VIBRATIONAL ENERGY TRANSFER PROCESSES IN GASEOUS SYSTEMS AT HIGH TEMPERATURES

by

G.E. MILLWARD A.R.I.C.

A thesis submitted to the University of Keele in partial fulfilment of the requirements for the Degree of Doctor of Philosophy

DEPARTMENT OF CHEMISTRY
UNIVERSITY OF KEELE

OCTOBER 1970

ACKNOWLEDGEMENTS

In presenting this thesis I would like to acknowledge the contributions of the following people:-

Dr. Peter Borrell for his valuable guidance and encouragement throughout this work.

Professor H.D. Springall for providing the laboratory facilities for this project.

Miss Jacqueline Marsden for typing the thesis.

The technical staff of the Chemistry Department, in particular Mr. Peter Holbrook and Mr. Frank Entwistle.

The staff of the computer centre for programming assistance, and Miss Pat Highfield for instruction in use of the computer.

The technical staff of the University Workshops, for the attention devoted to the construction of several parts of the apparatus.

The University of Keele for financial support.

All the work reported in this thesis was carried out by the author, under the supervision of Dr. Peter Borrell.

A B S T R A C T

A study has been made of the rate of vibrational excitation in shock heated CO for the temperature range 1300K - 2500K, by observation of the infrared emission behind the incident shock wave. Care was taken to eliminate impurity effects and the non uniformity of the flow was accounted for in the prescribed manner.

The first measurements were made on the fundamental and overtone of CO in the pure gas and CO/Ne mixtures. The experimental data was reduced using kinetically derived equations, which incorporated the Landau-Teller ratios between the rate constants. For τ_{CO-CO} the Landau-Teller constants were found to be A = -22.2; B = 160.2 and for τ_{CO-Ne} A = -21.66; B = 148.9. The separate observations of the levels indicated that the population of the v = 2 level was by successive single quantum transitions. It was concluded that the Landau-Teller ratio of the rate constants $k_{21} : k_{10} = 2 : 1$, was incorrect, in the case of the anharmonic oscillator. The coefficient was thought to lie between 2.2 and 2.4. It was demonstrated by computer calculations, using selected models, that the equations used in the reduction of experimental data were inadequate for real systems. Thus studies using the equations were thought to be subject to a small systematic error.

The second series of measurements was performed on CO/CO_2;

CO/N_2O and CO/COS mixtures, to measure the rate of vibration-vibration (V-V) energy exchange. Small concentrations of the faster relaxing gas (i.e. the polyatomic) were shown to dramatically reduce the relaxation time of the major component, CO. By using relaxation equations for a binary gas mixture, the probability of the V-V process was determined from the data. The probabilities were found to lie in the following sequence with respect to the energy discrepancy ΔE:-

$$P_{CO-CO_2} < P_{CO-N_2O} < P_{CO-COS}$$

$$\Delta E = 206 \qquad 80 \qquad 64 \quad cm^{-1}$$

These probabilities compared in magnitude and temperature dependence with the theories of Schwartz, Slawsky and Herzfeld and Rapp and Golden.

C O N T E N T S

1. INTRODUCTION

1.1 PRELIMINARY REMARKS

The molecules of a gas can possess energy in four different forms electronic, vibrational, rotational and translational. Each form of energy, excepting translational, has a discrete set of energy levels associated with it. The magnitude of the quanta associated with the levels decrease in the order:-

Electronic >> vibrational > rotational >> translational

The typical molecular energy spacings for the various forms of energy are shown below:-

TABLE 1.1

	Wavenumber cm^{-1}	Characteristic Temp K	ev	J mol^{-1}
Electronic	20,000	28,800	2.48	240,000
Vibrational	1000	1440	0.12	12,000
Rotational	10	14	0.0012	120

Transitions between the levels may be stimulated by electromagnetic radiation or molecular collisions. Neglecting radiative decay, both processes provide the disturbance which is necessary for the absorption

or emission of quanta of energy. The energy level spacings in the case of electronic energy are so large, that the excited states are not normally accessible by collision. The energy level spacings in the case of molecular vibrations and rotations do permit collisional excitation. In the case of translation the energy levels are so close that they are treated completely classically. The available thermal energy is equilibrated among the various degrees of freedom by the following processes:-

1. Rotation $\rightleftharpoons$ Translation
2. Vibration (1) $\rightleftharpoons$ Rotation * Translation
3. Vibration (1) $\rightleftharpoons$ Translation
4. Vibration (1) $\rightleftharpoons$ Vibration (2) * Translation

The exchange of translational energy with the internal degrees of freedom, processes 1, 3, are called simple processes. If a vibrational quantum in one molecule is converted into a quantum of a different vibration, then it is called a complex process, i.e. 4. This last case involves two vibrations and the difference between the two quanta is made up with translational energy. Process 2 which involves energy exchange between the internal degrees of freedom, vibrational and rotational, may also be called a complex process.

The probability per collision of energy exchange between vibration and translation is small and many collisions are often required to achieve energy conversion. The complex process is more

efficient, since less energy is required from translation. The efficiency of the complex process depends on the matching of the energy levels of the two vibrations.

The present work is concerned with information that can be obtained about these types of processes, when the system is disturbed by an external force. After the disturbance the system requires a finite time to return to the new equilibrium. The return to equilibrium via the processes is known as a relaxation process. The rate at which the energy E of a relaxing system returns to its equilibrium value $\bar{E}$ has been shown to be, by Landau and Teller,[1] proportional to its displacement from equilibrium:-

$$-\frac{dE}{dt} = \frac{1}{\tau}(E - \bar{E})$$

or

$$(E - \bar{E}) = (E_0 - \bar{E}) \exp(-t/\tau)$$

where τ is the time for the energy displacement $(E - \bar{E})$ to fall 1/e of the initial value $(E_0 - \bar{E})$ at $t = 0$, having the temperature held constant by a heat bath. The time scale for the molecular relaxation will be determined by the number of collisions within the region of observation. Since the collision rate is pressure dependent, the relaxation times will be similarly so. Convention dictates that the relaxation times should always be quoted at the standard pressure of 1 atmosphere.

In the present case the equilibrium was disturbed with a shock wave. The technique is well established, and has provided the majority of data on the temperature dependence of relaxation times. This method, together with several other important methods for studying energy transfer, will be reviewed below.

1.2 EXPERIMENTAL TECHNIQUES

1.2.a SHOCK TUBE TECHNIQUES

The shock tube is a device in which a shock wave is produced by the sudden bursting of a breakable diaphragm, which divides the tube into high pressure and low pressure sections. The pressure of the driver gas at which the diaphragm bursts depends on the diaphragm material and thickness. The formation of a shock wave by the bursting is understood by regarding the driver gas as a piston, which moves in small increments into the test gas. A pressure pulse is propagated, and this compression heats the gas slightly as it moves at the speed of sound. The second pulse also moves at the speed of sound but now in slightly hotter gas. The speed of sound increases with temperature, so that each pulse is moving faster than its predecessor. Eventually all the pulses coalesce to form a sharp front, i.e. the shock wave. This wave moves faster than the speed of sound. Thus the test gas molecules, which can only move at the speed of sound, are bound at some stage to be ingested by the shock front. The result is that there is a build up of pressure and density in the shock wave. Originally the waves were treated mathematically by Reimann,[2] who assumed that the shock wave was an adiabatic and reversible transition. Rankine[3] examined the theory and showed that the process was not adiabatic. Finally, Rayleigh[4] and Hugoniot[5] both showed that the shock transition must involve a change of entropy, and thus could not be adiabatic or reversible.

Using a system of coordinates where the shock front is stationary, see Figure 1.1, The Rankine-Hugoniot conservation equations may be written:-

FIGURE 1.1

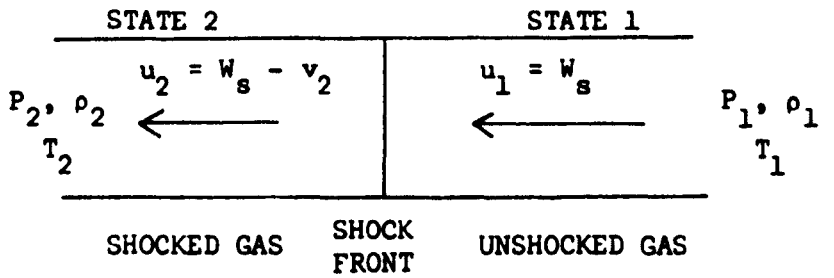

where W_s = velocity of shock front

v = velocity of gas molecules relative to the tube

P, ρ, T = pressure, density and temperature

The conservation of mass:-

$$\rho_1 u_1 = \rho_2 u_2 \qquad 1.1$$

The conservation of momentum:-

$$\rho_1 u_1^2 + P_1 = \rho_2 u_2^2 + P_2 \qquad 1.2$$

The conservation of energy:-

$$H_1 + \tfrac{1}{2}u_1^2 = H_2 + \tfrac{1}{2}u_2^2 \qquad 1.3$$

where H = enthalpy

In 1.3, the term $(\frac{1}{2}u_1^2 - \frac{1}{2}u_2^2)$ represents the amount of kinetic

energy which is changed into thermal energy, and thus the shock wave heats the gas. However, the heating produced by the shock wave is not the same as that produced in an adiabatic isentropic compression. This is due to the fact that $\Delta S > 0$ for the former, while $\Delta S = 0$ for the latter. The increase in entropy of the system which is compressed from state 1 to state 2 can be calculated:-

$$q = Tds$$

$$q = du + pdv \quad \text{(1st Law)}$$

$$\therefore \quad ds = \frac{du}{T} + \frac{p}{T}\,dv$$

$$\text{But} \quad du = C_v dT$$

$$\text{and} \quad RdT = pdv + vdp$$

$$\therefore \quad ds = \frac{dT}{T}\left[C_v + R\right] - \frac{vdp}{dT}$$

$$\frac{v}{T} = \frac{R}{p}$$

$$\therefore \quad ds = C_p \frac{dT}{T} - \frac{Rdp}{p}$$

$$\text{Integrating} \quad \Delta S = C_p \int_{T_1}^{T_2} \frac{dT}{T} - R \int_{p_1}^{p_2} \frac{dp}{p}$$

$$\Delta S = C_p \ln \frac{T_2}{T_1} - R \ln \frac{P_2}{P_1}$$

$$\text{Since} \quad R = C_p - C_v \quad \text{and} \quad \gamma = C_p/C_v$$

$$\Delta S = C_p \ln \left[\frac{(T_2/T_1)}{(P_2/P_1)^{\frac{\gamma-1}{\gamma}}} \right]$$

Thus:-

$$\frac{T_2}{T_1} = \left(\frac{P_2}{P_1}\right)^{\frac{\gamma-1}{\gamma}} \exp(\Delta S/C_p) \qquad 1.4$$

The equation 1.4 shows that for the same value of (P_2/P_1), an isentropic process where $\Delta S = 0$ (the exponential is one), the value of T_2 must always be less than T_2 across the shock front, where the exponential term is always greater than one. The change in entropy across the shock front may be calculated from:-

$$\Delta S = (R/(\gamma-1)) \ln \left[\left(\frac{P_2}{P_1}\right) \left(\frac{\rho_1}{\rho_2}\right)^{\gamma} \right]$$

The ratios (P_2/P_1) and (ρ_2/ρ_1) have been derived, in terms of known quantities, from the conservation equations. The ratios are to be found in section 6.2 of Chapter 6.

The shock wave is one of several waves produced after rupture of the diaphragm. The wave patterns are illustrated on the (x, t) diagram Figure 1.2, where x is the distance along the shock tube and t the time after the diaphragm bursts. The shock wave moves at a constant velocity in the test gas and is reflected on reaching the end plate. The test gas is heated by the initial shock wave, and is heated again by the reflected shock, but to a lesser degree, since the latter has a lower velocity. Following the shock wave is the contact surface, the point at which the test gas meets the driver gas, which moves with

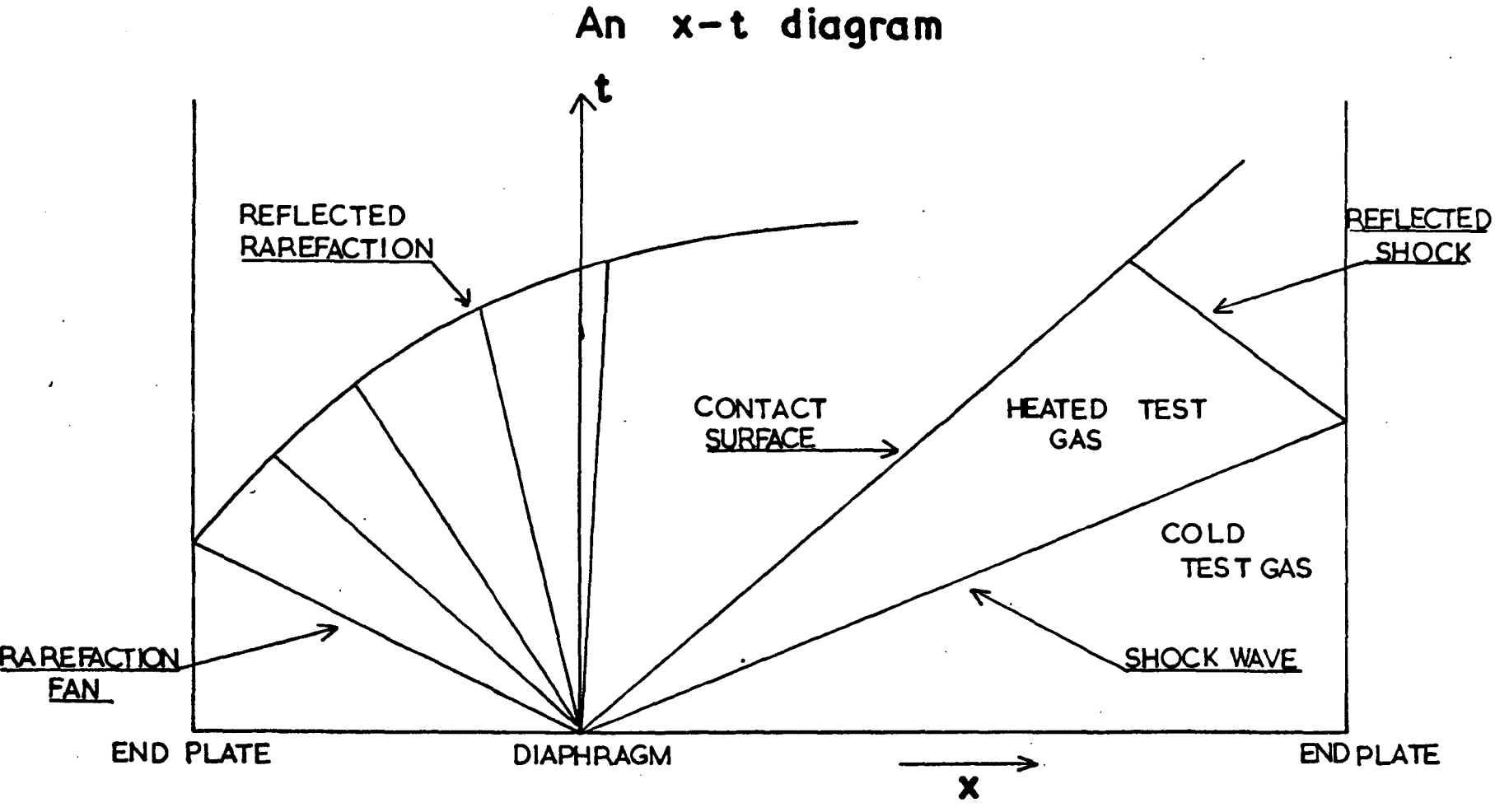
An x-t diagram
t
REFLECTED RAREFACTION
REFLECTED SHOCK
CONTACT SURFACE
HEATED TEST GAS
COLD TEST GAS
RAREFACTION FAN
SHOCK WAVE
END PLATE
DIAPHRAGM
END PLATE
x

Figure 1.2

a constant velocity, which is smaller than that of a shock wave. Thus at greater distances down the tube the separation between the shock front and the contact surface increases. The rarefaction fan, which is produced at the same time as the shock wave, moves into the driver gas at a sonic speed. The fan cannot coalesce to form a discontinuity and after reflection from the end plate accelerates towards the shock wave. The possibilities of interaction of the various wave forms depends upon the length of tube. This has been dealt with elsewhere.[6] The construction and operation of shock tubes is well defined and has been documented.[7,8,9,10] Particular emphasis has been placed on the measurement of shock speed, since this allows computation of the theoretical equilibrium state of the gas in the shock wave. Measurements of shock wave attenuation are also important, since in certain circumstances, boundary layer effects influence the shock properties,[11,12] see section 3.1.a of Chapter 3. The velocity is measured by devices which can respond rapidly, in the order of 1 μs. The methods available are pressure transducers, thin film temperature detectors and light detection devices. The techniques provide electric pulses which serve to trigger recording and timing devices.

It is the region between the shock front and the contact surface, which is of particular interest to kineticists, and it has facilitated an interesting range of chemical studies. There exists a large amount of data on the study of the unimolecular dissociations of

diatomic and polyatomic species, using shock techniques.[12,13,14] The studies of chemical reactions in shock waves have been tabulated,[10] and have been updated by Strehlow.[15] Recent ideas include cis-trans isomerization studies,[16] and homogeneous exchange reactions using radioactive tracers.[17] Hooker[18] has studied two phase systems, using a powder-gas aerosol for the test gas. However, the most exciting prospect seems to lie in the glow discharge shock tube,[19] which has been effectively used by Gross[20] and Cohen.[21,22]

The present work is concerned with the vibrational relaxation of gas molecules at high temperatures. The main measurement techniques involve those which can respond to changes of density; temperature and the emission of radiation. Shock front reflectance methods have been used to measure rotational relaxation.[23] Measurements of density changes have been made using a Mach-Zender interferometer.[24,25,26] The technique has been improved by the use of a laser light source.[27] Schlieren techniques have also been advanced by the use of lasers.[28,29,30] The vibrational temperature of the shocked gas may be followed by using the sodium line reversal method.[31] The infrared fluorescence methods allow the populations of individual vibrational levels to be followed during the relaxation period. The first work was done by Windsor, Davidson and Taylor,[32,33] who studied the infrared emission from the overtone of CO with a PbS detector. The technique is simple, the emission from the shock heated gas is passed through a filter, to isolate the wavelength of interest, and on to a detector, which is

usually of the photoconductive or photovoltaic type.[34] The infrared fluorescence technique has now been widely used[35,36,37,38,39] and its application in the present case is given in section 2.6 of Chapter 2.

Finally, the nozzle expansion flow technique,[40,41,42,43] which is an extension of the simple shock tube, has provided data[44,45] which bear comparison to shock tube results. The shock wave raises the translational temperature, so that the vibrational degrees of freedom may be excited. The expansion flow utilises the stationary gas at the end of the shock tube after the shock has reflected from the end plate. The gas is expanded through a nozzle, so that the gas is translationally cooled, and the deexcitation of the vibrationally excited gas may be followed. The vibrational temperature may be followed by the sodium line reversal technique. However the results may have been affected by impurities,[46] drawn from the boundary layer.

1.2.b ULTRASONIC METHODS

At relatively low temperatures the ultrasonic technique has provided a large bulk of data on vibrational relaxation. There are several good reviews on the subject, which also give the types of systems that have been studied.[47,48,49] The basis of the method is as follows. The velocity of sound through the gas is given by:-

$$v^2 = (1 + R/C_v)RT/M$$

where R = universal gas constant

v = velocity of sound

T = temperature

C_v = heat capacity of gas

M = molecular weight

The rate of energy transfer through the gas has an inverse dependence on the effective heat capacity of the gas. If the period of the sound wave is long enough for equilibrium to be established between all modes, then the heat capacity is given by:-

$$C_v = C_{trans} + C_{rot} + C_{vib}$$

where C_{trans}, C_{rot} and C_{vib} are the translational, rotational and vibrational heat capacities. If the period between the waves is gradually decreased a point is reached at which energy cannot be transferred in and out of the vibrational modes rapidly enough to maintain equilibrium. This energy is then lost from the sound wave and dissipated in the gas. At some point no energy is transferred to the vibration, and the vibration makes no contribution to the specific heat of the gas. The sound wave now travels through the gas at higher velocity. From measurements of the velocity at various sound frequencies, the Napier time may be calculated. The method has had success in measurements of vibrational relaxation in a temperature

range up to 1000K. However, it cannot be used for high frequency molecular vibrations which make a small contribution to the specific heat.

1.2.c MISCELLANEOUS METHODS

Experimental techniques have been developed, for the study of vibrational energy transfer, based on the radiative excitation of energy levels. Those vibrational modes of molecules which involve a change of dipole moment can take up quanta directly by absorption of radiation of the appropriate wavelength. A particular vibration will lose energy either by radiative decay of infrared fluorescence or by collisional deactivation, depending on the lifetimes of the two processes:-

$$A_2^* + M \rightleftharpoons A_2 + M + K.E.$$

$$A_2^* \rightleftharpoons A_2 + h\nu$$

The radiative lifetime of an infrared active mode is independent of the gas pressure whereas the collisional lifetime is inversely proportional to it. For all but a few diatomic molecules with high vibration frequencies (i.e. CO) the radiative lifetime is much longer than the collisional lifetime, and the latter dominates the vibrational relaxation.[50]

An apparatus which combines radiative excitation with

sound wave detection is the spectrophone. The gas is pulsed with infrared radiation and the time lag for the modulated radiation to appear as a sound pulse (optic-acoustic effect) provides a measure of the rate of vibration-translation energy transfer.[51,52,53]

The infrared resonance fluorescence technique of Millikan[54] employs both spectroscopic excitation and deexcitation to study CO ($\bar{\nu}$ = 2143 cm^{-1}), one of the molecules whose radiative lifetime is shorter than its collisional lifetime, at room temperature. Millikan studied the half quenching of fluorescence from CO by small additions of other gases. From this he obtained the probabilities of energy transfer in heteromolecular collisions. Important features of the experiment were an optically thin gas and the elimination of wall collisions as an effective quencher of CO by containing the gas sample in a streaming jacket of Argon.

The most recent infrared excitation technique is the use of laser pulsing to modulate the population of a particular vibrational energy level. The development of the high power CO_2-N_2 gas laser[55,56,57] has focussed considerable interest in the mechanism and kinetic rates of vibrational energy exchange between CO_2 and N_2. This method of excitation, combined with the observation of fluorescence from another vibrational mode has been used[58] to study vibration-vibration exchange in CH_4 and CO_2.[59] There are good reviews on the subject.[60,61]

Another spectroscopic method, which gives information on vibration-vibration energy transfer, is flash spectroscopy, described

by Norrish[62] and Callear.[63] The technique, used particularly with NO, consists essentially of triggering a powerful light flash, filtered for suitable wavelengths, in a tube next to the reaction vessel. The NO molecules in their ground electronic state $X^2\pi$ (v=0) are raised to higher vibrational levels of the exicted electronic states, usually $A^2\ \Sigma^+$. Relaxation of the vibrational energy can be studied in the excited state by observing the changing intensities of v=0 and v=1 progression in the fluorescent spectrum of the excited electronic state and the ground state by flash spectroscopy. In this last method the photoflash is followed, after a controlled delay, by a spectroscopic flash, enabling the absorption band of the transition $X^2\pi$ (v=1) to the excited $A^2\ \Sigma^+$ (v=0) to be photographed. The decay with time of this band provides a measure of the vibrational relaxation of the v=1 level in the ground electronic state of NO. Both fluorescent emission and flash spectroscopy have been used to study the relaxation of NO in homo and hetero molecular collisions.

1.2.d COMPARISON OF METHODS

The spectroscopic methods are concerned with exciting molecules vibrationally. They provide a means of studying high frequency vibrations whose vibrational energy levels are not appreciably populated at 300K. For these vibrations, as previously stated, there is little or no ultrasonic dispersion or absorption. On the other hand it is possible to measure relaxation processes

occuring in short times, by the ultrasonic technique. This is not always possible with the shock techniques. The spectroscopic and ultrasonic methods are complementary since in the former the direct perturbation of the vibrational energy facilitates the study of vibration-vibration energy transfer, while the latter is more suited to vibration-translation transfer. However, in the case of gas mixtures the two methods supplement each other. As with the acoustic method, the shock wave studies provide evidence primarily about vibration-translation transfer. Together the two techniques provide data on the temperature dependence of this process, which can be used to test the validity of theoretical calculations.

1.3 PREVIOUS SHOCK TUBE STUDIES OF VIBRATIONAL ENERGY TRANSFER

The object of this section is to review shock tube results which are relevant to the present study. The performance of the theoretical predictions is also given. There are several methods for the absolute calculations of Napier times, and these are given in Chapter 4. The most widely applied approach is the S.S.H. theory (section 4.5). It is a 3-Dimensional quantum mechanical treatment which predicts absolute values of the Napier times, to within an order of magnitude, for many systems over a wide temperature range. The details are tabulated.[48,64,65] For simple non polar molecules the dependence of temperature follows the Landau-Teller[1] relationship, $\ln\tau\alpha T^{-\frac{1}{3}}$. At lower temperatures and for non polar molecules the experimental times vary less steeply with temperature. The Millikan and White[66] (M.W.) correlation, derived on an empirical basis, has had reasonable success in predicting vibration-translation Napier times (see section 4.6). However there are notable exceptions to the S.S.H. theory and M.W. correlation, particularly H_2, D_2, the hydrogen halides and NO. H_2[29] and D_2[28] show Napier times almost two orders of magnitude longer than the S.S.H. theory predicts, while the M.W. correlation gives Napier times of 7 times too slow for D_2 and 40 times tooslow for H_2. The Napier times of HCl,[67,68,69] HBr,[70] HI[70,71] and DCl[68] have been measured. At 2000K HCl has a rough agreement with the S.S.H. value but HBr and HI are much lower than predicted by the theory and the M.W. correlation. These discrepancies may be due to the efficiency of

vibration-rotation energy exchange, of which the theories take no account. Moore[72] has developed a vibration-rotation transfer theory, and it gives a reasonable value for HCl, but not for HI. This may be due to the use of a single value of the repulsive potential parameter, ℓ, to fit the experimental data of a wide range of molecules. In the NO case, it is possible that an electronically excited state is formed, or that dimerization may have to be taken into account. A special potential function is needed for this molecule.

Linear triatomic molecules such as CO_2[73,74,75,76] and N_2O[82,83] have had much attention devoted to them. Opinion has been divided as to whether the molecules possess more than one relaxation time. However, recent experimental evidence has hardened the attitude that all the modes relax together.[77,78,79] This was certainly the case in Camac's[80] study above 2000K. The theoretical S.S.H. results do not agree well with the experimental values, the former having a too steep temperature dependence. N_2O has been studied in the shock tube and there is good agreement between various workers. These molecules are of interest in mixtures[81] since their vibrational modes will provide information on intermolecular vibration-vibration energy transfer, and also intramolecular vibration-vibration transfer.

Carbon monoxide, the basis of the present work, has been well studied,[32,36,84,85] The original work in the reflected shock region gave a longer Napier time than the subsequent studies using different techniques. This was probably due to the use of incident

shock wave parameters in the former work. The relaxation has been studied in the presence of various collision partners[86,87] and the Napier times agree well with the S.S.H. calculation, but are about a factor of 2 shorter than the M.W. predictions.

The overtone of CO was studied and it was shown[36] that the rate of populating the v=2 level by successive quantum jumps was ten times faster than the rate of direct excitation. The equilibrium population of the v=2 level of pure CO may be acheived in two ways:-

$$\text{Firstly} \quad CO_{v=0} + CO_{v=0} \underset{k'_{10}}{\overset{k'_{01}}{\rightleftharpoons}} CO_{v=1} + CO_{v=0} \qquad 1.5$$

$$\text{then} \quad CO_{v=1} + C_{v=0} \underset{k'_{21}}{\overset{k'_{12}}{\rightleftharpoons}} CO_{v=2} + CO_{v=0} \qquad 1.6$$

$$\text{or} \quad CO_{v=1} + CO_{v=1} \underset{k'_{-2}}{\overset{k'_{2}}{\rightleftharpoons}} CO_{v=2} + CO_{v=0} \qquad 1.7$$

where v = vibrational quantum number

k' = bimolecular rate constants

The mechanism was interpreted using a Landau-Teller model that, $k'_{01} : k'_{12} = 1 : 2$ etc., and it was concluded that the stepwise process dominated.[36] However no attempts were made to distinguish between the population of the overtone by reactions 1.5 and 1.6 from 1.5 and 1.7. It was found that both mechanisms reduced to the same

analytical equation, see Chapter 5. Higher vibrational levels of other molecules have been studied. In particular work on HCl[67] and HI[70] showed that transitions where $\Delta v > 1$ were possible, so that

$$k_{10} = k_{20} = k_{30}$$

It was suggested that this result may be explained on the basis of efficient energy exchange from vibration to rotation.

A large number of acoustical and spectroscopic measurements have been made in gas mixtures, which provide information about vibration-vibration energy transfer in heteromolecular collisions. Considering a binary gas mixture, whose molecules A and B contain only one vibrational mode, then if the quantum of vibrational energy is denoted * the processes are:-

1. $A^* + A \rightleftharpoons A + A$
2. $A^* + B \rightleftharpoons A + B$
3. $B^* + B \rightleftharpoons B + B$
4. $B^* + A \rightleftharpoons B + A$
5. $A^* + B \rightleftharpoons A + B^*$

The self relaxation of B is more rapid than that of A. For mixtures of gases A and B, the relative Napier times of the pure gases (1,3) and the relative matching of their vibrational energy levels ($\bar{\nu}_A$ and $\bar{\nu}_B$) can be so chosen to be closely similar or widely different. If the matching of A and B is poor, so that the vibration-vibration exchange is slow, then at all compositions, the reciprocal Napier time will be

linear, with slope depending on the relative rates of processes (1,2) for A, and (3,4) for B. Now consider the case in which the levels of A and B are nearly resonant so that for certain pairs of molecules the vibration-vibration reaction 5 will be more rapid than the simple deactivation of B. The mixture will show only one Napier time at any concentration, the time depending on the rates of processes 3,4.

The most notable shock tube work in this field has been by Taylor et al.,[38] who carried out experiments in these gas mixtures $NO-N_2$ (ΔE = 456 cm^{-1}); NO-CO (ΔE = 267 cm^{-1}); CO_2-N_2 (ΔE = 18 cm^{-1}). The first two systems provided data on "near-resonant" vibration--vibration exchange. The CO_2-N_2 mixture provided data on resonant energy exchange. Since this work, other studies have been carried out on a variety of systems.[39,88,89,90,91,92] For diatomic systems the general temperature dependence of the resonant rates is reasonable, but the magnitude of the experimental data is considerably less than the S.S.H. theory predicts. Simple molecules with additional vibrational modes have complex mechanisms for vibration-vibration energy transfer.[60] They are well studied at room temperature,[61] and the theory has been revised to take account of the possibilities of intramolecular energy exchange.[93,94] However, further work is required on the temperature dependence of systems containing such molecules.

1.4 OBJECTS OF THE PRESENT STUDY

i) The construction and development of a pressure driven shock tube. The tube was to be capable of producing conditions of high temperatures in gaseous systems, so that accurate infrared emission measurements could be made on the chosen systems.

ii) Infrared emission measurements on pure CO and CO/Ne mixtures. CO is a molecule with a dipole moment, and thus lends itself to this type of experiment. As indicated in section 1.3 the vibrational relaxation of the fundamental and overtone have been studied under carefully controlled conditions. It was decided to remeasure the Napier time for these vibrational modes of CO. Then to study the effect of the addition of an inert gas on the mechanism of the population of the fundamental and the overtone. This was done with the intention of being able to distinguish between the two mechanisms of population of the overtone. The experimental results were to be compared with computed relaxation curves using various models for the population of upper levels. It was intended that the comparison of theory and experiment would provide a stringent test of the models and assumptions used in the reduction of shock tube data.

iii) Infrared emission measurements on CO/polyatomic mixtures. The current interest in shock work lies in vibration--vibration exchange processes. Previous workers have used linear triatomic molecules[38,90] in a binary mixture and came to the conclusion that energy must be transferred from these molecules

via the ν_3 antisymmetric stretching mode. Thus for a mixture with CO, the infrared emission from the fundamental of CO, may give some measure of the rate of exchange between the fundamental of CO and the ν_3 mode of the triatomic. A series of mixtures which lend themselves to this study are (energy discrepancy in brackets):-

CO/CO_2 (ΔE = 206 cm^{-1})

CO/N_2O (ΔE = 81 cm^{-1})

CO/COS (ΔE = 64 cm^{-1})

The first system in the series, is of special interest since the low dissociation energy of CO_2, means that some CO is expected in electric discharges in CO_2-N_2 or in CO_2 lasers. Thus it was hoped to obtain information on vibration-vibration energy exchange in these systems.

iv) Theoretical calculations. Extensive calculations of the Napier times for the systems were carried out using the methods selected in Chapter 4.

v) Conclusions. A reasoned explanation of the kinetics of the processes studied under ii and iii was undertaken.

REFERENCES

1. L.D. Landau and E. Teller, Z. *Phys. Sowjetunion*, 1936, 10, 34.
2. B. Reimann, *Gesammelte Werke*, 1876, 144.
3. W.J.M. Rankine, *Trans. Roy. Soc. (London)*, 1870, 160, 277.
4. J. Rayleigh, *Proc. Roy. Soc. (London)*, 1910, 84, 247.
5. H. Hugoniot, *J. de l'École Polytechnique*, 1889, 58, 1.
6. I.I. Glass, *University of Toronto Aeronautics Review*, 1958, No.12.
7. J.N. Bradley, *Shock Waves in Chemistry and Physics*, (Methuen, London) 1962.
8. A.G. Gaydon and I.R. Hurle, *The Shock Tube in High Temperature Chemical Physics*, (Chapman and Hall, London) 1963.
9. J.K. Wright, *Shock Tubes*, (Methuen, London) 1961.
10. E.F. Greene and J.P. Toennies, *Chemical Reactions in Shock Waves*, (Arnold Publishers, London) 1964.
11. R.A. Strehlow and R.L. Belford, *Tech. Rept. A.A.E.*, 69-1, Univ. Illinois, Urbana, 1969.
12. R.L. Belford and R.A. Strehlow, *Ann. Rev. Phys. Chem.*, 1969, 20, 247.
13. S.H. Bauer, *Ann. Rev. Phys. Chem.*, 1965, 16, 245.
14. J. Troe and H. Wagner, *Ber. Bunsenges Physik Chem.*, 1967, 71, 937.
15. R.A. Strehlow, *Progress in High Temperature Physics and Chemistry*, (C.H. Rouse Ed. Pergamon Press, New York) 1969, 3.
16. P.M. Jeffers and W. Shaub, *J. Am. Chem. Soc.*, 1969, 91, 7706.

17. A.J. Kassman and D.S. Martini, *J. Am. Chem. Soc.*, 1969, 91, 6237.

18. W.J. Hooker and R.D. Main, *Physica*, 1969, 41, 35.

19. R.A. Hartunian, W.P. Thompson and E. Hewitt, *J. Chem. Phys.*, 1966, 44, 1765.

20. R.W.F. Gross, *J. Chem. Phys.*, 1968, 48, 1302.

21. R.W.F. Gross and N. Cohen, *J. Chem. Phys.*, 1968, 48, 2582.

22. N. Cohen and R.W.F. Gross, *J. Chem. Phys.*, 1969, 50, 3119.

23. E.F. Greene, G.R. Cowan and D.F. Hornig, *J. Chem. Phys.*, 1951, 19, 427.

24. H.K. Zienkiewicz and N.H. Johannesen, *J. Fluid Mech.*, 1963, 17, 499.

25. V.H. Blackman, *J. Fluid Mech.*, 1956, 1, 61.

26. D.R. White, *J. Chem. Phys.*, 1965, 42, 447.

27. A.L. Besse and J.G. Kelley, *Rev. Sci. Instr.*, 1966, 37, 1497.

28. J.H. Kiefer and R.W. Lutz, *J. Chem. Phys.*, 1966, 44, 658.

29. J.H. Kiefer and R.W. Lutz, *J. Chem. Phys.*, 1966, 44, 668.

30. J.H. Kiefer and R.W. Lutz, *J. Chem. Phys.*, 1966, 44, 3888.

31. A.G. Gaydon and I.R. Hurle, *Proc. Roy. Soc. (London) Ser. A*, 1961, 262, 38.

32. M.H. Windsor, N. Davidson and R. Taylor, *J. Chem. Phys.*, 1957, 27, 315.

33. M.H. Windsor, N. Davidson and R. Taylor, *7th Symp. Combustion*, (Butterworths, London) 1959, 80.

34. R.F. Potter and W.L. Eisenman, *Appl. Optics*, 1962, 1, 567.

35. P. Borrell, *Chem. Soc. (London) Spec. Publ.*, 1966, 20, 263.

36. W.J. Hooker and R.C. Millikan, *J. Chem. Phys.*, 1963, 38, 214.

37. D.R. White and R.C. Millikan, *A.I.A.A. Journal*, 1964, 2, 1844.

38. R.L. Taylor, M. Camac and R.M. Feinberg, *11th Symp. Combustion*, (Combustion Institute, Pittsburg, Pa.), 1967, 49.

39. Y. Sato, S. Tsuchiya and K. Kuratani, *J. Chem. Phys.*, 1969, 50, 1911.

40. I.R. Hurle, *J. Chem. Phys.*, 1964, 41, 3592.

41. I.R. Hurle, and A.L. Russo, *J. Chem. Phys.*, 1965, 43, 4434.

42. I.R. Hurle, A.L. Russo and J.G. Hall, *J. Chem. Phys.*, 1964, 40, 2076.

43. A.L. Russo, *J. Chem. Phys.*, 1966, 44, 1305.

44. I.R. Hurle, *Chem. Soc. (London), Spec. Publ.*, 1966, 20, 277.

45. A.L. Russo, *J. Chem. Phys.*, 1967, 47, 5201.

46. C.W. von Rosenburg, R.L. Taylor and J.D. Teare, *J. Chem. Phys.*, 1968, 48, 5731.

47. K.F. Herzfeld and T.A. Litovitz, *Absorption and Dispersion of Ultrasonic Waves*, (Academic Press, New York) 1959.

48. T.L. Cottrell and J.C. McCoubrey, *Molecular Energy Transfer in Gases*, (Butterworths, London) 1961.

49. J.L. Stretton, *Transfer and Storage of Energy by Molecules*, (Wiley - Interscience, London) 1969, 2, 1.

50. S.J. Lukasik, *J. Accust. Soc. Am.*, 1956, 28, 455.

51. T.L. Cottrell, T.F. Hunter and A.W. Read, *Proc. Chem. Soc.*, 1963, 272.

52. M.G. Ferguson and A.W. Read, *Trans. Faraday Soc.*, 1965, 61, 1559.

53. T.L. Cottrell, I.M. Macfarlane, A.W. Read and A.H. Young, *Trans. Faraday Soc.*, 1966, 62, 2655.

54. R.C. Millikan, *J. Chem. Phys.*, 1963, 38, 2855.

55. C.K.N. Patch, *Phys. Rev. Letters*, 1964, 13, 617.

56. F. Legay and N. Legay-Sommaire, *Compt. Rend.*, 1964, 259, 99.

57. N. Legay-Sommaire, L. Henry and F. Legay, *Compt. Rend.*, 1967, 260, 3339.

58. J.T. Yardley and C.B. Moore, *J. Chem. Phys.*, 1966, 45, 1066.

59. L.O. Hocker, M.A. Kovacs, C.K. Rhodes, G.W. Flynn and A. Javan, *Phys. Rev. Letters*, 1966, 17, 233.

60. C.B. Moore, *Acc. of Chem. Res.*, 1969, 2, 103.

61. R.L. Taylor and S. Bitterman, *Rev. Mod. Phys.*, 1969, 41, 26.

62. R.G.W. Norrish, *The Study of Energy Transfer in Atoms and Molecules by Photochemical Methods*, (Interscience, New York) 1962.

63. A.B. Callear, *Appl. Optics Suppl.*, 1965, 2, 145.

64. P. Borrell, *Transfer and Storage of Energy by Molecules*, (Wiley - Interscience, London) 1969, 2, 180.

65. B. Stevens, *Collisional Activation in Gases*, (Pergamon Press, London) 1967, 201.

66. R.C. Millikan and D.R. White, *J. Chem. Phys.*, 1963, 39, 3209.

67. P. Borrell and R. Gutteridge, *Recent Advances in Aerothermochemistry*, (Conference Proceedings 12, AGARD, Paris) 1967, 131.

68. W.D. Breshears and P.F. Bird, *J. Chem. Phys.*, 1969, 50, 333.

69. C.T. Bowman and D.J. Seery, *J. Chem. Phys.*, 1969, 50, 1904.

70. C.C. Chow and E.F. Greene, *J. Chem. Phys.*, 1965, 43, 324.

71. J.H. Kiefer, W.D. Breshears and P.F. Bird, *J. Chem. Phys.*, 1969, 50, 3641.

72. C.B. Moore, *J. Chem. Phys.*, 1965, 43, 2979.

73. N.H. Johannesen, H.K. Zienkiewicz, P.A. Blythe and J.H. Gerrard, *J. Fluid Mech.*, 1962, 13, 213.

74. I.R. Hurle and A.G. Gaydon, *Nature*, 1959, 184, 1858.

75. J. Daen and P.C.T. de Boer, *J. Chem. Phys.*, 1962, 36, 1222.

76. W.J. Witteman, *J. Chem. Phys.*, 1962, 37, 655.

77. D. Weaner, J.F. Roach and W.R. Smith, *J. Chem. Phys.*, 1967, 47, 3096.

78. C.J.S.M. Simpson, K.B. Bridgman and T.R.D. Chandler, *J. Chem. Phys.*, 1968, 49, 513.

79. C.J.S.M. Simpson, T.R.D. Chandler and A.C. Strawson, *J. Chem. Phys.*, 1969, 51, 2214.

80. M. Camac, *Avco Report*, 1964, 195.

81. C.J.S.M. Simpson, T.R.D. Chandler, *Proc. Roy. Soc. (London), Ser. A*, 1970, 317, 265.

82. W. Griffith, D. Brickl and V. Blackman, *Phys. Rev.*, 1956, 102, 1209.

83. C.J.S.M. Simpson, K.B. Bridgman and T.R.D. Chandler, *J. Chem. Phys.*, 1968, 49, 509.

84. A.G. Gaydon and I.R. Hurle, *8th Symp. Combustion*, (Williams and Wilkins, Baltimore) 1962, 309.

85. D.L. Matthews, *J. Chem. Phys.*, 1961, 34, 639.

86. R.C. Millikan, *J. Chem. Phys.*, 1964, 40, 2594.

87. R.C. Millikan and L.A. Osberg, *J. Chem. Phys.*, 1964, 41, 2196.

88. D.R. White, *J. Chem. Phys.*, 1968, 49, 5472.

89. G. Kamimoto and H. Matsui, *A.I.A.A. Journal*, 1969, 7, 2359.

90. J.F. Roach and W.R. Smith, *J. Chem. Phys.*, 1969, 50, 4114.

91. S.J. Colgan and B.P. Levitt, Private communication.

92. R.L. Taylor and S. Bitterman, *J. Chem. Phys.*, 1969, 50, 1720.

93. K.F. Herzfeld, *Discussions Faraday Soc.*, 1962, 33, 86.

94. K.F. Herzfeld, *J. Chem. Phys.*, 1967, 47, 743.

2. EXPERIMENTAL

2.1 INTRODUCTION

The shock tube has been used for energy transfer studies for a number of years.[1] The rise in temperature at the shock front provides rapid and uniform heating of the test gas, so that the various degrees of freedom exchange energy. By monitoring a suitable characteristic of the gas, information on the relaxation will be obtained.

The tube consisted essentially of a metal or glass tube of circular cross section, divided into two sections by a diaphragm of cellophane or metal foil. The shorter of the sections contained a driver gas at high pressure which acted as a piston when the diaphragm was ruptured. A shock wave was driven into the experimental gas, at a considerably lower pressure, in the longer section of the tube. It was then possible to measure the velocity of the shock, and to observe the infrared emission from the shock heated gas, by utilising a detector and display unit. Since the shock wave travelled at about 1 to 2 millimetres per μs, the relaxation process was completed within 500 μs and electronic methods were necessary to measure the relaxation process.

The following chapter describes the important parameters in the building of the shock tube, and in the choice and construction

of the ancillary equipment. Included also are details of the experimental procedure, together with some of the major difficulties which had to be overcome.

2.2 SHOCK TUBE

2.2.a CALCULATIONS OF TUBE DIMENSIONS

Before any tube design was undertaken, it was necessary to calculate lengths of driver and test section required. The important quantity in these calculations was the hot flow time, (laboratory time) that is, the time between the passage of the shock front and the contact surface, to an observer stationed in the test section. In the ideal situation, the time is limited solely by the interaction of the wave systems produced when the diaphragm is burst, after they are reflected from the ends of the tube. Expressions relating the hot flow time to the combination of driver and test gas, and shock speed have been derived.[2] The pertinent equations are given in Appendix 1. The calculations are made assuming ideal gases. However, the growth of the boundary layer behind the shock front affected the flow, so that the hot flow time was considerably reduced. A detailed account of the boundary layer, and its effects on shock conditions will be given in Chapter 3.

The calculations were made assuming that the driver gas was hydrogen, the test gas carbon monoxide, the shock wave travelled at Mach 5 and the hot flow time was 500 μs. The hot flow time was selected on the basis of previous results obtained on carbon monoxide.[3] Using these figures, the calculations showed that the ideal driver section was 1.5 m long, the minimum length of test

section was 3.61 m. However, the available laboratory space was restricted to a total length of 3.75 m. Thus the theoretical tube geometries were modified in accord with the ranges described by Hall.[4] This was an empirical approach, based on data of a number of tubes. The final lengths decided upon were:-

Driver Section - 1.15 m

Test Section - 2.55 m

It was also important to calculate the distance the observation station was to be placed from the end plate. At a distance of 0.42 m from the end plate, calculations showed that the initial hot flow should not undergo any interaction from the reflected shock.

2.2.b TUBE MATERIALS AND DESIGN

The shock tube will be considered in terms of its individual components, that is, the driver section, the connecting section and the test section. A tube of circular cross section was decided upon, since the absence of corners made it easy to keep clean, and the circular cross section gave structural strength. There are two effects to be considered on change of the internal tube diameter. Firstly, a decrease in the diameter leads to an increase in boundary layer effects, of the shock wave with the wall. Secondly, an increase in diameter leads to an increase in the pumping time. In this case it was decided to restrict

the pumping time, and to make the necessary corrections for the boundary layer.

The driver section was made of brass, and was 1.15 m in length, with an internal diameter of 2.54 cm. See Figure 2.1.a. At either end of the section, a brass flange, diameter 12.5 cm, was silver soldered to the tube. In one of the flanges were drilled three equally spaced holes, near the periphery of the flange. These were to house the securing bolts for the end plate. An 'O' ring made the vacuum seal. The other flange had a seating for an 'O' ring, 8 cm diameter. Pins for locating the driver section with the connecting section were placed diametrically opposite at a distance of 11 cm. Two grooves were cut into the edge of the flange, to accommodate the clamping screws of the connecting section. Located about midway on the tube was a hollow thread, which was silver soldered to a hole drilled into the section. This was the driver gas inlet.

The connecting section, Figure 2.1.b, was the piece which allowed the driver section to be joined to the test section. It was made of brass, with brass flanges, and was of length 10 cm, with internal diameter 2.54 cm. At the end nearer the driver section the flange had an 'O' ring 6.5 cm in diameter. Also two holes were drilled to coincide with the locating pins on the foward flange of the driver. This ensured that both sections had their diameters in coincidence when the sections were clamped together. The clamping was done by two butterfly screws,

Figure 2.1.a
Driver Section

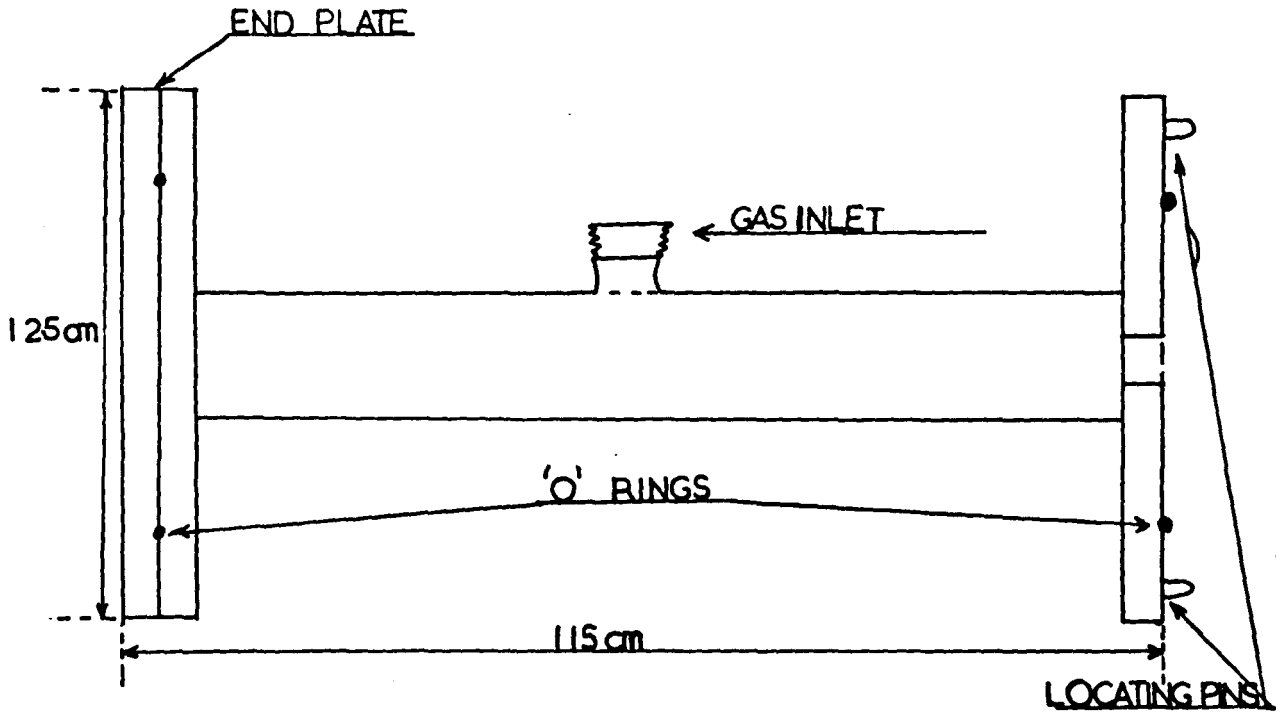

Figure 2.1.b
Connecting Section

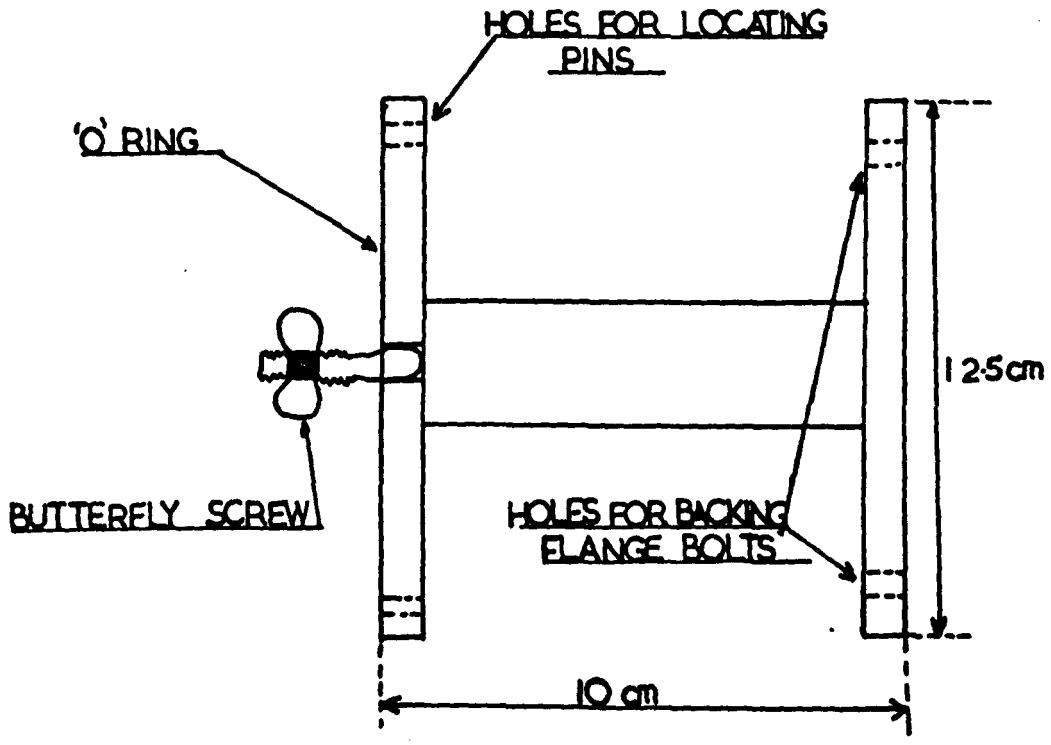

which fitted the grooves on the driver section's forward flange. Drilled at equidistant points near the periphery of the other flange were three holes, which coincided with the holes on a standard Q.V.F. backing flange, and which held the test section firmly against the connecting section.

For spectroscopic work it would be advantageous to use a glass tube as the test section. However, in the present studies this presented two disadvantages. Firstly, the thick curved wall of the glass tube presented optical difficulties, and secondly pyrex glass was opaque below 3800 cm^{-1}. It was decided to use pyrex tubing for the studies on the overtone of carbon monoxide, at 4260 cm^{-1}, and for the studies on the fundamental, at 2143 cm^{-1}, a pyrex tube-metal tube combination was used. The metal tube had calcium aluminate windows which transmitted in the region of interest. See Chapter 3. The pyrex tubing was standard Q.V.F. pipeline of 2.54 cm internal diameter. It had been tested to a maximum internal working pressure of 689.5 kNm^{-2}. The residual pressure in the tube after a shock experiment was calculated to be never greater than 305 kNm^{-2}. The pyrex tubing could be obtained in varying lengths, which were clamped together by two metal backing flanges. The joint between the glass tube was sealed by a P.T.F.E. crescent shaped ring. All the aforementioned parts are standard Q.V.F. pieces. The joint between the pyrex tube and the connecting section was made by clamping a metal

backing flange to the metal flange of the connecting section with a P.T.F.E. ring as the seal. For the measurement on the overtone of carbon monoxide the test section consisted of a 15 cm length and a 2.4 m length of pyrex tubing. The 15 cm length had a 5 mm internal diameter gas exit and entry port glass blown on to it. At the end of the longer length, an end plate was clamped with a backing flange.

For the studies on the fundamental of carbon monoxide, the following sections were used:- (i) 15 cm section with gas port as before, (ii) 75 cm section of pyrex tubing, (iii) 90 cm section of metal tube, with one window mounting, (iv) 90 cm section of metal tube with two window mountings. The couplings between glass-glass and glass-metal joints were as described before. The Figure 2.2.a shows the metal section with the two window mountings. The tube itself was constructed from stainless steel, with brass flanges, 8.75 cm in diameter, and silver soldered to the tube. The joining of the two metal sections was arranged so that large steps at the joint were avoided. This was achieved by having a lip on the periphery of the flange of one tube, which fitted into a groove on the other. An 'O' ring made the seal when the two flanges were bolted together. This system of mating the tubes gave not only a smooth tube, but also ensured a good vacuum. Mounted on the tubes were blocks of brass, which were machined to accommodate the window holders. The design of the holder is shown in Figure 2.2.b. The holders were clamped to the tube by means of screws, and an 'O' ring made the seal. Before the

Figure 2.2.a
Metal Observation Section

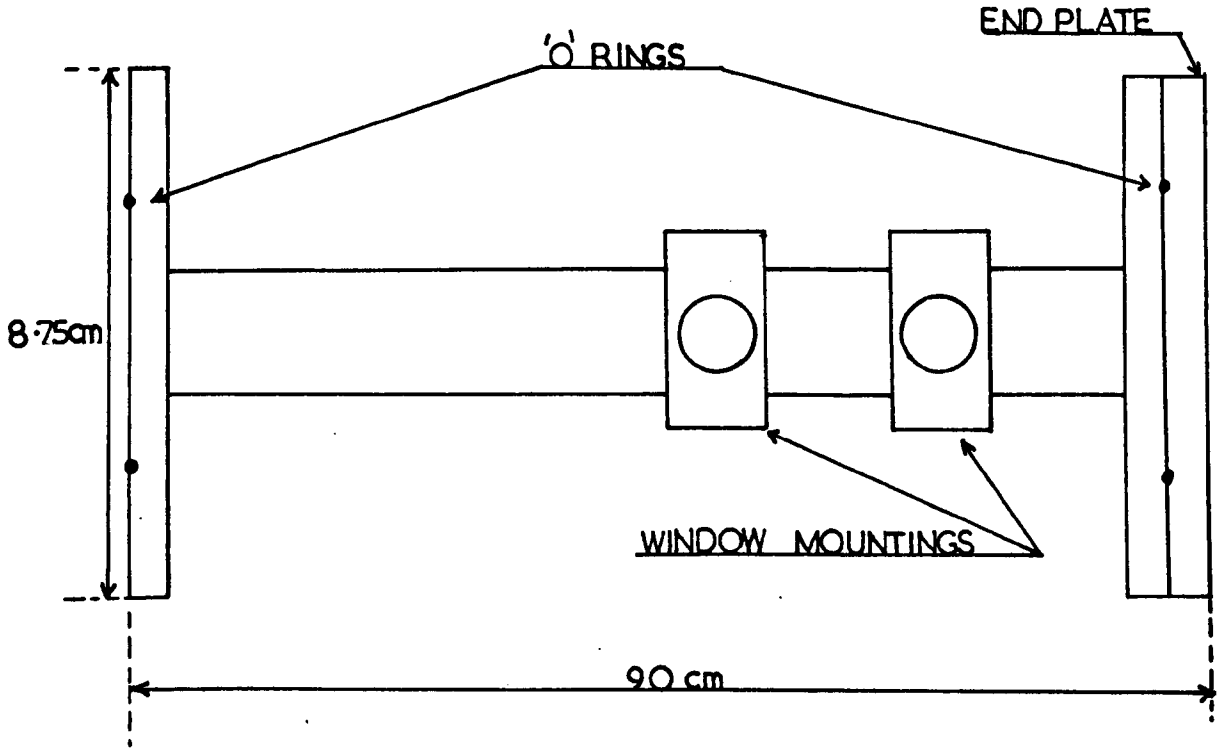

Figure 2.2.b
Window Holder

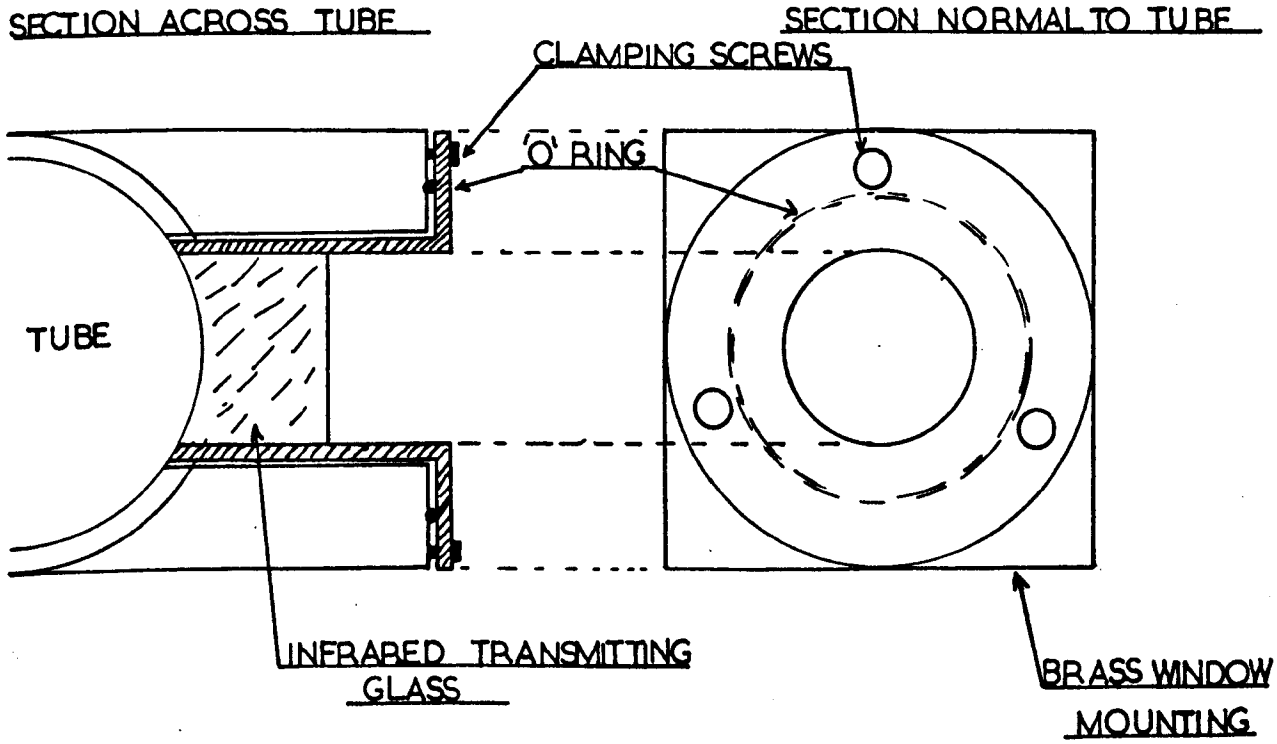

windows were cemented in position, the holders were clamped in position and both tubes were honed to a diameter of 2.54 ± 0.0025 cm. The windows used were of two types (i) Calcium Aluminate glass type BS 39B obtained from Messrs. Barr and Stroud Limited. This glass had an infrared transmission to about 1700 cm^{-1}, with a transmittance of 50%. (ii) Pyrex glass, which was obtained from Electronic Optics Limited. Both types of glass, were circular discs of 1.56 cm diameter and 0.63 cm maximum thickness, which had one surface ground to a radius of 1.27 cm. The other face was flat. The windows, were cemented into the holder, using Araldite, so that they were flush with the inside wall of the tube. The first and second pairs of windows were pyrex, used to measure the velocity of the shock by means of light screens. The last window was used for observing the infrared emission.

2.2.c SUPPORTS

Support for the shock tube and driver section was important. Considerable forces existed along the axis of the tube, in particular, when the diaphragm was broken and when the gas was brought to rest. Convenient rigid supports for the circular tube were standard Q.V.F. pipeline holders. These supports consisted of a split moulded rubber collar, kept in place by a U-bolt and back plate. The driver section was mounted on rollers to take up any recoil, and to facilitate changing of the diaphragm.

2.3 VACUUM AND PRESSURE TECHNIQUE

The high vacuum apparatus is represented in Figure 2.3. The taps, wherever possible, were of the greaseless type. The ultimate vacuum was realised by means of an oil diffusion pump (N.G.N. type OPW 125, with entrainment head) which was backed by an Edwards Two Stage Rotary Pump (Type ED 35). The rotary pump was separated from the diffusion pump by a liquid nitrogen cooled trap, and similarly the diffusion pump was separated from the system by a trap. This combination of traps and pumps enabled the following vacua and leak rates to be attained:-

	Vacuum	Leak Rate
Glass Tube	106 mNm^{-2}	0.74 $mNm^{-2}s^{-1}$
Glass-Metal Tube	133 mNm^{-2}	1.11 $mNm^{-2}s^{-1}$

Test gases were stored in 5 l. and 20 l. bulbs, point A in the diagram. The gases were distilled by trap to trap distillation, along the distillation train, point B. It turned out, that the bulbs were lightly used, since high purity gases were required. These are described later. The pressure of test gases was measured on Edwards Barometrically Independent Capsule Dial Gauges, at point C, calibrated in the ranges 0 - 2.66 kNm^{-2}, 0 - 5.32 kNm^{-2}, 0 - 101 kNm^{-2}. The vacuum was measured by an Edwards Pirani Gauge Head, mounted in a B14 glass joint, and the vacuum was read from an Edwards Control Unit.

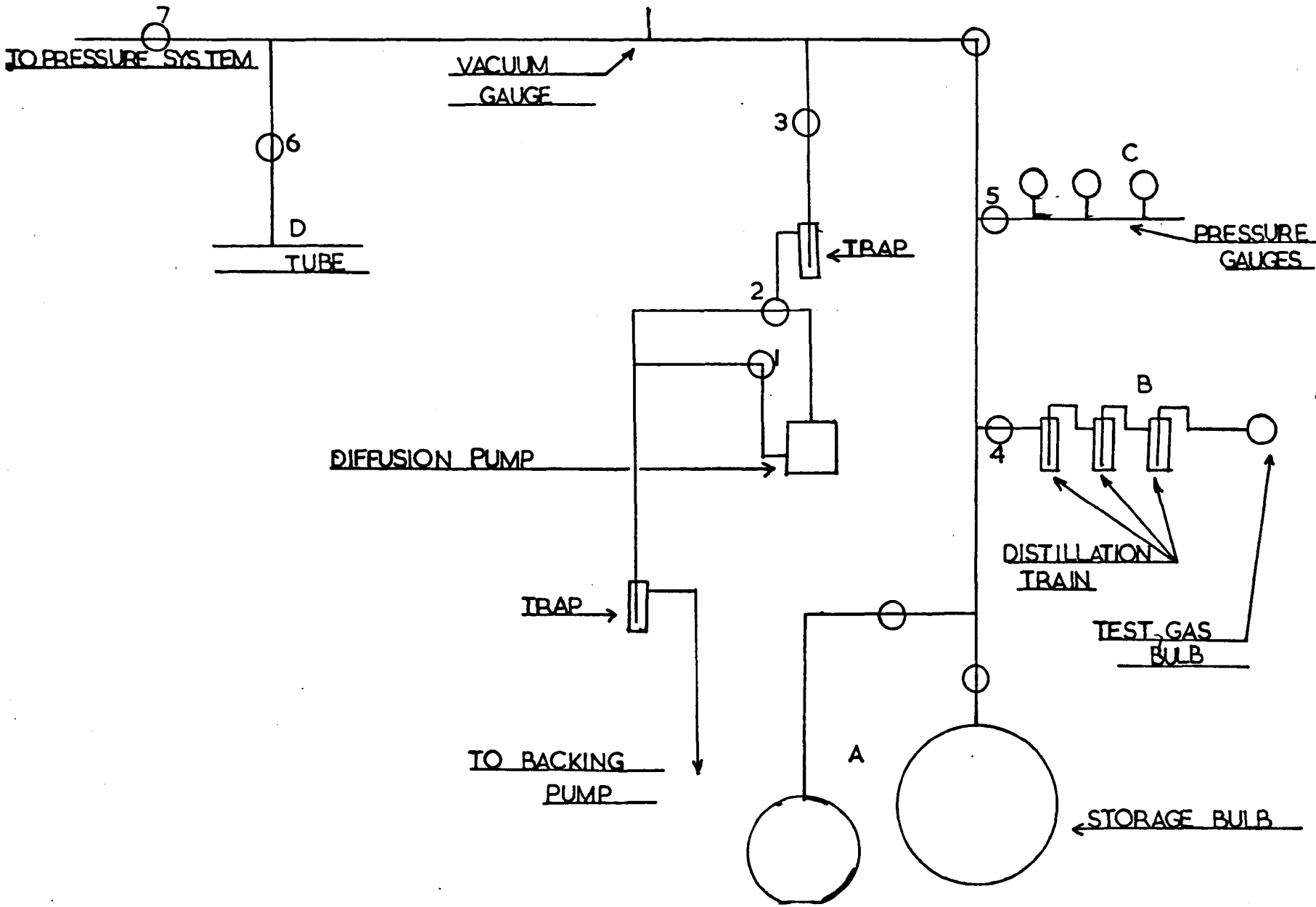

Figure 2.3 Vacuum System

Figure 2.4
High Pressure System

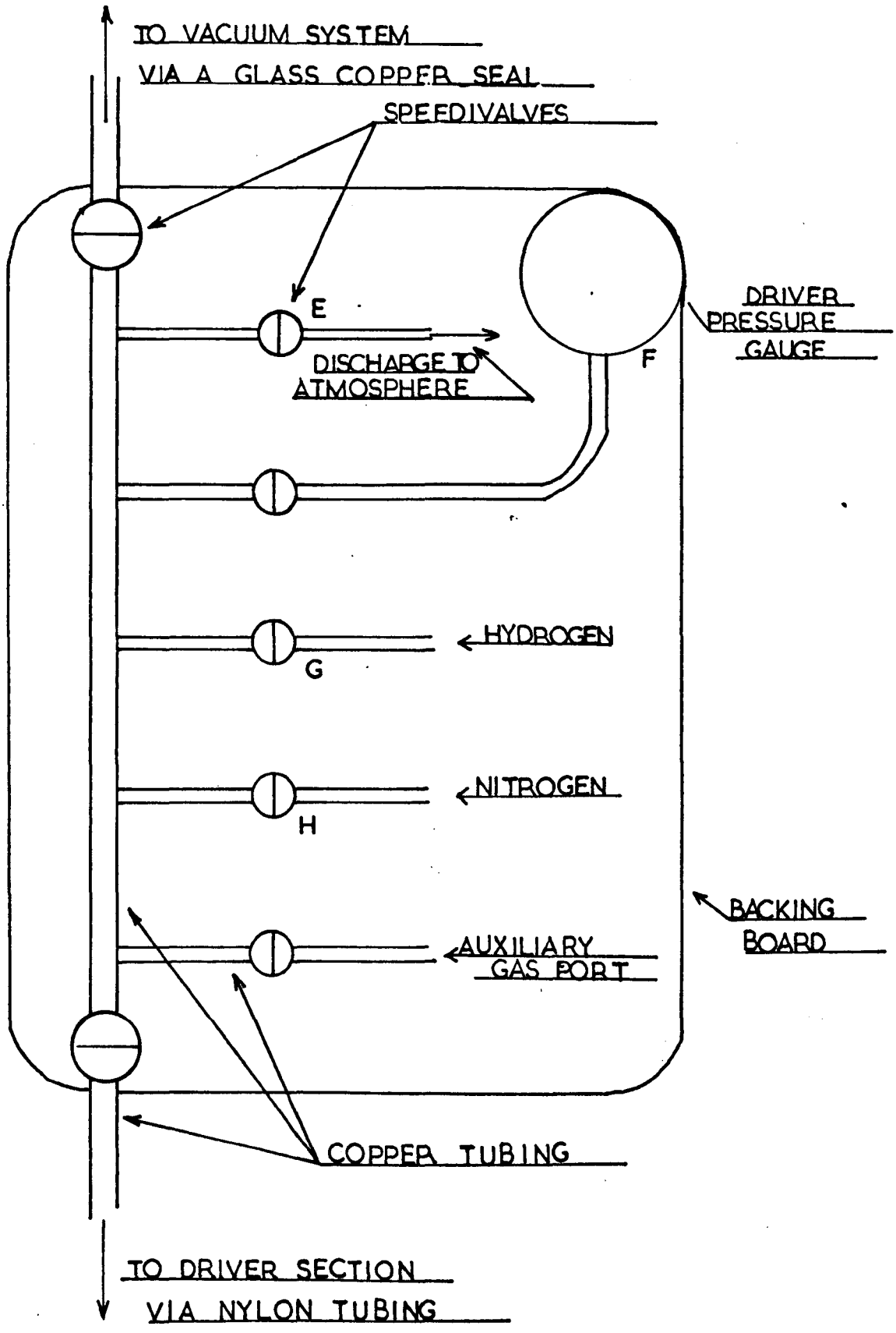

The entry to the tube was at point D.

The high pressure system is represented in Figure 2.4. All the taps on this system were Saunders-Edwards Speedivalves, which would stand the high pressures used in this section of the instrument. Discharge of any unwanted high pressure in the tube was via the tap at point E. The Bourdon gauge, at point F, was obtained from Budenburg Company Limited, had a range of 0 - 1.38 MNm^{-2}. The device also had an auxiliary pointer which enabled the driver pressure to be read accurately, after the shock. At point G, the driver gas hydrogen was taken from a cylinder. Nitrogen could be used as a driver gas, taken via point H.

2.4 DIAPHRAGMS

In this study the diaphragms were allowed to burst naturally, by gradually increasing the driver pressure. The choice of diaphragm material was reduced to Aluminium foil, supplied by G.W. Aluminium Company Limited, and Melinex Polyester Film made by I.C.I. Tests were carried out on both types of material using carbon monoxide as the test gas. The aluminium foil, 0.01 cm thick, burst on average at about 380 kNm^{-2}. In the first instance, the petals formed on bursting were torn off by the sharp edge of the connecting section. Thus the connecting section was tailored to give an edge over which the petals could fold. In this condition, most of the subsequent runs showed that the diaphragm petalled from the centre, into four pieces, without fragmentation. For those experiments in which fragmentation did occur, there was no apparent tube damage and the fragments were removed after each experiment. In general 150 gauge Melinex (0.0038 cm thickness) burst at 620 kNm^{-2}. It was found, on inspection after an experiment, that this material split rather than folded or petalled back, to allow the greatest area through which the driver gas could flow. It has been suggested[2] that this type of diaphragm was unsatisfactory for spectroscopic work, since the material shredded and burned to give an undesirable impurity spectrum. It was thus decided to use aluminium diaphragms.

The diaphragm was clamped between staggered 'O' rings on

the driver and connecting section. This gave good vacua in both sections. It was found that excessive tightening distorted the flanges, and that finger tightness, on the clamping screws was sufficient.

2.5 LIGHT SCREENS

Initially the velocity of the shock wave was measured by two sets of light screens, after the method of Bleakney[5] and his co-workers.[6] The arrangement is shown in Figure 2.5.a. In practice the light screens were independent of the frame. Their operation depended upon total reflection from the back of the shock wave of the incident light. The light source S, a 12 volt Tungsten projection lamp, was used in conjunction with a system of three knife edges k_1, k_2, k_3. The knife edges were arranged so that they lay in a line perpendicular to the axis of the flow. Then only rays lying in the plane so defined reach the photomultiplier P. The photomultiplier was an E.M.I. type 9660B, of a 9-stage "squirrel-cage" design, with a quartz envelope. The caesium antimony cathode had a maximum spectral response between $33 \times 10^3 cm^{-1}$ and $25 \times 10^3 cm^{-1}$ and a long wavelength cut-off at about $14 \times 10^3 cm^{-1}$. The rate of change of light flux on P was approximately proportional to the shock speed and the signal voltage rose rapidly with time. The output signal was fed to the circuit shown in Figure 2.5.b. The value of the load resistor, L, was large so that the output signal was large. The twin emitter follower, type TS 17, supplied by Venner Electronics Limited, was used as an impedance transformer. The emitter follower transmitted the signal from the high impedance source, to a low impedance at the output, in the co-axial cable of impedance about 50Ω. This combination

Figure. 2.5.a
Reflection Light Screen

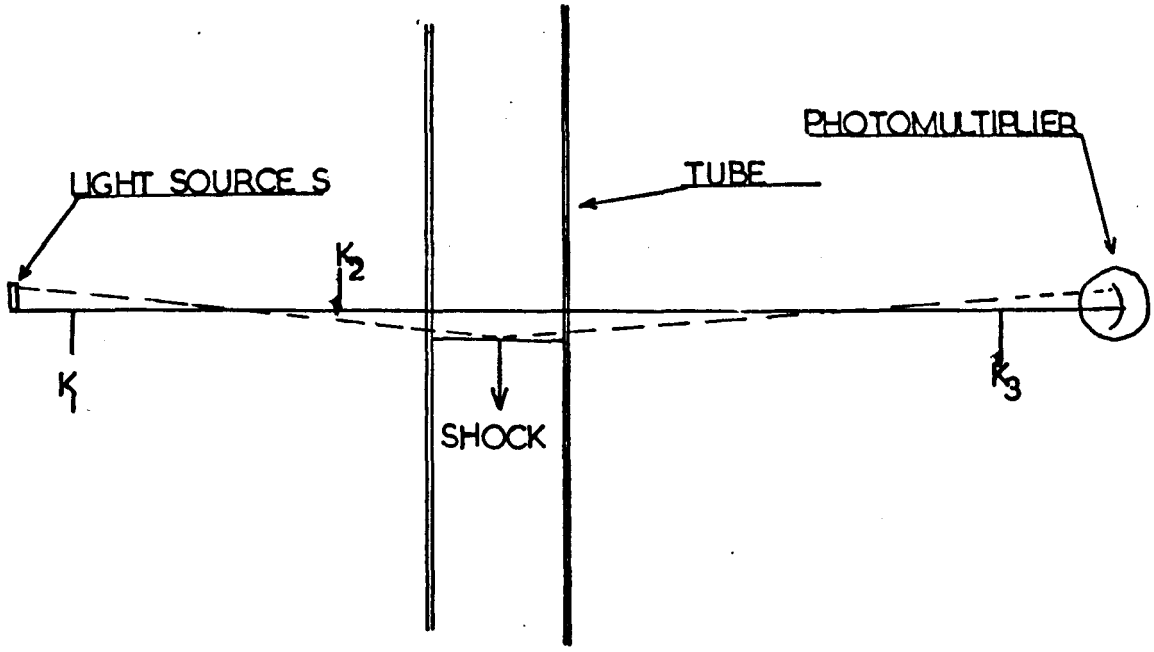

Figure 2.5.b
Photomultiplier Circuit

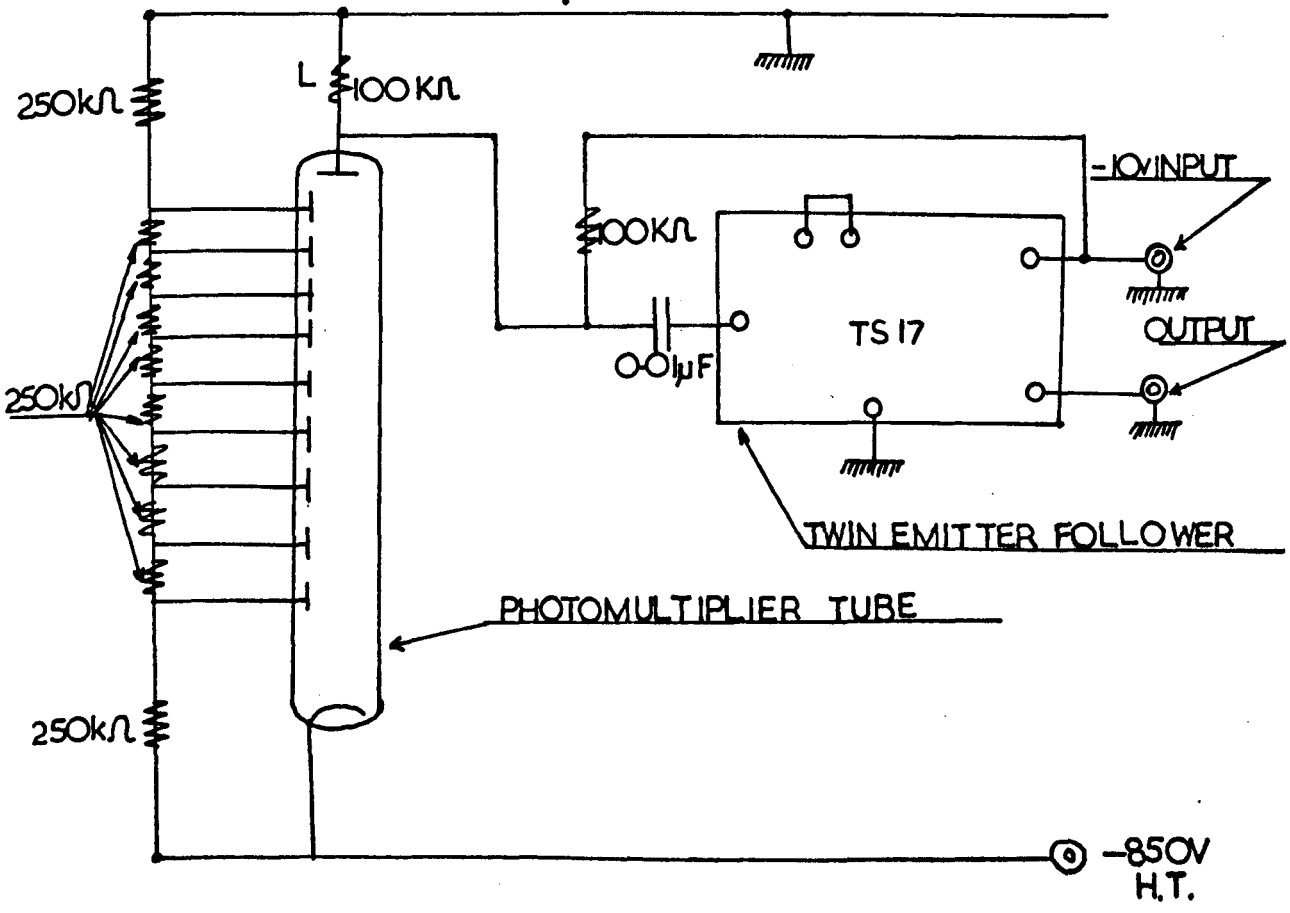

of optics and electronics afforded a pulse rise time of the order of 1 μs.

The sensitivity of the method depended on the signal to noise ratio from the photomultiplier. The most important factor in noise generation was the amount of stray light. Attempts were made to reduce the stray light to a minimum by covering the screens with black cloths.

In a series of test runs, using hydrogen as driver and nitrogen as test gas, the pulse depth was seen to fall off with increase in Mach number. The limit of operation was at a test gas pressure of 0.9 kNm^{-2}. This may be explained by considering the following equation, which was derived and used by Hornig and his associates in work on rotational relaxation.[7,8]

$$R = \frac{(1 + \tan^4\theta)}{4\rho_o^2} \quad (n_o - 1)^2 \quad (\Delta\rho)^2$$

where R = optical reflectivity = $\frac{\text{Intensity of reflected light}}{\text{Intensity of incident light}}$

θ = angle of incidence always large, that is grazing incidence $\approx 90^o$

n_o = refractive index of the gas at S.T.P.

ρ_o = density of the gas at S.T.P.

$\Delta\rho$ = total density change across the shock front

All other things being equal, the quantity $\Delta\rho$ was the factor which most influenced R. Since:-

$$\Delta\rho = (\rho_A - \rho_1)$$

$$\Delta\rho = (\frac{\rho_A}{\rho_1} - 1)\rho_1$$

where ρ_A = density at the shock front

ρ_1 = density of the downstream gas

Although at higher Mach numbers the ratio ρ_A/ρ_1 increased the value of ρ_1, which is pressure dependent, decreased due to a lower downstream pressure. Thus at higher Mach numbers the light screens ceased to function.

In 1965, J.H. Kiefer and R.W. Lutz,[9] developed a quantitative laser schlieren technique to measure the vibrational relaxation of deuterium. The method used photomultiplier detection of the deflection of a narrow laser beam, the technique being sensitive to rapid gas density changes. It was decided to adopt several features of this technique to improve the performance of the light screens. The system decided upon is shown in Figure 2.6. At position A was the laser, a helium-neon type, supplied by Ferranti Limited, which emitted a coherent beam of light at $15.81 \times 10^3 cm^{-1}$ (632.8 nm). At position B was a beam splitter of 50% transmittance and 50% reflectance. The other mirrors M_1, M_2 and M_3 are of the front surfaced type. k_1 and

Figure 2.6
Laser Light Screens

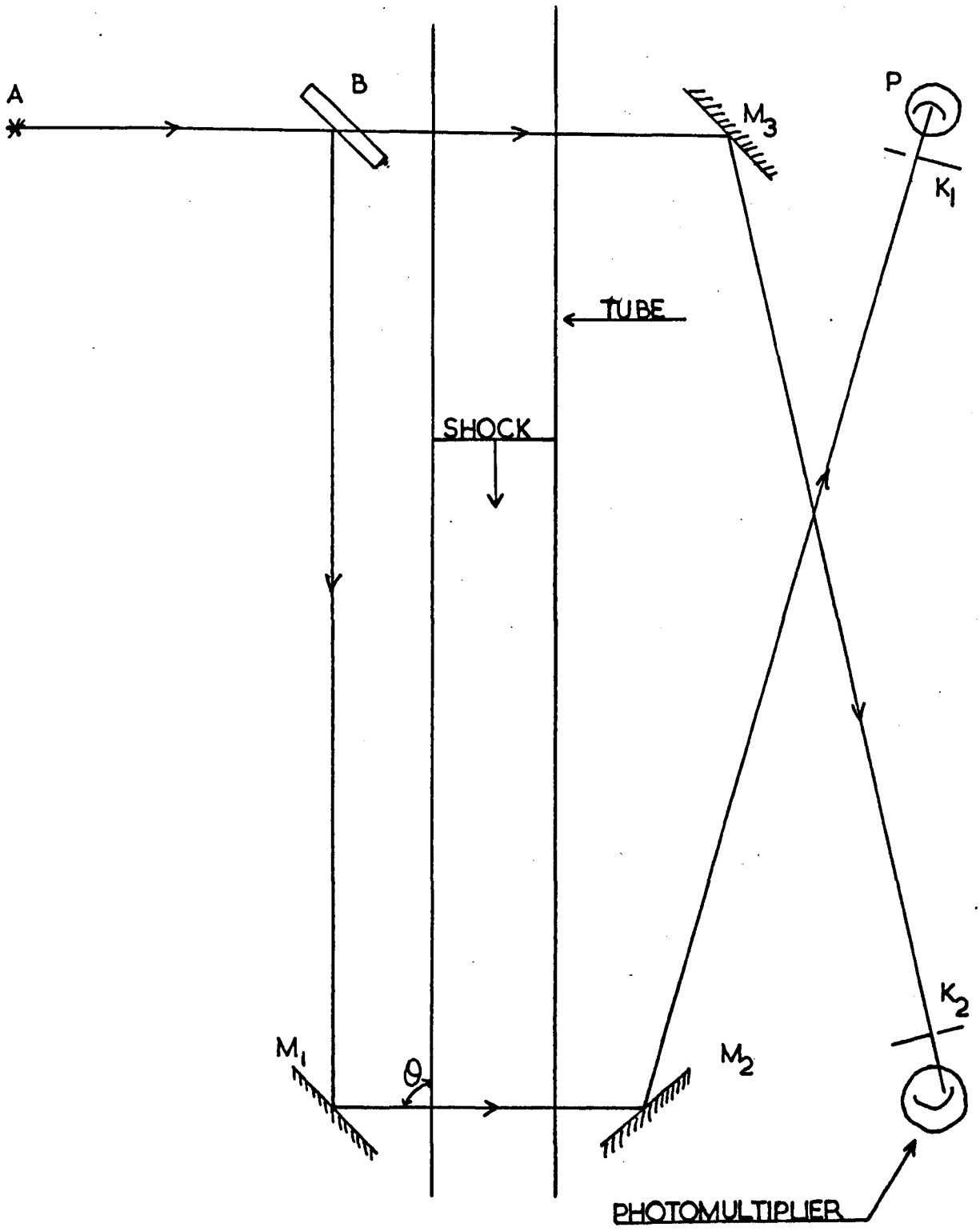

k_2 were knife edges onto which the laser light was focussed. The distance between the mirror M_2 and the photomultiplier was 1 m. This length of optical lever was found to be satisfactory. The incident light beam crossed the tube almost normally to the direction of flow, θ being 89.5°. It was assumed that the beam was not only reflected from the rear of the shock wave, but also it was refracted towards the higher density region. Test runs were carried out, using hydrogen as a driver gas and nitrogen as a test gas. Pulses of about 1 μs rise time were produced. Also pulse depths were increased by about 30% over those obtained using corresponding conditions in the original technique. The system also operated to a minimum test gas pressure of 0.2 kNm^{-2}.

Two problems emerged with the use of the laser system. Firstly, not having the beam exactly normal to the tube resulted in secondary reflections from the walls of the tube, and secondly the spacial resolution of the beam was lost due to the curvature of the tube walls. The loss of spacial resolution was more acute in the case of the windows on the metal tube. To compensate for the divergent effect of the windows, barrel shaped lenses of focal length 7.5 cm were used. Plate 2.1 shows the arrangement. To prevent any spurious reflections interfering with the incident beam, slits of adhesive tape were placed on the tube.

Finally, in recent years advances in solid state electronics

PLATE 2.1

have led to the production of photodiodes, which while retaining the essential characteristics, have a number of advantages over the photomultiplier tube. A P.I.N. photodiode was obtained from Plessey Microelectronics. At the present time a circuit which combined fast response with high gain had not been achieved. But, clearly, this is a field in which some further work is required.

2.6 INFRARED DETECTOR

2.6.a DETECTOR AND CIRCUIT

The detector was a Mullard RPY 36 Indium-Antimonide photoconductive cell. The photoconductive element, with a time constant of <2.0 μs, was mounted in a glass dewar vessel and was cooled by liquid nitrogen. It had a sapphire window which transmitted to about 1800 cm^{-1}. The element was mounted in the horizontal position with its longest edge parallel to the axis of the incident radiation. A surface aluminised mirror at 45°, reflected the incident radiation onto the element. During operating conditions, see Plate 2.1, a stream of dry air was played on the window to prevent condensation. Precautions were taken to exclude ambient radiation from the detector area, since visible radiation damaged the element. The electrical circuit of the detector is shown in Figure 2.7. The resistor-voltage combination was chosen to give a bias current of about 1.2 mA, which registered on ammeter A. The two outputs from the detector were fed to the positive and negative inputs of a differential amplifier. This was done, in part, to smooth the noise generated in each resistor R_1 and R_2. The variable resistance V.R. was used to prevent current surge in the detector and ammeter when the device was switched on. The resistor, V.R., was wound from 250 kΩ to zero, and the current rose from about zero to the bias value. The leads on the circuit were made as short as possible,

Figure 2.7
Detector Circuit

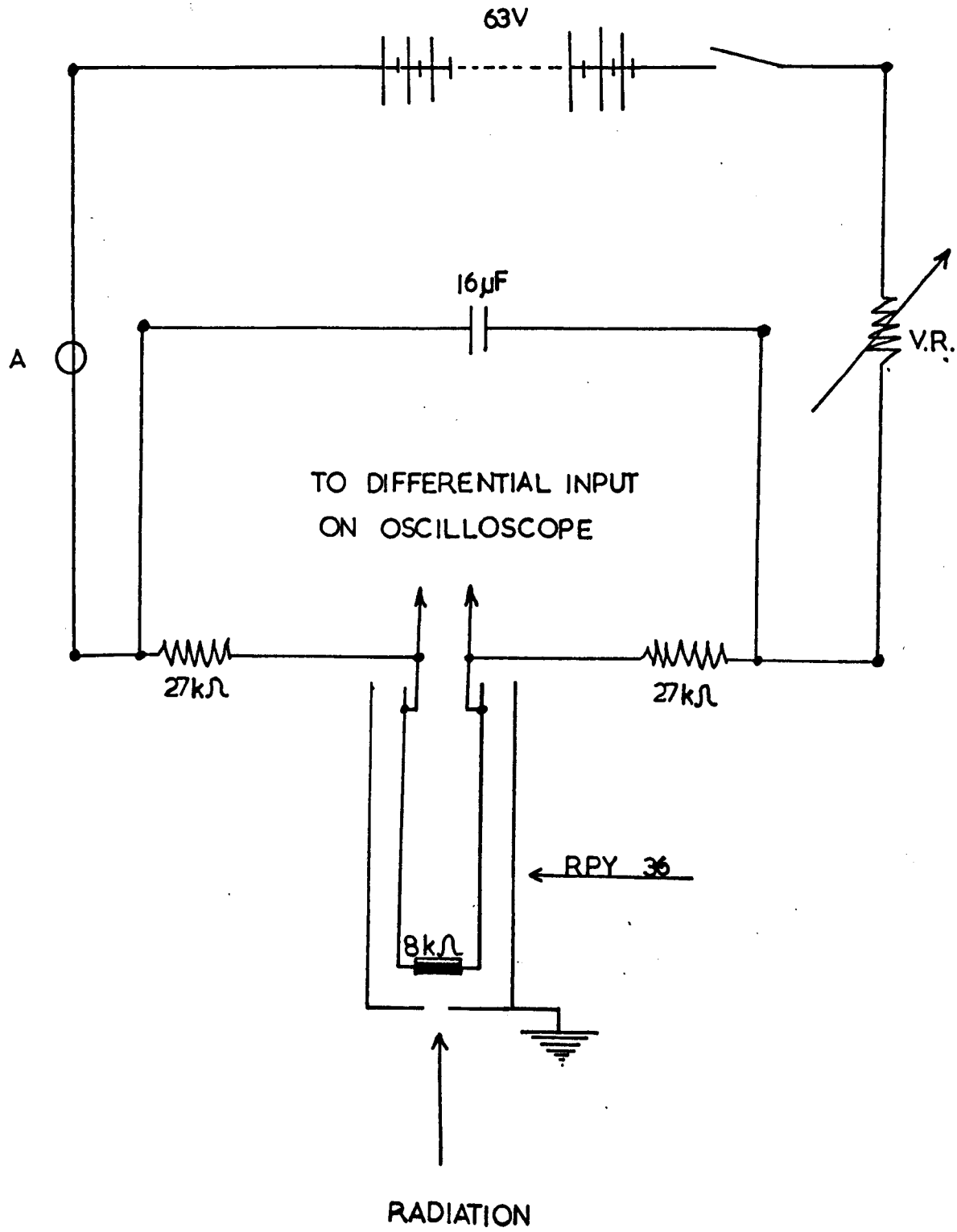

but capacitor, C, was included in the circuit to smooth any stray capacitance. A range of bias currents were tried from zero mA to 1.6 mA and it was found that the noise was minimal at 1.1 mA. The recommended value was 1.1 mA.

2.6.b OPTICAL ARRANGEMENT

The detector and its optical arrangement are shown in Figure 2.8. The optics were set up on a bench separated from the frame holding the shock tube. The slits were of 1 mm width. The filters, of the interference type, were supplied by S.T.C. Limited, and were cut-on or cut-off type. They were used to isolate the region of the fundamental of carbon monoxide. The pyrex glass tube, which had a zero transmittance at 2143 cm^{-1}, was used for the measurements on the overtone of carbon monoxide.

The detector was aligned, without the filter in position, by placing a lamp and slit on the opposite side of the tube. The detector element was then aligned by eye so that the pencil of light produced by the slits, illuminated the detector uniformly. The detector could not be aligned electronically, in the biased condition, since there was a risk of damaging the element.

Taking the limiting rays in the diagrams the optical rise time was calculated to be 2 μs for a shock travelling at about 1.5 mm/μs.

Figure 2.8

The Optical System - Not To Scale.

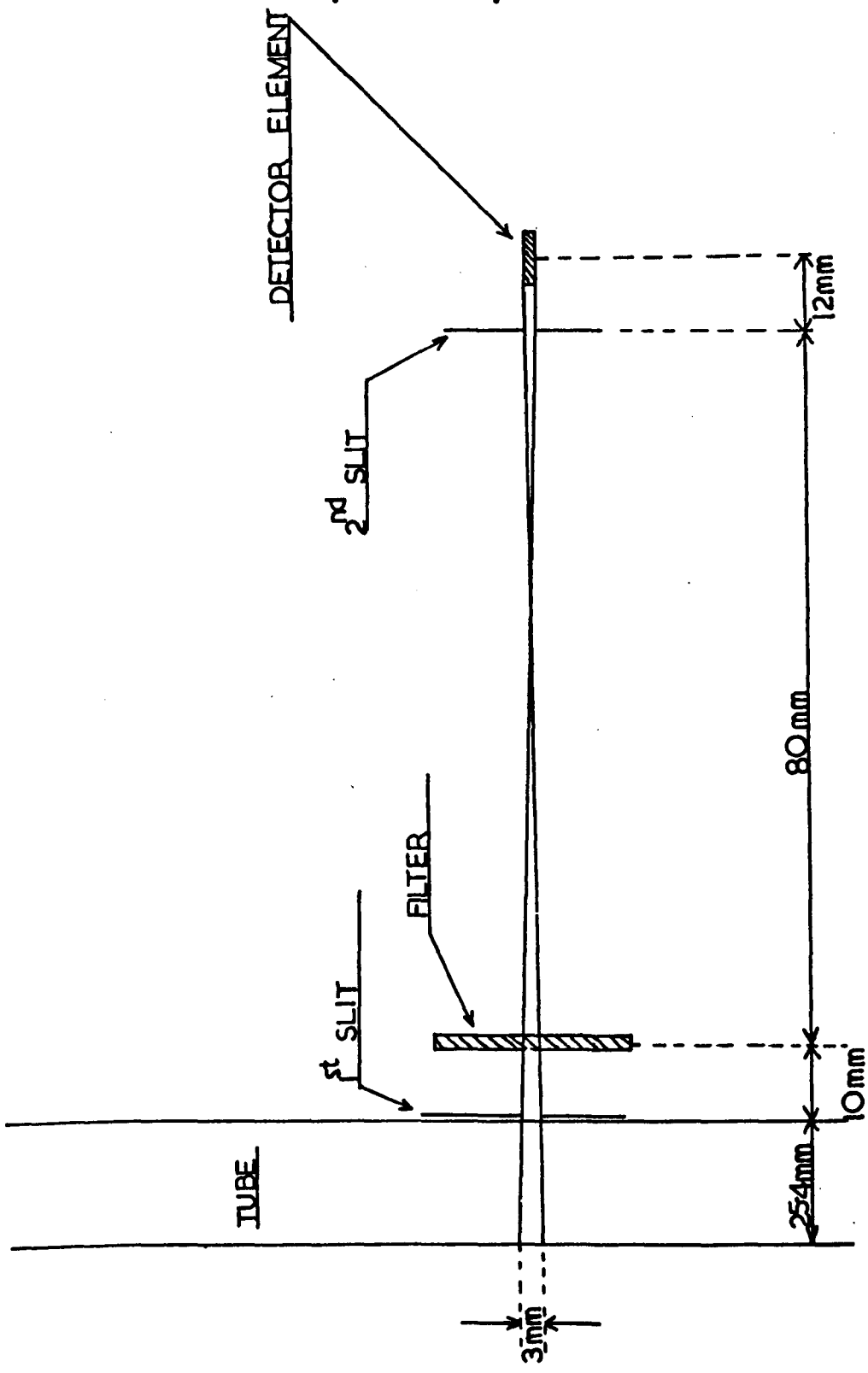

2.7 ELECTRONICS ARRANGEMENT

The electrical arrangement is shown in Figure 2.9. The outputs from the light screens were used to trigger a Venner microsecond time interval meter, type TSA 5536, and measure the time for the shock to traverse the two screens. The minimum pulse peak to peak amplitude required to trigger the timer was 1 V. The trigger levels were adjustable, on both inputs, between 3 V and -3 V. The pulses were also displayed on a Hewlett-Packard 141A storage oscilloscope with a type 1421A Dual Trace Amplifier. This provided a check on the pulses entering the time interval meter. The output from the first light screen was also used to trigger the delay on the Hewlett-Packard 140A oscilloscope, so that the main sweep was triggered as the shock wave approached the central detection station. The output from the detector was fed via a 2 m length of double-shielded two conductor cable to a 1403A Differential Amplifier, which was plugged into the 140A oscilloscope. The amplifier had thirteen calibrated ranges from 100 mV/cm to 0.01 mV/cm. The bandwidth was 0.1 Hz to 400 kHz (0.9 μs rise time) and the upper and lower limits of the bandwidth were independently selected. The bandwidth used was, upper limit >400 kHz, lower limit 100 Hz. This excluded interference from mains frequency. It was assumed that there was no distortion of the incoming pulse (frequency ≈ 1.6 kHz) due to the cut-off of the lower frequency components. The output from the

Figure 2.9
Electronics Arrangement

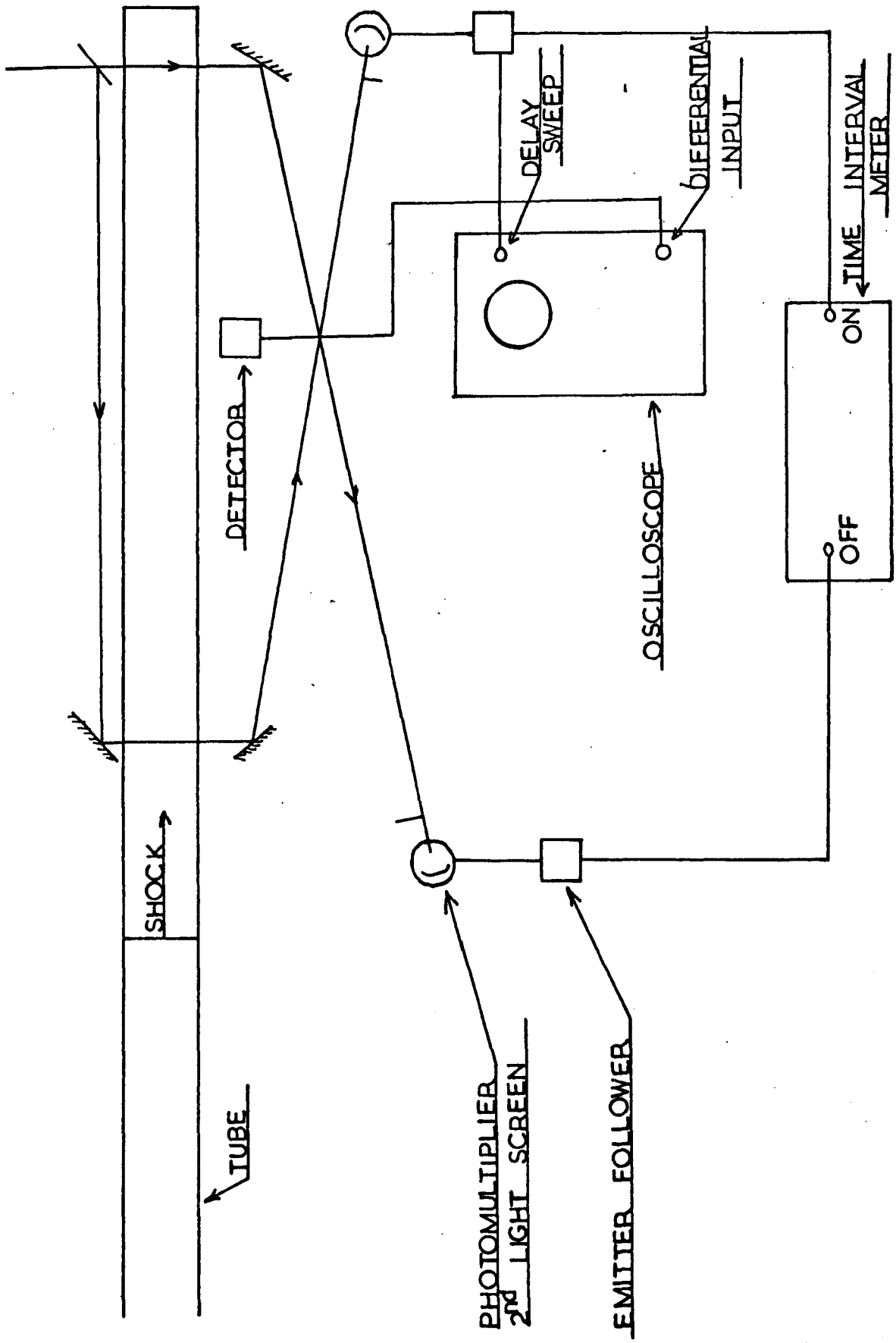

detector was displayed on the oscilloscope and the transient was photographed using a Hewlett-Packard 196B, 1:1 ratio polaroid camera. The photographs were taken using 3000 ASA polaroid film. A u.v. light incorporated in the camera provided illumination of the graticules, which were exposed separately.

From time to time performance checks were carried out on the oscilloscopes, camera and time interval meter.

The high tension for the photomultipliers was supplied from a power supply, type Pm 2500/R, obtained from Brandenburg Limited. This supplied an operating voltage of 850 V to the photomultipliers. The 10 V power supply required for the twin emitter follower was supplied from a Venner transistorized power supply, type TS 20/C.

2.8 MATERIALS

In past work[3,10] it was realised that impurities reduced the relaxation time of diatomic molecules. This was particularly so for polyatomic molecules with additional vibrational modes, and also for light molecules such as hydrogen. B.O.C. Limited Grade X gases were obtained, the gases being processed to the maximum feasible purity, under strict quality controlled conditions. The pure gases and gas mixtures were obtained in 1 l. pyrex flasks filled to 101.3 kNm^{-2}. The glass flasks had a 13.5 mm bore stem and the gas was contained by a 'swan-neck break seal'. The flasks were glass blown onto the system, and the seal could be broken by releasing a plunger. The following analyses on the test gases obtained from B.O.C.:-

(i) Carbon Monoxide:-

N_2	<0.04%
O_2	<0.001%
CO_2	0.0016%
H_2	<0.0025%
Hydrocarbons	0.0013%

(ii) Neon:-

He	<0.05%
N_2	<0.0001%
O_2	<0.0001%
CO_2	<0.00005%
H_2	<0.00005%

(iii) Carbon Dioxide:-

N_2, O_2, CO, H_2 all <0.0005%

(iv) Nitrous Oxide:-

N_2, O_2, H_2 all <0.0005%

Mixtures of gases were made up in the pyrex flasks, and were filled to ±0.1% tolerance.

Carbonyl sulphide could not be obtained in Grade X quality, but a cylinder of 97.5% purity was obtained. The gas was purified and the mixtures were made up using the apparatus shown in Plate 2.2. This apparatus was connected to the vacuum system via a Q.V.F. P.T.F.E. bellows, and the pressure was reduced to 133 mNm^{-2}. The carbonyl sulphide was then purified by a freeze-pump-thaw cycle, and a measured amount allowed to expand into the 2 l. storage bulb. Then a measured amount of Grade X carbon monoxide was admitted to the bulb. The pressures were read on a mercury manometer. The flask was sealed off, and the mixture allowed to stand overnight so that diffusion could take place. The flask was then removed and glass blown onto the system.

The driver gases were obtained from commercial cylinders. In the case of hydrogen the purity was 99.9%, and the nitrogen was 99.5%. Before entering the driver system the gases were passed through a B.O.C. line filter, which removed particles greater than 0.025 mm.

PLATE 2.2

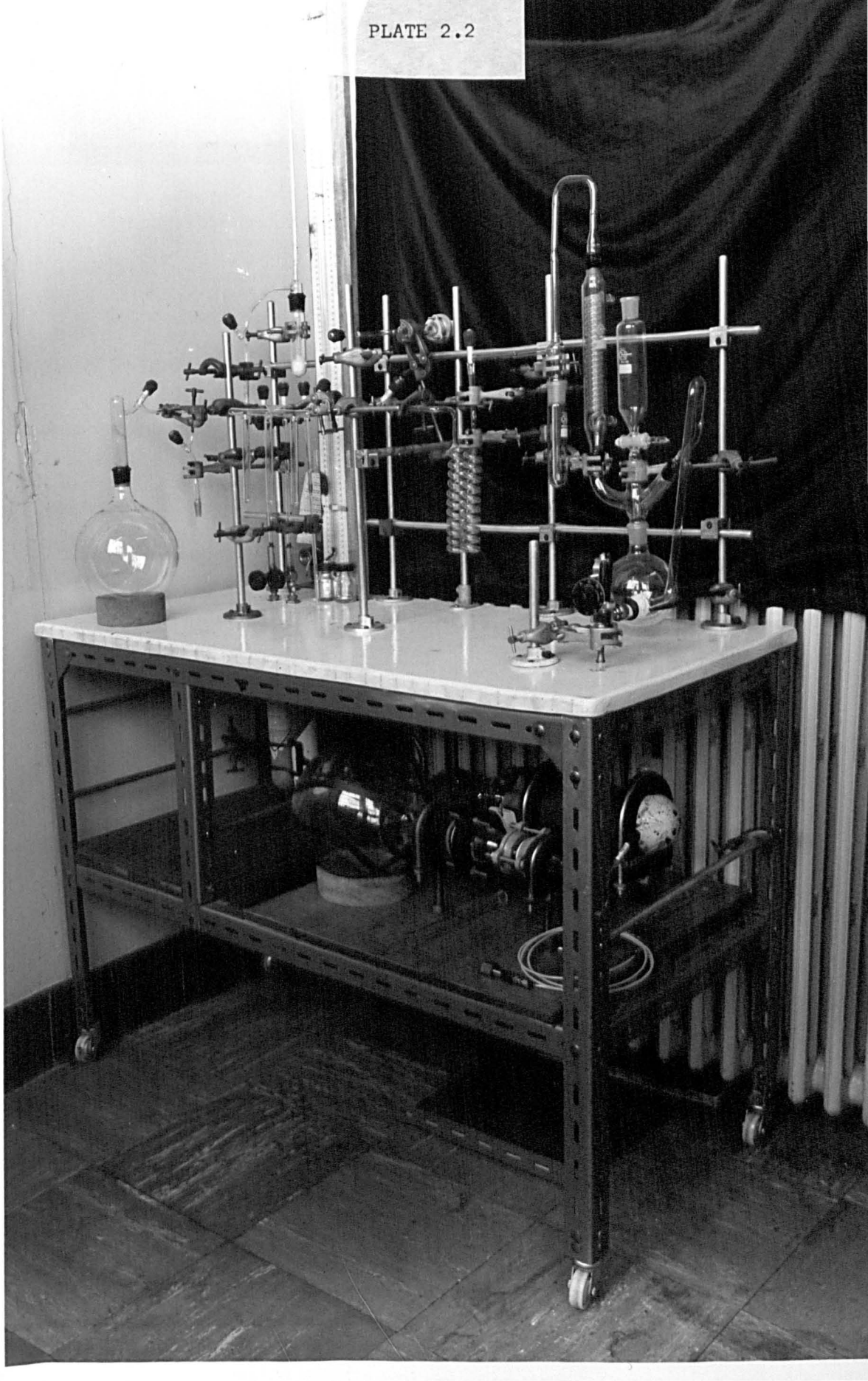

2.9 EXPERIMENTAL PROCEDURES

During this section reference is made to Figure 2.3 and Figure 2.4.

The operational procedure for a shock experiment is enumerated below:-

(i) The flask of test gas was glass blown onto the end of the distillation train at B. That part of the system was always well evacuated before the test gas was released.

(ii) The shock tube and pressure gauge section, C, were evacuated by opening taps 5 and 6. It was found that a pumping time of not less than 75 minutes was required in order to obtain the vacua and leak rates mentioned in Section 2.3.

(iii) After thorough evacuation tap 3 was closed and the test gas was admitted to the tube, the pressure being measured on the gauges at C.

(iv) Taps, 4, 5, 6 were closed and the taps 1 and 2 were adjusted to cut off the diffusion pump.

(v) Taps 7 and 3 were opened and the driver section was evacuated completely by the backing pump.

(vi) While (v) was being done, the detector was filled with liquid nitrogen and the graticules of the recording scope were exposed and photographed.

(vii) The taps 7 and 3 were closed and tap 1 opened.

(viii) The laser was switched on, the electronics set ready and the camera shutter opened.

(ix) The shock was initiated by increasing the driver pressure. The camera shutter was closed, the laser and detector were switched off. The time taken, from the injection of the test gas to the shock going off, was typically 4 minutes, but at no time was it greater than 8 minutes.

(x) The excess pressure in the tube was released and residual gases pumped away. The tube was then raised to atmospheric pressure with nitrogen.

(xi) The diaphragm and end plate were removed, and the tube was cleaned by pulling a rag, soaked in diethyl ether, through the tube. This removed fragments of diaphragm material.

(xii) A new diaphragm was clamped in position, and the end plate replaced.

(xiii) The driver section was roughly pumped out, with the backing pump only.

(xiv) The test section was then roughly pumped and the diffusion pump was turned into the system, to reduce the pressure further.

(xv) The photograph was removed from the camera, developed and fixed.

In a typical experiment, the test gas pressures were typically between 5.32 kNm^{-2} - 0.53 kNm^{-2}, and the driver pressure was about 380 kNm^{-2}.

Finally it is important to stress three major difficulties encountered while attempting to obtain a clean uniform flow.

(i) In the present study, it was found that the diaphragm station was one of the most sensitive parts of the tube. It was pointed out in Section 2.4 that the diaphragm be made to burst evenly with little fragmentation, and with no tearing. This was partly achieved by bevelling the leading edge on which the diaphragm burst. Also it was found that a finger tightness was all that was required on the diaphragm clamp, since it was thought that overtightening may have affected the opening time and the bursting characteristics.[11,12]

(ii) It was made sure that the tubes were aligned as closely as possible at the joints. Efforts were made to ensure that the windows and their holders fitted exactly as possible to the contour of the tube. This was done by honing them 'in situ'. At the ends of the pyrex tubing there was a slight increase in test section area, 0.35 cm^2, which facilitated the clamping of the backing flanges. Thus to avoid any 'steps' in the tube, the metal sections, in glass-metal joints, were machined to meet this requirement.

(iii) Before any of the Q.V.F. pipeline was used, it was cleaned with chromic acid, washed thoroughly with distilled water and dried. The metal sections were cleaned with organic solvents. The new tubes were always pumped thoroughly, approximately three days before being used. During operation, the cleanliness of the tube was maintained by pulling a rag moistened with an organic solvent

through the tube. This removed not only fragments of diaphragm, but also contaminants which came from the driver gas cylinder. Test runs were carried out using nitrogen as a test gas. The emission from the tube was studied using the RPY 36 detector. For the runs in which no cleaning took place, a steady increase in spurious emission was observed. In the cases where the tube was cleaned, and for short pumping times 30 minutes, a large emission was observed. This was ascribed to emission from the cleaning fluid, which was absorbed on the wall and windows of the tube. A longer pumping time reduced the emission to a level which was considered insignificant. The long pumping times necessitated that the backing pump and diffusion pump were maintained frequently.

REFERENCES

1. R.A. Strehlow, *Tech. Rept. A.A.E.*, 68-1, Univ. Illinois, Urbana, 1968.

2. A.G. Gaydon and I.R. Hurle, *The Shock Tube in High Temperature Chemical Physics*, (Chapman and Hall Limited, London) 1963, Chapter IV.

3. W.J. Hooker and R.C. Millikan, *J. Chem. Phys.*, 1963, 38, 214.

4. J.G. Hall, *University of Toronto Aeronautics Review*, 1958, No.12, 196.

5. W. Bleakney, *High Speed Aerodynamics and Jet Propulsion*, (Oxford University Press, London) 1958, Vol. IX, 159.

6. W. Bleakney, D.K. Weimer and C.H. Fletcher, *Rev. Sci. Instrum.*, 1949, 20, 807.

7. D.F. Hornig, *High Speed Aerodynamics and Jet Propulsion*, (Oxford University Press, London) 1958, Vol. IX, 203.

8. D.F. Hornig, E.F. Greene and G.R. Cowan, *J. Chem. Phys.*, 1951, 19, 427.

9. J.H. Kiefer and R.W. Lutz, *J. Chem. Phys.*, 1966, 44, 658.

10. M. Windsor, N. Davidson and R. Taylor, *7th Symposium on Combustion*, (Butterworths, London) 1959, 80.

11. C.J.S.M. Simpson, T.R.D. Chandler and K.B. Bridgman, *Phys. Fluids*, 1967, 10, 1894.

12. D.R. White, *General Electric Research Laboratory Report*, 58-RL-1999, 1958.

3. CALIBRATIONS AND RADIATION CHARACTERISTICS

This chapter contains two sections. Firstly, a discussion of calibration experiments, with a particular emphasis on the estimation of the performance of the shock tube. The second section will contain some important features of the observed radiation.

3.1 CALIBRATION MEASUREMENTS

3.1.a SHOCK TUBE

It is now well known that non idealities in shock tube flows affect the history of a gas sample. This is reflected particularly in terms of the hot flow time, which is always less than that predicted by ideal shock tube theory. In the ideal case, the shock wave and contact surface move with different, but constant velocities. Since the shock wave moves faster than the contact surface, the hot flow time increases as the shock progresses down the tube. In an actual shock tube flow the presence of a boundary layer causes the shock wave to decelerate and the contact surface to accelerate, thus reducing the hot flow time. The situation in the present case is shown in Figure 3.1. It is seen that the hot flow time is reduced by about one half to one third of the theoretical value, over a range of Mach

Figure 3.1

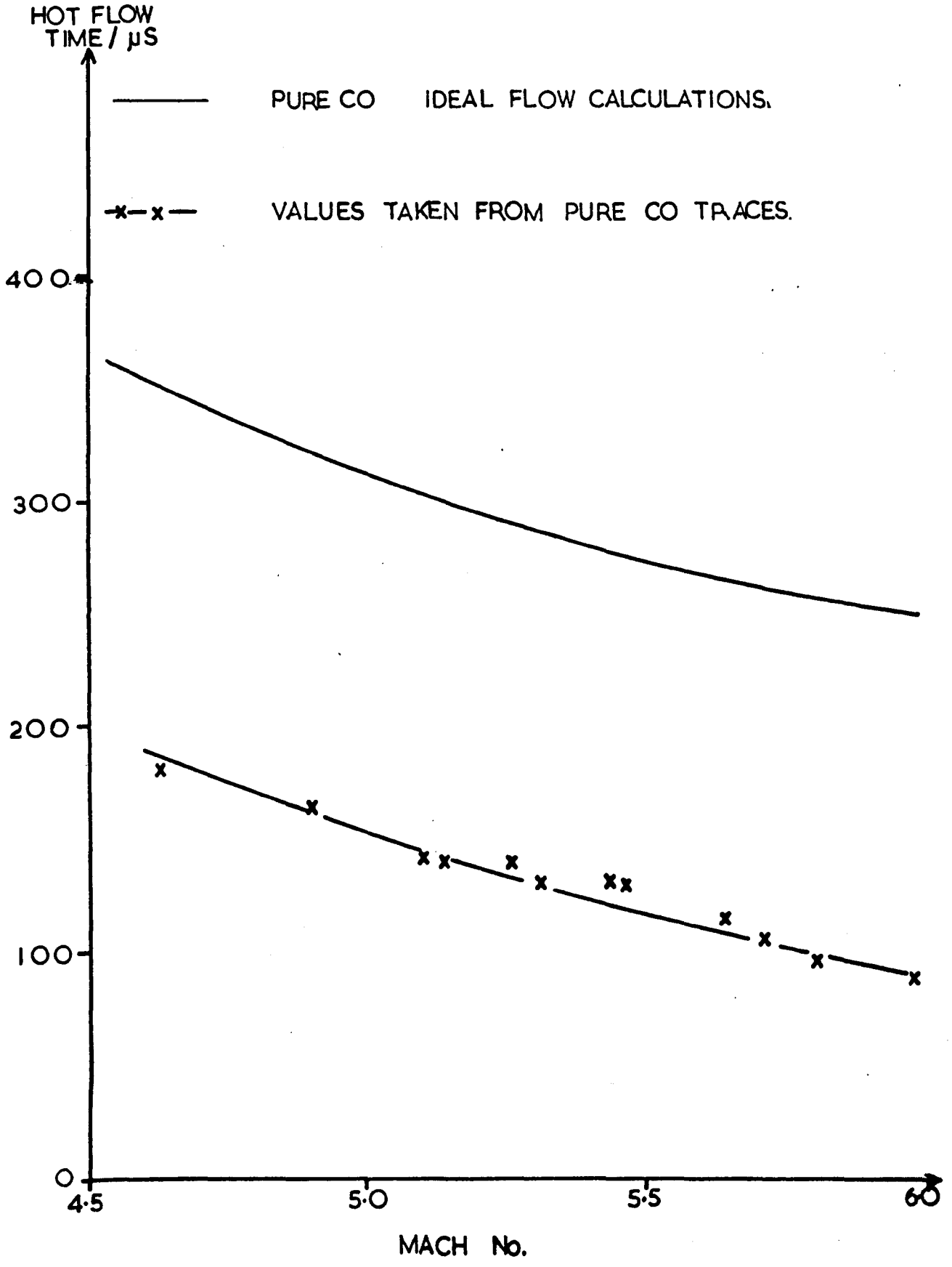
HOT FLOW TIME / μS
PURE CO IDEAL FLOW CALCULATIONS.
VALUES TAKEN FROM PURE CO TRACES.
400
300
200
100
0
4·5
5·0
5·5
6·0
MACH No.

numbers. This magnitude of hot flow time reduction has been observed generally. The flow conditions are shown on the (x, t) diagram, Figure 3.2.a, and Figure 3.2.b indicates the growth of the boundary layer in the shock tube. The presence of the boundary layer is due to the loss of heat to the walls by conduction and the loss of momentum by friction with the walls. Early measurements[1] with a small diameter shock tube showed that non idealities could be acribed to the formation of a laminar boundary layer. Also, as the length-to-diameter ratio of the tube was increased and the initial downstream pressure was reduced, the boundary layer effects increased. The situation is further complicated by the fact that the shock wave may be decelerating over the period of measurement. These effects serve to influence the temperature and density of the hot flow.

In recent years the effects of flow non idealities on shock parameters have been treated theoretically by Mirels.[2,3,4] Strehlow and Belford[5,6] have arranged the equations into explicit form, which is of particular interest to kineticists. Since previous workers have calibrated their shock tube,[7,8] the present study will also take account of the non idealities and the effect on shock parameters. The method used is given below.

The first stage of the calculations is to find the real particle testing time, t_p, from the observed hot flow time. The maximum hot flow time, t_m, at an observation station is given by:-

Figure 3.2

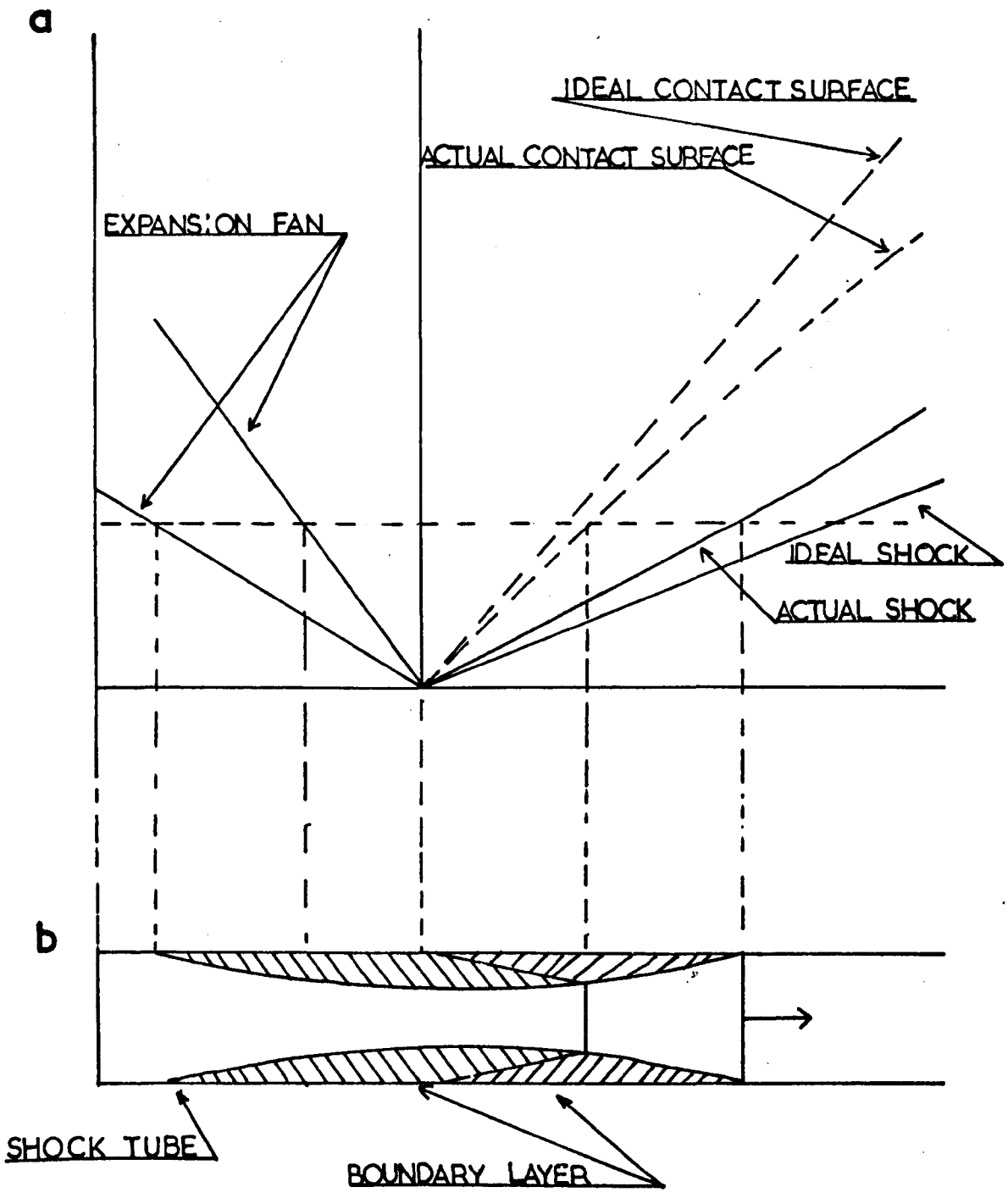
a
IDEAL CONTACT SURFACE
ACTUAL CONTACT SURFACE
EXPANSION FAN
IDEAL SHOCK
ACTUAL SHOCK
b
SHOCK TUBE
BOUNDARY LAYER
\\\\ — DRIVER GAS IN BOUNDARY LAYER
//// — TEST GAS IN BOUNDARY LAYER

$$t_m = \frac{5.85\ d^2\ P_1}{M_s^{1.7}\ a_1} \quad cm^{-1}\ torr^{-1} \qquad 3.1$$

where d = hydraulic diameter

$= \frac{4A}{L}$

A = cross sectional rea of tube in cm^2

L = perimeter of the tube, cm

P_1 = initial pressure, torr

M_s = shock Mach number

a_1 = velocity of sound in gas cm s^{-1}

The equation 3.1 was obtained by fitting Mirels theoretical curve (Figure 6, reference 2) of $t_m/d^2\ P_1$ versus Mach number for a number of gases. The equation 3.1 fits the results of Mirels, over a range $2.5 < M_s < 8$, for all cases to within 3%.

The ideal particle heating time $(t_p)_i$ is related to the hot flow time t_ℓ, by the equation;

$$(t_p)_i/t_\ell = (\rho_2/\rho_1)_{av}$$

where $(\rho_2/\rho_1)_{av}$ = average shock density ratio

The real particle heating time t_p has been shown to be,[9]

$$t_p = t_\ell\left(\frac{\rho_2}{\rho_1}\right)_{av}\left[1 + 0.7\ (t_\ell/t_m)^{\frac{1}{2}}\right] \qquad 3.2$$

Equation 3.2 being valid for $t_\ell/t_m < 0.1$.

Errors in the temperature tend to move in the form of a temperature increase behind the shock, during the observation period. The rise in temperature has two causes:-

a) the deceleration of the flow because of the boundary growth behind a steady shock. The relationship has been evaluated by Mirels to be:-

$$\left(\frac{\Delta T}{T_2}\right)_b = \left(\frac{t_\ell}{t_m}\right)^{\frac{1}{2}} \left[\frac{M_{2s}^2 - 1}{(\gamma-1)\, M_{2s}^2}\right] \qquad 3.3$$

where ΔT = temperature increase K

T_2 = temperature behind the shock where the observation is made K

M_{2s} = value of Mach number behind the shock (subsonic)

b = correction to boundary layer

$$M_{2s} = \left[\frac{(\gamma-1)\, M_s^2 + 2}{2\gamma M_s^2 - (\gamma-1)}\right]^{\frac{1}{2}} \qquad 3.4$$

M_s = shock Mach number.

b) the decleration of the shock wave produces the following temperature increase:-

$$\left(\frac{\Delta T}{T_2}\right)_d = t_p \left[\frac{2(M_s^2-1)}{(1+((\gamma-1)/2)M_s^2)((2\gamma M_s^2/(\gamma-1))-1)}\right] \frac{d\ln M_s}{dt} \qquad 3.5$$

where t_p = calculated from equation 3.2

d = refers to correction due to deceleration

$$\frac{d\ln M_s}{dt} = \frac{Ya_1 M_s}{(Ya_1 t_m+1)} \qquad 3.6$$

Y = velocity decrement (% m^{-1})

The derivation of 3.6 is shown in Appendix 1. The two effects may be treated independently and added to give the total effect of boundary layer growth and deceleration on the temperature.

$$\left(\frac{\Delta T}{T_2}\right)_{TOTAL} = \left(\frac{\Delta T}{T_2}\right)_b + \left(\frac{\Delta T}{T_2}\right)_d \qquad 3.7$$

Then the correction to the density is given by:-

$$\left(\frac{\Delta \rho}{\rho_{av}}\right) = \left(\frac{\Delta T}{T_2}\right)_{TOTAL} \Big/ (\gamma-1) \qquad 3.8$$

where $\rho_{av} = \left(\frac{\rho_2}{\rho_1}\right)_{av}$

To estimate the magnitude of the corrections the following factors must be known:-

a) Diameter of the tube, a measurable quantity.

b) The initial downstream pressure P_1, a measurable quantity.

c) The hot flow time t_ℓ measured from the infrared traces of

emission versus time. Since an average value of the density ratio and the shock temperature were taken, for the analysis of the results, an average value of the hot flow time was used. Thus for the CO/Ne runs, where in most cases equilibrium was reached just before the contact surface arrived, half the hot flow time was taken. In the CO/polyatomic runs, where in some cases equilibrium was reached near the shock front, t_ℓ was taken as half the time from onset of the shock to the onset of equilibrium.

d) The shock Mach number, this is a value calculated from the equations set out in Chapter 6, section 2.

e) The ideal average shock temperature, is also calculated by the equations set out in Chapter 6, section 2.

f) The ideal average shock density ratio, see Chapter 6, section 6.

g) Velocity decrement. In the present study only two velocity measuring stations were possible, and the value of Y had to be estimated with the aid of the emission traces. It was found that for most of the runs involving the CO/Ne and CO/polyatomic systems, where the Mach number ranged from 4.0 - 6.5 that the velocity decrement was on average 2% m^{-1}. Generally for Mach numbers lower than 4 it was found that the velocity decrement was 1% m^{-1}.

As an example of the corrections involved in a typical shock tube run, consider a shock wave of $M_s = 4.3$, travelling in CO in a 2.54 cm diameter tube at an initial pressure of 1.066 kNm^{-2} and an

initial temperature of 300 K with a velocity decrement of 1% m^{-1}. For this case t_m = 0.483 ms and $d(\ln M_s)/dt$ = 19.1 s^{-1}. The observations are made at t_ℓ = 60 μs after the passage of the shock. The temperature shift becomes:-

$$\frac{\Delta T}{T_2} = 0.0285 + (0.00047)\ (19.1) = 0.037$$

In this case $(T_2)_{av}$ = 1903 K

$$\therefore \Delta T = 71.2 \text{ K}$$

and since $(\rho_2/\rho_1)_{av}$ = 5.47

$$\Delta\rho = 0.51$$

If the velocity decrement is now set at 2% m^{-1}, all other factors being the same then:-

$$\frac{\Delta T}{T_2} = 0.0285 + (0.00047)\ (38.2) = 0.046$$

$$\Delta T = 88.2 \text{ K}$$

and $\Delta\rho$ = 0.63

Thus it is shown that in the two cases above the temperature is increased by 3.7% in one case and 4.7% in the other. The density increase is 9.3% and 11.6%. Since the increases are small, even in the case of the higher shock attenuation, it was felt that they could be added to the ideal temperature $(T_2)_{av}$ and the density ratio $(\rho_2/\rho_1)_{av}$, to give the final corrected flow properties in the shock

tube. Chapter 6 deals in detail with the calculation of the shock parameters of temperature and density. The ideal values of the shock parameters are compared with the corrected ones in Figure 6.6 of Chapter 6. In the present study the corrected shock parameters were always used to calculate the Napier time. How the Napier time is affected by using corrected and uncorrected shock parameters, is shown in Chapter 7. A computer programme was written to calculate the corrected shock parameters. The programme is presented in Appendix 2.

3.1.b RISE TIME OF THE SYSTEM AND PREEMISSION

The limiting response time of the whole system, optics, detector and electronics was determined by using strong shocks in a CO_2/Ar mixture, with 5% CO_2. At a temperature of 2000 K the vibrational relaxation of the CO_2 was less than 1 μs.[10] The observed emission was that of the CO_2 asymmetric stretching mode near 2350 cm^{-1}. The rise of the infrared emission signal was displayed on an oscilloscope, a typical record is shown in Figure 3.3. If the rise time is taken to be from 10% to 90% of the equilibrium emission, then the record gives a rise time of about 8 μs. However, the record shows a significant (≈12% of total emission) rise in emission, prior to the arrival of the shock front. It is thought that preemission can arise from two sources. Firstly, resonance fluorescence, which arises from the absorption and reemission of

Figure 3.3

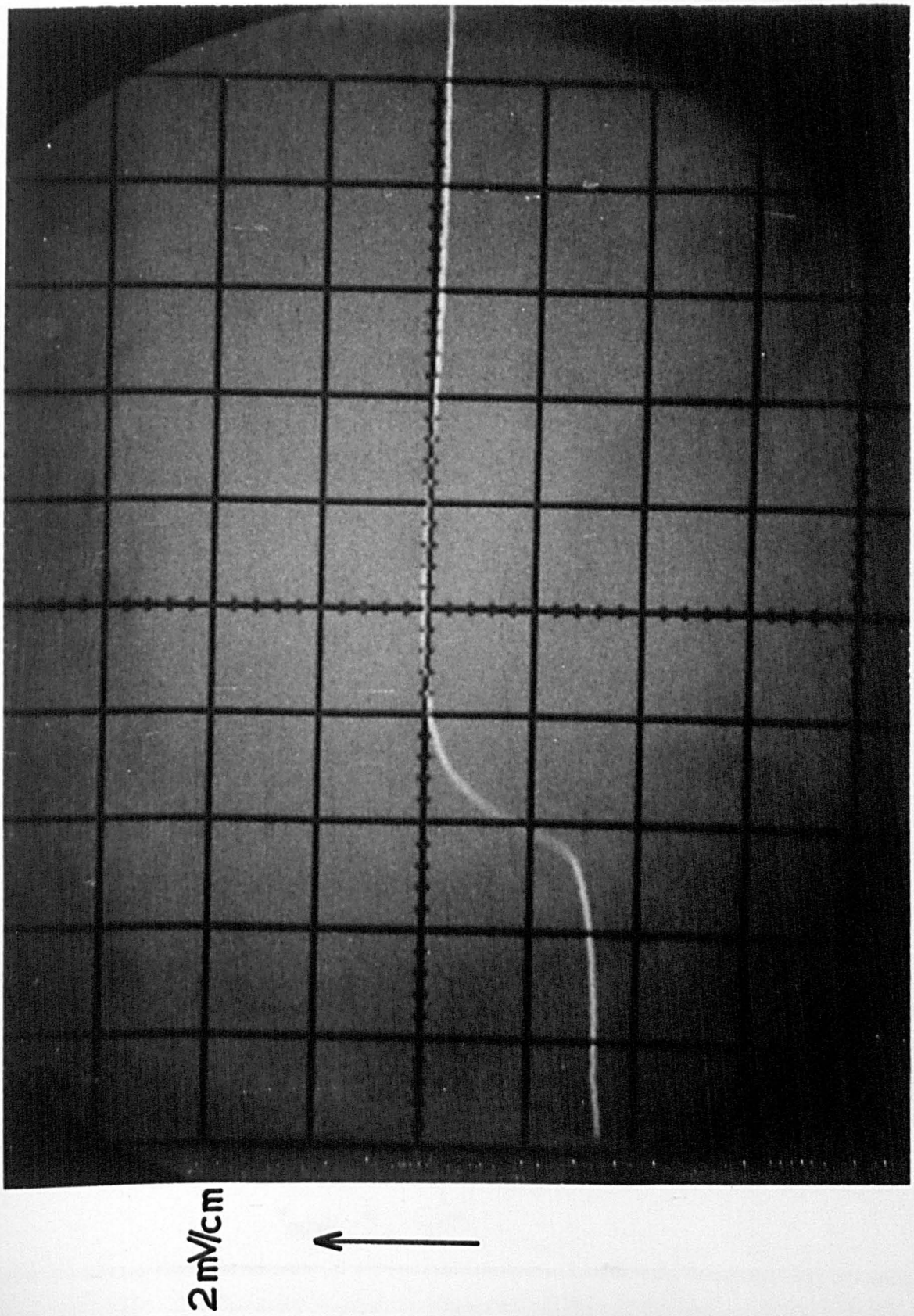

radiation, by the unshocked gas. As will be shown in Section 3.2.d the contribution to preemission from resonance fluorescence is very small. The second and more important pheomena, is multiple reflections from the tube walls which may cause radiation to enter the detection system prior to the shock arrival. Brabbs,[11] using 3% CO_2 in Argon, has shown that it is possible to observe emission from the shock front when the shock wave is about 0.1 m away from the observation point. The walls of the shock tube were coated with colloidal graphite, and Brabbs[11] then showed that a comparison of the equilibrium intensities for coated and uncoated gave the emission of the coated wall less by 30%. In view of the significant amount of preemission, it was felt that a realistic value of the rise time was ≈4 μs. This value was consistent with that obtained, by considering the rise time of the combination:-

$$T_{OUT} = \sqrt{(T_1^2 + T_2^2 + T_3^2 + \text{etc})}$$

In this case T_1 = optical rise time

T_2 = detector rise time

T_3 = amplifier rise time

As mentioned in Chapter 2, section 2.6.b, the optical rise time was ≈2 μs. The values of T_2 and T_3 were as stated in Chapter 2.

$$\therefore \quad T_{OUT} = \sqrt{(2^2 + 2^2 + 1^2)}$$

$$T_{OUT} = 3 \text{ μs}$$

This value was not disadvantageous to the CO/Ne runs where the processes were completed within 50 μs. However, in the case of the CO/polyatomic runs, it restricted the observations to a narrow range of concentrations of polyatomic species.

3.2 RADIATION CHARACTERISTICS

3.2.a SPECTRA

The fundamental vibration-rotation band spectrum, Figure 3.4, was obtained with a gas cell, with sodium chloride windows. Figure 3.5 shows the spectrum of a mixture of 5% N_2O and 95% CO. The P branch of the asymmetric stretching mode of the N_2O is seen to overlap with some of higher rotational transitions of the R branch of the CO. The overlap was also present with CO_2 and COS.

The transmission characteristics of the Calcium Aluminate glass is shown in Figure 3.6. The glass had a transmission of 45% in the region of the fundamental of CO. A cut on filter, Figure 3.7, was used to isolate the region of the fundamental of CO, it had a transmission of about 80% in the region of interest. The effect of the Calcium Aluminate glass-filter combination was to remove several of the higher rotational transitions in the P branch of the CO i.e. j(19→18), j(20→19) etc. One further disadvantage of the combination was that it allowed the emission from the polyatomic species to enter the detection system. However, in the experiments up to a 2% maximum concentration of polyatomic gas was used, and it was assumed that these species did not make a significant contribution to the radiation arriving at the detector.

Observations on the overtone of CO were made in a pyrex tube,

Figure 3.4

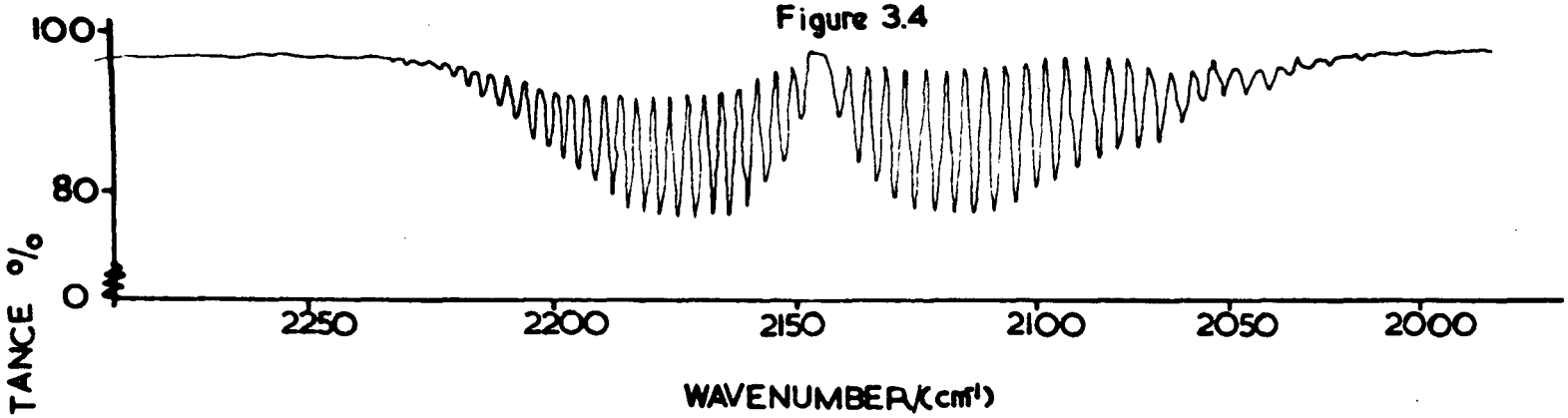

Figure 3.5

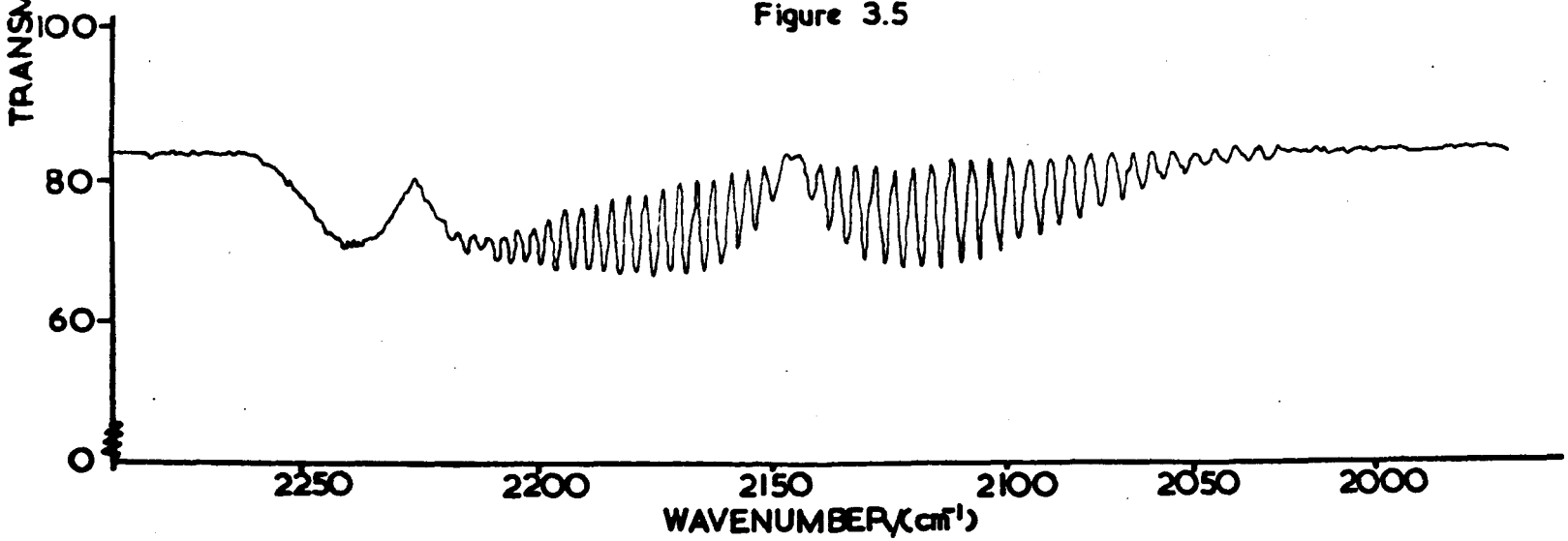

Figure 3.6

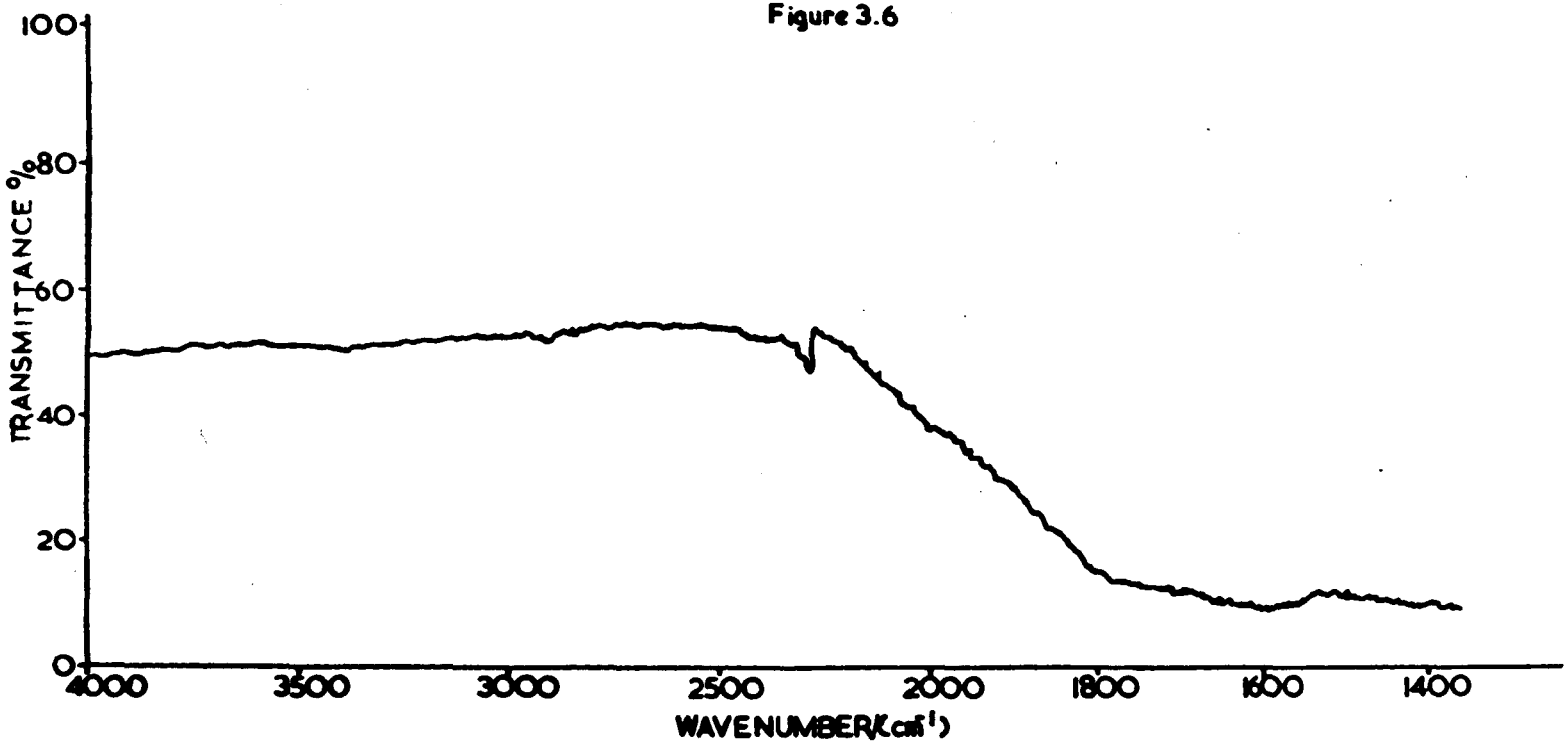
100
80
60
40
20
0
TRANSMITTANCE %
4000
3500
3000
2500
2000
1800
1600
1400
WAVENUMBER(Kcal⁻¹)

Figure 3.7

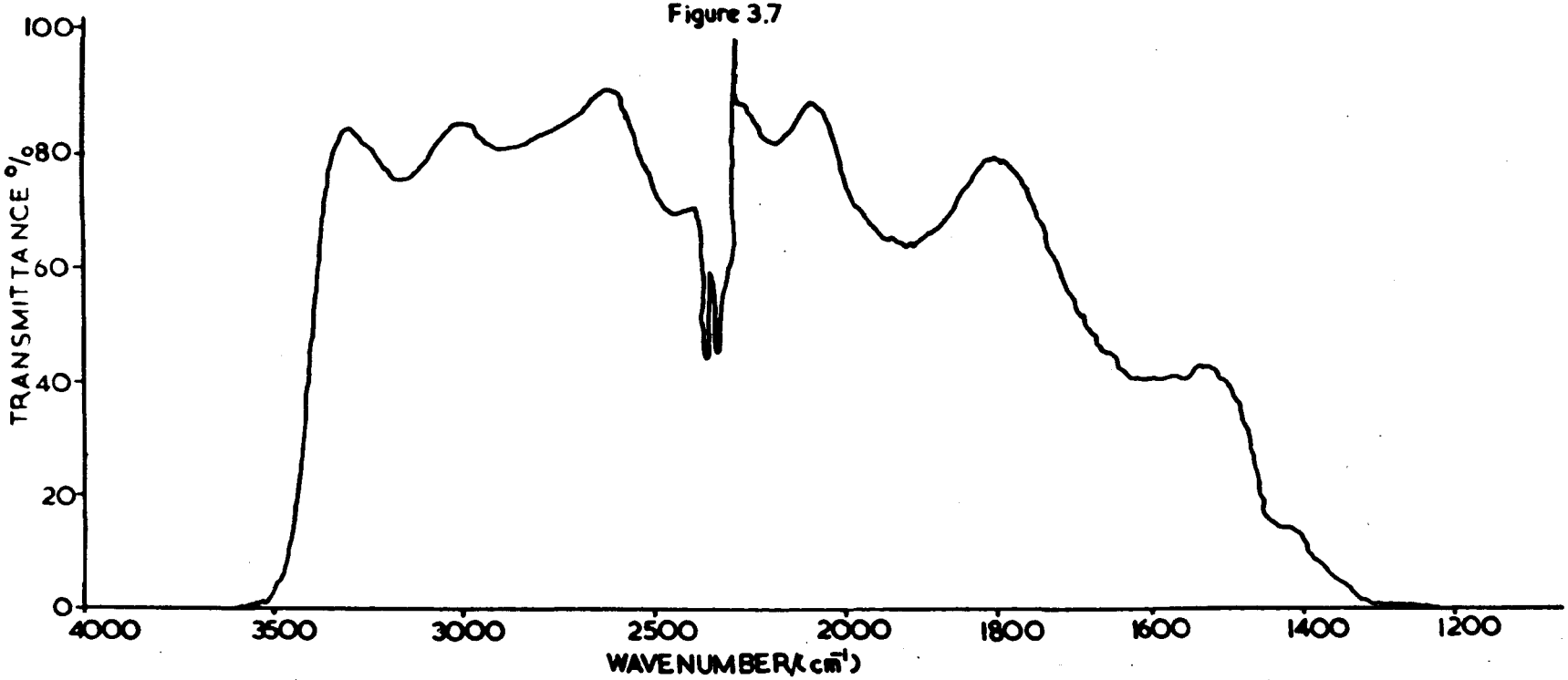
100
80
60
40
20
0
TRANSMITTANCE %
4000
3500
3000
2500
2000
1800
1600
1400
1200
WAVENUMBER(cm⁻¹)

the infrared spectra of this glass showed that there was a zero transmission in the region of the fundamental of CO.

3.2.b RADIATIVE LIFETIME

The radiative lifetime, τ_2, corresponds to the radiative process:-

$$X_{2\,v=0} + M \underset{k_{10}}{\overset{k_{01}}{\rightleftharpoons}} X_{2\,v=1} + M$$

$$X_{2\,v=1} \xrightarrow{k_2} X_{2\,v=0} + h\nu$$

The radiative lifetime can be calculated using a formula derived originally by Ladenburg,[12] which relates the radiative lifetime with the band strength:-

$$\frac{1}{k_2} = \tau_2 = 3.210 \times 10^{28}/S\nu^2$$

where τ_2 = radiative lifetime s

S = integrated absorption at S.T.P. in $cm^{-2}\ atm^{-1}$

ν = frequency s^{-1}

The values obtained[13] for the band strengths of CO are:-

$0 \rightarrow 1$ $S = 235.6\ cm^{-2}\ atm^{-1}$

$0 \rightarrow 2$ $S = 1.7\ cm^{-2}\ atm^{-1}$

Thus the radiative lifetimes are found to be:-

$$\text{Fundamental} \quad \tau_2^{10} = 3.288 \times 10^{-2} \text{ s}$$

$$\text{Overtone} \quad \tau_2^{20} = 1.09 \text{ s}$$

However the second vibrational level may depopulate in a stepwise fashion:- i.e.

$$CO_{v=2} \xrightarrow[\tau_2^{21}]{} CO_{v=1} + h\nu$$

$$CO_{v=1} \xrightarrow[\tau_2^{10}]{} CO_{v=0} + h\nu$$

If a harmonic oscillator is assumed then:-

$$k_{21} = 2k_{10}$$

$$\therefore \quad \tau_2^{21} = \frac{\tau_2^{10}}{2} = 1.644 \times 10^{-2} \text{ s}$$

Thus the second level depopulates preferentially via a stepwise mechanism. The relaxation processes by collision are completed with 200 μs or less. Thus the radiative process will serve to indicate the population of the observed state without affecting it significantly.

3.2.c CONCENTRATION OF EXCITED STATE AND DETECTOR OUTPUT

The rate of population of a particular vibrational level was followed by observing the emission of the infrared radiation from this state, by a suitable detector. It is believed that the intensity of the emission, as recorded by the detector, is directly proportional to the concentration of molecules in the excited state. This is shown in the equations below:-

$$\text{(Ref. 14)} \quad D^* = \frac{V_S/V_N \; (A\Delta f)^{\frac{1}{2}}}{I} \qquad 3.9$$

where D^* = detectivity cm $(Hz)^{\frac{1}{2}}$ W^{-1}

A = area of sensitive element cm^2

Δf = bandwidth of amplifier Hz

V_S/V_N = signal to noise ratio

I = incident light intensity on the sensitive element W

$$\text{(Ref. 15)} \quad I = I_0 K p x \qquad 3.10$$

K = spectral absorption coefficient cm^{-1} atm^{-1}

p = $(CO_{v=1})$ concentration of emitting species atm

x = thickness of emitting layer cm

I_0 = intensity of blackbody, radiation W

Substituting 3.10 in 3.9

$$D^* = \frac{V_S/V_N \; (A\Delta f)^{\frac{1}{2}}}{I_0 \; K \; x \; (CO_{v=1})}$$

At any wavelength and for a fixed path length:-

I_0, D^*, A, Δf, K and x are constant

$$\therefore \quad \frac{V_S}{V_N} \quad \alpha \quad (CO_{v=1})$$

3.2.d RESONANCE FLUORESCENCE

Resonance fluorescence arises from the absorption of radiation emanating from the shock front, and the reemission of the radiation, by gas downstream of the shock wave. Considering an infinitely long tube of emitting gas at pressure p_2:-

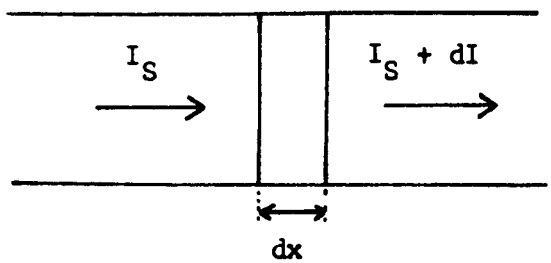

The increase in light along the incremental length dx is:-

$$dI_S = I' - I_S p_2 K dx \qquad 3.14$$

where I_S = incident radiation intensity from shock heated gas in watts cm^{-2}

I' = radiation intensity in watts cm^{-2} generated by the emitters in dx

K = spectral absorption coefficient in cm^{-1} atm^{-1}

The spectral emissivity of the layer, ε, is given by:-

(Ref. 15) $\varepsilon = Kp_2 dx$

$I' = I_0 Kp_2 dx$

I_0 = intensity of radiation in watts cm^{-2} of a black body

$\therefore$ 3.14 becomes:-

$$dI_S = I_0 Kp_2 dx - I_S p_2 K dx \qquad 3.15$$

where the first term on the right represents the emitted light and the second term measures the attenuation produced by the absorbers in dx.

$$\therefore \frac{dI_S}{(I_0 - I_S)} = Kp_2 dx$$

Integrating and applying $x = 0$, $I_S = 0$

$$I_S = I_0(1-\exp(-Kp_2 x)) \qquad 3.16$$

Thus a unit cube of shocked gas emits intensity I_S into the unshocked gas and toward the detector. The amount of light absorbed, I_{Abs} is given by:-

$$I_{Abs} = I_S - I_{trans} = I_S(1-\exp(-Kp_1))$$

where I_{trans} = transmitted light watts cm^{-2}

p_1 = downstream pressure atm

The amount of light reemitted is determined by the radiative lifetime, τ_2, see section 3.2.b. Thus the fraction of molecules reemitting:-

$$dN/N = K_2\, dt$$

$$\frac{\Delta N}{N} = K_2 \Delta t = \tau_2^{-1} \Delta t$$

where Δt = time available before the shock wave reaches the observation point

Assuming about $^1/6$ of the reemitted light reaches the detector. Thus the intensity of light reaching the detector prior to the shock is:-

$$I_{P.S.} = \frac{\frac{\Delta N}{N}\,(1-\exp(-Kp_1))I_S}{6}$$

Thus the ratio of light before the shock to the light after is:-

$$\frac{I_{P.S.}}{I_S} = \frac{\frac{\Delta N}{N}\,(1-\exp(-Kp_1)I_S}{6\ I_S}$$

In the present case $\Delta t = 10^{-5}$ s

For the first vibrational level:-

$$\frac{\Delta N}{N} = 3 \times 10^{-4}$$

$$\therefore \frac{I_{P.S.}}{I_S} = 5 \times 10^{-5} (1-\exp(-Kp_1)) \qquad 3.17$$

In the case of the second vibrational level:-

$$\frac{\Delta N}{N} = 10^{-5}$$

$$\therefore \frac{I_{P.S.}}{I_S} = 1.6 \times 10^{-6} (1-\exp(-Kp_1)) \qquad 3.18$$

Thus for the first vibrational level equation 3.17 shows that at a maximum the amount of resonance radiation reaching the detector prior to shock is 5×10^{-5} that reaching the detector after the shock. As is seen from equation 3.18 the amount of light reaching the detector from the overtone is very much less. In the case of CO it was assumed that resonance fluorescence made little or no contribution to any preemission seen on the infrared traces.

The above calculations are only very approximate. Detailed calculations of shock tube precursor radiation have been carried out by Lapp,[16] who concluded that in the case of CO that the effect of resonance fluorescence was only of slight magnitude.

REFERENCES

1. R.E. Duff, *Phys. Fluids*, 1959, 2, 207.
2. H. Mirels, *Phys. Fluids*, 1963, 6, 1201.
3. H. Mirels, *A.I.A.A. Journal*, 1964, 2, 84.
4. H. Mirels, *Phys. Fluids*, 1966, 9, 1907.
5. R.A. Strehlow and R.L. Belford, *Tech. Rept. A.A.E.*, Univ. Illinois, Urbana, 1969, 69-1.
6. R.L. Belford and R.A. Strehlow, *Ann. Rev. Phys. Chem.*, 1969, 20, 247.
7. W.J. Hooker, *Phys. Fluids*, 1961, 4, 1451.
8. W.J. Hooker and R.C. Millikan, *J. Chem. Phys.*, 1963, 38, 214.
9. J.N. Fox, I.I. McLaren and R.M. Hobson, *Phys. Fluids*, 1966, 9, 2345.
10. C.J.S.M. Simpson, K.B. Bridgman and T.R.D. Chandler, *J. Chem. Phys.*, 1968, 49, 513.
11. T.A. Brabbs, *J. Chem. Phys.*, 1968, 49, 1433.
12. R. Ladenburg, *Z. Physik*, 1921, 4, 451.
13. W.S. Benedict and E.K. Plyler, *Energy Transfer In Hot Gases, National Bureau of Standards, Washington, D.C.*, 1954, p. 57-73.
14. P.W. Kruse, L.D. McGlauchlin and R.B. McQuistan, *Elements of Infrared Technology*, (J. Wiley and Sons, New York) 1962, 265.
15. S.S. Penner, *Quantitative Molecular Spectroscopy and Gas Emissivities*, (Addison-Wesley Publishing Company Inc., Massachusetts) 1959, Chapter 1.

4. VIBRATIONAL TRANSFER PROBABILITIES

4.1 INTRODUCTION

Exact solutions to rigorous calculations of the transition probability, P, for any process is not possible. This is due to the fact that realistic intermolecular potentials are not yet available, and some of the equations involved are too complex to be solved by computer. In the three quantitative approaches, i.e. classical, semiclassical and quantum mechanical, approximations are made to ease the problem.

This chapter will briefly outline each of the methods, with special emphasis on those used to compare the present results with. There will be no detailed derivations, since they are well documented elsewhere.[1,2,3,4] The relative merits of the assumptions and limitations of each method have been described.[2,3,4] Also mentioned are empirical methods, and those involving long range forces.

Energy transfer between translational and vibrational degrees of freedom, during a non reactive collision can be described in terms of the Ehrenfest Adiabatic Principle. This principle states that the duration of the collision must be short compared to the period of vibration, if energy exchange is to take place. The classical situation is understood by considering a vibrating mechanical spring, which if

given a sudden blow will be left oscillating vigorously. The other extreme is that of a 'soft' force where the oscillator is able to adjust to the collision, during its period of vibration. This type of collision is adiabatic. The quantum mechanical case is that of a force field perturbing an oscillator. If the force field is only slowly varying then the oscillator can readjust to the perturbation, whereas if the perturbation is changing rapidly, then there is a high probability of a quantum transition. The physical situation which applies to all three 1-dimensional approaches, is represented in Figure 4.1. Atom A initially at infinite distance, approaches the simple harmonic oscillator BC, along their internuclear axis. The equilibrium internuclear distance of BC is y, and the displacement from equilibrium is χ. The distance, r, between the centres of gravity of A and BC is:-

$$r = d + \chi + y/2$$

The total energy of the two species will be conserved throughout the collision and it is the relative kinetic energy which is converted into vibrational energy, the centre of gravity of BC being taken as stationary. Full details of the collision problem have been described.[5,6] Rapp[5,7] has compared the three approaches, and found that they give identical results at high velocities of approach when the amount of net energy transfer to the oscillator is small.

Figure 4.1

Two Particle Problem For A-BC Collisions

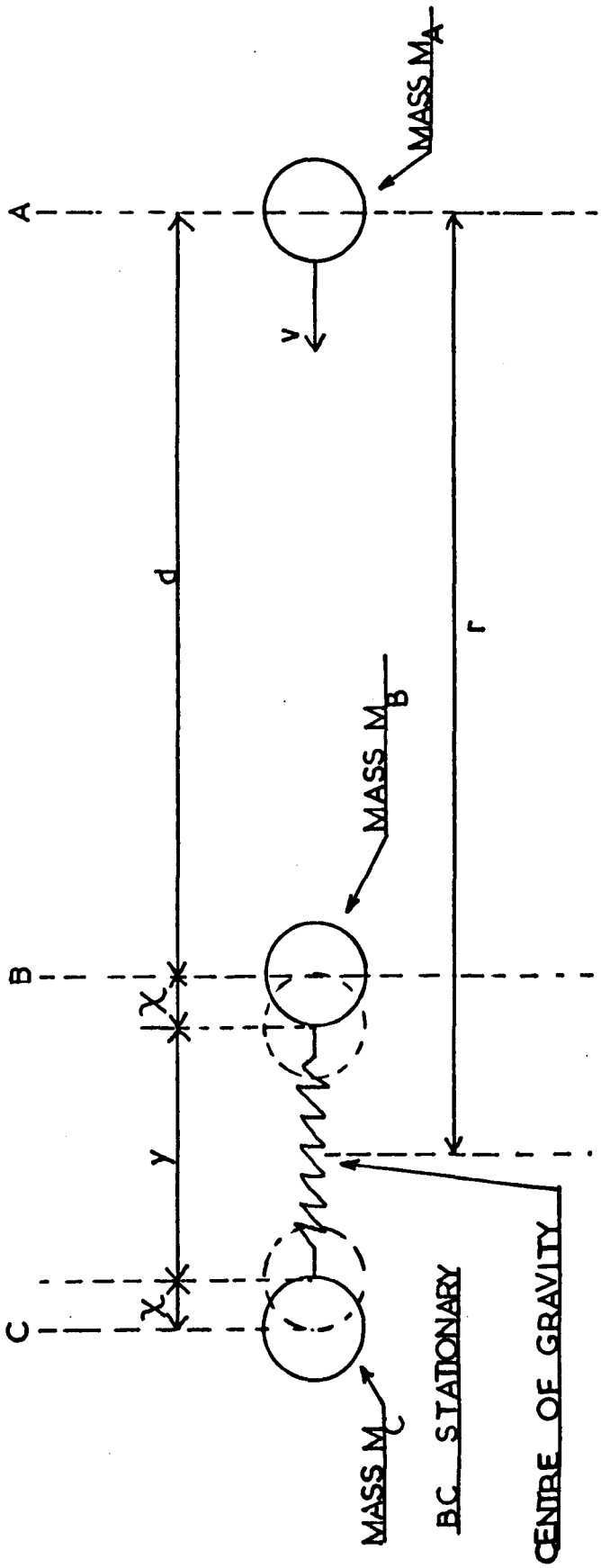

4.2 PARAMETER RELATIONSHIPS

In the following sections the parameters involved in vibration excitation are as follows:-

(a) P_{10}, transition probability

(b) Z_{10}, collision number

(c) k_{10}, rate constant

(d) τ, relaxation time

The subscript 10 refers to the de-excitation process. Similar parameters, subscripted 01, exist for the excitation process.

In the case of a 2 state model, where the molecule has 2 vibrational levels then:-

$$\tau = (k_{01} + k_{10})^{-1}$$

However in a multi state model:-

$$\tau = (k_{10} - k_{01})^{-1}$$

At equilibrium

$$\frac{k_{01}}{k_{10}} = \exp(-h\nu/kT)$$

Then for $T \ll h\nu/k$

$$\tau \approx \frac{1}{k_{10}}$$

Also $P_{10} = 1/Z_{10}$

$\tau = Z_{10}\ \tau_c$

Similarly $P_{10} = k_{10}\ \tau_c$

where $\tau_c = \eta/1.271 \times P$

η = viscosity μP

P = 1 atmosphere pressure

$$\eta = \frac{266.93 \times \sqrt{\frac{2 \times M_A \times M_{BC} \times T}{M_A + M_{BC}}}}{\Omega^{(2,2)} \times r_o^2 \times 10^7}$$

M_A, M_{BC} = masses of colliding species

r_o = constant in L-J potential values

$\Omega^{(2,2)}$ = viscosity data tabulated by Hirschfelder

T = temperature K

The values of τ_c were obtained from a computer programme see Appendix 2.

4.3 CLASSICAL METHOD

The purely classical approach is where the external and internal coordinates are given by the classical equations of motion. The energy levels of the oscillator are considered to be a continuum, and only the total energy transfer is calculated. The most notable workers in the field, Benson and co-workers,[8,9,10,11,12] base their method on a 1 dimensional collision model, using a Morse interaction potential. The method has been extended to treat rotation-vibration[13] and vibration-vibration[14] energy exchange. Some of their earlier work gave erroneous results,[10] and the more recent papers have been criticised by Rapp and Kassal.[2] Classical calculations have been carried out also by Parker[15] and Wilson[16,17] and co-workers. The results of numerical classical calculations on a large number of systems, under various conditions, are given by Kelley and Wolfsberg.[18]

4.4 SEMICLASSICAL METHOD

In this method the molecule BC is treated as a quantum mechanical system with discrete energy levels. The motion of the incident particle A is treated classically. The first approaches to the problem were made by Zener[19] and Landau and Teller.[20] Landau and Teller assumed that the interaction potential between the colliding species was exponential and of the form:-

$$V(r) = A \exp(-r/\ell)$$

where $V(r)$ = potential energy

A = constant

r = distance between species nm

ℓ = range of repulsive forces nm

They then showed that the probability of vibrational de-excitation, P_{10}:-

$$P_{10} \propto \exp\left(-\frac{\text{Duration of Collision}}{\text{Period of Vibration}}\right)$$

$$P_{10} = C \exp(-\ell \nu/v) \qquad 4.1$$

Thus the probability of energy transfer is favoured by a high relative velocity, v, and by a low value of the vibration frequency, ν. To obtain P_{10} as a function of temperature equation 4.1 was integrated over all possible velocities. The following expression was obtained:-

$$P_{10} = K_1 T^{-\frac{1}{3}} \exp(-K_2/T^{\frac{1}{3}}) \qquad 4.2$$

where K_1 and K_2 are constants which depend on collision across sections.

Also $NP_{10} = k_{10} = \frac{1}{\tau}$ (see section 4.2)

where N = number of collision per unit time

k_{10} = rate constant for deactivation

τ = relaxation time

$\frac{1}{\tau} = NP_{10}(1 - \exp(-h\nu/kT))$

and $N \alpha pT^{-\frac{1}{2}}$

Thus equation 4.2 becomes

$$\tau = \frac{K_1' T^{\frac{1}{6}} \exp(K_2/T^{\frac{1}{3}})}{p(1 - \exp(-h\nu/kT))}$$

Therefore:-

$\ln\tau \alpha T^{-\frac{1}{3}}$ approximately

The original calculations have been extended, in particular by Cottrell and Ream,[21] Rapp and Sharp[22,23] and Takayanagi.[24] The $T^{-\frac{1}{3}}$ dependence was given by most approaches, and in general the relaxation time can be expressed as:-

$$\ln\tau = A + BT^{-\frac{1}{3}} \qquad 4.3$$

In the process:-

$$AB_{(v=1)} + CD_{(v=0)} \rightleftharpoons AB_{(v=0)} + CD_{(v=1)}$$

there is a non zero, ΔE, interconversion of vibrational and translational energy. A semiclassical calculation of the probabilities of near resonant vibrational energy transfer has been accomplished by Rapp and Golden.[25,26] The calculation was made with a two state approximation (i.e. 0, 1 and 1, 0), and using an exponential potential between B and C. The result is:-

$$P_{10\rightarrow01} = 3.7 \quad 10^{-6} \quad T \quad \text{sech}^2 \left(\frac{0.174 \quad \Delta E}{T^{\frac{1}{2}}}\right) \qquad 4.4$$

where T = temperature K.

ΔE = difference in vibration frequency of the colliding species, measured in cm^{-1}

Thus increase in ΔE tends to decrease the transition probability for the exchange of vibrational energy. See Figure 4.2. The above method has been expanded to a multistate procedure.[27]

Figure 4.2

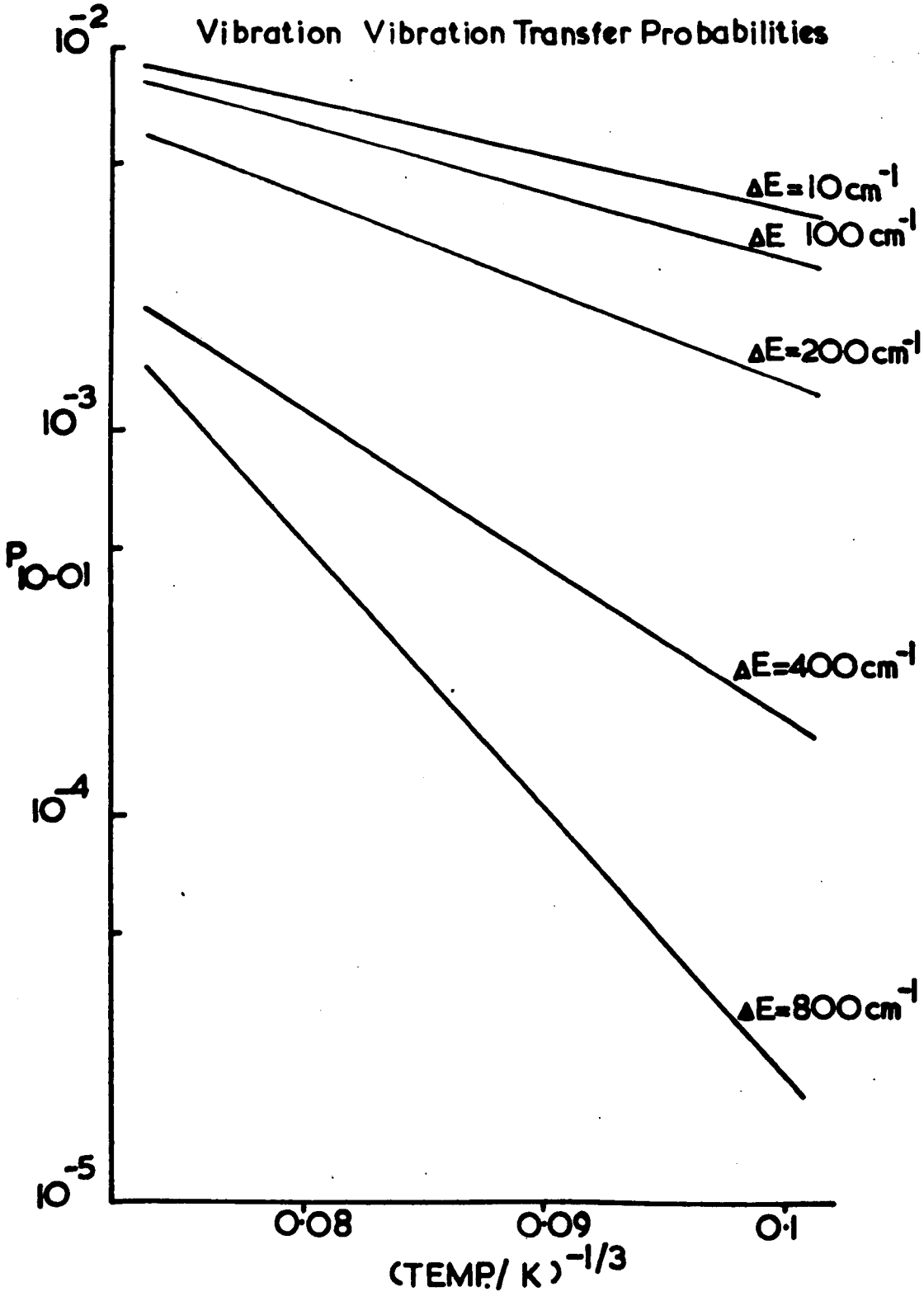
Vibration Vibration Transfer Probabilities
10^{-2}
10^{-3}
10^{-4}
10^{-5}
P_{10-01}
ΔE=10cm^{-1}
ΔE 100cm^{-1}
ΔE=200cm^{-1}
ΔE=400cm^{-1}
ΔE=800cm^{-1}
0·08
0·09
0·1
(TEMP./ K)$^{-1/3}$

4.5 QUANTUM MECHANICAL METHOD

This section is divided into three parts. Firstly, a discussion of the method, secondly a discussion of how the molecular interaction potential may best be refined, and thirdly a comparison of tabulated and computed results.

4.5.a THE METHOD

In this treatment the approaching and retreating atom is represented by a wave. If the wave corresponding to the retreating atom has the same wave number as the incident wave, then there has been no change in the internal energy of the oscillator. However, if the retreating atom has a different wave number, then there has been a change in internal energy. This method of treating the collision problem, in 1-dimension, has been described in detail,[1,28,29] and Jackson and Mott[30] have dealt with the solution of the integrals involved.

The three dimensional molecular model is more realistic. This problem has been treated and refined by Herzfeld and his co-workers.[31,32] In this case the approaching atom and the receding atom are represented by a system of spherical waves. The oscillator is treated as being spherically symmetrical, that is the vibration is considered as a symmetrical increase and decrease in the size of a

sphere. In the original calculations an exponential potential was assumed between the colliding species, since it made the mathematics simpler. However, this type of collision problem could not be solved exactly, but only by an approximate method. At low collision velocities, where the total transition probability is small, the approximate solution is found by using the First Order Distorted Wave Approximation (F.O.D.W.A.).

The final Schwartz-Slawsky-Herzfeld (S.S.H.) equation for estimating vibration-translation probabilities is:-

$$P_{10} = \frac{1}{Z_{10}} = \left(\frac{r_c}{r_o}\right)^2 \times \frac{\exp(\varepsilon/kT) \times (1 - \exp(\theta/kT))}{1.017 \times Z_o \times Z_{osc} \times Z_{tr} \times Y(2,2)}$$

where r_c = distance of closest approach

r_o = length constant in the Lennard-Jones Equation

ε = well depth in Lennard-Jones potential

θ = $h\nu/k$ = characteristic temperature of the vibration

$Y(2,2)$ = a viscosity factor

Z_o = orientation factor

Z_{osc} = vibrational collision number

Z_{tr} = translational collision number

The method has been refined further so that the probabilities of vibration-vibration energy transfer may be calculated. The details

of this equation are given in Appendix 2. For this type of calculation to be successful, a realistic estimation of the quantity, ℓ, the range of repulsive forces must be obtained. The value of ℓ depends on the choice of intermolecular potential. The fitting of the purely repulsive potential, used in the derivation, to a reasonable potential is shown in the next section.

4.5.b THE INTERMOLECULAR POTENTIAL

At short intermolecular distances where repulsive forces dominate, the foregoing treatment is based on a purely repulsive potential. For real gases the field between two molecules is usually represented by the Lennard-Jones(L-J) potential. This potential contains an attractive, as well as a short range repulsive component. The attractive component accelerates the particles during their approach. The equation is:-

$$V_{L-J}(r) = -4\varepsilon \left[\left(\frac{r_o}{r}\right)^6 - \left(\frac{r_o}{r}\right)^{12} \right]$$

where ε = potential well depth

$V_{L-J}(r)$ = potential energy with a minimum at $r = 2^{\frac{1}{6}} r_o$

r_o = constant

The constant $-\varepsilon$ is introduced into the exponential potential, to make the slopes of the two potentials compatible at small distances, which are important in determining energy transfer probabilities.

The range of collision velocities has a minimum value of r at r_c. There are two recognized methods of fitting the two potentials.

Method A was developed originally by Schwartz, Slawsky and Herzfeld.[29] In this case the repulsive potential is made tangent to the L-J potential at r_c. Thus at this point the potential energy and slopes of the potentials are set equal. It is found that:-

$$\frac{r_o}{\ell} = 12 \left[\tfrac{1}{2}(1 + \sqrt{Em/\varepsilon + 1})\right]^{\frac{1}{6}} \left[1 + (Em/\varepsilon + 1)^{-\frac{1}{2}}\right]$$

where Em = effective energy of collision

Method B is due to De Wette and Slawsky,[33] who fitted the exponential potential by requiring that the curves have 2 points in common. The first point is as before, where both curves have some potential energy, and the second point is where V(r) = 0 and $r = r_A$. From this condition it is found that:-

$$\frac{r_o}{\ell} = \left[\ln(Em/\varepsilon + 1)\right] \left[1 - \left(\tfrac{1}{2}\left[1 + \sqrt{Em/\varepsilon + 1}\right]\right)^{-\frac{1}{6}}\right]^{-1}$$

The fitting of the exponential potential to the L-J potential is shown in Figure 4.3. The value of r_o/ℓ as a function of $\log_{10} Em/\varepsilon$ for both methods is plotted in Figure 4.4. It is seen that method B gives a reasonably constant value of r_o/ℓ over a wide range of $\log_{10} Em/\varepsilon$. Also, method B has been used by many workers since it

Figure 4.3
Fitting Of Exponential To L-J Potential

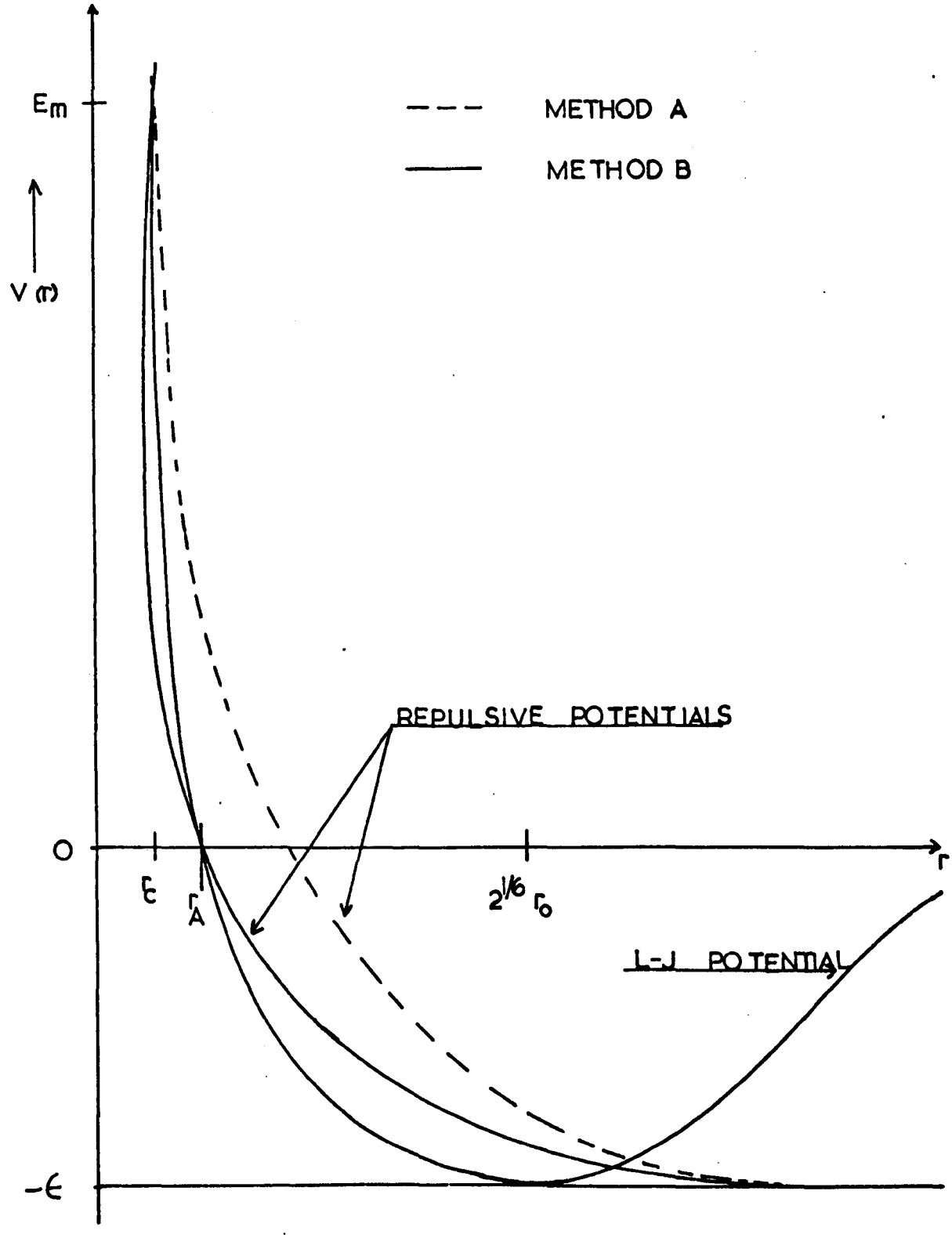

Figure 4.4
Comparison Of Methods A & B

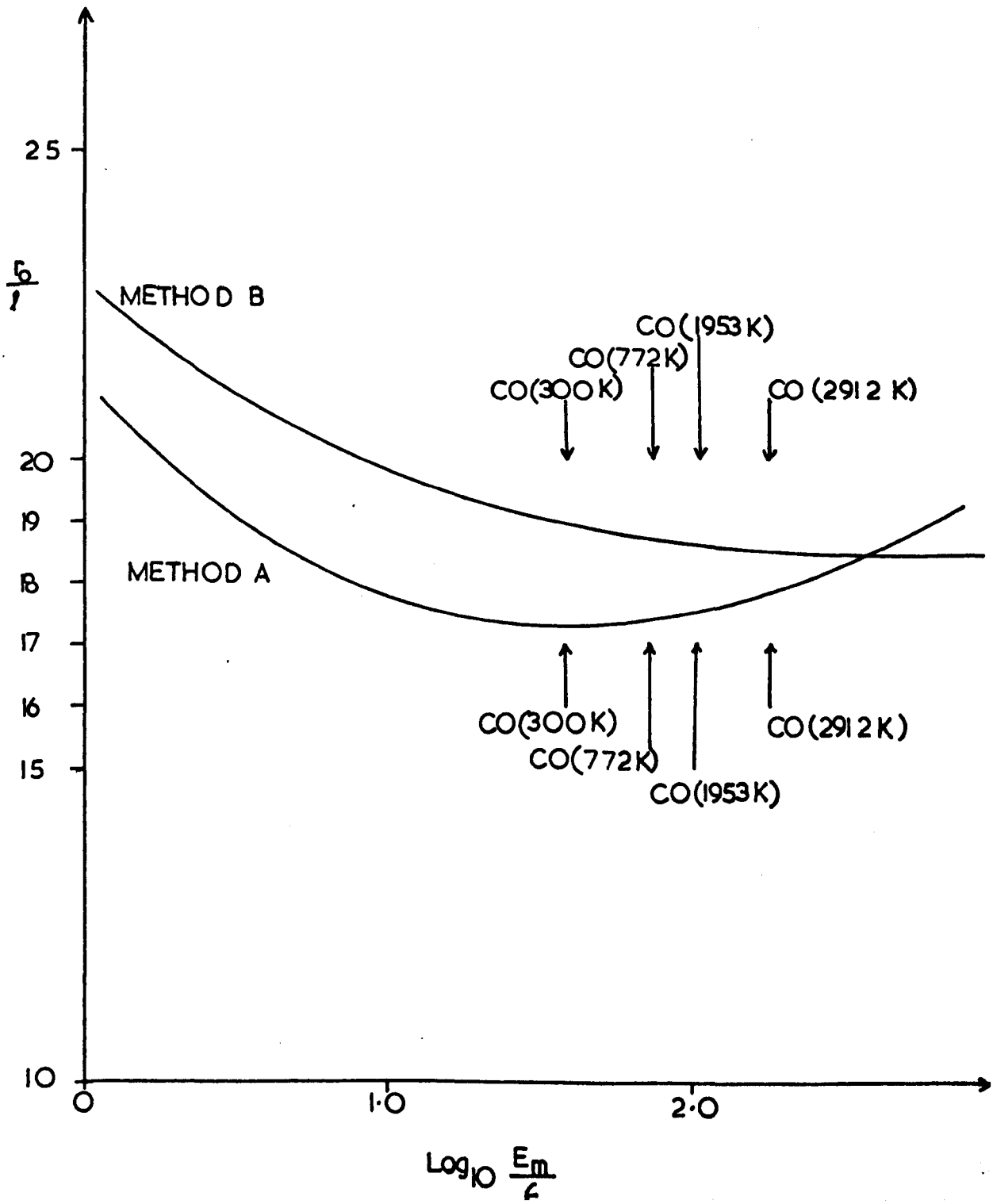

gives a smaller value of ℓ, which has usually led to better agreement with experiment. In this study method B was used. The important quantity obtained from the curve matching was the range of repulsive forces ℓ.

4.5.c COMPARISON OF COMPUTED AND TABULATED RESULTS

A computer programme to deal with the S.S.H. calculations was devised. Details of the programme, together with the calculational method are set out in Appendix 2. The value of ℓ was calculated by an iterative procedure, and for most systems lay between 1.5 and 2.5 nm. Figure 4.5 compares the computer results with those tabulated by Herzfeld and Litovitz[1] for method B, and for vibration-translation energy transfer. The molecular constants used were obtained from Hirschfelder et al,[34] and are found in Table 4.1. The calculated values of ℓ and Em/ε are compared to the tabulated values[1] in Table 4.2. It is seen that the agreement for the value of ℓ is good, the discrepancy between the results never being greater than 2%. The values of Em/ε agree also to within 3% of each other.

Figure 4.5 shows a difference between the tabulated probabilities and the calculated ones. This is due to the selection of a value for Z_o. Herzfeld[1] chose a value of 3 for Z_o, whereas the present calculations find Z_o from the following:-

TABLE 4.1

Molecule	$\bar{\nu}$ cm^{-1}	r_0 nm	ε/k K
O_2	1548.61	34.33	113.2
N_2	2330.22	36.81	91.5
Cl_2	562.64	41.15	357.0
CO_2	667.0	39.96	190.0

TABLE 4.2

Colliding Species	Temperature K	Repulsion Parameter - ℓnm		Em/ϵ	
		Computed Result	Herzfeld & Litovitz	Computed Result	Herzfeld & Litovitz
O_2-O_2	288	1.787	1.787	25.21	25.35
	1372	1.834	1.833	70.66	71.33
	1953	1.841	1.840	89.64	90.5
N_2-N_2	778	1.970	1.971	78.9	79.39
	4630	1.992	1.991	262.27	262.6
Cl_2-Cl_2	288	2.037	1.998	5.80	5.57
	1000	2.119	2.090	13.29	13.15
	1372	2.158	2.106	16.50	16.32
CO_2-CO_2	288	2.008	2.011	10.29	10.30
	1000	2.076	2.076	23.48	23.47

Figure 4.5

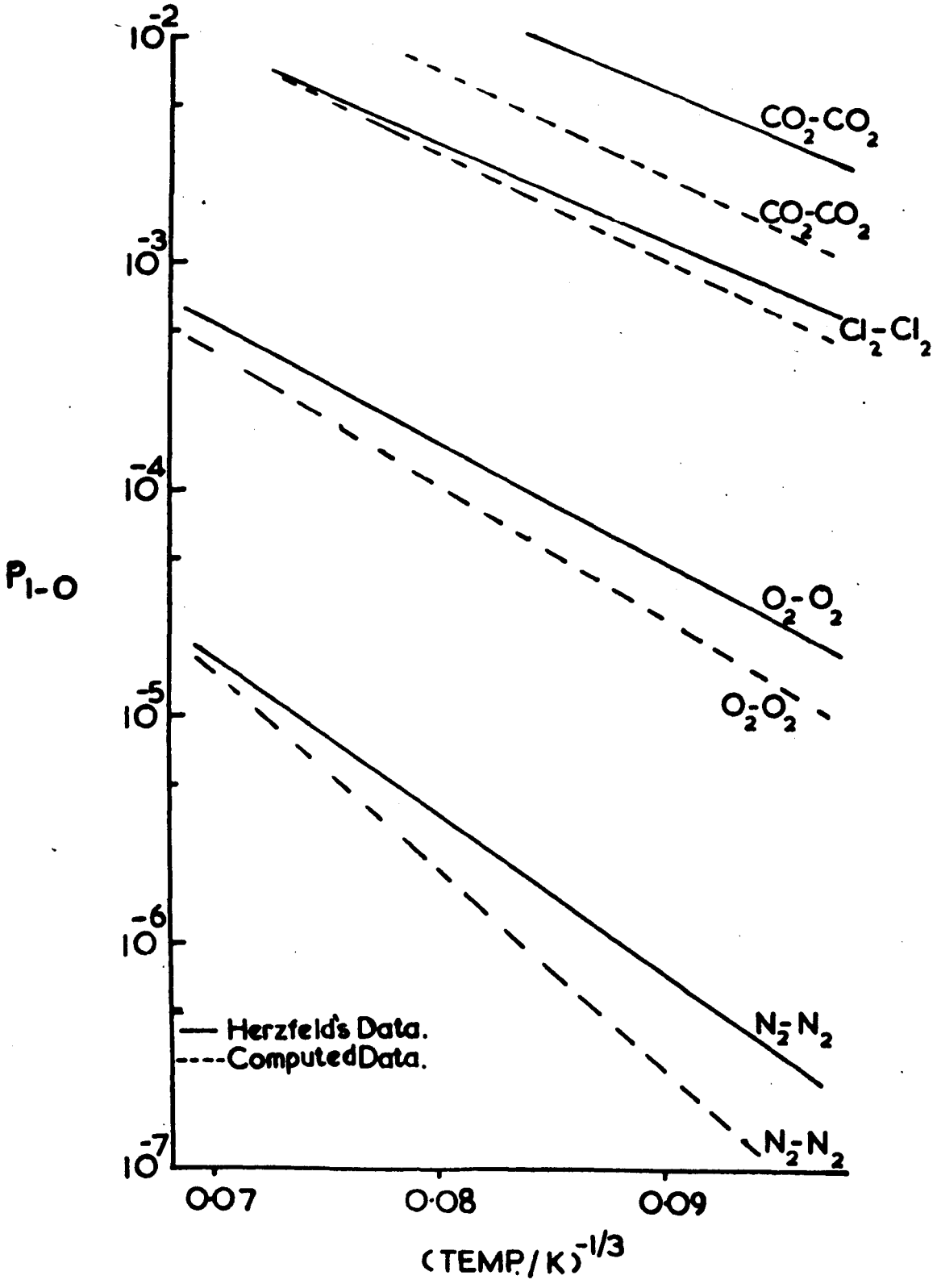
10^{-2}
10^{-3}
10^{-4}
10^{-5}
10^{-6}
10^{-7}
P_{1-0}
CO_2-CO_2
CO_2-CO_2
Cl_2-Cl_2
O_2-O_2
O_2-O_2
N_2-N_2
N_2-N_2
— Herzfeld's Data.
---- Computed Data.
0·07
0·08
0·09
(TEMP./K)$^{-1/3}$

$$Z_o = 2.5 \times (\ell/L)^2 + L/\ell \qquad 4.6$$

where L = interatomic distance of BC

ℓ = range of repulsive forces

From this equation it was found that for most systems Z_o ranged between 5 and 10. Equation 4.6 is proceding toward a more realistic value for Z_o, but the recent work of Shin[35] has refined it still further.

In conclusion, it is believed that the present computational method is sound, since the values of important molecular parameters can be reproduced accurately. Although discrepancy exists between the probabilities, computed and tabulated, the present values may be more accurate due to the calculation of Z_o. Thus the procedure contains no adjustable parameters.

4.6 EMPIRICAL METHODS

Losev and Osipov[36] suggested an empirical method for calculating vibrational relaxation times. This was developed by Millikan and White.[37] It was found that linear plots of $\log_{10}\tau$ (at unit pressure) against $T^{-\frac{1}{3}}$ had a common origin for many diatomic gases of similar reduced mass. The relaxation times of the gases over a wide range of temperatures are given by the formula:-

$$\log_{10}\tau = 5.0 \times 10^{-4} \times \mu^{\frac{1}{2}} \times (\theta)^{\frac{4}{3}} \times (T^{-\frac{1}{3}} - 0.015 \times \mu^{\frac{1}{4}}) - 8.00$$

where μ = the reduced mass of the colliding system

θ = characteristic temperature of the vibration.

The equation is valid for the following limits:-

$$1.75 < \mu < 127$$

$$310\ K < \theta < 3395\ K$$

$$280\ K < T < 8000\ K$$

This relationship applies only to vibration-translation energy exchange, and takes no account of vibration-vibration exchange.

4.7 LONG RANGE INTERACTION METHODS

De Wette and Slawsky[33] made a theoretical investigation of two cases in which long range forces are strong. They studied the dipole-dipole interaction of 2 HCl molecules and the quadrupole-quadrupole interaction in the case of 2 CO molecules. The interactions were divided into two possibilities a) long range (adiabatic) interaction, b) short range (nonadiabatic) interaction. The work confirmed that the effect of the long range forces was to accelerate the approaching particle, and this would affect the transition probability directly.

The probability of vibration-vibration energy transfer between infrared active modes, due to dipole-dipole interaction, has been considered by Mahan.[38] The resonance interaction was assumed to diminish at great distances as r^{-3}. The calculations showed that; a) the resonant transfer of energy may be more rapid than is indicated by the calculations using the repulsive potential, b) the probability decreases as the temperature increases, whereas the probability due to repulsive forces increases with increase in temperature. These calculations have been extended by Yardley[39] to the case of non-resonant vibration-vibration transfer, due to dipole-dipole interactions.

Sharma and Brau[40,41] have shown that anomalous behaviour of the N_2-CO_2 system below 1000 K, can be explained in terms of a

long range dipole quadrupole interaction. The probabilities calculated by this method show a negative temperature dependence, in contrast to the behaviour predicted by the S.S.H. theory. Recent experimental evidence has been provided by Roach and Smith,[42] who have worked on the N_2-N_2O system. However, it is assumed that above 1000 K short range repulsive forces will dominate the translation-vibration transfer process. The method will not be considered in the present study.

4.8 DISCUSSION OF METHODS

It is not easy to compare the theories with experiment, since vibrational energy transfer is extremely sensitive to the slope of the repulsive part of a potential. Thus the value of the range of the repulsive force, ℓ, is not well known. Herzfeld[43] found that a better evaluation of ℓ could be obtained by fitting the exponential potential to an L-J potential. A double exponential potential of the Morse type has been used,[44] and Monchick and Mason[45] have modified the L-J potential to a 12-6-3 potential which takes account of dipole-dipole interaction in polar molecules. Molecular beams enable measurements of the repulsive forces to be made more directly. Mueller and Marchi[46] have concluded that the L-J 12-6 potential does not provide a sound basis for the observed scattering patterns and a broader minimum is required. Further studies of this nature will lead to a better understanding of the interaction potentials between colliding species.

The classical calculations of Parker[15] and Benson and Berend[12] have fitted their data to the Landau-Teller theory, and have obtained reasonable agreement. The plots of Log P_{10} are not simple linear functions of $T^{-\frac{1}{3}}$ over a large temperature range, but tend to show an 'S' shaped behaviour. One of the reasons why this theory is not well applied is the need for careful computing procedures to solve the integrals involved.

The S.S.H. theory has been widely applied since the equations are presented in an explicity soluble form. It is possible to calculate the relaxation times of pure gases and gas mixtures to within an order of magnitude, and log τ is a linear function of $T^{-\frac{1}{3}}$. There are notable exceptions, where the relaxation times predicted by S.S.H. are different from the experimental values. H_2[47] relaxes abnormally rapidly, as does NO. The case for NO has been explained[48] by assuming the formation of an electronically excited state. Results for the hydrogen halides, and in particular the HI/HI system[49] show that Z is several powers of 10 smaller than the S.S.H. prediction. In the case of the hydrogen halides and some hydrides there is the possibility of vibration-rotation rather than vibration-translation energy exchange. Some 25 molecules have been fitted to a semi-quantitative vibration-rotation model[50] with reasonable success. However, this theory is unable to fit the hydrogen halides well.

Vibration-vibration energy transfer probabilities were calculated from equation 4.4, section 4.4. This method has had reasonable success in giving close agreement with room temperature data[51] and more recent high temperature data,[52] with the CO-NO and N_2-NO systems. However the work of White[53] on N_2-O_2 vibration exchange had less agreement. Sato et al[54] have studied vibrational energy exchange, by the shock tube technique, and the experimental

data agreed well with the equation derived by S.S.H. for vibration-vibration exchange. Recently, Riley and Kuppermann[55] have made numerically exact quantum mechanical calculations of collisional energy transfer probabilities. They found that the F.O.D.W.A. used in derivation of the S.S.H. theory, was very accurate for the (0, 1) → (1, 0) process. The one quantum translation-vibration processes were found to be an order of magnitude too large.

Figure 4.6 compares the probabilities of vibration-vibration energy transfer calculated from equation 4.4, and those calculated by the S.S.H. method. Specific systems were taken for the S.S.H. calculations, as shown in the figure. The two approaches compare most favourably with increase in the value of ΔE, the energy discrepancy. It is reasonable to assume that the quantum mechanical method should compare best with experimental data.

The Millikan and White[37] correlation has been criticised[12] on the basis that the correlation ignores some low temperature data not lying on the extrapolated curves. The equation contains no terms relating to the intermolecular potential, and a common value for ℓ is assumed. However as pointed out previously the transition probability is sensitive to ℓ. The correlation does not work for H_2, D_2 the hydrogen halides and polyatomic molecules in general. The correlation is successful in predicting vibration-translation probabilities for diatomic molecules.

Figure 4.6

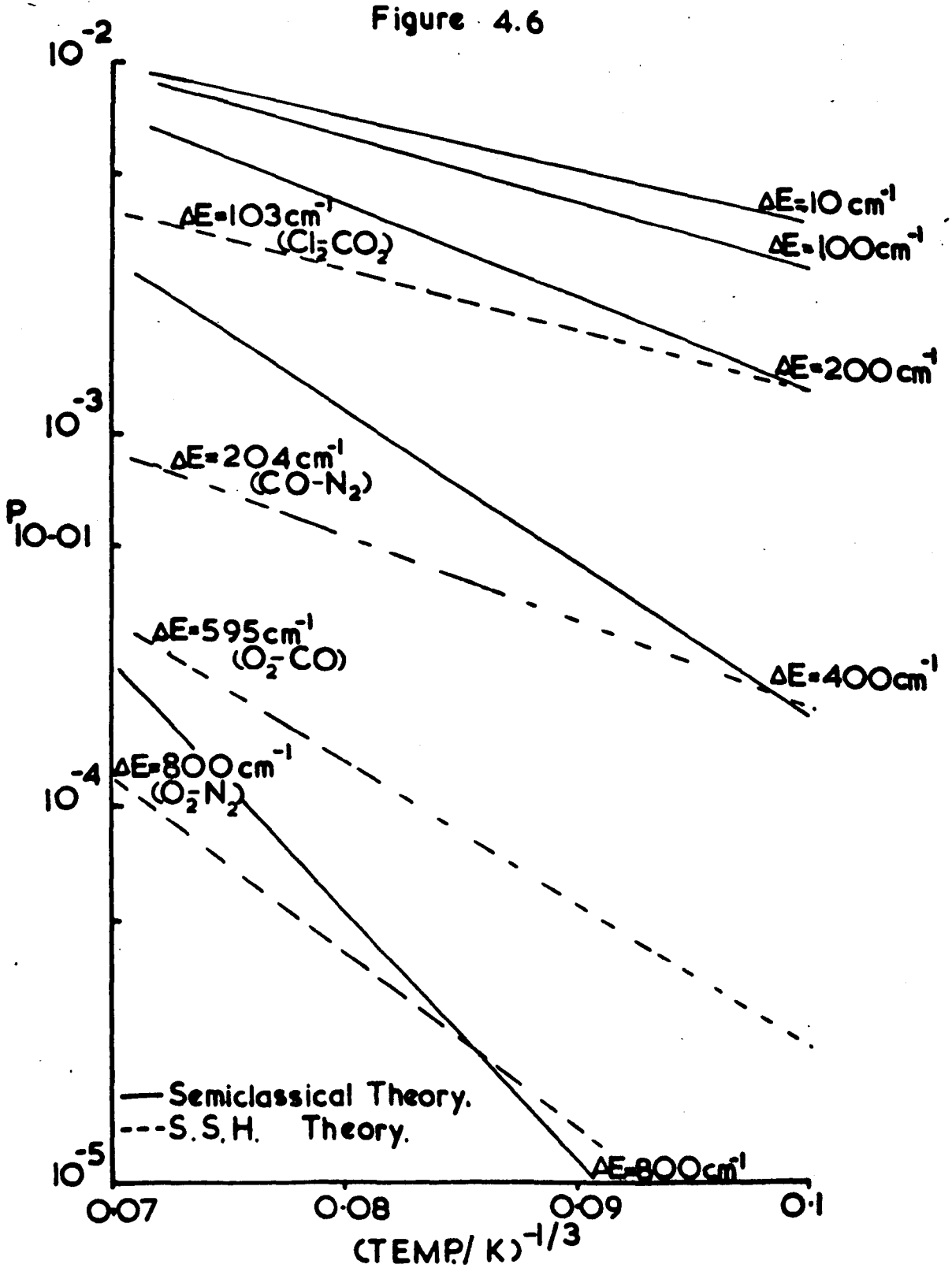
10^{-2}
10^{-3}
10^{-4}
10^{-5}
P
10-01
ΔE=10 cm⁻¹
ΔE=100cm⁻¹
ΔE=103cm⁻¹
(Cl₂-CO₂)
ΔE=200 cm⁻¹
ΔE=204cm⁻¹
(CO-N₂)
ΔE=595cm⁻¹
(O₂-CO)
ΔE=400cm⁻¹
ΔE=800 cm⁻¹
(O₂-N₂)
— Semiclassical Theory.
---S.S.H. Theory.
ΔE=800cm⁻¹
0·07
0·08
0·09
0·1
(TEMP./ K)⁻¹/³

REFERENCES

1. K.F. Herzfeld and T.A. Litovitz, *Absorption and Dispersion of Ultrasonic Waves*, (Academic Press, New York) 1959.
2. D. Rapp and T. Kassal, *Grumman Research Department Report*, 1968, RE-345.
3. J.L. Stretton, *Transfer and Storage of Energy by Molecules*, (Wiley, London) 1969, Vol 2, 58.
4. T.L. Cottrell and J.C. McCoubrey, *Molecular Energy Transfer in Gases*, (Butterworths, London) 1961.
5. D. Rapp, *J. Chem. Phys.*, 1964, 40, 2813.
6. K. Takayanagi, *Advan. At. Mol. Phys.*, 1965, 1, 149.
7. D. Rapp, *J. Chem. Phys.*, 1960, 32, 735.
8. S.W. Benson, G.C. Berend and J.C. Wu, *J. Chem. Phys.*, 1962, 37, 1386.
9. S.W. Benson, G.C. Berend and J.C. Wu, *J. Chem. Phys.*, 1963, 38, 25.
10. S.W. Benson and G.C. Berend, *J. Chem. Phys.*, 1963, 39, 2777.
11. S.W. Benson and G.C. Berend, *J. Chem. Phys.*, 1964, 40, 1289.
12. S.W. Benson and G.C. Berend, *J. Chem. Phys.*, 1966, 44, 470.
13. S.W. Benson and G.C. Berend, *J. Chem. Phys.*, 1966, 44, 4247.
14. S.W. Benson and G.C. Berend, *J. Chem. Phys.*, 1969, 51, 1480.
15. D.G. Parker, *Phys. of Fluids*, 1959, 2, 444.
16. E.B. Alterman and D.J. Wilson, *J. Chem. Phys.*, 1965, 42, 1957.

17. R.J. Harter, E.B. Alterman and D.J. Wilson, *J. Chem. Phys.*, 1964, 40, 2137.

18. J.D. Kelley and M. Wolfsberg, *J. Chem. Phys.*, 1966, 44, 324.

19. C. Zener, *Phys. Rev.*, 1931, 37, 556.

20. L.D. Landau and E. Teller, *Z. Phys. Sowjetunion.*, 1936, 10, 34.

21. T.L. Cottrell and N. Ream, *Trans. Faraday Soc.*, 1955, 51, 1453.

22. D. Rapp and T.E. Sharp, *J. Chem. Phys.*, 1963, 38, 2641.

23. T.E. Sharp and D. Rapp, *J. Chem. Phys.*, 1965, 43, 1233.

24. K. Takayanagi, *Progr. Theoret. Phys. (Kyoto)*, 1963, Suppl. 25, 1.

25. D. Rapp and P.E. Golden, *J. Chem. Phys.*, 1964, 40, 573, *Ibid*, 1964, 40, 5123.

26. D. Rapp, *J. Chem. Phys.*, 1965, 43, 316.

27. A. Zelechow, D. Rapp and T.E. Sharp, *J. Chem. Phys.*, 1968, 49, 286.

28. N.F. Mott and H.S.W. Massey, *The Theory of Atomic Collisions*, (Oxford University Press, Oxford) 1949, 2nd Edn.

29. R.N. Schwartz, Z.I. Slawsky and K.F. Herzfeld, *J. Chem. Phys.*, 1952, 20, 1591.

30. N.F. Mott and J.M. Jackson, *Proc. Roy. Soc.*, 1932, 137A, 703.

31. R.N. Schwarz and K.F. Herzfeld, *J. Chem. Phys.*, 1954, 22, 767.

32. K.F. Herzfeld, *J. Chem. Phys.*, 1967, 47, 743.

33. F.W. de Wette and Z.I. Slawsky, *Physica*, 1954, 20, 1169.

34. J.O. Hirschfelder, C.F. Curtiss and R.B. Bird, *Molecular*

Theory of Gases and Liquids, (Wiley, New York) 1954.

35. H.K. Shin, *J. Chem. Phys.*, 1967, 47, 3302.

36. S.A. Losev and A.I. Osipov, *Soviet Phys. Usp. (English Transl.)*, 1962, 4, 525.

37. R.C. Millikan and D.R. White, *J. Chem. Phys.*, 1963, 39, 3209.

38. B.H. Mahan, *J. Chem. Phys.*, 1967, 46, 98.

39. J.T. Yardley, *J. Chem. Phys.*, 1968, 50, 2464.

40. R.D. Sharma and C.A. Brau, *Phys. Rev. Letters*, 1967, 19, 1273.

41. R.D. Sharma and C.A. Brau, *J. Chem. Phys.*, 1969, 50, 924.

42. J.F. Roach and W.R. Smith, *J. Chem. Phys.*, 1969, 50, 4114.

43. K.F. Herzfeld, *Thermodynamics and Physics of Matter*, (Princeton University Press, Princeton, N.J.) 1965.

44. S.L. Thomson, *J. Chem. Phys.*, 1968, 49, 3400.

45. L. Monchick and E.A. Mason, *J. Chem. Phys.*, 1961, 35, 1676.

46. C.R. Mueller and R.P. Marchi, *J. Chem. Phys.*, 1963, 38, 745.

47. J.H. Keifer and R.W. Lutz, *J. Chem. Phys.*, 1966, 44, 668.

48. E.E. Nikitin, *Optika Spektrosk.*, 1960, 9, 8.

49. C.C. Chow and E.F. Greene, *J. Chem. Phys.*, 1965, 43, 324.

50. C.B. Moore, *J. Chem. Phys.*, 1965, 43, 2979.

51. N. Basco, A.B. Callear and R.G.W. Norrish, *Proc. Roy. Soc. (London)* 1961, A260, 459; 1962, A269, 180.

52. R.L. Taylor, M. Camac, R.M. Feinberg, *Symp. Combust. 11th*, 1967, 49, 1966.

53. D.R. White, *J. Chem. Phys.*, 1968, 49, 5472.

54. Y. Sato, S. Tsuchiya and K. Kuratani, *J. Chem. Phys.*, 1969, 50, 1911.

55. M.E. Riley and A. Kuppermann, *Chem. Phys. Letters*, 1968, 1, 537.

5. RELAXATION EQUATIONS

The following chapter will contain details of the mechanisms of the reactions used in this study, their respective kinetic equations and the solution of these equations. The introduction will deal with the mechanisms. Then methods will be presented which deal with a) a binary mixture of diatomic and inert gases, b) a binary mixture of gases with the possibility of a complex reaction.

5.1 INTRODUCTION

In a pure diatomic gas, A, of two vibrational states, neglecting radiative loses, the reaction for excitation and de-excitation of the first vibrational level is:-

$$A_0 + A \underset{k_{10}^{AA}}{\overset{k_{01}^{AA}}{\rightleftharpoons}} A_1 + A$$

$$x_{A0} \qquad\qquad x_{A1}$$

where A = diatomic molecule, subscripts 1, 0 refer to 1st excited state and ground state respectively.

k_{10}^{AA} , k_{01}^{AA} = bimolecular rate constants for deexcitation and excitation respectively

x_{A0}, x_{A1} = concentrations of ground and excited state of A respectively

The addition of an inert gas, B, to the system, introduces another reaction possibility:-

$$A_0 + B \underset{k_{10}^{AB}}{\overset{k_{01}^{AB}}{\rightleftharpoons}} A_1 + B$$

where k_{01}^{AB}, k_{10}^{AB} = bimolecular rate constants

x_B = concentration of B

Also:- $x_A = x_{A0} + x_{A1}$

$x_B = x_B$

$x = x_A + x_B$

$(1-X) = \frac{x_A}{x}$ X = mole fraction

$\therefore X = x_B/x$

In this case the energy exchange can occur by collision of A with A or A with B. The overall rate constant for any mixture is given by:-

$$k_{mix} = k_{10}^{AA}(1 - X) + k_{10}^{AB}X \qquad 5.1$$

Assuming $k_{10} > k_{01}$

where k_{10}^{AA} = rate constant for a pure diatomic gas

k_{10}^{AB} = rate constant for 1 molecule of A in pure B.

Equation 5.1 has a linear dependence upon concentration, experimental results may be extrapolated to give k_{10}^{AB}.

The excitation of the upper levels of a diatomic molecule is an example of a series mechanism, see Figure 5.1.a. The energy is fed into the molecule by translation, so that the lowest vibrational mode is vibrationally excited. This energy is then redistributed to other modes.

$$A_0 + A \underset{k_{10}}{\overset{k_{01}}{\rightleftharpoons}} A_1 + A$$

$$A_1 + A \underset{k_{21}}{\overset{k_{12}}{\rightleftharpoons}} A_2 + A$$

etc.

In contrast to the series mechanism, the parallel mechanism is the case where the vibrational modes can exchange energy with translation independently. Examples of this are i) a pure polyatomic molecule, which has several vibrational modes, ii) that of a binary mixture of diatomic or polyatomic gases where both species interchange energy with translation independently. In both cases the molecules relax towards equilibrium without disturbing each other and two

Figure 5.1
Relaxation Mechanisms

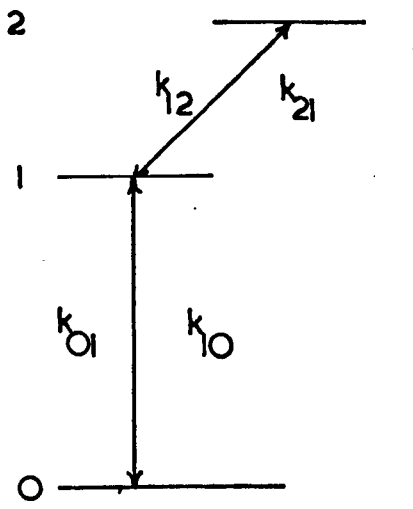

a. SERIES MECHANISM

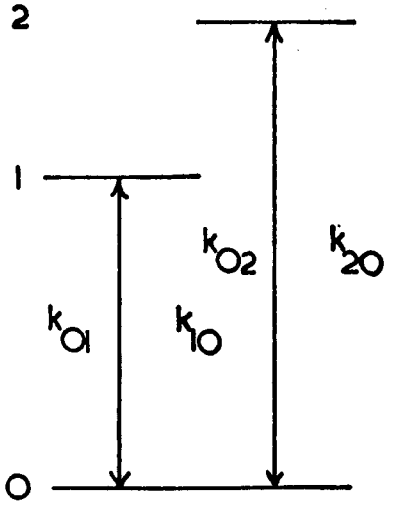

b. PARALLEL MECHANISM

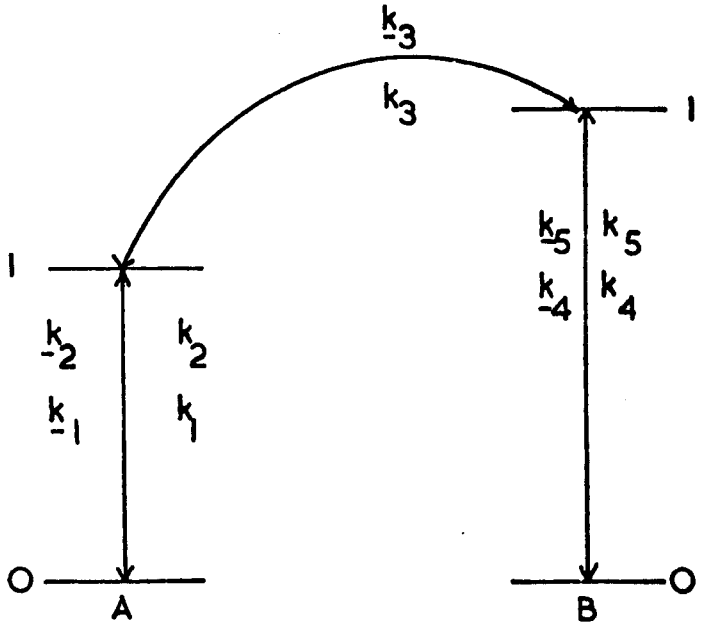

c. COMPLEX MECHANISM

relaxation processes are distinguishable.

In the examples just considered the processes were those involving vibration-translation energy exchange. However, it is possible, in a binary mixture of diatomic or polyatomic gases, for a complex process to take place. The complex process involves vibration-vibration energy exchange. The reactions describing the process are given below. The colliding species are A and B (now diatomic), subscripted 1 if they are vibrationally excited. The rate constants are k_1, k_2 etc. for de-excitation and k_{-1}, k_{-2} etc. for excitation.

1) $A_1 + A \underset{k_{-1}}{\overset{k_1}{\rightleftharpoons}} A_0 + A$ vib.-trans.

2) $A_1 + B \underset{k_{-2}}{\overset{k_2}{\rightleftharpoons}} A_0 + B$ vib.-trans.

3) $A_1 + B_0 \underset{k_{-3}}{\overset{k_3}{\rightleftharpoons}} A_0 + B_1$ vib.-vib. (complex process)

4) $B_1 + B \underset{k_{-4}}{\overset{k_4}{\rightleftharpoons}} B_0 + B$ vib.-trans.

5) $B_1 + A \underset{k_{-5}}{\overset{k_5}{\rightleftharpoons}} B_0 + A$ vib.-trans.

The concentration of the various species are:-

$$A_1 = x_{A1} \qquad A_0 = x_{AO}$$

$$B_1 = x_{B1} \qquad B_0 = x_{BO}$$

$$x_A = x_{A1} + x_{AO}$$

$$x_B = x_{B1} + x_{BO}$$

$$x = x_A + x_B$$

$$1-X = \frac{x_A}{x} \qquad X = \frac{x_B}{x}$$

where X = mole fraction

It is convenient to denote 1) as slower than 4) i.e. pure A has a longer relaxation time than pure B. The mechanism is shown schematically in Figure 5.1.c. Reactions 1, 2 and 4, 5 are simple excitation and de-excitation of A and B. However reaction 3 couples the equilibria of 1, 2 and 4, 5. Thus the relaxation times are not only of 1, 2 and 4, 5 but independent linear combinations of them, which gives a single relaxation behaviour.

The two methods used to analyse the mechanisms are given in the next section.

5.2 KINETIC APPROACH

The basis of this method is to write down the mechanism, derive the rate equations and integrate them in terms of the concentration of a species which is measured experimentally.

5.2.a 1st VIBRATIONAL LEVEL

The excitation to the first vibrational level can be considered in terms of two models.

5.2.a.i 2 STATE MODEL

This model has two vibrational levels, the ground and the first. The reaction is written generally, so that the collision partner M is either another molecule A, or an inert atom B. The concentration of M, x, is the sum of the concentrations of A and B. For clarity the concentration of A_0 and A_1 will be designated x_0 and x_1 respectively.

$$A_0 + M \underset{k'_{10}}{\overset{k'_{01}}{\rightleftharpoons}} A_1 + M$$

$$\therefore \quad \frac{dx_1}{dt} = x(x_0 - x_1)\, k'_{01} - xx_1\, k'_{10}$$

The bimolecular rate constant k'_{01} and k'_{10} may be replaced by the concentration dependent quantities k_{01} and k_{10} equal to $k'_{01}\, x$ and

k'_{10} x respectively.

$$\therefore \quad \frac{dx_1}{dt} = x_0 k_{01} - x_1(k_{01} + k_{10})$$

when $t = 0$, $x_1 = 0$ (a typical condition prior to a shock experiment)

the equation integrates to:-

$$x_1 = \frac{k_{01}}{k_{01} + k_{10}} x_0(1-\exp(-t(k_{01} + k_{10}))) \qquad 5.2$$

Applying the equilibrium conditions (shocked gas fully relaxed)

$$t \rightarrow \infty, \; x_1 \rightarrow x_1^{\infty}$$

5.2 becomes:-

$$x_{1\infty} = \frac{k_{01}}{(k_{01} + k_{10})} x_0$$

$$\therefore \quad \frac{x_1}{x_{1\infty}} = (1-\exp(-t(k_{01} + k_{10}))) \qquad 5.3$$

The relaxation time τ,

$$\tau = (k_{01} + k_{10})^{-1} \qquad 5.4$$

Euqation 5.3 gives an exponential approach to equilibrium. If equation 5.3 is rearranged:-

$$-\ln\left(1 - \frac{x_1}{x_{1\infty}}\right) = \frac{t}{\tau} \qquad 5.3.a$$

Plotting the L.H.S. versus time, a straight line of slope τ^{-1} is obtained.

5.2.a.ii HARMONIC OSCILLATOR MODEL

This model was first treated by Landau and Teller.[1] It is assumed that the molecule is a harmonic oscillator, and that transitions can only occur between adjacent vibrational levels, of which there are an infinite number.

$$M + A_{j-1} \underset{k'_{j,j-1}}{\overset{k'_{j-1,j}}{\rightleftharpoons}} A_j + M \underset{k'_{j+1,j}}{\overset{k'_{j,j+1}}{\rightleftharpoons}} A_{j+1} + M$$

A further condition is that the rate constants have a simple relation to each other:-

$$k_{j+1,j} : k_{j,j-1} = (j+1) : j$$

The equation for the change of population of the j^{th} level:-

$$\frac{dx_j}{dt} = k_{j-1,j}\, x_{j-1} - k_{j,j-1}\, x_j - (k_{j,j+1}\, x_j - k_{j+1,j}\, x_{j+1}) \qquad 5.5$$

and for the lowest state:-

$$\frac{dx_0}{dt} = k_{10} x_1 - k_{01} x_0 \qquad 5.6$$

The change in the total number of quanta is obtained by summing equations 5.5 and 5.6 over all levels. Then the relaxation time is found to be:-

$$\tau = (k_{10} - k_{01})^{-1}$$

In both the two state model and the multistate model the following relationships may apply:-

$$\frac{k_{01}}{k_{10}} = \exp(-h\nu/kT)$$

so that providing:-

$$T << h\nu/k$$

the relaxation time in both cases reduces to:-

$$\tau = k_{10}^{-1} \qquad 5.7$$

The rate constants are temperature dependent so that the equation 5.7 is only valid for oscillators relaxing in a constant temperature heat bath. In most shock tube work this assumption has been made, even for pure gases with vibrational modes.

5.2.b 2nd VIBRATIONAL LEVEL

Three mechanisms explaining the population of the second vibrational level are possible.

5.2.b.i DIRECT MECHANISM

$$A_0 + M \underset{k'_{20}}{\overset{k'_{02}}{\rightleftharpoons}} A_2 + M$$

This reaction is analysed as a 2 state system, see section 5.2.a.i. The result is:-

$$\frac{x_2}{x_{2\infty}} = (1-\exp(-t(k_{02} + k_{20})) \qquad 5.8$$

5.2.b.ii STEPWISE MECHANISM

$$A_0 + M \underset{k'_{10}}{\overset{k'_{01}}{\rightleftharpoons}} A_1 + M$$

$$A_1 + M \underset{k'_{21}}{\overset{k'_{12}}{\rightleftharpoons}} A_2 + M$$

The rate equations are:-

$$\frac{dx_0}{dt} = k_{10} x_1 - k_{01} x_0$$

$$\frac{dx_1}{dt} = k_{01}\,x_0 + k_{21}\,x_2 - k_{12}\,x_1 - k_{10}\,x_1$$

$$\frac{dx_2}{dt} = k_{12}\,x_1 - k_{21}\,x_2$$

These equations were solved by the 'Operator Method', full details of this technique are available.[2] The basis of the method is to let the derivative, d/dt, be designated by P, the operator. Treating P as a constant, many differential equations are reduced to ordinary algebraic equations. The equation can then be solved for the unknown in terms of P. If the transform is known then the final solution can be derived. The operations of setting up the transformed functions and replacing the latter by the originals are based on the Laplace transform. There are a large number of tables (specially for kinetics)[2] relating the transform to the original. The result of applying this method to the above rate equations, with the condition that $x_2 = 0$ when $t = 0$:-

$$x_2 = \frac{x_0 k_{01} k_{12}}{(k_{21}+k_{12}-k_{10}-k_{01})}\left[\frac{(k_{21}+k_{12}-k_{10}-k_{01})}{(k_{01}+k_{10})(k_{21}+k_{12})} - \frac{\exp(-t(k_{01}+k_{10}))}{(k_{10}+k_{01})} + \frac{\exp(-t(k_{12}+k_{21}))}{(k_{12}+k_{21})}\right] \qquad 5.10$$

Applying the Landau-Teller result:-[1]

$$k_{12} = 2k_{01}$$

$$k_{21} = 2k_{10}$$

Thus equation 5.10 reduces to:-

$$x_2 = \frac{k_{01}^2 x_0}{(k_{01}+k_{10})} \left[1-\exp(-t(k_{10}+k_{01})) \right]^2 \qquad 5.11$$

Applying the equilibrium conditions:-

$$t \rightarrow \infty \quad x_2 \rightarrow x_{2\infty}$$

$$\therefore \quad x_0 = \frac{x_{2\infty}\,(k_{01}+k_{10})}{k_{01}^2}$$

$$\therefore \quad \frac{x_2}{x_{2\infty}} = \left[1-\exp(-t(k_{01}+k_{10})) \right]^2 \qquad 5.12$$

Put $\tau = k_{10}^{-1}$ and rearranging:-

$$-\ln(1-(x_2/x_{2\infty})^{\frac{1}{2}}) = t/\tau \qquad 5.12a$$

Plotting the L.H.S. versus time gives a straight line of slope τ^{-1}.

5.2.b.iii RESONANCE MECHANISM

$$A_0 + M \underset{k'_{10}}{\overset{k'_{01}}{\rightleftharpoons}} A_1 + M$$

$$A_1 + A_1 \underset{k_{-2}}{\overset{k_2}{\rightleftharpoons}} A_2 + A_0$$

The second reaction is a complex vibration-vibration energy transfer, of exact resonance (harmonic oscillator) and is assumed to be very rapid. The rate constants k_2 and k_{-2} are for excitation and de-excitation.

The rate equations are:-

$$\frac{dx_1}{dt} = k_{01} x_0 + k_{-2} x_2 x_0 - k_{10} x_1 - k_2 x_1^2 \qquad 5.13$$

$$\frac{dx_2}{dt} = k_2 x_1^2 - k_{-2} x_2 x_0 \qquad 5.14$$

If $x_2 \ll x_1 \ll x_0$ then 5.13 reduces to:-

$$\frac{dx_1}{dt} = k_{01} x_0 - k_{10} x_1$$

the solution of which is:-

$$\frac{x_1}{x_{1\infty}} = (1-\exp(-t/\tau))$$

this is substituted in 5.14

$$\frac{dx_2}{dt} = k_2(x_{1\infty}(1-\exp(-t/\tau)))^2 - k_{-2} x_2 x_0 \qquad 5.15$$

as $t \to \infty$ $\frac{dx_2}{dt} \to 0$

and $x_2 \rightarrow x_{2\infty}$

$$\therefore \quad x_{2\infty} = \frac{k_2 \, x_{1\infty}^2}{k_{-2} \, x_0} \qquad 5.16$$

Substituting 5.16 in 5.15.

$$\frac{d(x_2/x_{2\infty})}{dt} = k_{-2} \, x_0 \, (1-\exp(-t/\tau))^2 - \frac{k_{-2} \, x_2 x_0}{x_{2\infty}}$$

This is rearranged to:-

$$\frac{d(x_2/x_{2\infty})}{dt} + k_{-2} \, x_0 \left(\frac{x_2}{x_{2\infty}}\right) = k_{-2} \, x_0 \, (1-\exp(-t/\tau))^2 \qquad 5.17$$

This is a linear differential of the type:-

$$\frac{dy}{dx} + Py = Q$$

where P and Q are functions of x only or constants. Standard methods can be used for the solution.

$$\therefore \quad \frac{x_2}{x_{2\infty}} = k_{-2} \, x_0 \left[\frac{(1-\exp(k_{-2} \, x_0 t))}{k_{-2} \, x_0} - \frac{2}{(k_{-2} \, x_0 - \tau^{-1})} \right.$$

$$\left. (\exp(-t/\tau)-\exp(-k_{-2} \, x_0 t)) + \frac{1}{(k_{-2} \, x_0 - 2\tau^{-1})} \, (\exp(-2t/\tau)-\exp(-k_{-2} x_0 t)) \right]$$

Putting $k_{-2}\, x_0 \gg \tau^{-1}$

$$\frac{x_2}{x_{2\infty}} = \left[1-2\exp(-t/\tau) + \exp(-2t/\tau)\right]$$

$$\frac{x_2}{x_{2\infty}} = (1-\exp(-t/\tau))^2 \qquad 5.18$$

Thus the result is the same as that deduced in section 5.2.b.ii.

5.2.c BINARY MIXTURES OF EXCITABLE GASES

The kinetic analysis of a binary mixture reaction scheme, see section 5.1, was first attempted by Tuesday and Boudart.[3] The analysis relies upon two hypotheses, a)

$$x_{A1},\ x_{B1} \ll 1-X,\ X$$

$$X \ll 1$$

and, b) $dx_2/dt = 0$ that is that x_2 adjusts very quickly, after being perturbed from equilibrium. Thus it can be shown that:-

$$\frac{1}{\tau_o} = k_1 + (k_2 + (k_3k_5/(k_{-3}+ k_5)))X + ((k_{-3}k_3k_4)|(k_{-3}+ k_5)^2)X^2 \qquad 5.19$$

The full derivation, refinements and experimental observations are to be found elsewhere.[4,5,6,7] There are deficiencies in this technique. These will be commented upon later.

5.3 THE BAUER APPROACH

The Bauer approach[8] is to consider the excitation and de-excitation processes as a series of reactions to which the laws of irreversible thermodynamics apply. During a reversible process a system passes through a continuous series of states of equilibrium. However, during an irreversible process there is a displacement from equilibrium and the 'degree of irreversibility' determines the rate at which the system returns to equilibrium.

The set of relaxation equations are conveniently handled by matrix algebra and solved as an eigenvalue problem, whose latent roots are the desired relaxation times of the various modes.

Bauer has applied the method to consider the relaxation of all the levels of a harmonic oscillator, a binary mixture of excitable gas and inert gas and probably the most important a binary mixture of excitable gases. The full description of the method together with examples is available.[8] The present work will concern itself with the utility of the final equations.

5.3.a BINARY MIXTURES OF EXCITABLE GASES

For clarity the reaction scheme presented in section 5.1 is repeated below:-

1) $A_1 + A \underset{k_{-1}}{\overset{k_1}{\rightleftharpoons}} A_0 + A$

2) $A_1 + B \underset{k_{-2}}{\overset{k_2}{\rightleftharpoons}} A_0 + B$

3) $A_1 + B_0 \underset{k_{-3}}{\overset{k_3}{\rightleftharpoons}} A_0 + B_1$

4) $B_1 + B \underset{k_{-4}}{\overset{k_4}{\rightleftharpoons}} B_0 + B$

5) $B_1 + A \underset{k_{-5}}{\overset{k_5}{\rightleftharpoons}} B_0 + A$

The equation representing this scheme is given by:-

$$\left[\frac{1}{\tau_0} - (1+(x_{A1}/x_{A0}))\,(k_1(1-X) + (k_2+k_3/(1+(x_{B1}/x_{B0})))X) \right]$$

$$\left[\frac{1}{\tau_0} - (1+(x_{B1}/x_{B0}))\,((k_5+k_{-3}/(1+(x_{A1}/x_{A0})))(1-X) + k_4X) \right]$$

$$-k_3k_{-3}(1-X)X = 0 \qquad 5.20$$

The equation 5.20 is quadratic in $\tau^{o\,-1}$ and x_A and x_B. Since $x_A + x_B = 1$, the equation represents a conic section, the four extremities of the section being given by:-

$x_B \to 0$

$$\tau^{o\,-1}_{AA} = (1+(x_{A1}/x_{AO}))k_1$$

$$\tau^{o\,-1}_{BA} = (1+(x_{B1}/x_{BO}))(k_5+k_{-3}/(1+(x_{A1}/x_{AO})) \qquad 5.21$$

$x_A \to 0$

$$\tau^{o\,-1}_{BB} = (1+(x_{B1}/x_{BO}))k_4$$

$$\tau^{o\,-1}_{AB} = (1+(x_{A1}/x_{AO}))(k_2+k_3/(1+(x_{B1}/x_{BO})) \qquad 5.22$$

These four values can be substituted in 5.20:-

$$\left[\frac{1-X}{\tau^{o}_{AA}} + \frac{X}{\tau^{o}_{AB}} - \frac{1}{\tau^{o}}\right]\left[\frac{1-X}{\tau^{o}_{BA}} + \frac{X}{\tau^{o}_{BB}} - \frac{1}{\tau^{o}}\right] - k_3k_{-3}(1-X)X=0 \qquad 5.23$$

A typical conic section, given by 5.23, is shown in Figure 5.2.

where τ^{o} = a measured isothermal relaxation time at unit pressure

τ^{o}_{AA}, τ^{o}_{BB} = isothermal relaxation times in pure A and B

τ^{o}_{AB} = isothermal relaxation time of one molecule of A in B

Figure 5.2
The Conic Section

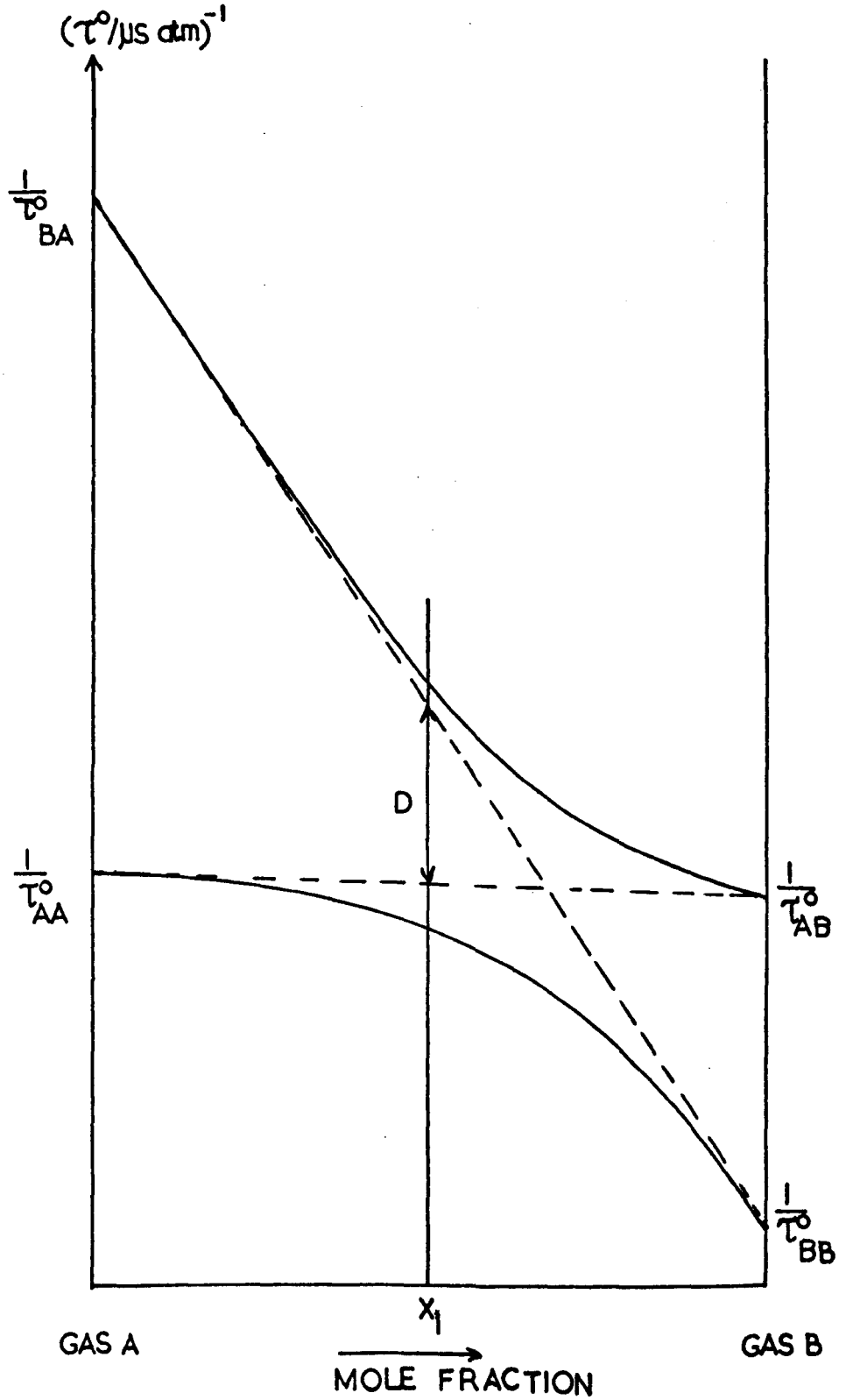

τ^{o}_{BA} = isothermal relaxation time of one molecule of B in A

It should be noted that τ^{o}_{AB} and τ^{o}_{BA} are composite values see equations 5.21 and 5.22, in the respect that they have a vibration-vibration term as well as a vibration-translation term. Thus it is the value of k_3 and k_{-3} which partly governs the position of τ_{AB} and τ_{BA} on the ordinate. If the modes are strongly coupled and k_3 is large then the lines may cross, as shown in the diagram. However when $k_3 \to 0$, the case of two decoupled relaxation processes is obtained, the separate relaxation times τ^{o}_{1}, τ^{o}_{2} being given by:-

$$\frac{1}{\tau^{o}_{1}} = \frac{1-X}{\tau^{o}_{AA}} + \frac{X}{\tau^{o}_{AB}} \qquad 5.24$$

$$\frac{1}{\tau^{o}_{2}} = \frac{1-X}{\tau^{o}_{BA}} + \frac{X}{\tau^{o}_{BB}} \qquad 5.25$$

In this case the conic section is reduced to two straight lines, which do not intersect. In general values of τ^{o}_{1} and τ^{o}_{2} are known, as a function of concentration, and τ^{o}_{AA}, τ^{o}_{BB}, τ^{o}_{AB}, τ^{o}_{BA} can be found. Then the rate constant k_3 is given by:-

$$\frac{1}{\tau^o_1, \tau^o_2} = \frac{1}{2}\left[\frac{1-X}{\tau^o_{AA}} + \frac{X}{\tau^o_{AB}} + \frac{1-X}{\tau^o_{BA}} + \frac{X}{\tau^o_{BB}}\right]$$

$$\pm \frac{1}{2}\sqrt{\left[\frac{1-X}{\tau^o_{AA}} + \frac{X}{\tau^o_{AB}} - \frac{1-X}{\tau^o_{BA}} - \frac{X}{\tau^o_{BB}}\right]^2 - 4k_3k_{-3}(1-X)X} \qquad 5.26$$

The term in brackets under the square root sign is equal to the distance between the pair of lines given by 5.24, 5.25.

$\therefore$ For a specific composition, X_1 on Figure 5.2:-

$$k_3k_{-3} = \frac{(\tau^{o\,-1}_1 - \tau^{o\,-1}_2)^2 - D^2}{4(1-X)X} \qquad 5.27$$

where $k_3 = k_{-3}\,\frac{x_{AO}x_{B1}}{x_{A1}x_{BO}}$ at any temperature the ratios $\frac{x_{A1}}{x_{AO}}$ and $\frac{x_{B1}}{x_{BO}}$ are calculable.

If only a small part of theconic section has been measured, usually near the pure gas value $\tau^{o\,-1}_{AA}$, then starting with $x_B = 0$ the value of $\tau^{o\,-1}_{AA}$ is obtained. The variation of $\tau^{o\,-1}$ caused by small amounts of additive may be expanded in the form of a Taylor series:-

$$\frac{1}{\tau^o} = \frac{1}{\tau^o_{AA}} + w_1x_B + w_2x_B^2 + \text{----} \qquad 5.28$$

The coefficients of which are found to be:-

$$w_1 = k_2 - k_1 + (k_3 k_5 / (k_{-3} + k_5)) \qquad 5.29$$

$$w_2 = k_3 k_{-5} (k_4 - w_1) / (k_{-3} + k_5)^2 \qquad 5.30$$

Substituting 5.29, 5.30 in 5.28

$$\frac{1}{\tau^o} = \frac{1}{\tau^o_{AA}} + (k_2 - k_1 + (k_3 k_5 / (k_{-3} + k_5)))X$$

$$+ (k_3 k_{-3} (k_4 - w_1) / (k_{-3} + k_5)^2) X^2 \qquad 5.31$$

This equation shows a quadratic dependence of τ^o on concentration, similar to the result of Tuesday and Boudart[3] equation 5.19.

Bauer and his co-workers[9,10,11,12] have used this technique to study vibrational relaxation in N_2-CO_2; CH_4-H_2S; CH_4-CO_2; CO-O_2; N_2-O_2 mixtures with an ultrasonic apparatus.

5.4 COMMENTS ON THE METHODS

5.4.a 1st VIBRATIONAL LEVEL

The relaxation times obtained by both the 2 state and harmonic oscillator models are temperature dependent. In most cases a constant shock temperature is assumed and many workers specify the relaxation times at an average temperature of the frozen and relaxed temperature. Methods[13] have been developed to estimate the relaxation times as the temperature changes during a single experiment.

It also should be noted that the population of the first vibrational level, observed in spectroscopic experiments would be given by:-

$$\tau = (k_{01} + k_{10})^{-1}$$

Whereas in measurements of the overall properties of the system such as the vibrational energy or the density, the harmonic oscillator model is probably more realistic:-

$$\tau = (k_{10} - k_{01})^{-1}$$

The application of the condition that $T << h\nu/k$, reduces both approaches to the same result:-

$$\tau = k_{10}^{-1}$$

It is probable that differences in the approaches may only be shown by calculation, since experimental techniques may not be sensitive enough to measure the small difference in τ.

5.4.b 2nd VIBRATIONAL LEVEL

In sections 5.2.b.ii and 5.2.b.ii the equations were derived on the basis of a 3 state model. It has been shown[8] that whether a 3 state or a multistate model be used, then the same relaxation time would be observed, in the pure gas, for the second level as for the first. The reason for this is either a) the correctness of the Landau-Teller ratios 1:2:3 etc. for the rate constants or b) the inclusion of the efficient vibration-vibration exchange reaction in the mechanism. Further comment on this will be made in a later chapter.

One of the factors neglected by the Landau-Teller theory is that of anharmonicity. In this case:-

$$CO_{v=1} + CO_{v=0} \underset{k_{21}}{\overset{k_{12}}{\rightleftharpoons}} CO_{v=2} + CO_{v=0}$$

which means that:-

$$k_{21}\ (\text{Landau-Teller}) < k_{21}\ (\text{Anharmonic})$$

It has been shown theoretically,[14,15] in the case of N_2, that

anharmonicity makes little difference to the relaxation rate, compared to the Landau-Teller result.

Decius[16] has used the multistate harmonic oscillator model with $\Delta v = 1$, to treat the fundamental and overtone emission of a system of oscillators. This model forbids the direct $0 \rightarrow 2$ process. The emission of the fundamental is assumed to arise from all $\Delta v = 1$ down transitions, and the overtone to $\Delta v = 2$ down transitions. Summing over all the vibrational levels equations 5.3.a and 5.12.a were obtained. The same relaxation time is obtained for the fundamental and overtone, in the pure gas, when treated this way.

In the present case the runs involving CO/Ne mixtures equations 5.3.a and 5.12.a were used for analysing the first and second vibrational levels respectively. The relaxation times were plotted against $T^{-\frac{1}{3}}$. The experimentally obtained relaxation times were compared with computer calculations. Relaxation curves of population (intensity) versus time were plotted for given initial conditions. The calculated curves were treated in exactly the same way as the experimental curves, to obtain the relaxation times. Further details will be given in Chapter 8.

5.4.c BINARY MIXTURES OF EXCITABLE GASES

Bauer[8] has criticised the use of the kinetic approach for analysing relaxation processes, on the basis that a rigorous solution

to the rate equations is difficult. It is customary to approximate by invoking a steady state condition for the fast relaxing component. This, according to Bauer, leads to a 'freeway for fallacy'. Henderson et al[6] worked on the O_2/H_2O; O_2/HDO; O_2/D_2O systems. In the O_2/H_2O mixture, they found a disagreement of about a factor of 10 in the results from a direct measurement of the relaxation of pure water, and the indirectly infrared values from the O_2/H_2O measurements, using the Tuesday and Boudart method (section 5.2.c). One of the reasons for failure may be the assumption that:-

$$\frac{dx^*_{H_2O}}{dt} = 0$$

$x^*_{H_2O}$ = concentration of excited water molecule.

Bauer[23] has shown that expansion as a Taylor series of the Tuesday and Boudart method for small concentrations of additive gives the following coefficients:-

$$w_{1\ TB} = k_2 - k_1 + (k_3k_5/(k_{-3} + k_5))$$

$$w_{2\ TB} = k_3k_{-3}k_4/(k_{-3} + k_5)^2$$

These coefficients are to be compared with those obtained by Bauer,[23] namely equations 5.29, 5.30. The value of w_1 is the same in both cases, but w_2 differs. This may be a consequence of assuming the state steady

in the kinetic approach.

It should be noted that the kinetic and Bauer approaches, for binary mixtures of excitable gases, use a two state model for each vibration. However, at temperatures experienced in the shock tube the two state approximation may be inaccurate. Bauer[10] has stated that the same results, the same conic sections, would be obtained if a harmonic oscillator model was used, with Landau-Teller ratios between the rate constants.

In the present case the CO/polyatomic mixtures, the first level of CO was observed and the relaxation time was extracted by use of equation 5.3.a. The Bauer approach was used to analyse these mixtures. Further discussion will be left until Chapter 8.

REFERENCES

1. L.D. Landau and E. Teller, Z. *Phys. Sowjetunion*, 1936, 10, 34.

2. N.M. Rodiguin and E.N. Rodiguina, *Consecutive Chemical Reactions* (D. Van Nostrand Co. Inc., New Jersey) 1964.

3. C.S. Tuesday and M. Boudart, *Tech. Note 7, Contract AF35 (038)-23976*, Princeton University, 1955.

4. K.F. Herzfeld and T.A. Litovitz, *Absorption and Dispersion of Ultrasonic Waves* (Academic Press, London) 1959, 212.

5. D.G. Jones, J.D. Lambert and J.L. Stretton, *Proc. Phys. Soc.*, 1965, 86, 857.

6. M.C. Henderson, A.V. Clark and P.R. Lintz, *J. Acoust. Soc. Amer.*, 1965, 37, 457.

7. M.C. Henderson and K.F. Herzfeld, *J. Acoust. Soc. Amer.*, 1965, 37, 986.

8. H.-J. Bauer, *Physical Acoustics* (Academic Press, London) 1965, Vol II-A, 47.

9. H.-J. Bauer and H. Roesler, *Z. Naturforsch*, 1964, 19, 656.

10. H.-J. Bauer and H. Roesler, *Molecular Relaxation Processes* (Academic Press, London) 1966, No. 20, 245.

11. H.-J. Bauer and R. Schotter, *6th International Congress on Acoustics*, Tokyo, Japan, 1968, J-13.

12. H.-J. Bauer and R. Schotter, *J. Chem. Phys.*, 1969, 51, 3261.

13. N.H. Johannesen, *J. Fluid Mech.*, 1961, 10, 25.

14. K.N.C. Bray, *Fluid Mechanic Laboratory Publication, Massachusetts Institute of Technology*, 1967, 67-3.

15. K.N.C. Bray, *J. Phys. B (Proc. Phys. Soc.)* 1968, Ser 2, Vol 1, 705.

16. J.C. Decius, *J. Chem. Phys.*, 1960, 32, 1262.

17. H.-J. Bauer, *J. Accoust. Soc. Amer.*, 1967, 42, 258.

6. TREATMENT OF RESULTS

6.1 CALCULATION OF RELAXATION TIMES

To calculate the relaxation times from the photographs of intensity versus time, it was necessary to assume a model for the relaxation process. The details of the processes and the analytical equations are set out in Chapter 5. Figure 6.1 shows the ideal relaxation curves for the first (I) vibrational level of a 2 state system and second (II) vibrational level of a 3 state system. Curve I was constructed using the equation:-

$$\frac{x_1}{x_{1\infty}} = (1 - \exp(-t/\tau)) \qquad 6.1$$

and curve II:-

$$\frac{x_2}{x_{2\infty}} = (1 - \exp(-t/\tau))^2 \qquad 6.2$$

In the present example, τ the relaxation time, was chosen to be 20 μs, and x, x_∞ are the intensities of emission at times t and ∞ respectively. The figure will serve to exemplify the methods by which the relaxation times were obtained.

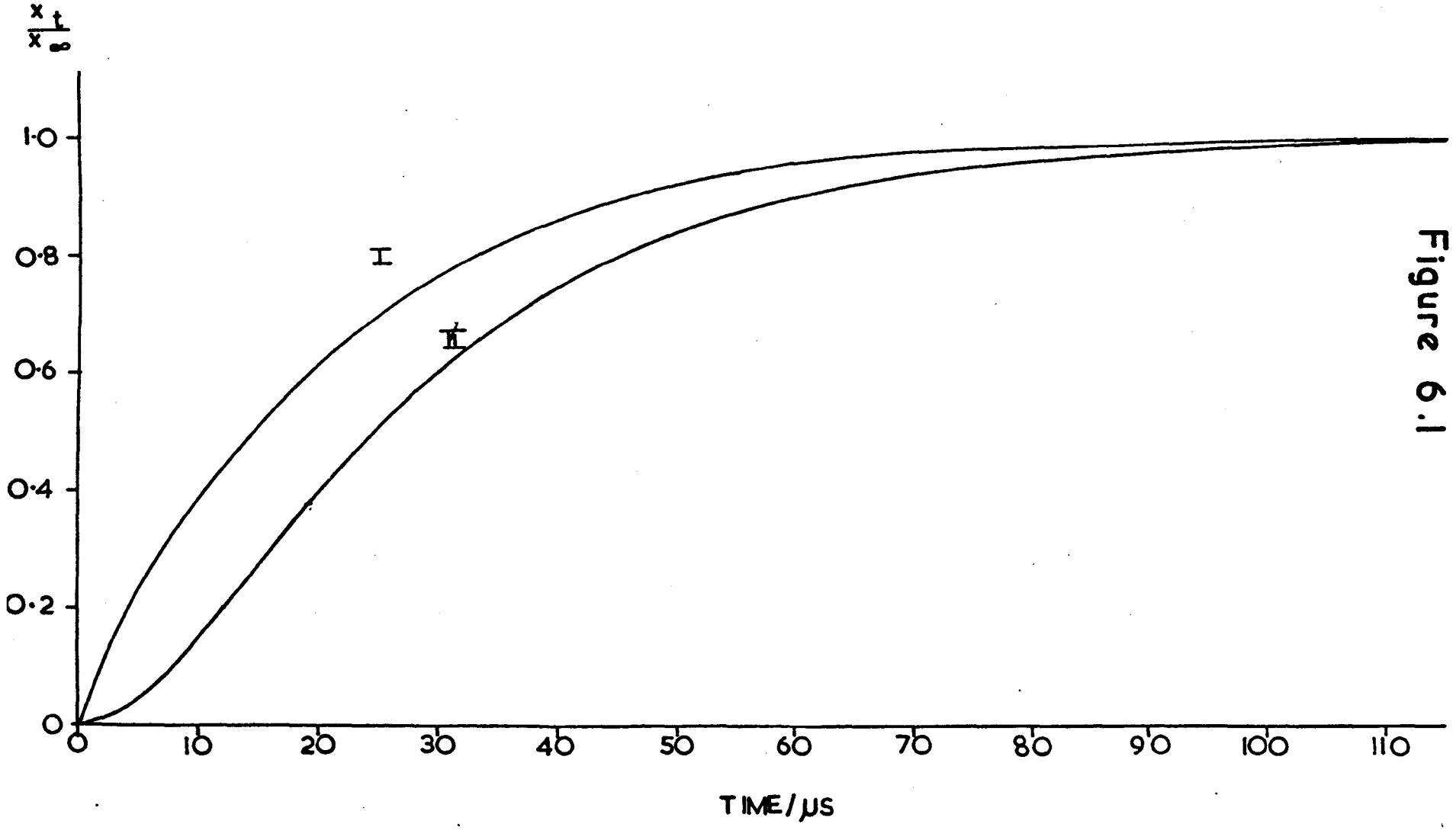
$\frac{x_t}{x_\infty}$
1·0
0·8
0·6
0·4
0·2
0
I
II
0
10
20
30
40
50
60
70
80
90
100
110
TIME/μs

Figure 6.1

Equations 6.1 and 6.2 can be rearranged:-

$$-\ln(1 - \frac{x_1}{x_{1\infty}}) = t/\tau \qquad 6.3$$

and

$$-\ln(1 - (\frac{x_2}{x_{2\infty}})^{\frac{1}{2}}) = t/\tau \qquad 6.4$$

In both cases the plotting of the L.H.S. versus time yielded the slope which was the reciprocal of the relaxation time. It was possible to take the intensity-time data from the Figure 6.1, by the use of a Demac Pencil Follower. This device consisted of a table, to which the figure could be attached, and which was mapped out in XY coordinates. The X coordinates had a digital readout value ranging from 0000 through 9999, and the Y coordinate 0000 through 4500. The XY coordinate of any point was registered on a digital display unit and the values could be punched onto paper tape. A computer programme[1] was devised to process the paper tape. The table coordinates were converted into the figures coordinates, and plots of the L.H.S. of equations 6.3 and 6.4 versus time made on the computer graph plotter. The results of the analysis of curves I and II is shown in Figures 6.2, 6.3 respectively, together with the relaxation times. A least squares routine was included in the computer programme to calculate the relaxation time. One further method was available for the solution of curve II.

Figure 6.2

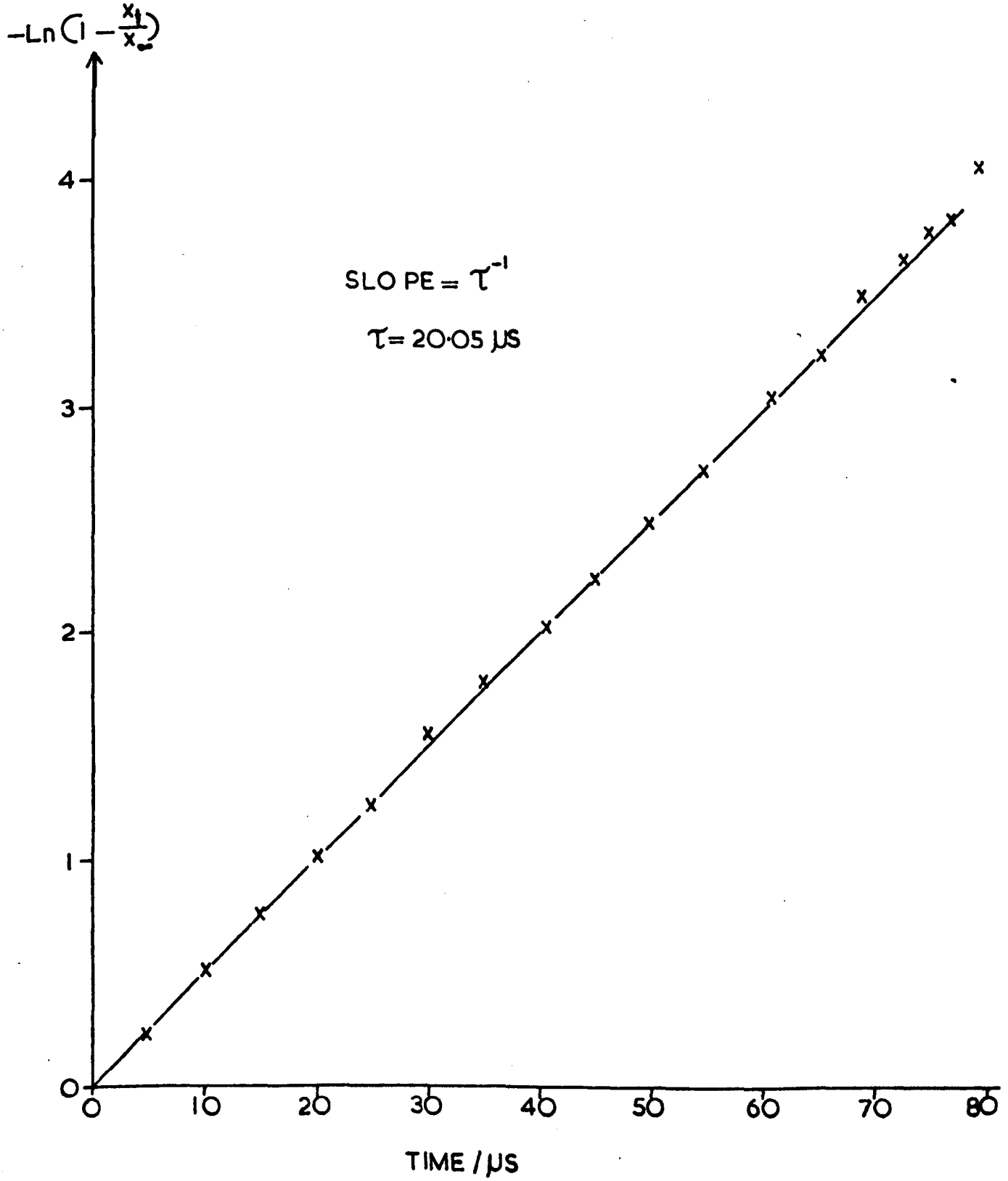
$-Ln\left(1-\frac{x_1}{x_\infty}\right)$
4
3
2
1
0
SLOPE = τ^{-1}
τ = 20·05 μS
0
10
20
30
40
50
60
70
80
TIME / μS

Figure 6.3

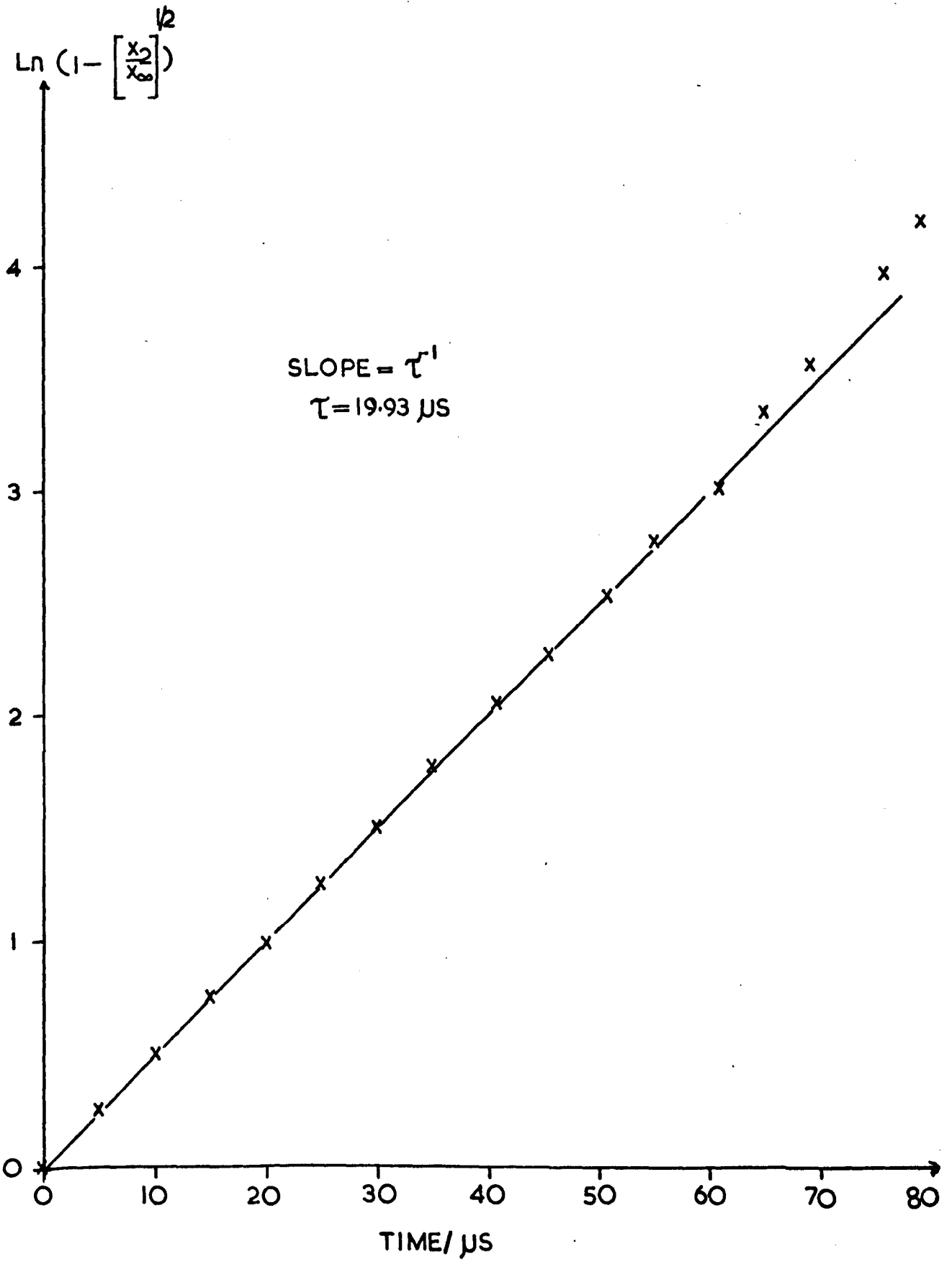

$$\frac{x_2}{x_{2\infty}} = 1 - 2\exp(-t/\tau) + \exp(-2t/\tau) \qquad 6.5$$

$$\frac{d\left(\frac{x_2}{x_{2\infty}}\right)}{dt} = \frac{2}{\tau}\exp(-t/\tau) - \frac{2}{\tau}\exp(-2t/\tau) \qquad 6.6$$

$$\frac{d^2\left(\frac{x_2}{x_{2\infty}}\right)}{dt^2} = -\frac{2}{\tau^2}\exp(-t/\tau) + \frac{4}{\tau^2}\exp(-2t/\tau)$$

At the point of inflexion:-

$$\frac{d^2\left(\frac{x_2}{x_{2\infty}}\right)}{dt^2} = 0$$

$\therefore$ $\exp(-t/\tau) = \frac{1}{2}$

$\therefore$ Taking 6.5.

$$\frac{x_2}{x_{2\infty}} = \frac{1}{4}$$

Taking 6.6.

$$\frac{\text{Slope}}{x_{2\infty}} = \frac{1}{2\tau} \quad \text{at} \quad x_2 = \frac{x_{2\infty}}{4}$$

$$\text{Slope} = \frac{2x_2}{\tau} \qquad 6.7$$

The comparison of the results obtained is given below:-

TABLE 6.1

Theoretical Relaxation Time = 20 μs

	Plot	Least Squares	Eq. 6.7
Curve I	20.05 μs	20.03 μs	-
Curve II	19.93 μs	20.01 μs	21.4 μs

Thus the chosen method of analysis reproduced the relaxation time to an excellent degree of accuracy. The method involving equation 6.7 had an error of 7%.

The same procedure was used to analyse the experimentally obtained photographs. The measured time axis on the photographs was expressed in laboratory coordinates, and it was shorter than the actual time elapsed after the shock had passed. The conversion from laboratory to particle time required a knowledge of conditions in the shocked region.

6.2 CALCULATION OF SHOCK PARAMETERS

The shock tube study required many calculations of the state of the gas behind the shock wave as energy was taken up by the various degrees of freedom. The experimental data consisted of the measured shock wave velocity, the initial pressure, the temperature, the molecular weights and the composition of the mixture. The heat capacity as a function of temperature for each gas in the mixture was required. From this data it was possible to calculate the gas conditions behind the shock.

The equations used were derived assuming, ideal gases, one-dimensional flow and no interaction with the walls. Thus mass, momentum and energy were conserved across the shock wave. The derivations and methods of solution have been dealt with.[2,3,4] The method used in this study was an iterative method, using a computer, suggested by Millikan.[5,6] The details of the technique are given below.

The pressure, density and temperature ratio, across the shock wave were calculated from:-

$$\frac{P_A}{P_1} = \frac{2\ \bar{\gamma}\ M^2 - (\bar{\gamma} - 1)}{(\bar{\gamma} + 1)}$$

$$\frac{\rho_A}{\rho_1} = \frac{(\bar{\gamma} + 1)\ M^2}{(\bar{\gamma} - 1)\ M^2 + 2}$$

$$\frac{T_A}{T_1} = \frac{P_A}{P_1} \Big/ \frac{\rho_A}{\rho_1}$$

where $M = \frac{u}{a}$ = Mach number

u = shock velocity

$a = \frac{1}{10} (0.8313\ \bar{\gamma}\ T_1 / \overline{M.W.})^{\frac{1}{2}}$

a = speed of sound in the gas

$\bar{\gamma}$ = average specific heat ratio

$\overline{M.W.}$ = average molecular weight

T_1, P_1, ρ_1 = initial temperature, pressure and density.

The conditions obtained for the state A corresponded to the uptake of energy behind the shock, by the translational and rotational degrees of freedom only. The gas properties in state 2, that is after vibrational energy is taken up, were then calculated. This was achieved by a method successive approximations involving an energy balance across the shock wave. For the first iteration the gas properties of state A were used. The energy required to heat the gas to temperature T_A was calculated from:-

$$\Delta H = H_{T_A} - H_{T_1}$$

$$= g(T_A) - g(T_1)$$

The enthalpy function g(T) is described below.

The enthalpy difference ΔH can also be calculated from the fluid dynamic equation:-

$$\Delta H^{*} = 119.503\ u^2\ \overline{M.W.}\ \left(1 - \left(\frac{\rho_1}{\rho_2}\right)^2\right)$$

where the enthalpy is in cal mol^{-1}. Then the energy difference was found.

$$\Delta E = \Delta H - \Delta H^{*}$$

A new rough temperature may be calculated:-

$$T' = T_A - (\Delta E / C_P)$$

C_P is the average heat capacity, assumed here to be 10 cal mol^{-1} (41.8 J mol^{-1}). This gives a 1% temperature error in T_2. New values of the density and pressure ratios corresponding with T' were obtained from:-

$$\frac{\rho'}{\rho_1} = \frac{P_A}{P_1} \Big/ \frac{T'}{T_1}$$

$\frac{P_A}{P_1}$ being used since the pressure was usually constant.

$$\frac{P'}{P_1} = 1 + \frac{120.274\ \overline{M.W.}\ u^2}{T_1}\ \left(1 - \frac{\rho_1}{\rho'}\right)$$

This completed one round of the iteration. If E is larger than 10 cal mol^{-1}, then a second iteration was begun using T', ρ'/ρ_1

and P'/P_1 as the initial values.

The enthalpy function for the mixture g(T) was related to the enthalpy function for the individual species $f_j(T)$ by:-

$$g(T) = \sum_{j=1}^{s} F_j f_j(T) \quad s < 5$$

where F_j = the mole fraction of species j

and $f_j(T) = A + BT^2 + CT^3 + DT^4$ 6.8

The coefficients of equation 6.8 were obtained from a curve fitting of the tabulated enthalpy data.[7] A computer programme[1] was available to obtain the coefficients. The comparison between the tabular values and those calculated from equation 6.8 are shown in Figure 6.4. The diatomic molecules CO and N_2 showed little variation in the region of interest, 1200 K - 2500 K, the temperature error being at a maximum of about 0.25%. However, the polyatomic molecules showed a wider fluctuation over the temperature range, the maximum error being about 1%. Since the polyatomic species were only in small concentrations (2% maximum) in mixtures, then their effect on the overall calculated temperatures of the mixture was very small.

An analytical method for the solution of the equations for shock conditions in state 2 has been suggested by Campbell and Klimas.[8]

The results of the present calculations are shown in Figure 6.5 for pure carbon monoxide. The density and pressure have larger values in the relaxed gas than in the frozen gas, while the value of

Figure 6.4
Comparison Of Tabulated And Calculated Enthalpies

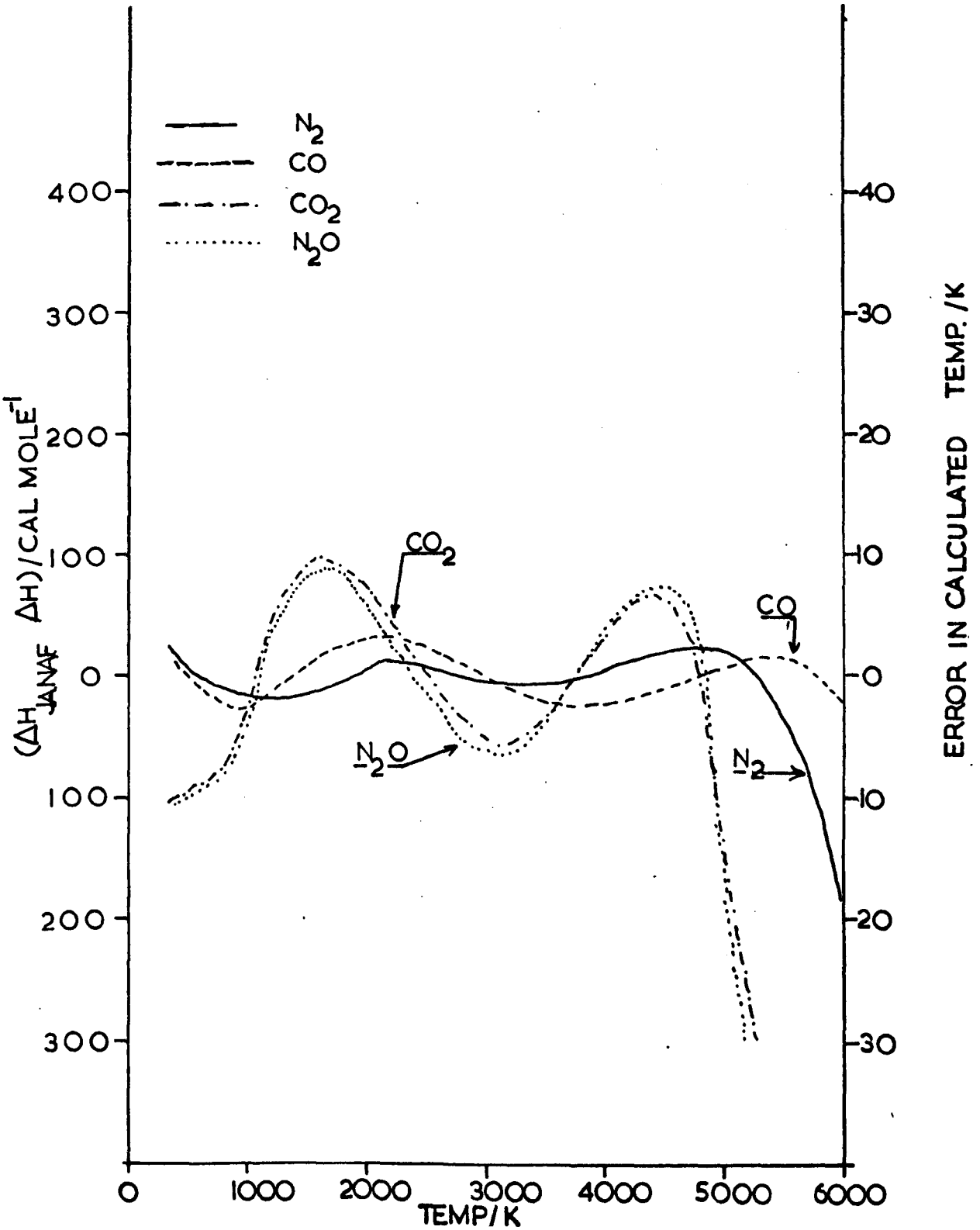

Figure 6.5
Shock Parameters In Pure CO

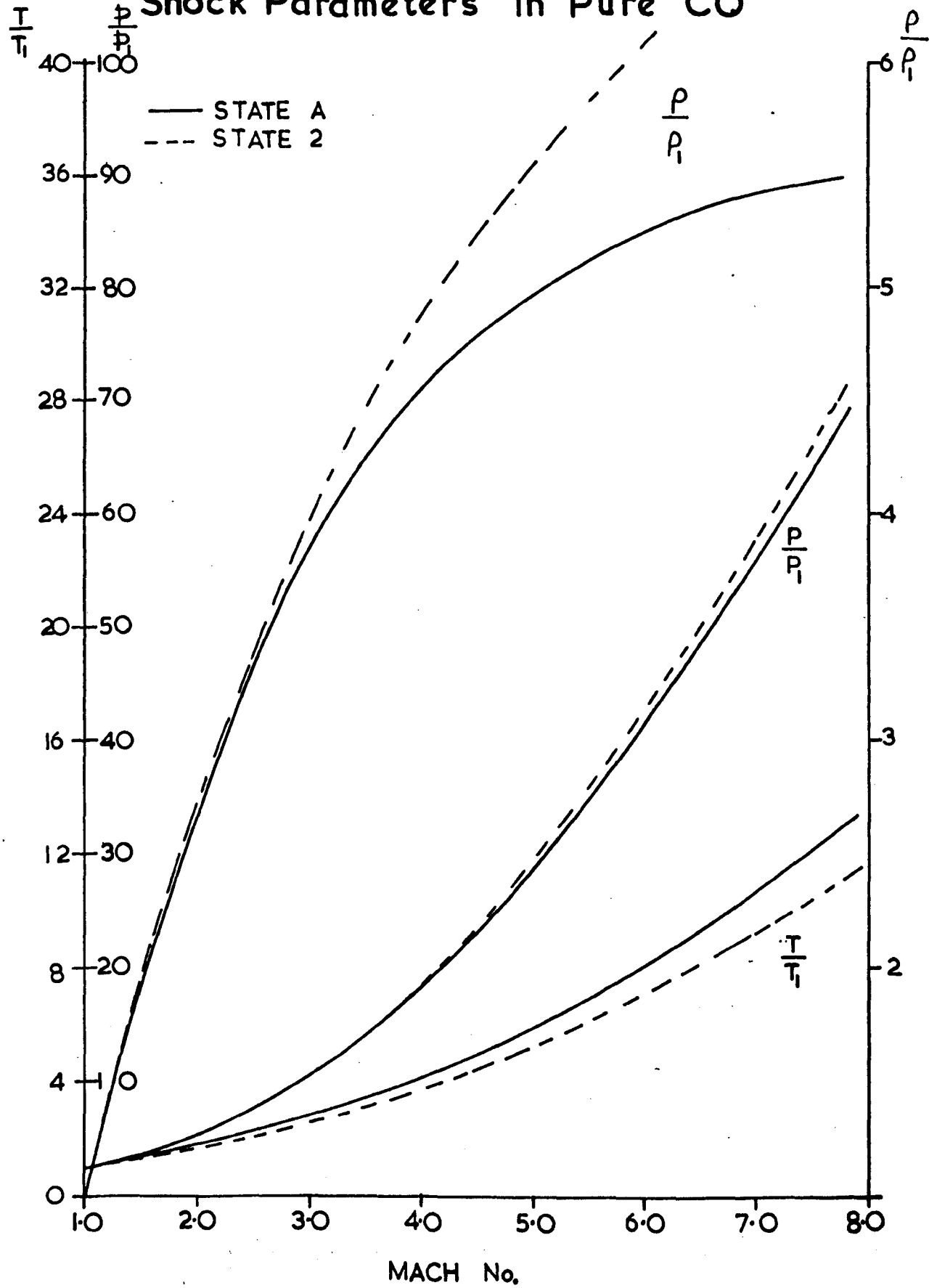

the temperature is less. These results were calculated assuming ideal flow conditions. As was pointed out in Chapter 3, the formation of a boundary layer and the deceleration of the shock wave required that adjustments must be made to the conditions behind the shock. The density and temperature were corrected, according to the procedures laid out in Chapter 3. The corrected results are compared to those calculated from ideal conditions, in Figure 6.6, for pure carbon monoxide. It can be seen that the correction to the average density ratio ranges between 8% - 13% and the average shock temperature ranges between 3% - 5%, with increase in Mach number. The corrected values were always used in the present calculations.

Figure 6.6

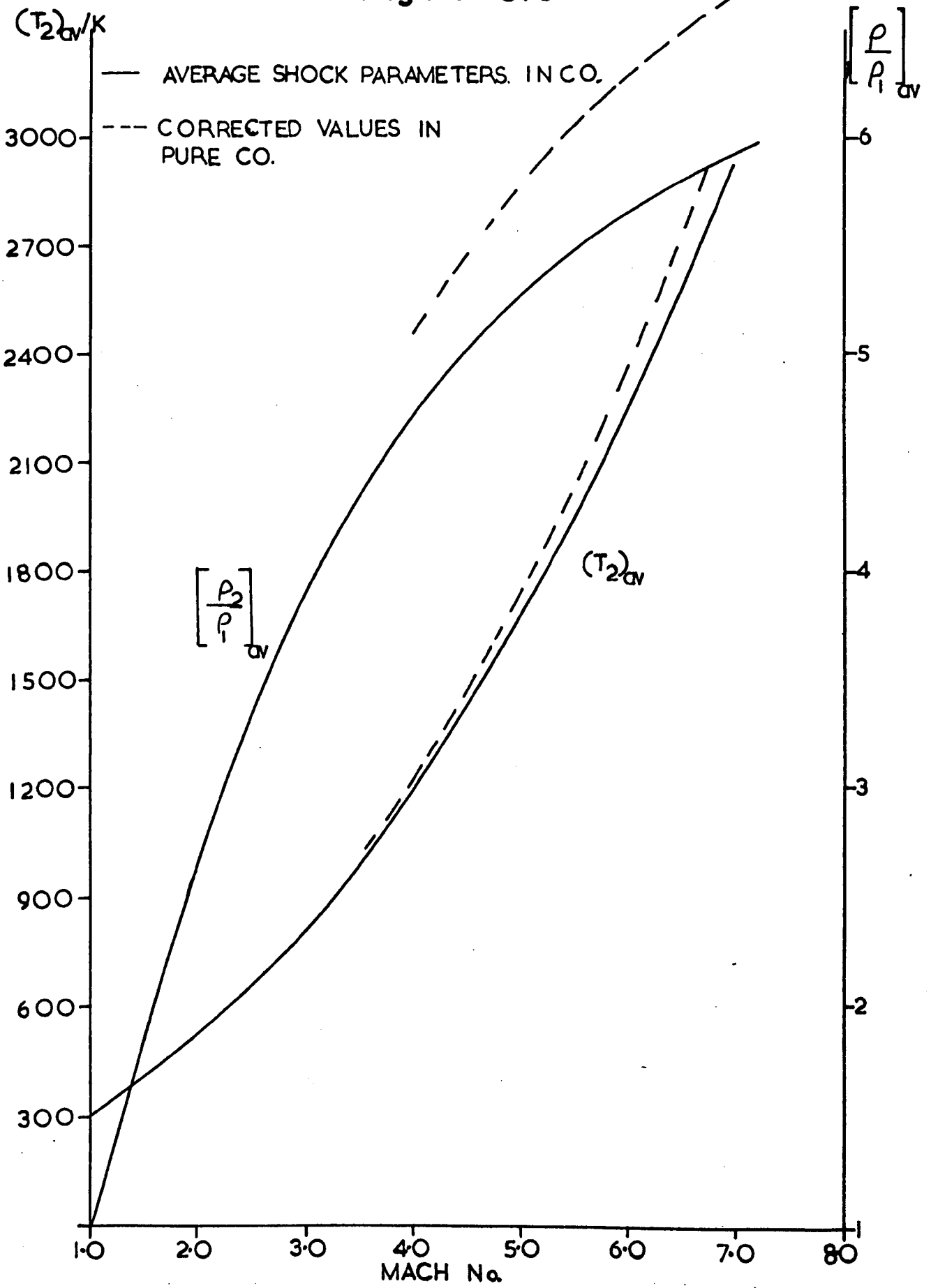
$(T_2)_{av}$/K
AVERAGE SHOCK PARAMETERS. IN CO.
CORRECTED VALUES IN PURE CO.
$\left[\frac{\rho}{\rho_1}\right]_{av}$
3000
2700
2400
2100
1800
1500
1200
900
600
300
6
5
4
3
2
1
$\left[\frac{\rho_2}{\rho_1}\right]_{av}$
$(T_2)_{av}$
1·0
2·0
3·0
4·0
5·0
6·0
7·0
8·0
MACH No.

6.3 PARTICLE TIME AND NAPIER TIME

Figure 6.7 represents the compression of the observation time. The particles are travelling behind the shock front at a velocity v_2, which is less than the shock velocity v_1. The particle time, t_p, is the time for the particle to reach the observer after being shocked. During this time the shock front has travelled $v_1 t_p$, and the particle $v_2 t_p$. The laboratory time is the time since the shock passed the observer and it has travelled a distance $v_1 t_\ell$.

$$\therefore \quad v_1 t_p = v_2 t_p + v_1 t_\ell$$

$$\therefore \quad \frac{t_p}{t_\ell} = \frac{v_1}{v_1 - v_2}$$

This is related to fixed shock coordinates by:-

$$\frac{t_p}{t_\ell} = \frac{v_1}{v_1 - v_2} = \frac{u_1}{u_2} = \frac{\rho_2}{\rho_1}$$

Thus to compensate for the time compression the relaxation time, obtained in laboratory coordinates, was corrected to the particle time by multiplying by the average density ratio.

In the relaxation of gas phase systems the energy is transferred between degrees of freedom, during bimolecular collisions. Thus, τ, is a pressure dependent quantity, and the value of τ is quoted for standard conditions of pressure. The resulting quantity is called the Napier time.

Figure 6.7
Compression Of The Observation Time

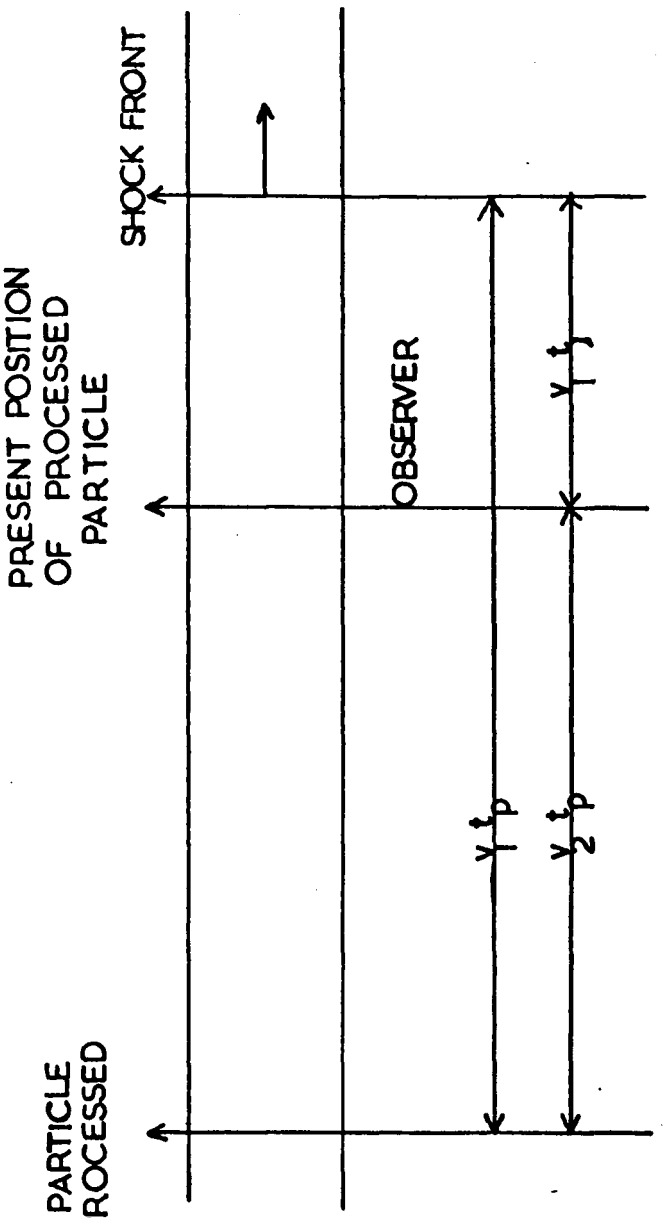

Thus in the present studies the value of τ was calculated from:-

$$\tau_p = \tau_\ell \times \left(\frac{\rho_2}{\rho_1}\right)_{av} \times \left(\frac{P_2}{P_1}\right)_{av} \times \frac{P_1}{760} \quad \mu s \text{ atm}$$

where τ_p = particle relaxation time μs atm

τ_ℓ = laboratory relaxation time μs

P_1 = downstream pressure mm

$\left(\frac{\rho_2}{\rho_1}\right)_{av}$, $\left(\frac{P_2}{P_1}\right)_{av}$ = average density and pressure ratios at temperature $(T_2)_{av}$.

REFERENCES

1. R. Gutteridge, *Ph.D. Thesis*, to be published.

2. A.G. Gaydon and I.R. Hurle, *The Shock Tube in High Temperature Chemical Physics*, (Chapman and Hall Limited, London), 1963, Chapter II.

3. J.N. Bradley, *Shock Waves in Chemistry and Physics*, (Methuen and Company Limited, London), 1962, Chapter II.

4. I.I. Glass, *Theory and Performance of Simple Shock Tubes*, Institute of Aerophysics, Rpt. No. 12, 1958.

5. R.C. Millikan, *General Electric Research Laboratory Rpt.*, (Schenectady, New York), 1964, No. 64-RL-3700C.

6. R.C. Millikan, *General Electric Research Laboratory Rpt.*, (Schenectady, New York), 1965, No. 65-C-106.

7. J.A.N.A.F., *Thermochemical Tables*, The Dow Chemical Company, Midland, Michigan, 1965.

8. G.S. Campbell and P.C. Klimas, *A.I.A.A. Journal*, 1967, 5, 1713.

7. RESULTS

This chapter contains the results obtained in the present study. Section 7.1 shows that the energy of the observed emissions corresponded to the energy of the $1 \rightarrow 0$ and $2 \rightarrow 0$ transitions. Section 7.2 shows the effect of the flow corrections on the relaxation times of the first vibrational level of pure carbon monoxide.

7.1 ENERGY OF THE OBSERVED EMISSION

The equilibrium population of the ith vibrational level with energy ε_i, of a harmonic oscillator is given by:-

$$n_i = N \exp(-\varepsilon_i/kT)/p.f. \qquad 7.1$$

where N = total number of molecules

n_i = number of molecules in level i

T = absolute temperature K

k = Boltzmann constant

The partition function, p.f., is given by:-

$$p.f. = \exp(-\varepsilon/2kT)/(1-\exp(-\varepsilon/kT)) \qquad 7.2$$

ε = energy separation of the vibrational levels.

Substituting 7.2 in 7.1

$$n_i/N = \exp(-\varepsilon_i/kT)\ (1-\exp(-\varepsilon/kT))/\exp(-\varepsilon/2kT)$$

Rearranging:-

$$\ln n_i/N = -(\varepsilon_i/kT-\varepsilon/2kT) + \ln(1-\exp(-\varepsilon/kT))$$

Differentiating:-

$$\frac{d \ln n_i/N}{dT^{-1}} = -(\varepsilon_i-\varepsilon/2)k^{-1} + \varepsilon/k\ (\exp(\varepsilon/kT) - 1) \qquad 7.3$$

$$N = \frac{P_1}{760} \times \frac{\rho_2}{\rho_1}$$

ρ_2/ρ_1 = density ratio

P_1 = downstream pressure

n_i corresponds to the concentration of oscillators in state i at equilibrium, and is equated to I_∞. To a good approximation, a plot of $\ln(n_i/N)$ versus T^{-1}, should give straight lines of slope $(\varepsilon_i - \varepsilon/2)k^{-1}$. The second term in 7.3, has a small value when the temperature is low. The term has more effect as the temperature increases, and the value of $\exp(\varepsilon/kT)$ decreases. At 2000K the value of the second term is $\approx 800\ K^{-1}$ compared to $(\varepsilon_i - \varepsilon/2)k^{-1}$ which is $\approx 3100\ K^{-1}$. Plots were carried out for the first and second vibrational levels of pure carbon monoxide. The Tables 7.1 and 7.2 contain the data, and Figure 7.1 shows the points plotted. For

the first vibrational level, the slope from Figure 7.1 was found to be $3333K^{-1}$ and $(\varepsilon_i - \varepsilon/2)$ was 27.64 kJ mol^{-1}. The energy of the first vibrational level is known to be 25.64 kJ mol^{-1}. Similarly for the seond vibrational level, the value of $(\varepsilon_i - \varepsilon/2)$ is 52.70 kJ mol^{-1} and the known value is 50.95 kJ mol^{-1}. The figures indicate that the emission is due largely from the experimentally observed levels. Thus in the case of the first vibrational level contributions to the emission from transitions such as $2 \rightarrow 1$, $3 \rightarrow 2$ etc. are expected to be small. Similar applies to the second vibrational level where transitions such as $3 \rightarrow 1$, $4 \rightarrow 2$ are involved.

TABLE 7.1

FIRST VIBRATIONAL LEVEL

Photo No.	P_1 mm	$(\rho_2/\rho_1)_{av}$	I_∞	$\ln n_i/N$	$(T_2)_{av}$ K	$(T_2)^{-1}_{av} \times 10^4$
1103	8.5	6.011	11.5	6.528	1890	5.291
1104	12.5	5.755	12	6.245	1671	5.984
2101	11.9	5.799	11.5	6.311	1691	5.913
2102	9.9	5.949	12	6.429	1856	5.388
2103	9.1	6.058	12.5	6.536	1945	5.141
2104	8.0	6.098	12	6.617	1991	5.022
2105	7.0	6.224	12.5	6.771	2104	4.753
2106	5.9	6.231	12.5	6.941	2116	4.726
2107	8.7	6.054	12	6.541	1925	5.194

TABLE 7.2

SECOND VIBRATIONAL LEVEL

Photo No.	P_1 mm	$(\rho_2/\rho_1)_{av}$	I_∞	$\ln n_i/N$	$(T_2)_{av}$ K	$(T_2)_{av}^{-1} \times 10^4$
1201	11.4	5.98	15.5	5.152	1773	5.64
1202	8.1	5.994	15.5	5.491	1818	5.501
1203	8.5	6.093	16	5.459	1930	5.18
1204	7.4	6.201	16	5.580	2022	4.945
2205	7.8	6.177	17	5.59	2014	4.965
2206	4.2	6.30	16	6.188	2184	4.58

Figure 7.1

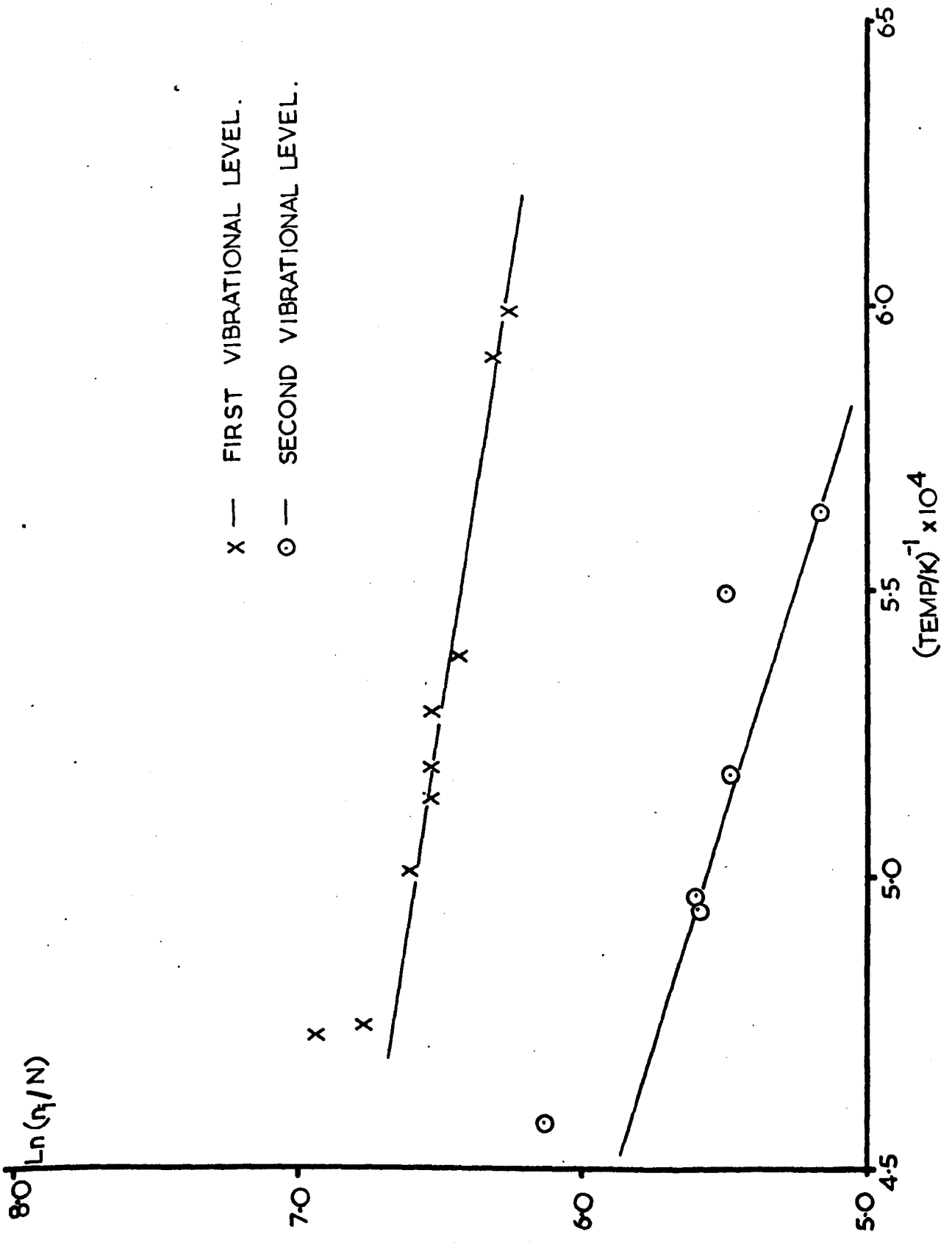
X — FIRST VIBRATIONAL LEVEL.
⊙ — SECOND VIBRATIONAL LEVEL.
Ln(n_J/N)
8·0
7·0
6·0
5·0
4·5
5·0
5·5
6·0
6·5
(TEMP/K)^-1 x 10^4

7.2 EFFECT OF FLOW CORRECTION

The following section shows the effect, on the relaxation time, of applying the corrections, due to non uniform flow (Chapter 3), to the shock parameters (Chapter 6) of density and temperature. Table 7.3, Figure 7.2 show the uncorrected data with respect to the work of Hooker and Millikan.[1] The present work gives relaxation times which are lower by approximately 26%. If the corrections are applied to the data, using a 1% m^{-1} velocity decrement, the points are adjusted to give relaxation times approximately 4.2% lower than the values of Hooker and Millikan.[1] This is shown in Table 7.4, Figure 7.3. The velocity decrement in the present case was found to be 2% m^{-1} and the result of using this value in the corrections is shown in Table 7.5, Figure 7.4. The data gives good agreement with the previous work. The corrections for non uniform flow were applied in every case in the present work. A velocity decrement of 2% m^{-1} was observed for the majority of mixtures, and this value was used in the calculations.

It is believed that the present calculational procedure is sound, and that the corrected values of the shock parameters are more realistic estimates of the conditions behind the shock wave. Belford and Strehlow[2] have urged workers to always make estimates of the non uniform flow corrections, and to present them so that others may assess them. This has been done by several workers.[3,4,5,6,7]

TABLE 7.3

PURE CO 1ST VIBRATIONAL LEVEL UNCORRECTED DATA

Photo No.	P_1 mm	Shock Speed$_1$ mm μs^{-1}	Shock Mach No.	Av.Shock Temp K	$(\text{Temp})^{-\frac{1}{3}}$	$(\rho_2/\rho_1)_{av}$	$(P_2/P_1)_{av}$	Lab Time μs	Napier Time μs atm
1101	9.9	1.8164	5.154	1752	0.08295	5.358	31.21	43.9	95.6
1103	8.5	1.8528	5.257	1809	0.08206	5.401	32.50	38.4	75.4
1104	12.3	1.7205	4.882	1606	0.08539	5.235	27.87	58.7	138.6
2101	11.9	1.7313	4.913	1622	0.08510	5.249	28.33	59.5	138.5
2102	9.9	1.8344	5.205	1780	0.08251	5.379	31.84	41.1	91.6
2103	9.1	1.8844	5.347	1860	0.08131	5.438	33.63	33.0	72.2
2104	8.0	1.9103	5.421	1903	0.08069	5.468	34.58	34.0	67.7
2105	7.0	1.9715	5.594	2004	0.07932	5.534	36.85	28.1	52.8
2106	5.9	1.9786	5.614	2016	0.07916	5.541	37.12	31.0	49.5
2107	8.7	1.8716	5.311	1840	0.08160	5.424	33.16	39.0	80.3

Figure 7.2

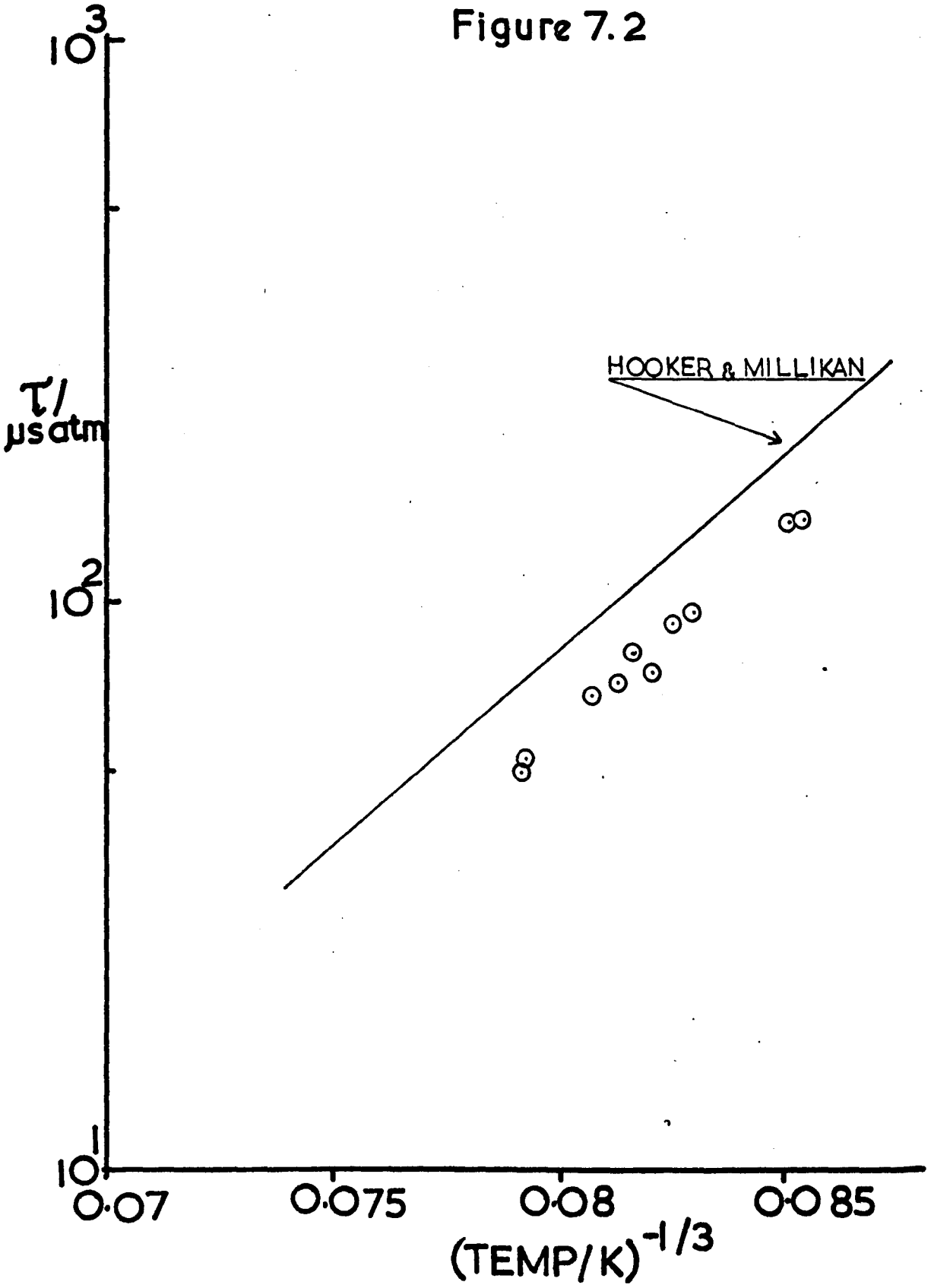
10^3
10^2
10^1
τ/ μs atm
HOOKER & MILLIKAN
0·07
0·075
0·08
0·085
(TEMP/K)$^{-1/3}$

TABLE 7.4

PURE CO 1ST VIBRATIONAL LEVEL - 1% VELOCITY DECREMENT

Photo No.	P_1 mm	Shock Speed$_1$ mm μs^{-1}	Shock Mach No.	Av.Shock Temp K	$(\text{Temp})^{-\frac{1}{3}}$	$(\rho_2/\rho_1)_{av}$	$(P_2/P_1)_{av}$	Lab Time μs	Napier Time μs atm
1101	9.9	1.8164	5.154	1832	0.8172	5.818	31.21	43.9	103.9
1103	8.5	1.8528	5.257	1875	0.08109	5.901	32.50	38.4	82.4
1104	12.3	1.7205	4.882	1657	0.08450	5.655	27.87	58.7	149.7
2101	11.9	1.7313	4.913	1677	0.08416	5.689	28.33	59.5	150.2
2102	9.9	1.8344	5.205	1842	0.08158	5.849	31.84	41.1	99.7
2103	9.1	1.8844	5.347	1929	0.08033	5.938	33.63	33.0	78.9
2104	8.0	1.9103	5.421	1975	0.07970	5.988	34.58	34.0	74.0
2105	7.0	1.9715	5.594	2086	0.07826	6.104	36.85	28.1	58.2
2106	5.9	1.9786	5.614	2099	0.07809	6.111	37.12	31.0	54.6
2107	8.7	1.8716	5.311	1909	0.08061	5.934	33.16	39.0	83.9

Figure 7.3

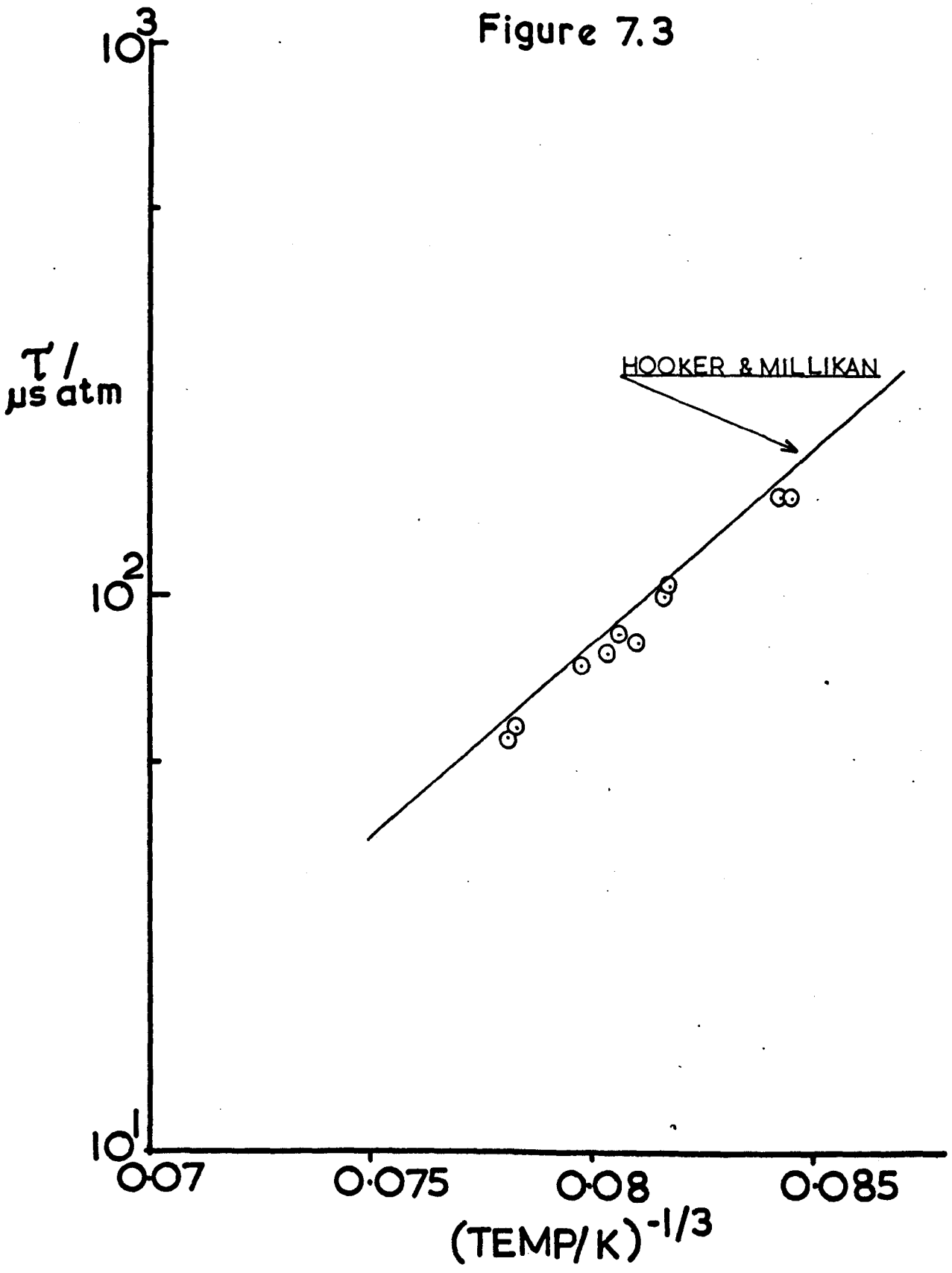
10^3
10^2
10^1
τ / μs atm
HOOKER & MILLIKAN
0·07
0·075
0·08
0·085
(TEMP/K)$^{-1/3}$

TABLE 7.5

PURE CO 1ST VIBRATIONAL LEVEL - 2% VELOCITY DECREMENT

Photo No.	P_1 mm	Shock Speed$_1$ mm μs^{-1}	Shock Mach No.	Av.Shock Temp K	$(\text{Temp})^{-\frac{1}{3}}$	$(\rho_2/\rho_1)_{av}$	$(P_2/P_1)_{av}$	Lab Time μs	Napier Time μs atm
1101	9.9	1.8164	5.154	1852	0.08143	5.918	31.21	43.9	105.6
1103	8.5	1.8528	5.257	1890	0.08088	6.011	32.5	38.4	83.9
1104	12.3	1.7205	4.882	1671	0.08427	5.755	27.87	58.7	152.2
2101	11.9	1.7313	4.913	1691	0.08393	5.799	28.33	59.5	153.0
2102	9.9	1.8344	5.205	1856	0.08137	5.949	31.84	41.1	100.3
2103	9.1	1.8844	5.342	1945	0.08011	6.058	33.64	33.0	80.4
2104	8.0	1.9103	5.421	1991	0.07948	6.098	34.58	34.0	75.5
2105	7.0	1.9715	5.594	2104	0.07804	6.224	36.85	28.1	59.4
2106	5.9	1.9786	5.614	2116	0.07789	6.231	37.12	31.0	55.7
2107	8.7	1.8716	5.311	1925	0.08038	6.054	33.16	39.0	89.6

Figure 7.4

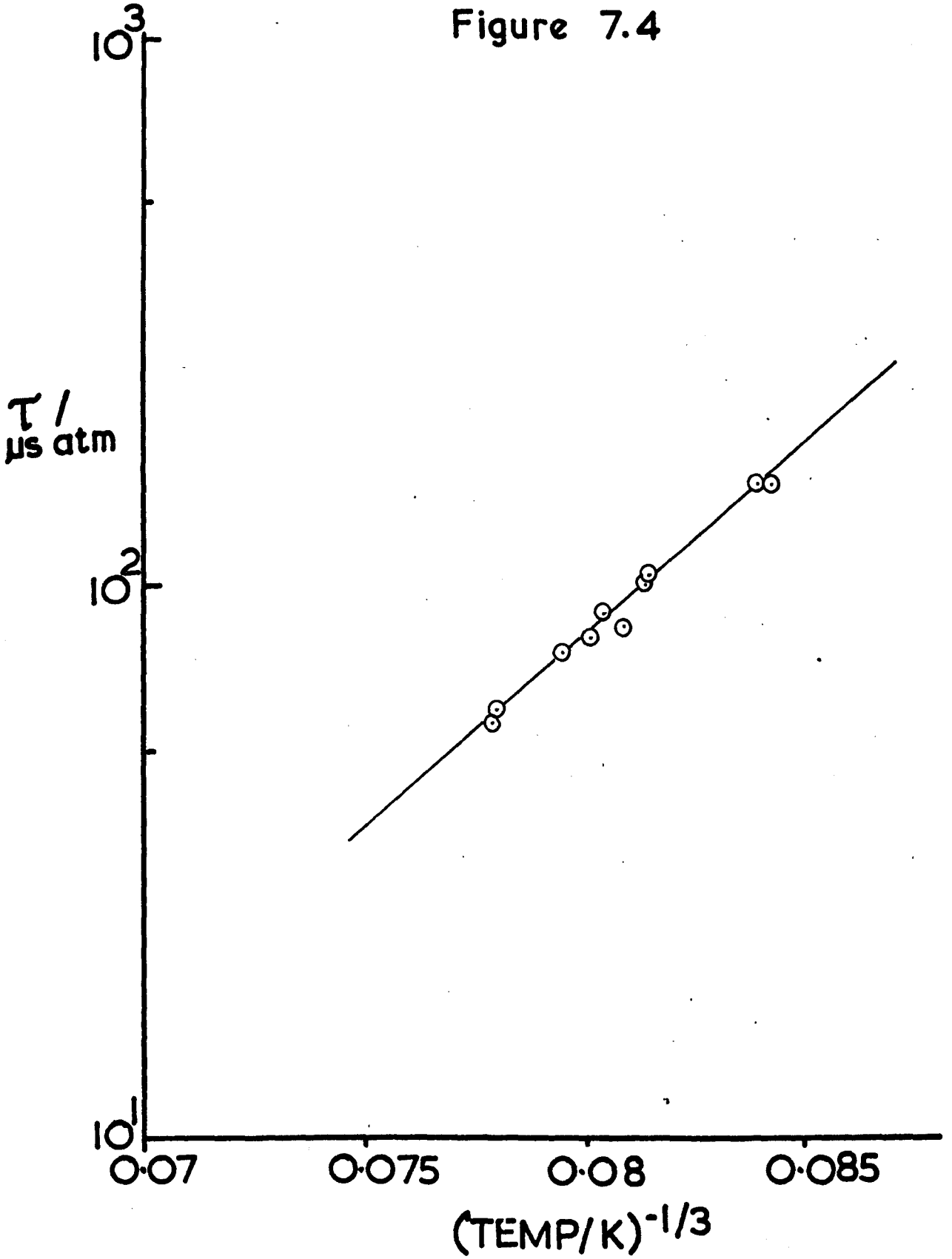

7.3 DATA OF CO/Ne MIXTURES FOR 1ST VIBRATIONAL LEVEL

The data for each mixture is tabulated on a separate page and, for clarity, a Landau-Teller plot of the data follows each mixture. In certain cases where few data were available, e.g. section 7.3f and 7.3g, the gradients of the lines were drawn with reference to the slopes of previous data as well as the available points. A typical experimental record of the infrared emission due to the $1 \rightarrow 0$ transition (2143 cm^{-1}) is shown in Figure 7.5. The data corresponding to this trace is to be found in section 7.3b, photograph number 1144. The horizontal sweep speed is 20 $\mu s\ cm^{-1}$ (i.e. in the Figure 7.5 20 μs/large square), and the emission of the CO rises vertically, and exponentially. The rise and the intensity shown on this figure bears comparison to Figure 7.13.

Figure 7.5

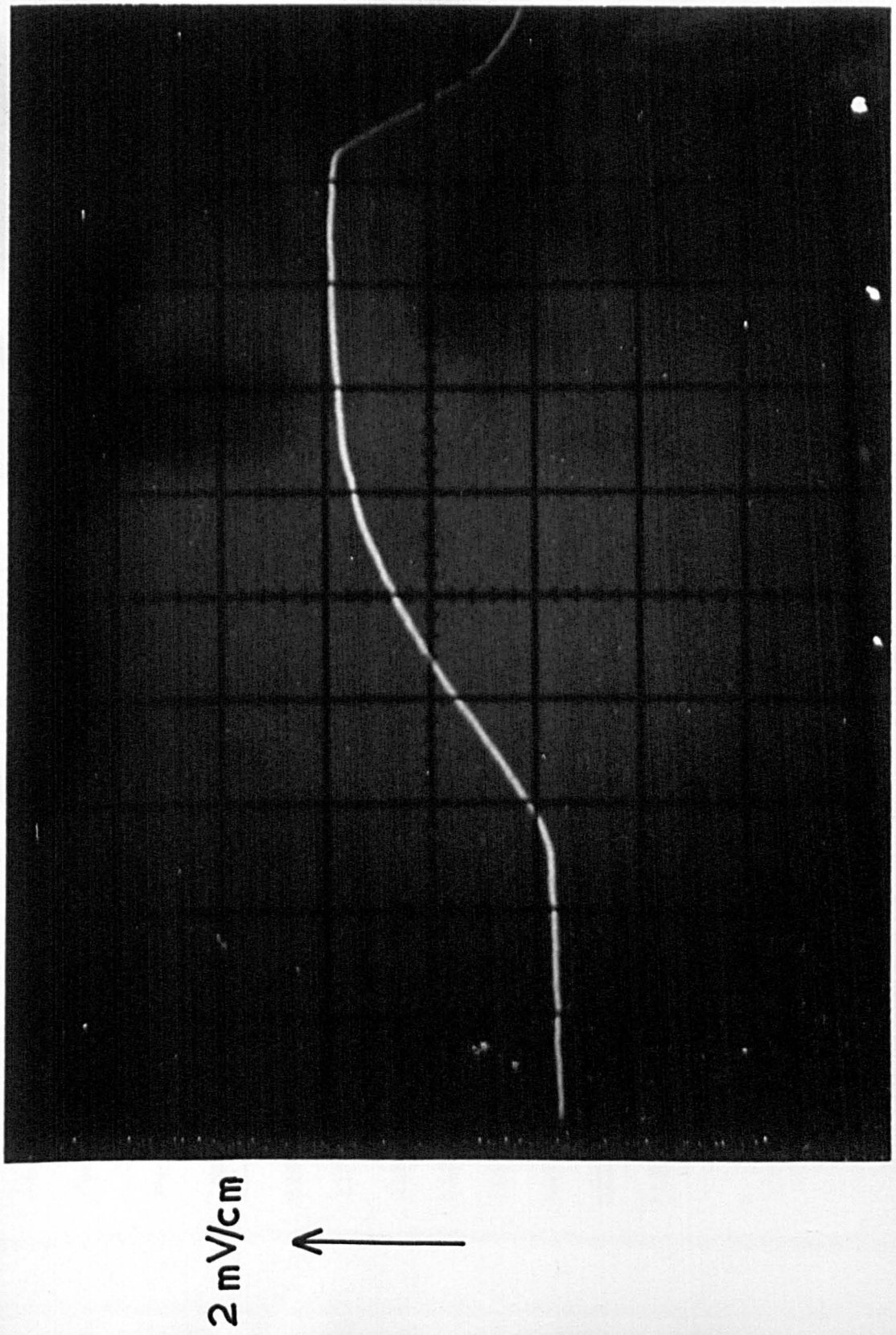

7.3.a 90% CARBON MONOXIDE - 10% NEON

Speed of Sound - 0.360 km s^{-1}; Specific Heat Ratio - 1.417; Av. Mol. Wt. - 27.23

Photo No.	P_1 mm	Shock Speed$_1$ mm μs^{-1}	Shock Mach No.	Av.Shock Temp K	$(Temp)^{-\frac{1}{3}}$	$(\rho_2/\rho_1)_{av}$	$(P_2/P_1)_{av}$	Lab Time μs	Napier Time μs atm
1121	10.9	1.8164	5.04	1828	0.08178	5.718	30.1	30.4	75.1
1122	8.9	1.8653	5.18	1912	0.08058	5.804	31.67	40.1	86.3
1124	12.0	1.7699	4.91	1750	0.08298	5.633	28.47	48.0	121.5
1125	11.1	1.7814	4.94	1771	0.08264	5.667	28.85	47.4	113.0
1126	9.8	1.8405	5.11	1872	0.08113	5.776	30.82	44.0	101.0
1127	8.2	1.8972	5.27	1973	0.07973	5.889	32.78	36.3	75.6
2121	6.9	1.9576	5.43	2079	0.07835	5.962	34.92	32.0	60.4
2122	6.1	1.9786	5.49	2124	0.07779	6.043	35.70	31.0	53.7

Figure 7.6

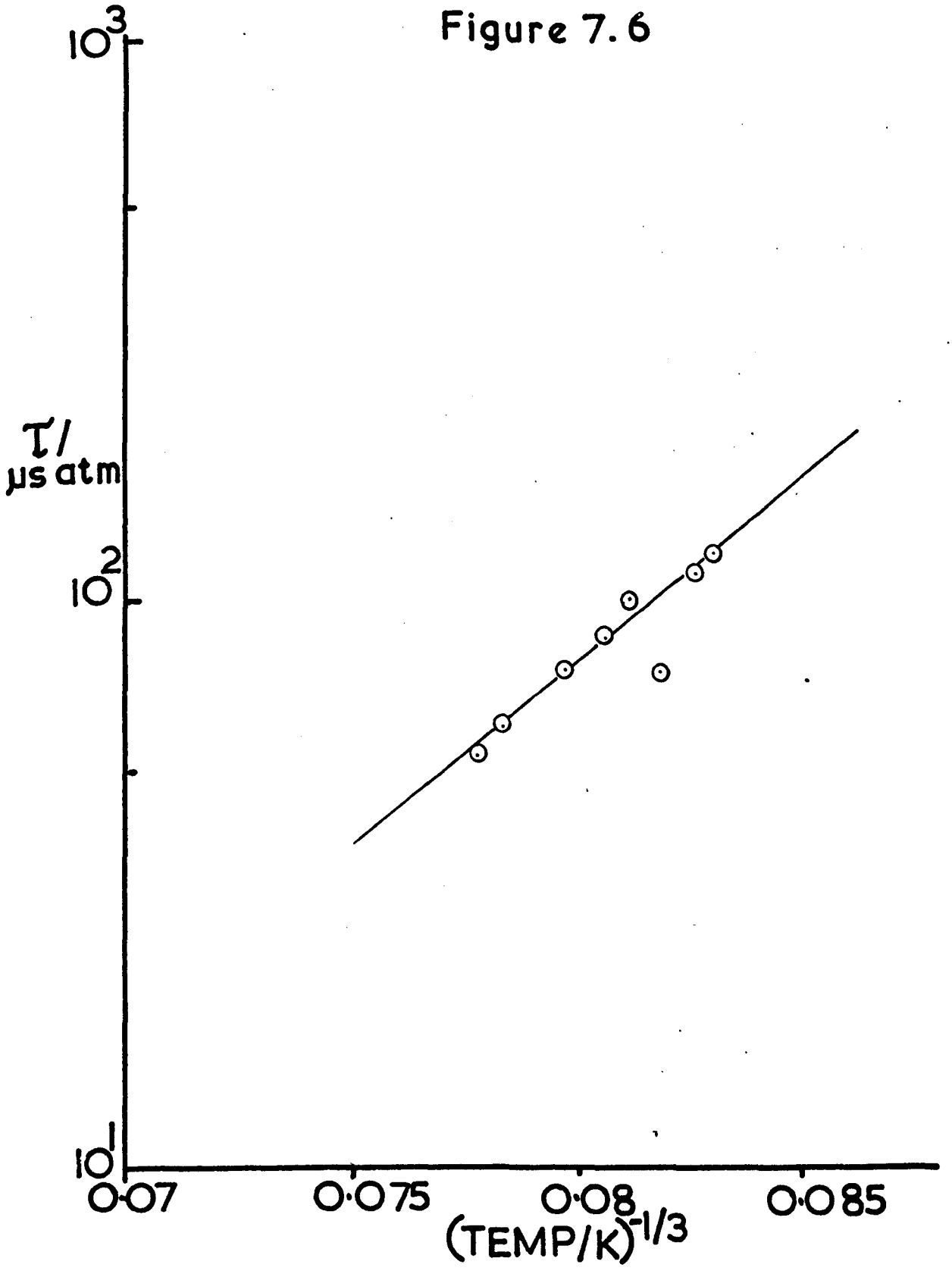

7.3.b 80% CARBON MONOXIDE - 20% NEON

Speed of Sound - 0.368 km s^{-1}; Specific Heat Ratio - 1.435; Av. Mol. Wt. - 26.44

Photo No.	P_1 mm	Shock Speed$_1$ mm μs^{-1}	Shock Mach No.	Av.Shock Temp. K	$(Temp)^{-\frac{1}{3}}$	$(\rho_2/\rho_1)_{av}$	$(P_2/P_1)_{av}$	Lab Time μs	Napier Time μs atm
1141	10.8	1.8105	4.92	1832	0.08172	5.545	28.72	40.8	92.3
1142	9.6	1.8349	4.99	1872	0.08114	5.571	29.50	44.2	91.8
1143	8.9	1.8843	5.13	1957	0.07995	5.644	31.15	36.4	74.9
1144	7.2	1.9370	5.27	2057	0.07863	5.737	32.94	32.4	57.9
1145	6.6	1.9715	5.36	2114	0.07792	5.76	34.14	34.0	57.5
1146	11.5	1.8046	4.91	1813	0.08201	5.378	28.54	46.4	108.0
1147	12.4	1.7587	4.78	1723	0.0834	5.406	27.08	56.0	113.8

Figure 7.7

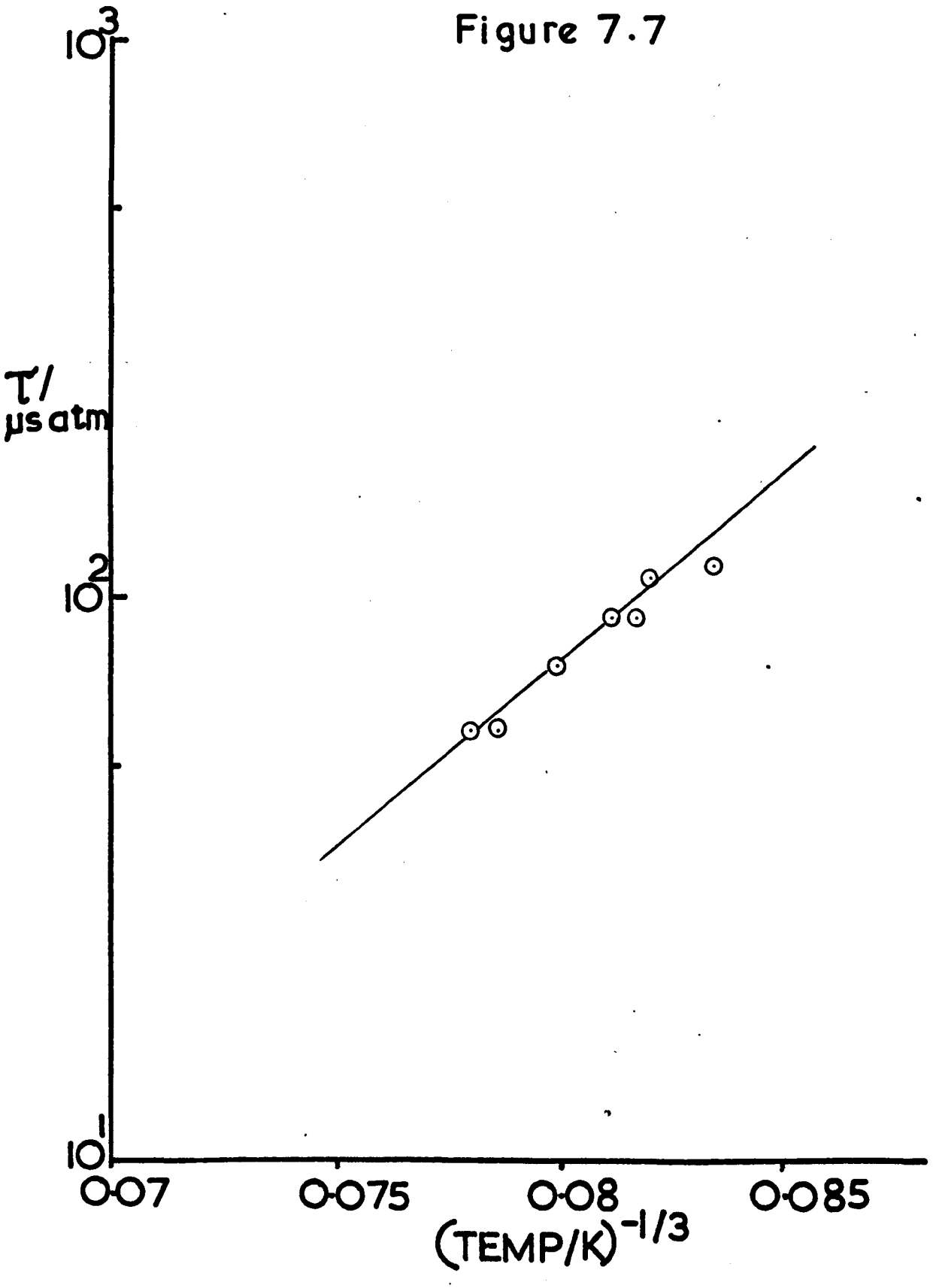

7.3.c 60% CARBON MONOXIDE - 40% NEON

Speed of Sound - 0.385 km s^{-1}; Specific Heat Ratio - 1.476; Av. Mol. Wt. - 24.88

Photo No.	P_1 mm	Shock Speed $mm\ \mu s^{-1}$	Shock Mach No.	Av.Shock Temp K	$(Temp)^{-\frac{1}{3}}$	$(\rho_2/\rho_1)_{av}$	$(P_2/P_1)_{av}$	Lab Time μs	Napier Time μs atm
1181	10.4	1.8779	4.88	1958	0.07993	5.174	28.55	36.0	73.6
1182	9.9	1.8844	4.90	1966	0.07983	5.15	28.76	37.2	71.7
1183	11.1	1.8105	4.71	1839	0.08162	5.071	26.52	48.3	94.8
1184	12.9	1.7971	4.67	1811	0.08204	5.027	26.12	43.4	96.7
1185	14.1	1.7699	4.60	1765	0.08275	4.99	25.3	48.0	112.4

Figure 7.8

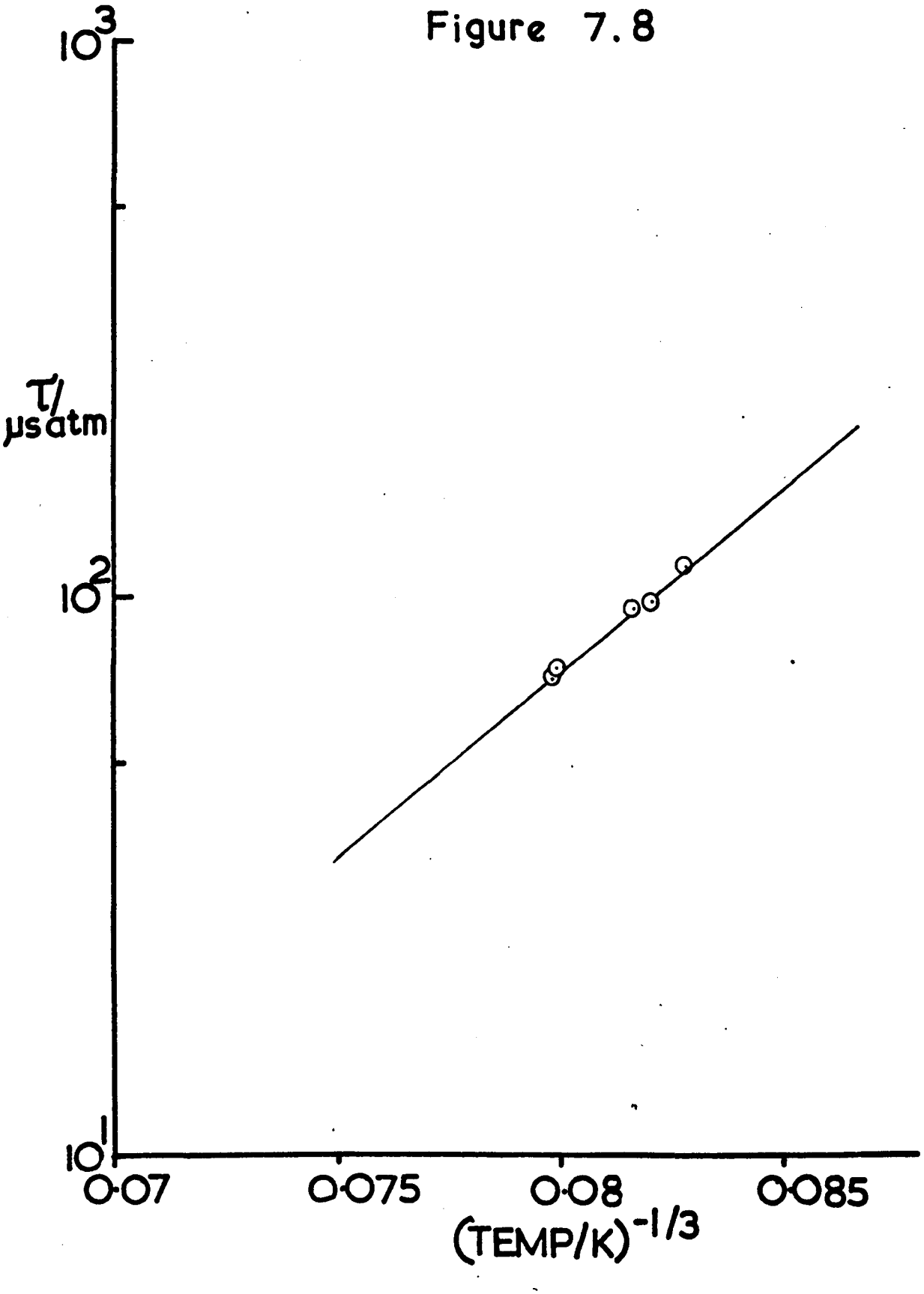

7.3.d 50% CARBON MONOXIDE - 50% NEON

Speed of Sound - 0.394 km s^{-1}; Specific Heat Ratio - 1.5; Av. Mol. Wt. - 24.09

Photo No.	P_1 mm	Shock Speed$_1$ mm μs^{-1}	Shock Mach No.	Av.Shock Temp K	$(Temp)^{-\frac{1}{3}}$	$(\rho_2/\rho_1)_{av}$	$(P_2/P_1)_{av}$	Lab Time μs	Napier Time μs atm
1101	12.1	1.8844	4.78	1986	0.07956	4.928	27.54	29.18	63.1
1102	15.0	1.7756	4.51	1779	0.08253	4.77	24.41	46.3	106.4
1103	16.7	1.7643	4.48	1746	0.08304	4.689	24.11	45.0	112.0
1104	17.8	1.7421	4.42	1708	0.08365	4.647	23.49	49.0	125.3
1105	19.4	1.7205	4.37	1672	0.08425	4.626	22.90	52.0	140.0
1106	11.1	1.9038	4.83	2006	0.07929	4.944	28.13	32.1	65.0

Figure 7.9

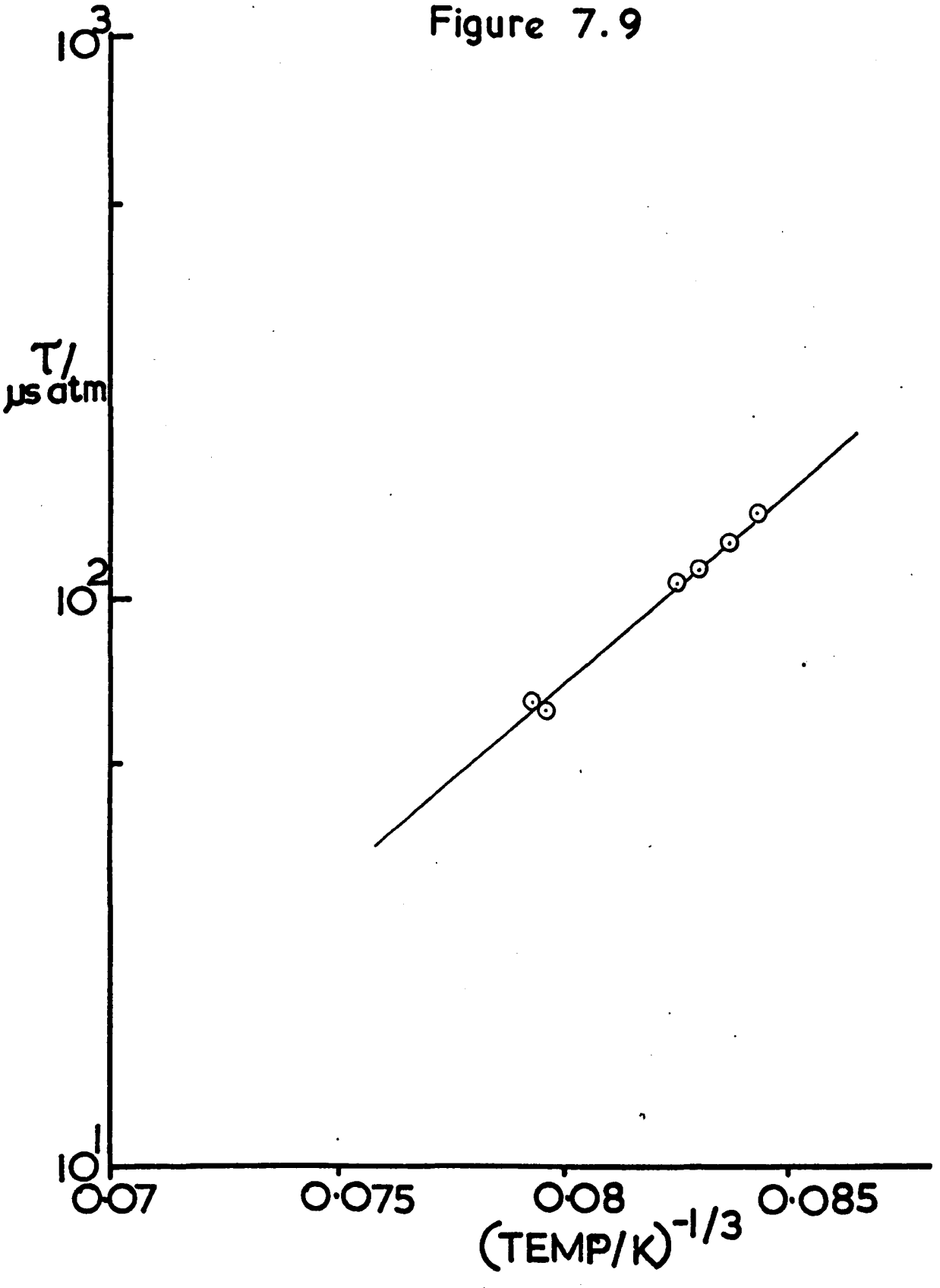

7.3.e 40% CARBON MONOXIDE - 60% NEON

Speed of Sound - 0.404 km s^{-1}; Specific Heat Ratio - 1.526; Av. Mol. Wt. - 23.31

Photo No.	P_1 mm	Shock Speed mm μs^{-1}	Shock Mach No.	Av.Shock Temp K	$(Temp)^{-\frac{1}{3}}$	$(\rho_2/\rho_1)_{av}$	$(P_2/P_1)_{av}$	Lab Time μs	Napier Time μs atm
1121	12.2	1.8528	4.58	1925	0.08038	4.67	25.44	36.8	70.2
1122	14.5	1.8284	4.52	1878	0.08104	4.63	24.77	35.6	77.9
1123	19.9	1.7699	4.38	1691	0.08393	4.484	21.89	50.1	128.8
1124	25.0	1.6152	4.00	1518	0.08700	4.328	19.25	70.0	191.8
1125	16.7	1.7205	4.38	1779	0.08253	4.569	23.18	41.1	95.7

Figure 7.10

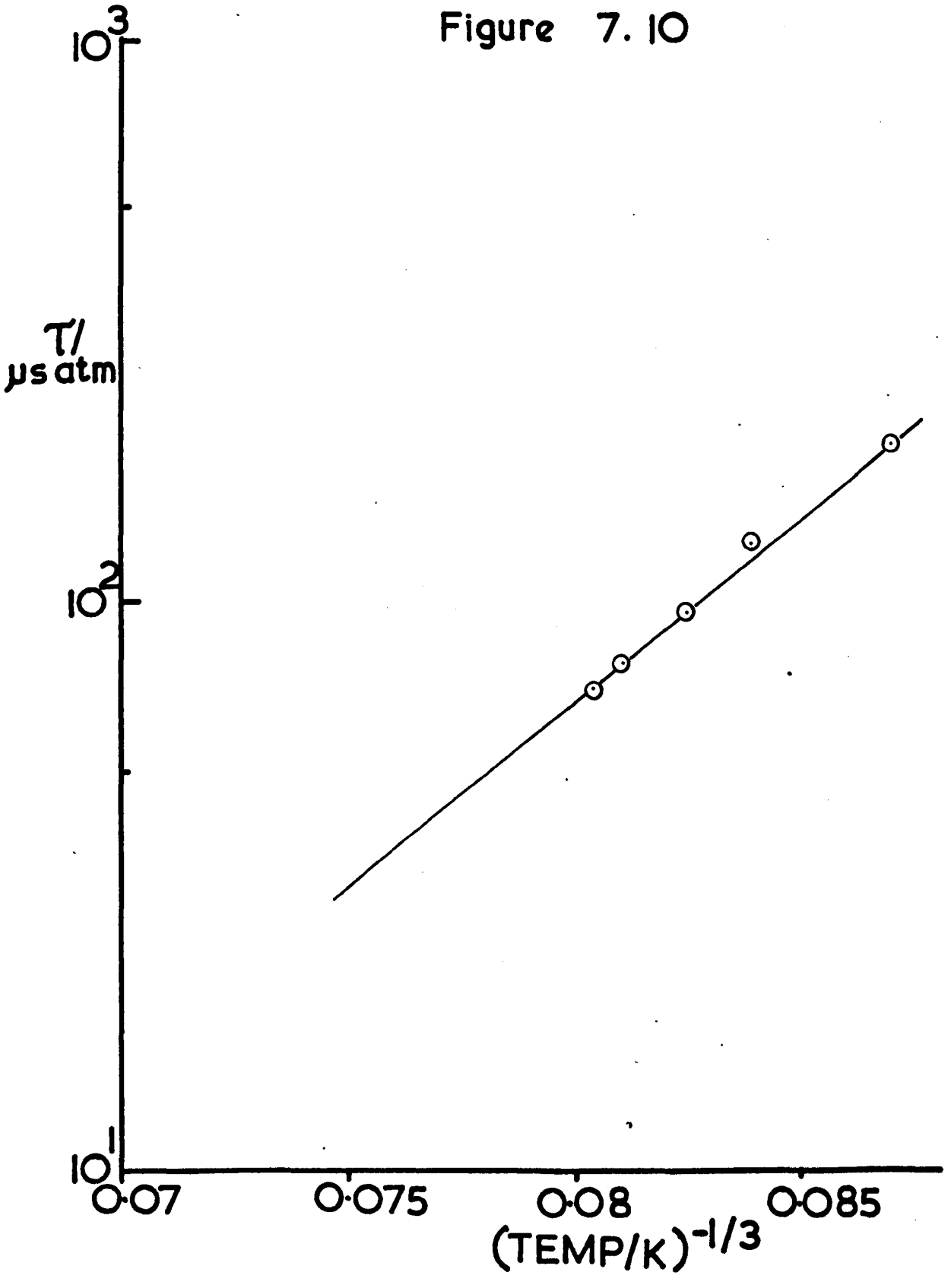

7.3.f 20% CARBON MONOXIDE - 80% NEON

Speed of Sound - 0.426 km s^{-1}; Specific Heat Ratio - 1.588; Av. Mol. Wt. - 21.75

Photo No.	P_1 mm	Shock Speed $_1$ mm μs^{-1}	Shock Mach No.	Av.Shock Temp K	$(Temp)^{-\frac{1}{3}}$	$(\rho_2/\rho_1)_{av}$	$(P_2/P_1)_{av}$	Lab Time μs	Napier Time μs atm
1161	20.0	1.7587	4.12	1768	0.0827	4.107	20.74	41.6	93.3
1162	23.0	1.7152	4.02	1689	0.08396	4.043	19.71	46.0	110.9
1163	25.0	1.6687	3.91	1612	0.08529	3.984	18.64	59.0	144.1
1164	20.6	1.7367	4.07	1729	0.08331	4.13	20.21	54.7	123.8

Figure 7.11

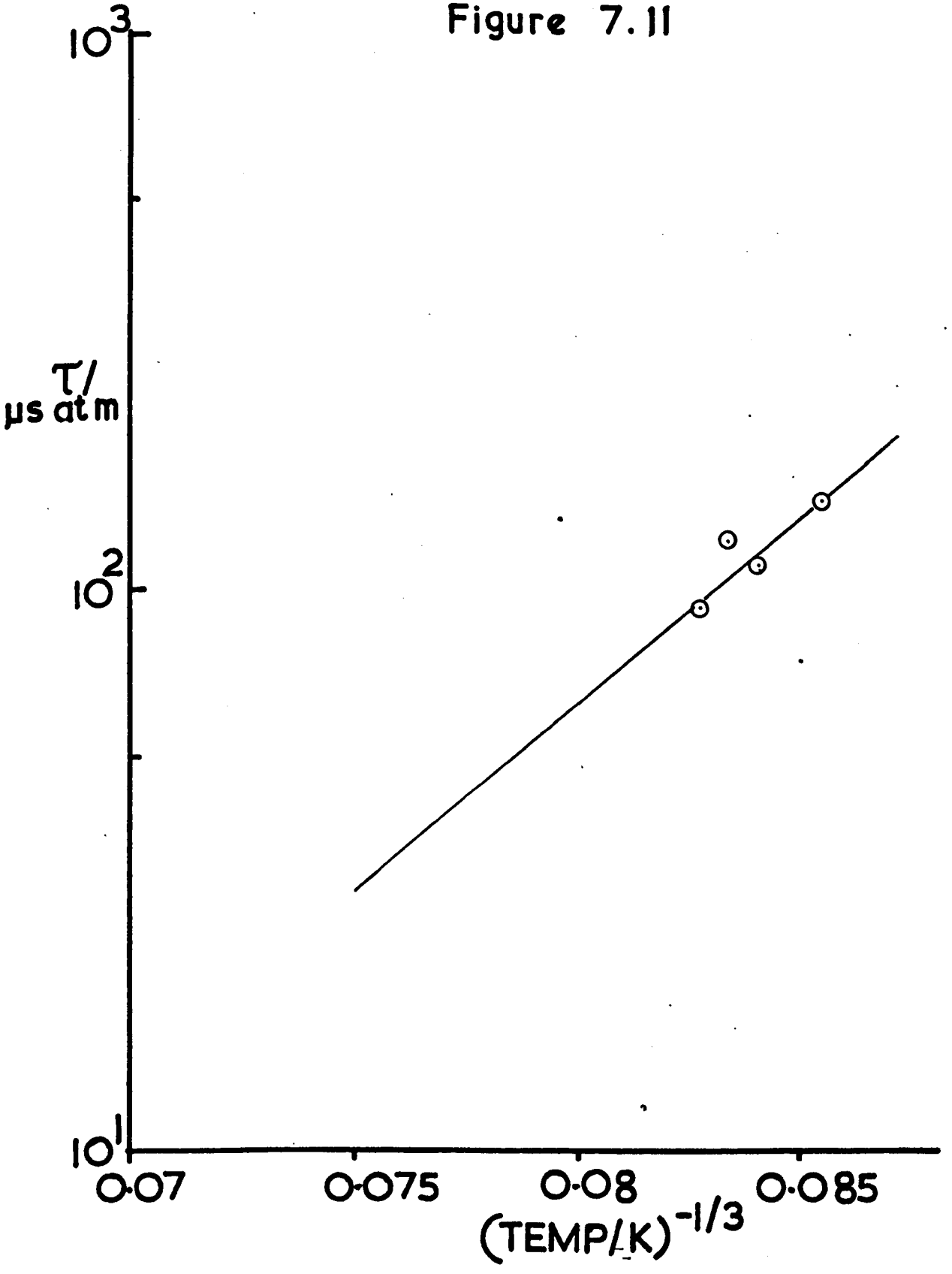

7.3.g 10% CARBON MONOXIDE - 90% NEON

Speed of Sound - 0.439 km s^{-1}; Specific Heat Ratio - 1.625; Av. Mol. Wt. - 20.963

Photo No.	P_1 mm	Shock Speed mm μs^{-1}	Shock Mach No.	Av.Shock Temp K	$(Temp)^{-\frac{1}{3}}$	$(\rho_2/\rho_1)_{av}$	$(P_2/P_1)_{av}$	Lab Time μs	Napier Time μs atm
1182	25.0	1.6737	3.81	1578	0.08589	3.698	17.75	68.0	146.8
1183	22.9	1.8405	4.19	1853	0.08142	3.835	21.53	37.2	92.4
1185	22.1	1.7532	3.99	1706	0.08368	3.767	19.51	47.1	100.7

Figure 7.12

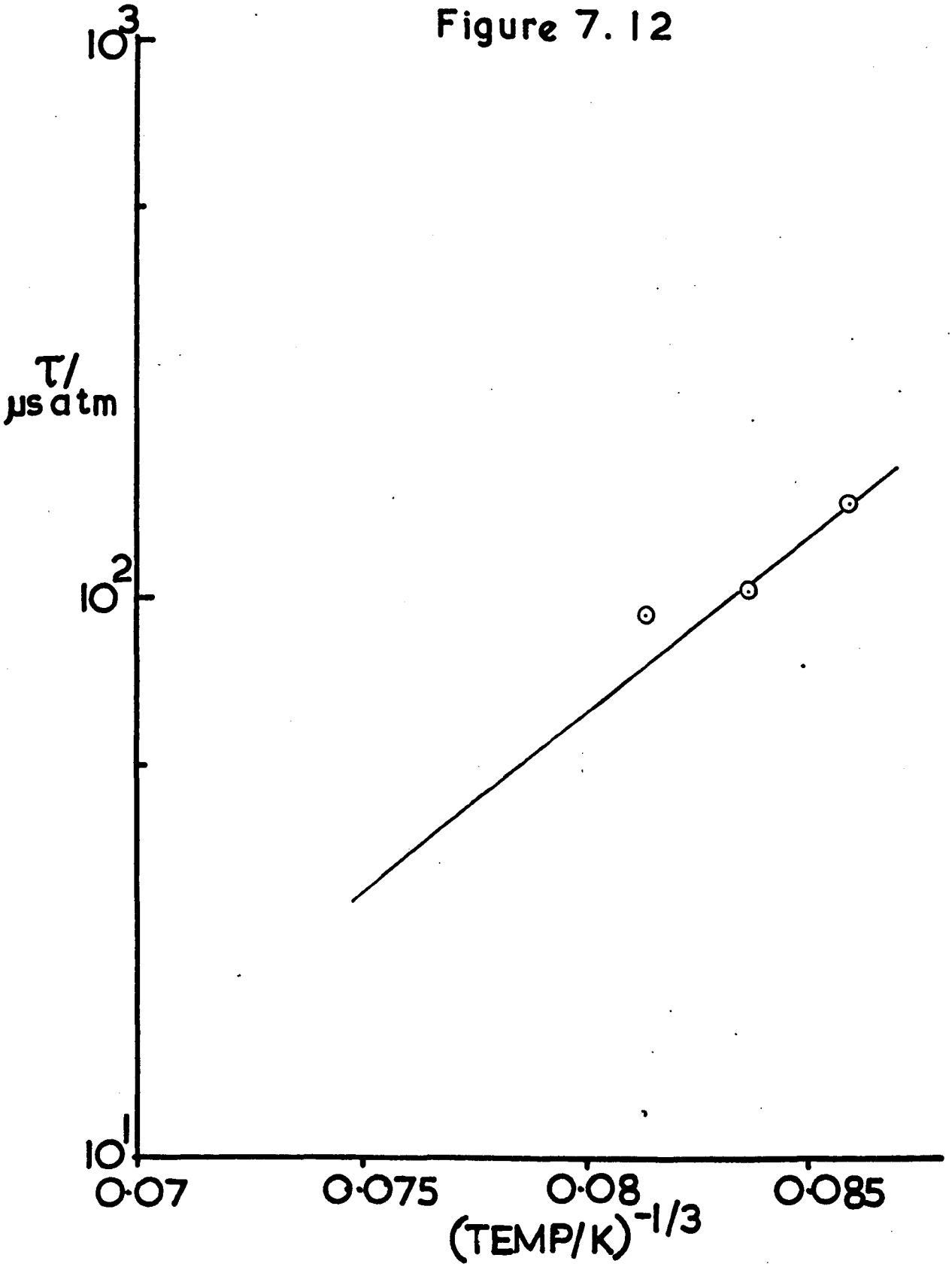

7.4 DATA OF CO/Ne MIXTURES FOR 2ND VIBRATIONAL LEVEL

The data for each mixture is tabulated on a separate page and, for clarity, a Landau-Teller plot of the data follows each mixture.

A typical experimental record of the infrared emission due to the 2 → 0 transition (4260 cm^{-1}) is shown in Figure 7.13. The data corresponding to this trace is to be found in section 7.4.e photograph number 1251. The horizontal sweep is 20 μs cm^{-1} (i.e. in the Figure 7.13 20 μs/large square), and the emission of the CO rises vertically. The emission in this case does not rise exponentially, as does the emission in Figure 7.5, but it shows an initial 'toe'. The emission in this case is only 0.25 that shown in Figure 7.5.

Figure 7.13

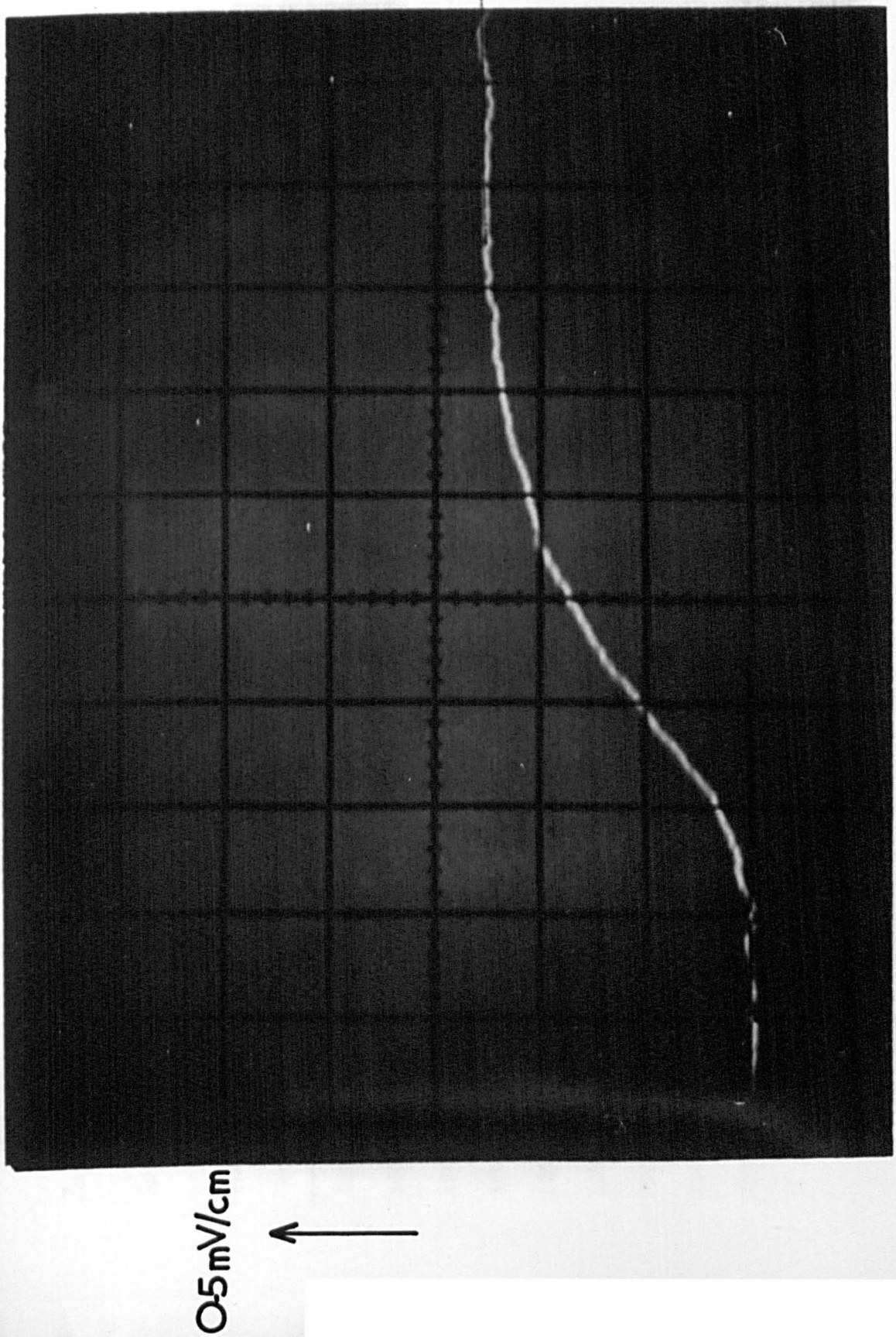

7.4.a PURE CARBON MONOXIDE

Speed of Sound - 0.353 km s^{-1}; Specific Heat Ratio - 1.40; Av. Mol. Wt. - 28.01

Photo No.	P_1 mm	Shock Speed$_1$ mm μs^{-1}	Shock Mach No.	Av.Shock Temp K	$(Temp)^{-\frac{1}{3}}$	$(\rho_2/\rho_1)_{av}$	$(P_2/P_1)_{av}$	Lab Time μs	Napier Time μs atm
1201	11.4	1.7702	5.023	1773	0.08262	5.98	29.63	46.24	122.8
1202	8.1	1.8051	5.132	1818	0.08193	5.994	30.83	52.5	103.5
1203	8.5	1.8714	5.310	1930	0.08032	6.093	33.16	39.1	88.4
1204	7.4	1.9224	5.455	2022	0.07908	6.201	35.02	35.7	75.5
1205	7.8	1.9184	5.444	2014	0.07918	6.177	34.88	33.9	75.0
1206	5.9	1.9891	5.644	2136	0.07765	6.253	37.53	30.2	54.9
2201	3.6	2.1080	5.982	2369	0.07501	6.478	42.19	26.9	34.9
2203	2.3	2.2149	6.285	2583	0.07288	6.638	46.65	25.4	23.8
2206	4.2	2.0153	5.719	2184	0.07707	6.30	38.54	38.0	51.0

Figure 7.14

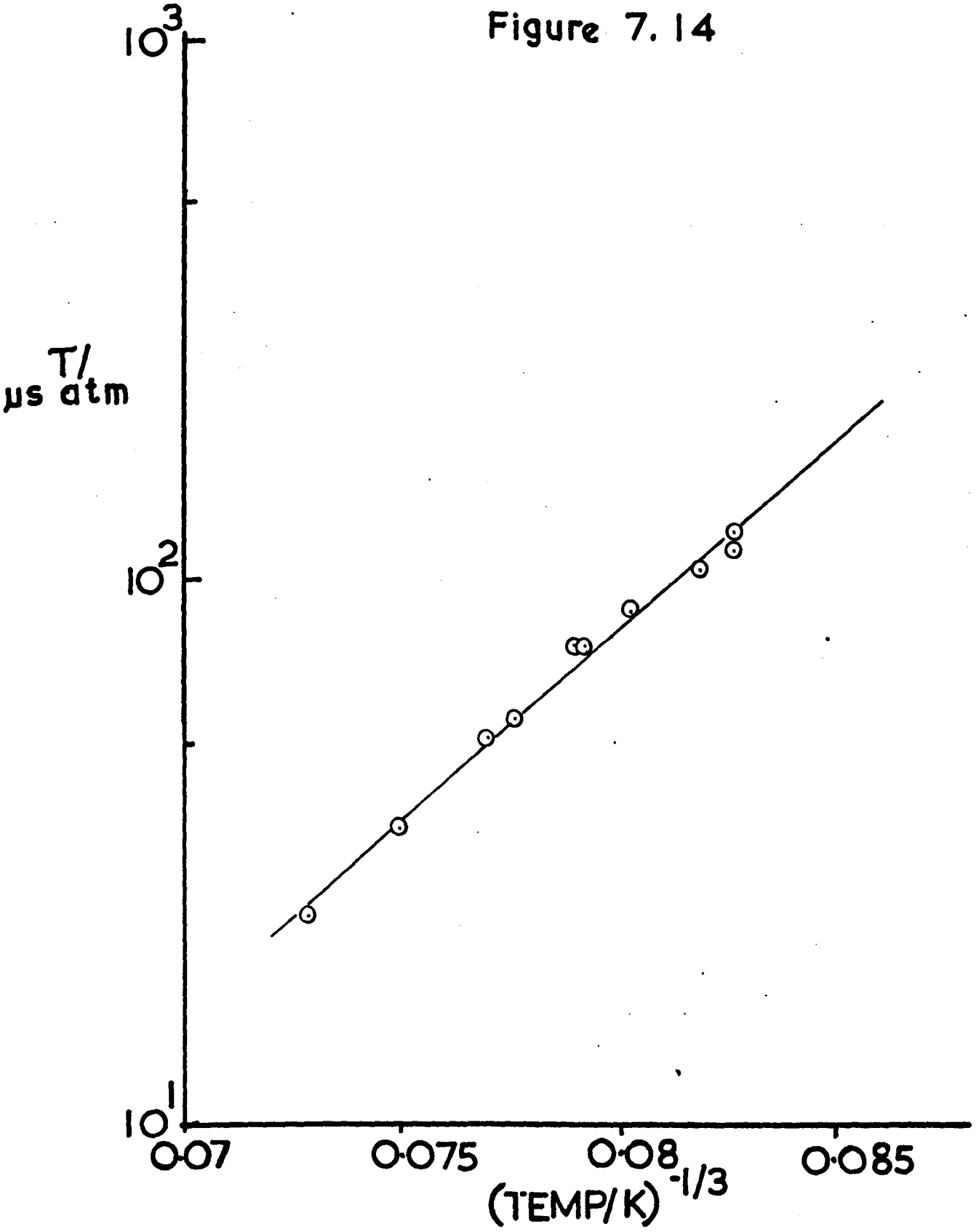

7.4.b 90% CARBON MONOXIDE - 10% NEON

Speed of Sound - 0.360 km s^{-1}; Specific Heat Ratio - 1.417; Av. Mol. Wt. - 27.23

Photo No.	P_1 mm	Shock Speed$_1$ mm μs^{-1}	Shock Mach No.	Av.Shock Temp K	$(Temp)^{-\frac{1}{3}}$	$(\rho_2/\rho_1)_{av}$	$(P_2/P_1)_{av}$	Lab Time μs	Napier Time μs atm
1221	6.3	1.9224	5.34	2022	0.07908	5.986	33.67	38.0	63.5
1224	4.5	2.0560	5.71	2267	0.07612	6.138	38.58	28.9	40.5
1225	7.5	1.9024	5.28	1984	0.07958	6.024	32.96	36.0	70.8
1226	8.3	1.8376	5.10	1878	0.08104	5.842	30.73	32.8	64.3
1227	9.8	1.7840	4.95	1786	0.08242	5.75	28.95	51.3	110.1
1228	8.0	1.8868	5.24	1959	0.07991	5.897	32.43	37.3	75.0
2221	4.8	2.0514	5.70	2255	0.07626	6.114	38.4	30.0	44.5

Figure 7.15

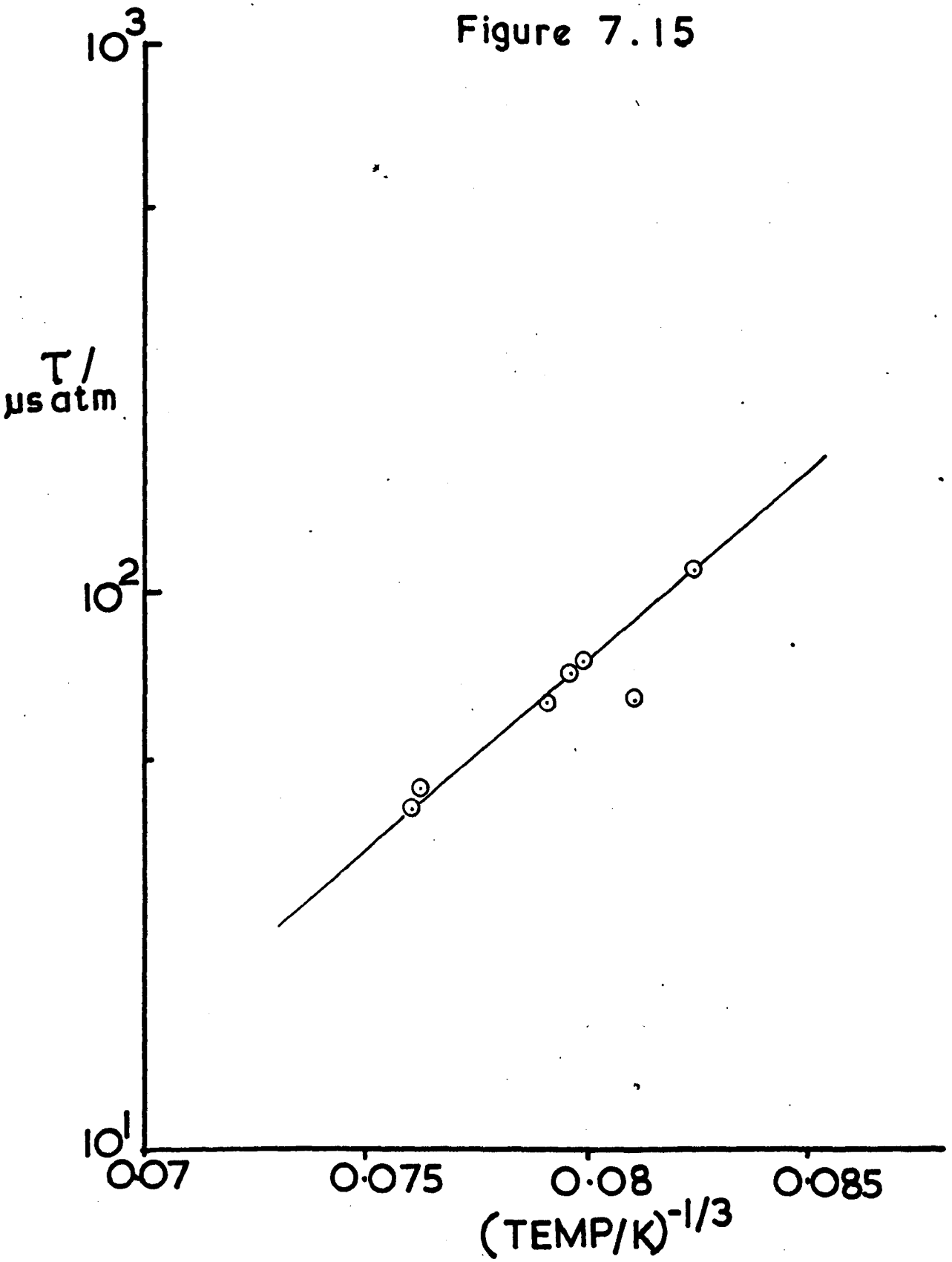

7.4.c 85% CARBON MONOXIDE - 15% NEON

Speed of Sound - 0.364 km s^{-1}; Specific Heat Ratio - 1.426; Av. Mol. Wt. - 26.84

Photo No.	P_1 mm	Shock Speed$_1$ mm μs^{-1}	Shock Mach No.	Av.Shock Temp K	$(Temp)^{-\frac{1}{3}}$	$(\rho_2/\rho_1)_{av}$	$(P_2/P_1)_{av}$	Lab Time μs	Napier Time μs atm
1232	9.7	1.8377	5.05	1878	0.08105	5.723	30.16	39.5	87.0
1233	9.7	1.8791	5.16	1947	0.08008	5.759	31.57	34.7	80.5
1234	7.6	1.9184	5.27	2021	0.07909	5.839	32.91	29.1	55.9
2231	13.3	1.7771	4.88	1776	0.08256	5.625	28.19	40.0	111.0
2232	14.4	1.7204	4.73	1681	0.0841	5.516	26.39	49.7	137.0
2233	5.9	2.0109	5.52	2188	0.07702	5.92	36.21	28.5	47.4

Figure 7. 16

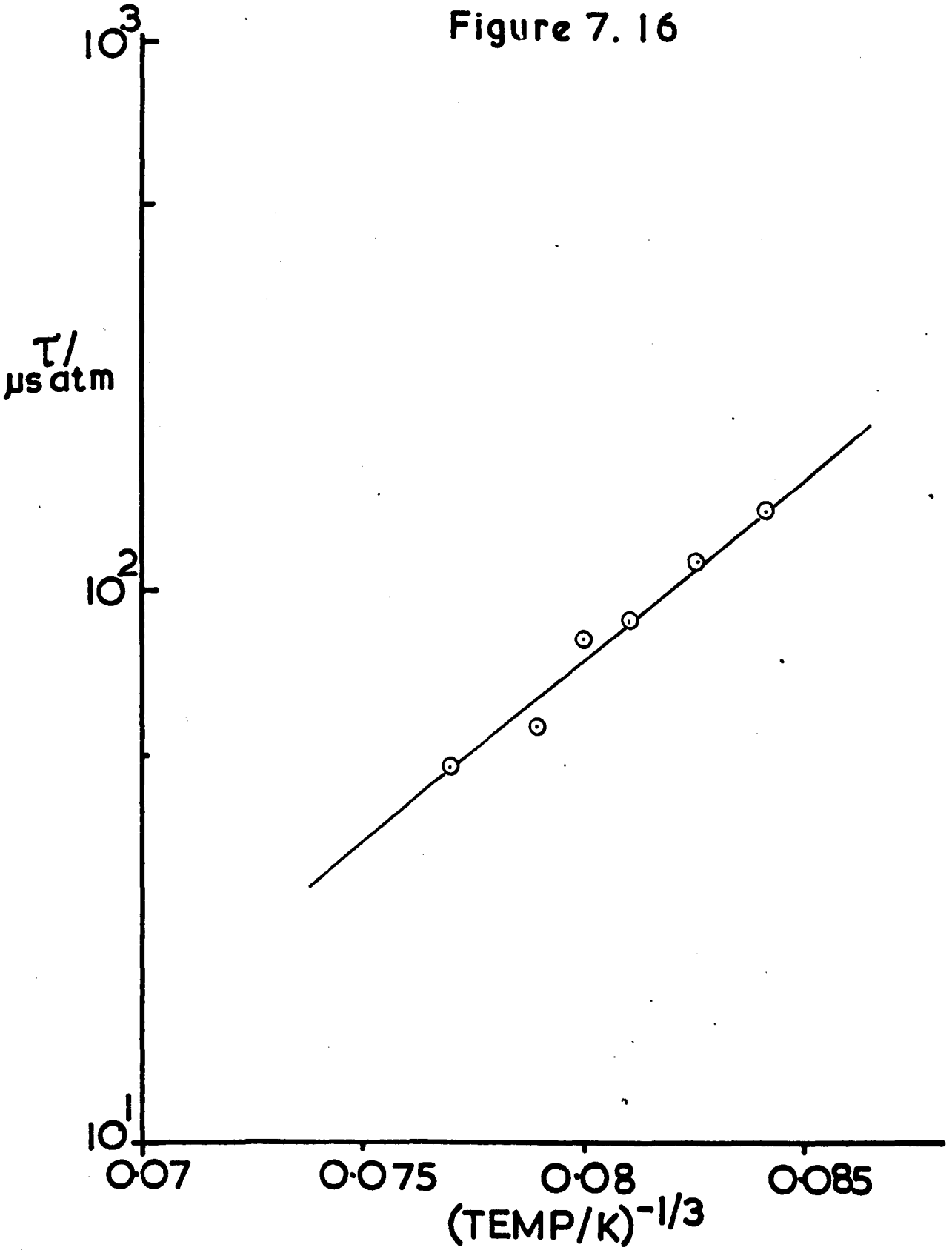

7.4.d 80% CARBON MONOXIDE - 20% NEON

Speed of Sound - 0.368 km s^{-1}; Specific Heat Ratio - 1.435; Av. Mol. Wt. - 26.44

Photo No.	P_1 mm	Shock Speed mm μs^{-1}	Shock Mach No.	Av.Shock Temp K	$(Temp)^{-\frac{1}{3}}$	$(\rho_2/\rho_1)_{av}$	$(P_2/P_1)_{av}$	Lab Time μs	Napier Time μs atm
1241	7.4	1.9427	5.28	2069	0.07848	5.762	33.13	28.0	52.0
1242	5.9	1.9934	5.42	2166	0.07728	5.86	34.9	27.0	43.6
1246	9.6	1.8430	4.99	1821	0.08188	5.66	29.48	43.1	90.9
1247	8.6	1.8638	5.07	1929	0.08033	5.652	30.45	38.5	74.9
2241	10.8	1.7875	4.86	1797	0.08225	5.529	27.99	44.1	96.8
2243	7.0	1.9635	5.34	2103	0.07805	5.772	33.85	28.7	51.6
2245	4.9	2.0423	5.55	2240	0.07643	5.805	36.61	27.5	37.7
2246	4.6	2.0483	5.57	2252	0.07621	5.81	36.88	25.0	32.5
2247	14.8	1.7204	4.68	1683	0.08406	5.40	25.9	49.8	135.6
2242	12.3	1.7466	4.75	1728	0.08333	5.462	26.7	53.4	126.0

Figure 7 . 17

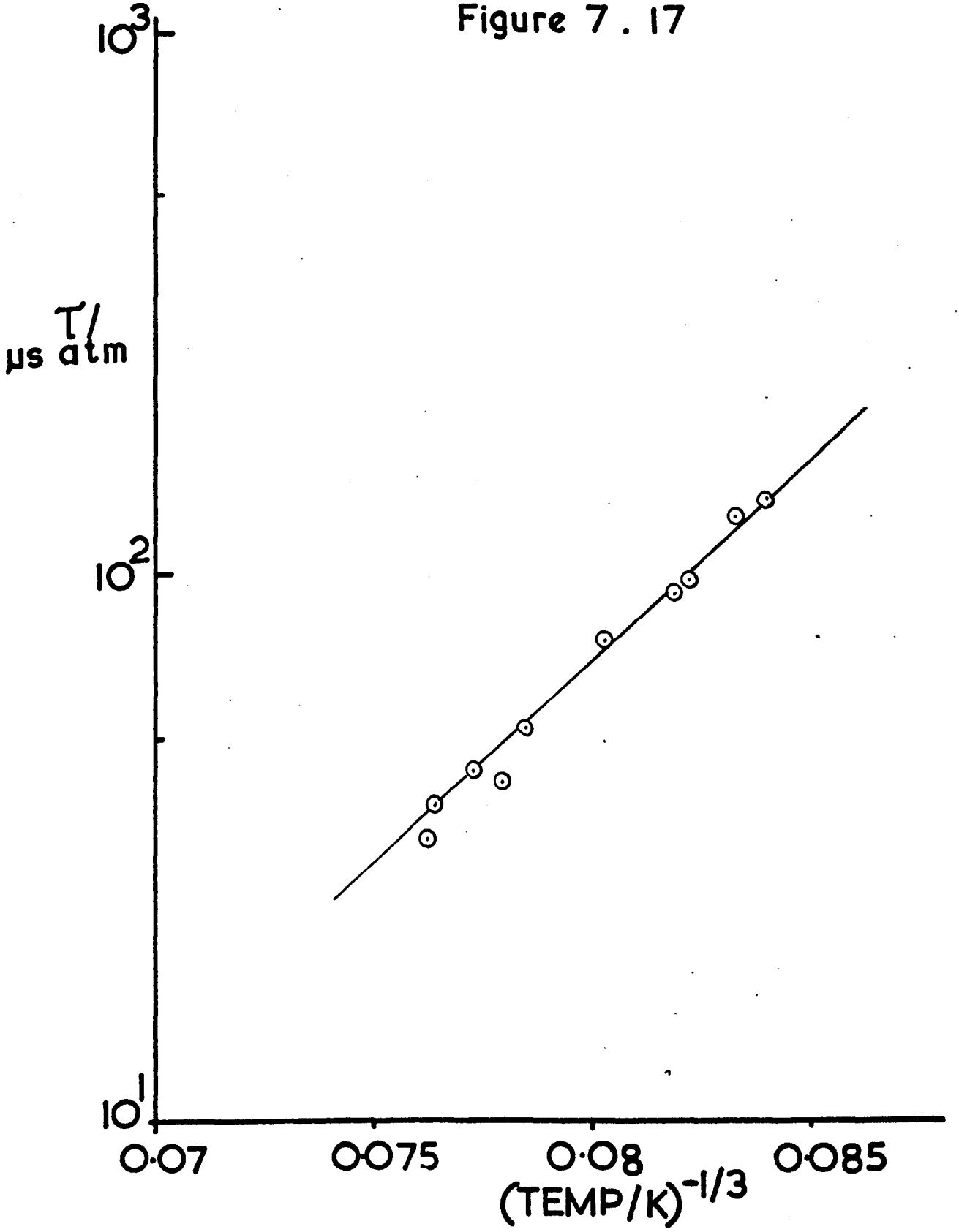

7.4.e 75% CARBON MONOXIDE - 25% NEON

Speed of Sound - 0.372 km s^{-1}; Specific Heat Ratio - 1.444; Av. Mol. Wt. - 26.05

Photo No.	P_1 mm	Shock Speed mm μs^{-1}	Shock Mach No.	Av. Shock Temp K	$(Temp)^{-\frac{1}{3}}$	$(\rho_2/\rho_1)_{av}$	$(P_2/P_1)_{av}$	Lab Time μs	Napier Time μs atm
1251	11.0	1.8194	4.89	1856	0.08136	5.486	28.46	36.3	82.0
1252	9.9	1.8562	4.99	1920	0.08045	5.534	29.63	34.8	74.4
1253	7.8	1.9264	5.18	2044	0.07879	5.624	31.95	31.1	57.4
1254	5.8	2.0242	5.44	2222	0.07663	5.744	35.33	26.6	41.2
1255	4.6	2.0746	5.58	2328	0.07545	5.857	37.12	25.2	33.2
1256	10.9	1.7635	4.74	1761	0.08280	5.395	26.72	50.4	104.1
1258	15.4	1.7013	4.58	1651	0.08461	5.312	24.84	52.0	139.0

Figure 7.18

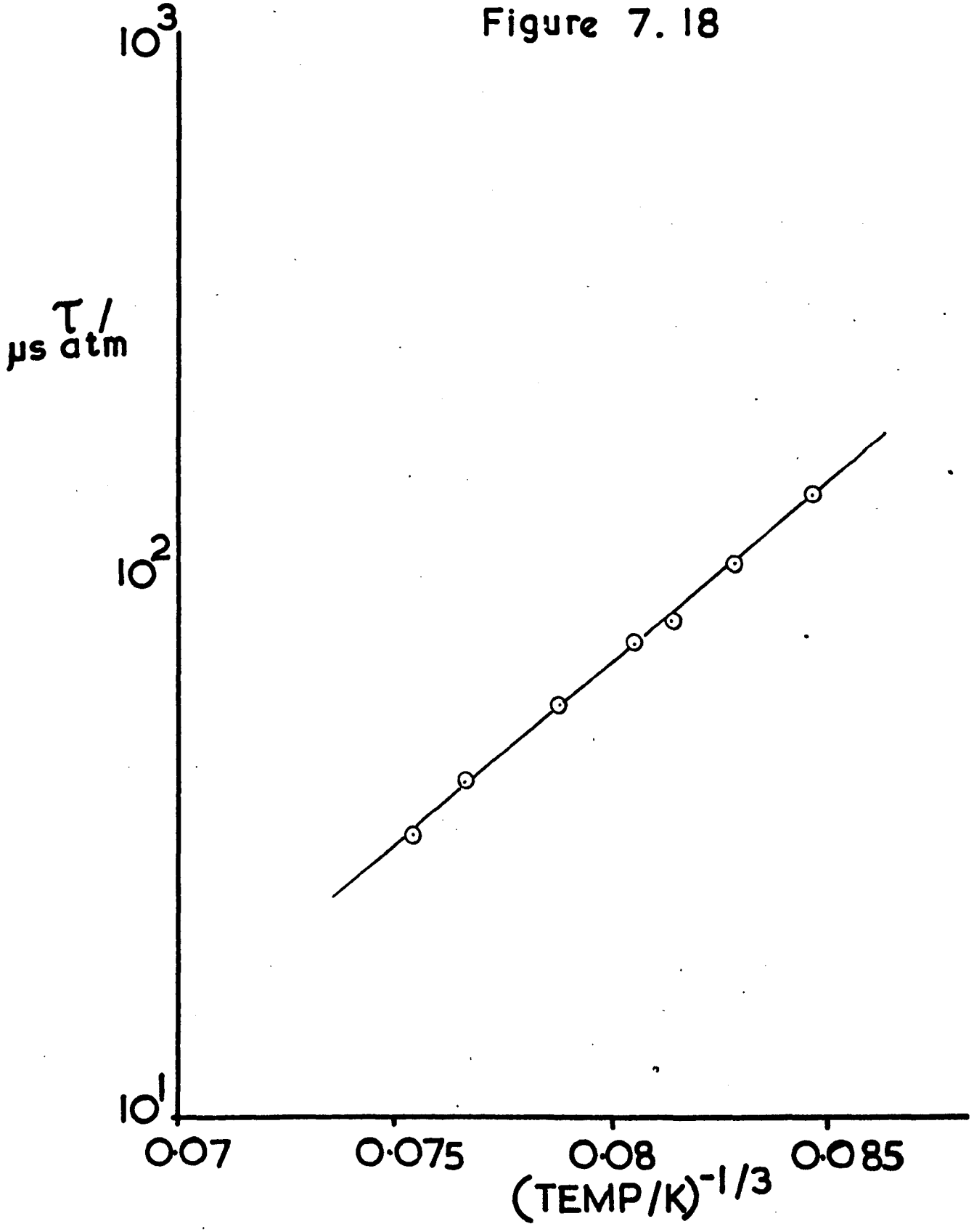

7.4.f 65% CARBON MONOXIDE - 35% NEON

Speed of Sound - 0.380 km s^{-1}; Specific Heat Ratio - 1.465; Av. Mol. Wt. - 25.27

Photo No.	P_1 mm	Shock Speed$_1$ mm μs^{-1}	Shock Mach No.	Av.Shock Temp K	$(Temp)^{-\frac{1}{3}}$	$(\rho_2/\rho_1)_{av}$	$(P_2/P_1)_{av}$	Lab Time μs	Napier Time μs atm
1271	12.2	1.7875	4.70	1806	0.0821	5.205	26.38	40.7	89.8
1272	10.0	1.8488	4.86	1911	0.08058	5.287	28.24	36.2	71.2
1274	8.8	1.8868	4.96	1975	0.07969	5.313	29.43	33.4	60.4
1276	6.3	2.0065	5.28	2182	0.07710	5.40	33.34	28.5	42.6
1277	5.3	2.0699	5.44	2317	0.07556	5.44	34.50	23.5	31.7
1278	3.8	2.1227	5.58	2443	0.07425	5.702	37.36	22.8	24.3
2271	14.5	1.7335	4.56	1719	0.08348	5.088	24.79	47.1	113.4
2273	9.7	1.8714	4.92	1949	0.08005	5.299	28.94	34.2	66.9

Figure 7. 19

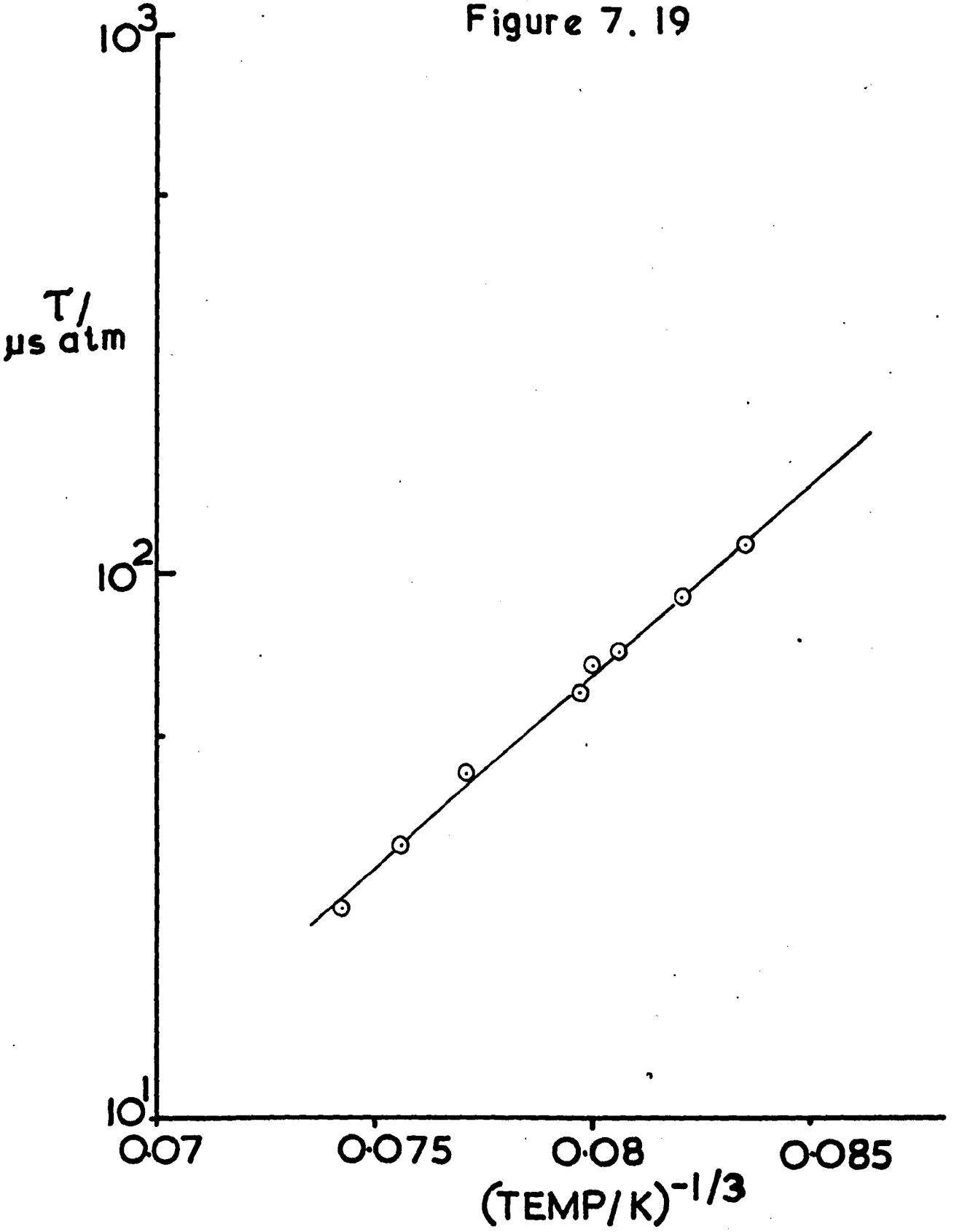

7.4.g 60% CARBON MONOXIDE - 40% NEON

Speed of Sound - 0.385 km s^{-1}; Specific Heat Ratio - 1.476; Av. Mol. Wt. - 24.88

Photo No.	P_1 mm	Shock Speed$_1$ mm μs^{-1}	Shock Mach No.	Av.Shock Temp K	$(Temp)^{-\frac{1}{3}}$	$(\rho_2/\rho_1)_{av}$	$(P_2/P_1)_{av}$	Lab Time μs	Napier Time μs atm
1282	11.9	1.8231	4.74	1866	0.08132	5.122	26.89	34.9	75.3
1283	9.4	1.8638	4.84	1938	0.08020	5.171	28.13	39.4	70.8
1284	8.1	1.9224	4.99	2045	0.07879	5.264	29.94	31.4	52.8
1286	5.4	2.0378	5.30	2258	0.07620	5.38	33.69	26.3	33.9
1287	4.9	2.0653	5.37	2308	0.07566	5.391	34.63	26.8	32.3
2281	15.4	1.7269	4.49	1707	0.08366	5.005	24.09	45.2	110.5
2282	14.4	1.7533	4.56	1748	0.08301	5.023	24.84	46.4	109.7
2283	8.5	1.9064	4.94	2014	0.07918	5.23	29.44	33.0	56.8

Figure 7.20

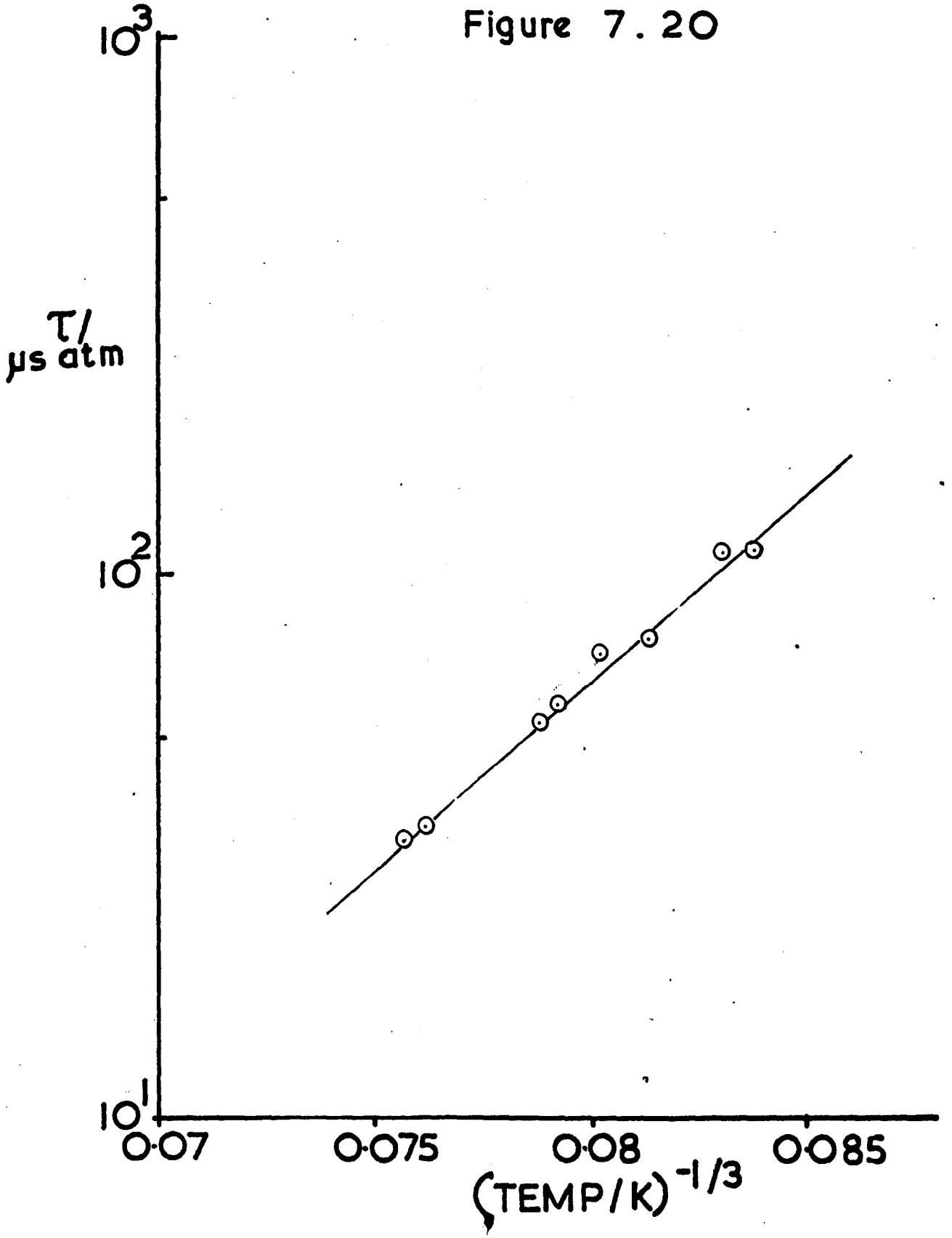

7.4.h 50% CARBON MONOXIDE - 50% NEON

Speed of Sound - 0.394 km s^{-1}; Specific Heat Ratio - 1.5; Av. Mol. Wt. - 24.09

Photo No.	P_1 mm	Shock Speed$_1$ mm μs^{-1}	Shock Mach No.	Av.Shock Temp K	$(Temp)^{-\frac{1}{3}}$	$(\rho_2/\rho_1)_{av}$	$(P_2/P_1)_{av}$	Lab Time μs	Napier Time μs atm
1201	12.9	1.8303	4.64	1874	0.08111	4.85	25.95	34.3	73.3
1202	11.1	1.8563	4.71	1930	0.08031	4.923	26.71	33.6	64.6
1203	9.1	1.9144	4.86	2034	0.07892	4.993	28.45	30.9	51.2
1205	9.9	1.8868	4.79	1987	0.07954	4.98	27.62	32.5	58.2
1206	8.0	1.9952	4.96	2112	0.0779	5.046	29.68	28.6	45.1
1207	7.8	1.9184	4.87	2046	0.07877	5.006	28.56	36.6	47.2
1209	18.1	1.7108	4.34	1681	0.08411	4.736	22.64	47.2	120.6
2201	10.2	1.8946	4.81	1984	0.07957	4.906	27.84	31.7	58.1
2202	12.2	1.8421	4.67	1893	0.08083	4.851	26.30	34.4	70.4
2203	14.9	1.7771	4.51	1786	0.08247	4.811	24.45	38.9	89.7

Figure 7.21

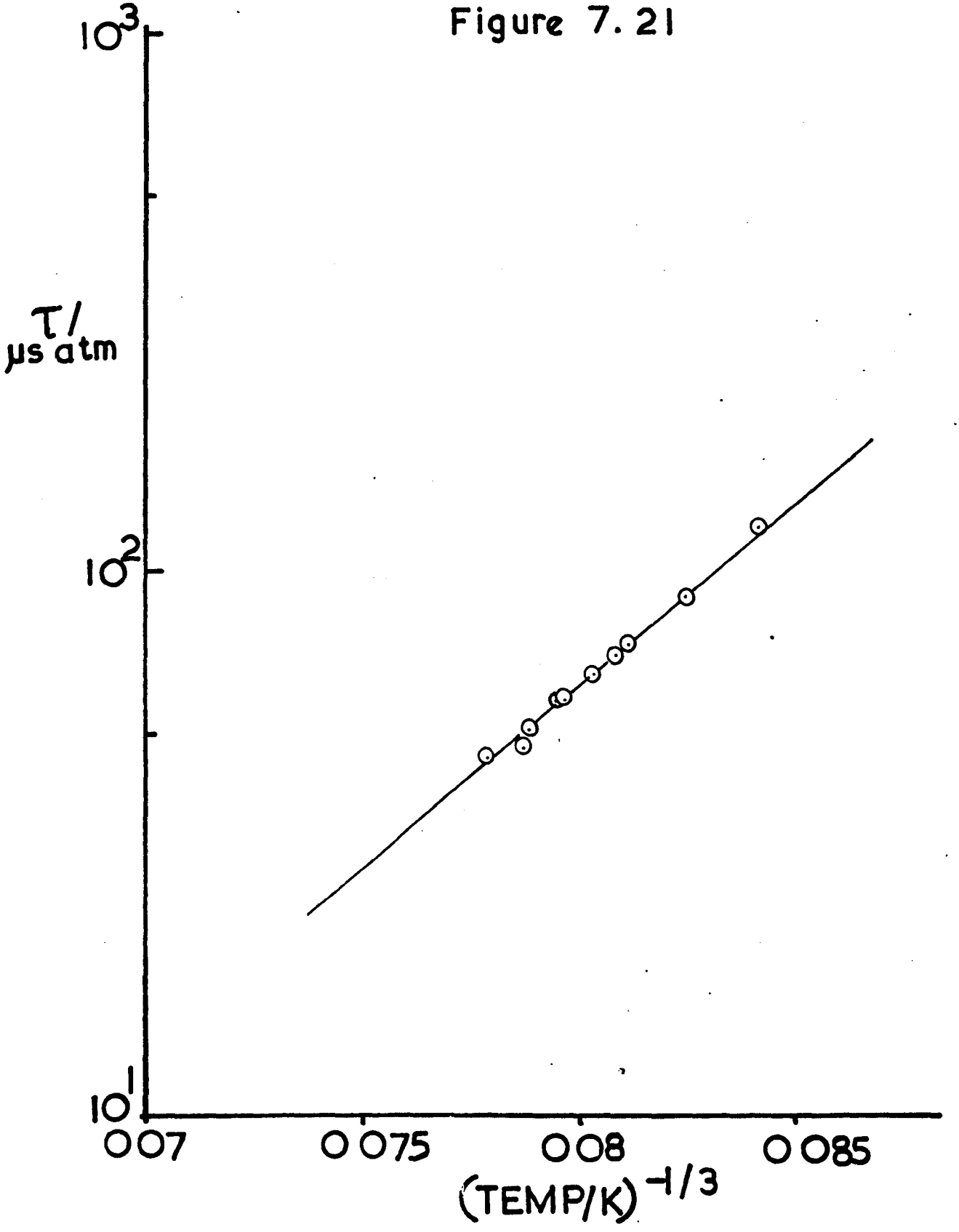

7.4.i 45% CARBON MONOXIDE - 55% NEON

Speed of Sound - 0.399 km s^{-1}; Specific Heat Ratio - 1.513; Av. Mol. Wt. - 23.70

Photo No.	P_1 mm	Shock Speed$_1$ mm μs^{-1}	Shock Mach No.	Av.Shock Temp K	$(Temp)^{-\frac{1}{3}}$	$(\rho_2/\rho_1)_{av}$	$(P_2/P_1)_{av}$	Lab Time μs	Napier Time μs atm
1211	13.1	1.8051	4.52	1850	0.08145	4.759	24.69	35.5	71.9
1212	12.1	1.8266	4.58	1881	0.08101	4.777	25.28	37.4	71.9
1213	11.2	1.8600	4.66	1943	0.08005	4.826	26.23	32.9	61.3
2212	10.6	1.8829	4.72	1985	0.07957	4.855	26.90	31.6	57.6
2213	14.1	1.7980	4.51	1831	0.08173	4.742	24.5	38.5	83.0
2214	16.9	1.7237	4.32	1703	0.08373	4.643	22.48	46.8	108.5

Figure 7.22

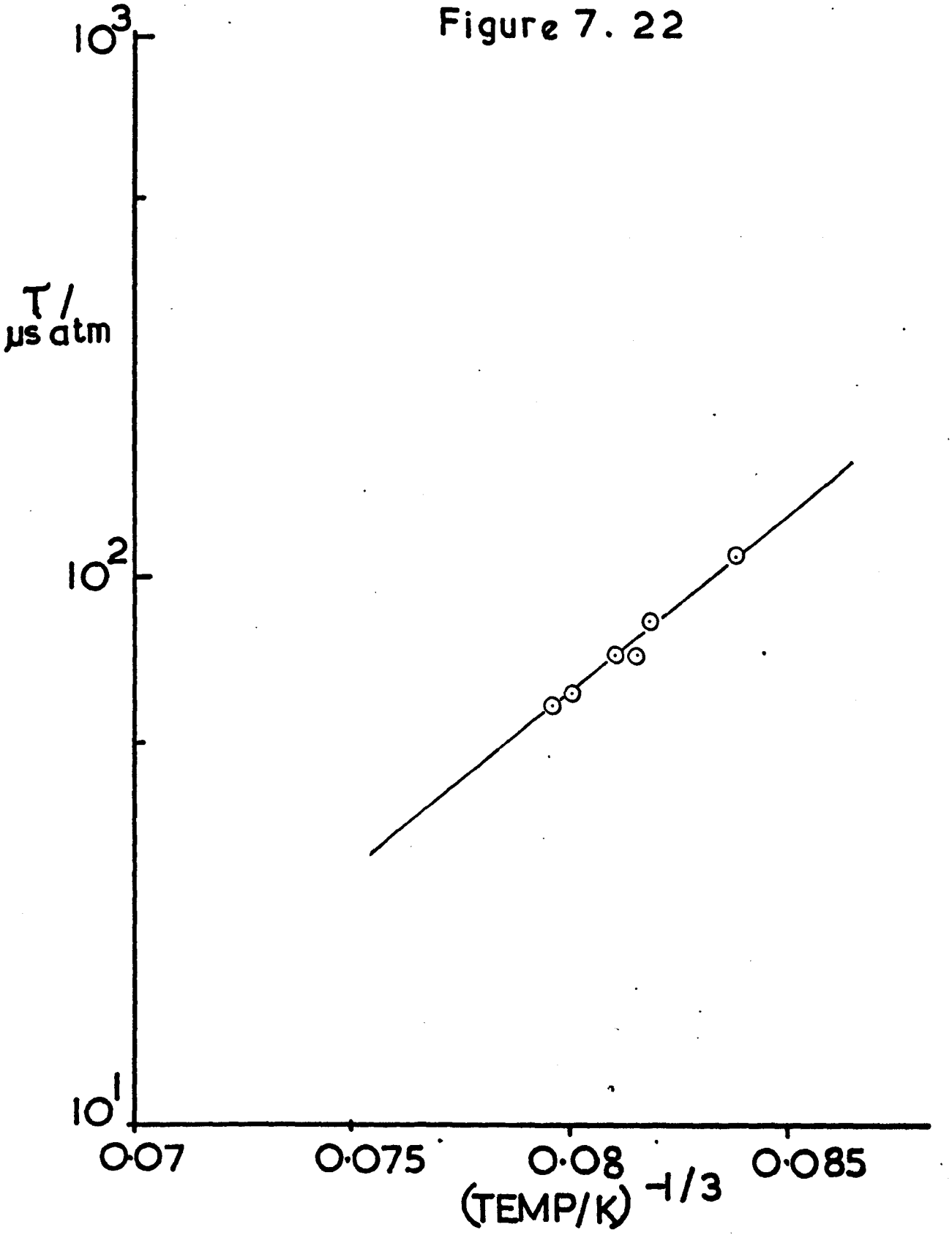

7.4.j 40% CARBON MONOXIDE - 60% NEON

Speed of Sound - 0.404 km s^{-1}; Specific Heat Ratio - 1.526; Av. Mol. Wt. - 23.31

Photo No.	P_1 mm	Shock Speed$_1$ mm μs^{-1}	Shock Mach No.	Av.Shock Temp K	$(Temp)^{-\frac{1}{3}}$	$(\rho_2/\rho_1)_{av}$	$(P_2/P_1)_{av}$	Lab Time μs	Napier Time μs atm
1221	13.4	1.8231	4.51	1880	0.08102	4.675	24.62	35.0	71.1
1222	11.9	1.8525	4.58	1934	0.08026	4.71	25.44	33.2	62.3
1223	11.0	1.8896	4.68	2001	0.07936	4.749	26.47	31.2	56.8
1224	11.5	1.8868	4.67	1995	0.07943	4.737	26.39	31.8	60.1
1225	9.4	1.9184	4.75	2052	0.07869	4.771	27.29	29.2	47.0
1226	9.0	1.9346	4.79	2085	0.07827	4.803	27.77	29.7	46.9
1227	15.1	1.7601	4.36	1767	0.08271	4.58	22.92	43.7	91.2
1228	18.0	1.7302	4.28	1715	0.08353	4.533	22.15	40.0	95.1
1229	20.0	1.6880	4.18	1649	0.08464	4.473	21.08	49.8	122.8

Figure 7. 23

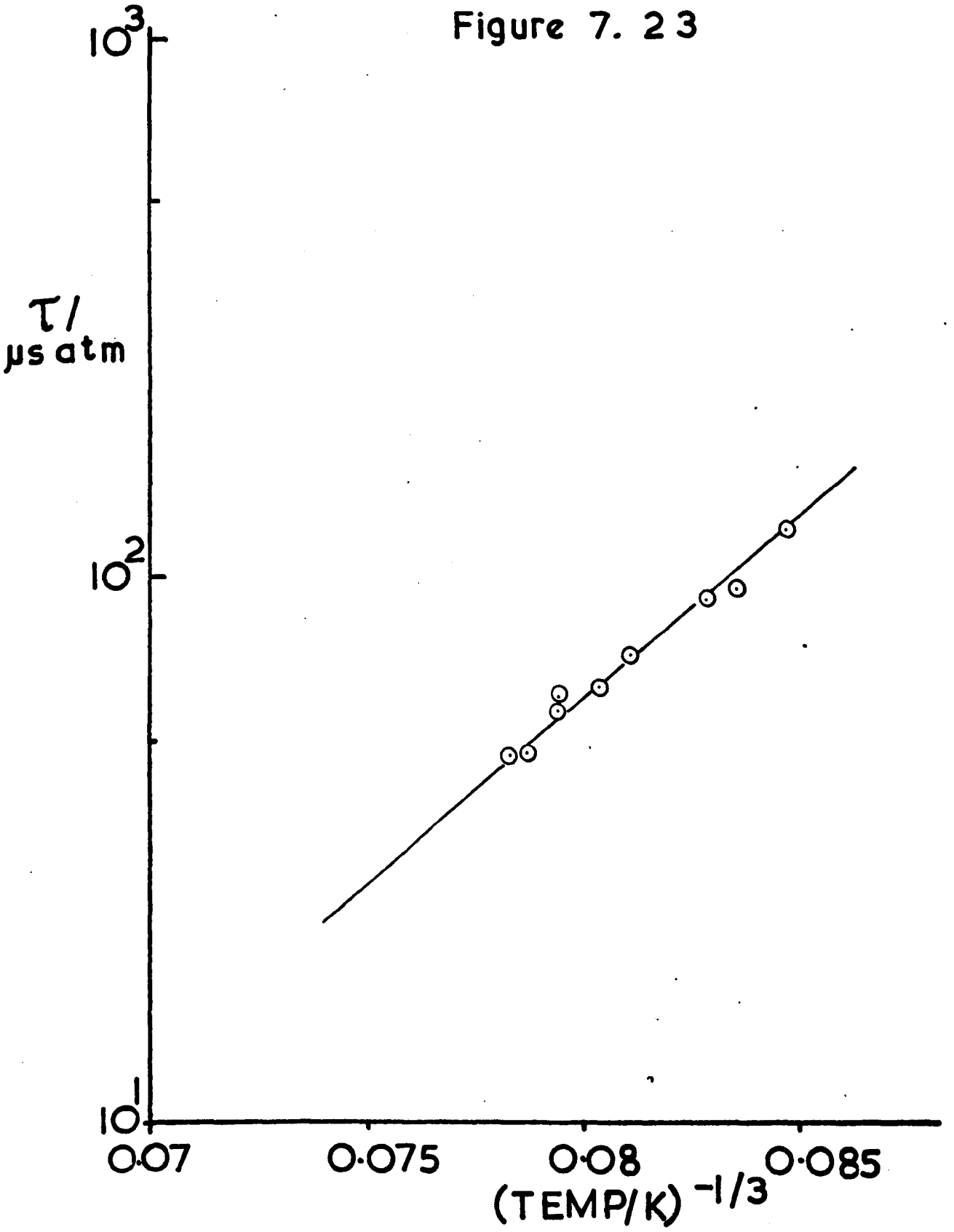

7.4.k 35% CARBON MONOXIDE - 65% NEON

Speed of Sound - 0.409 km s^{-1}; Specific Heat Ratio - 1.541; At. Mol. Wt. - 22.92

Photo No.	P_1 mm	Shock Speed $mm\ \mu s^{-1}$	Shock Mach No.	Av.Shock Temp K	$(Temp)^{-\frac{1}{3}}$	$(\rho_2/\rho_1)_{av}$	$(P_2/P_1)_{av}$	Lab Time μs	Napier Time μs atm
1232	12.2	1.8414	4.50	1919	0.08046	4.59	24.54	35.1	63.5
1233	11.3	1.8829	4.60	1993	0.07946	4.632	25.67	32.4	55.1
1234	10.0	1.9144	4.68	2058	0.07862	4.685	26.55	27.8	45.5
1235	9.0	1.9104	4.67	2035	0.07890	4.622	26.44	29.0	41.9
2231	20.0	1.6764	4.09	1626	0.08503	4.346	20.28	55.3	128.2
2232	17.8	1.7269	4.22	1711	0.08361	4.413	21.54	47.1	104.8

Figure 7. 24

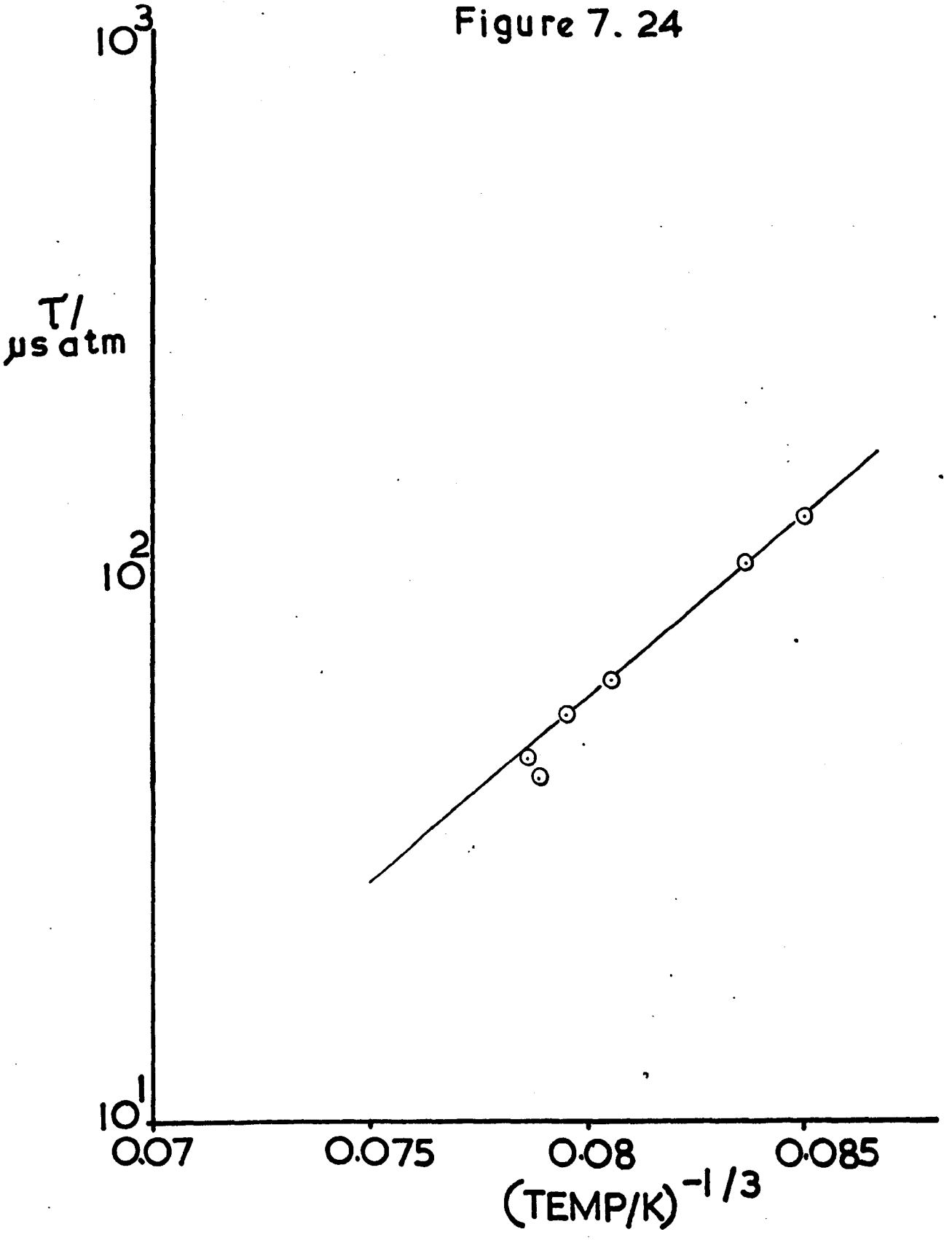

7.4.1 20% CARBON MONOXIDE - 80% NEON

Speed of Sound - 0.426 km s^{-1}; Specific Heat Ratio - 1.588; Av. Mol. Wt. - 21.75

Photo No.	P_1 mm	Shock Speed$_1$ mm μs^{-1}	Shock Mach No.	Av.Shock Temp K	$(Temp)^{-\frac{1}{3}}$	$(\rho_2/\rho_1)_{av}$	$(P_2/P_1)_{av}$	Lab Time μs	Napier Time μs atm
1265	15.1	1.8051	4.23	1865	0.08124	4.212	21.86	40.3	73.7
1266	16.7	1.7737	4.16	1651	0.08460	4.041	21.09	58.9	126.3
1267	21.2	1.6888	3.96	1651	0.08460	4.041	19.09	57.5	123.7
1268	14.7	1.8087	4.24	1872	0.08113	4.213	21.95	44.6	80.1
2261	13.4	1.8267	4.28	1884	0.08097	4.208	22.39	42.1	69.8
2262	19.4	1.737	4.04	1705	0.08371	4.05	19.91	55.2	113.6
2263	22.8	1.6764	3.93	1619	0.08515	3.981	18.81	61.3	137.7

Figure 7.25

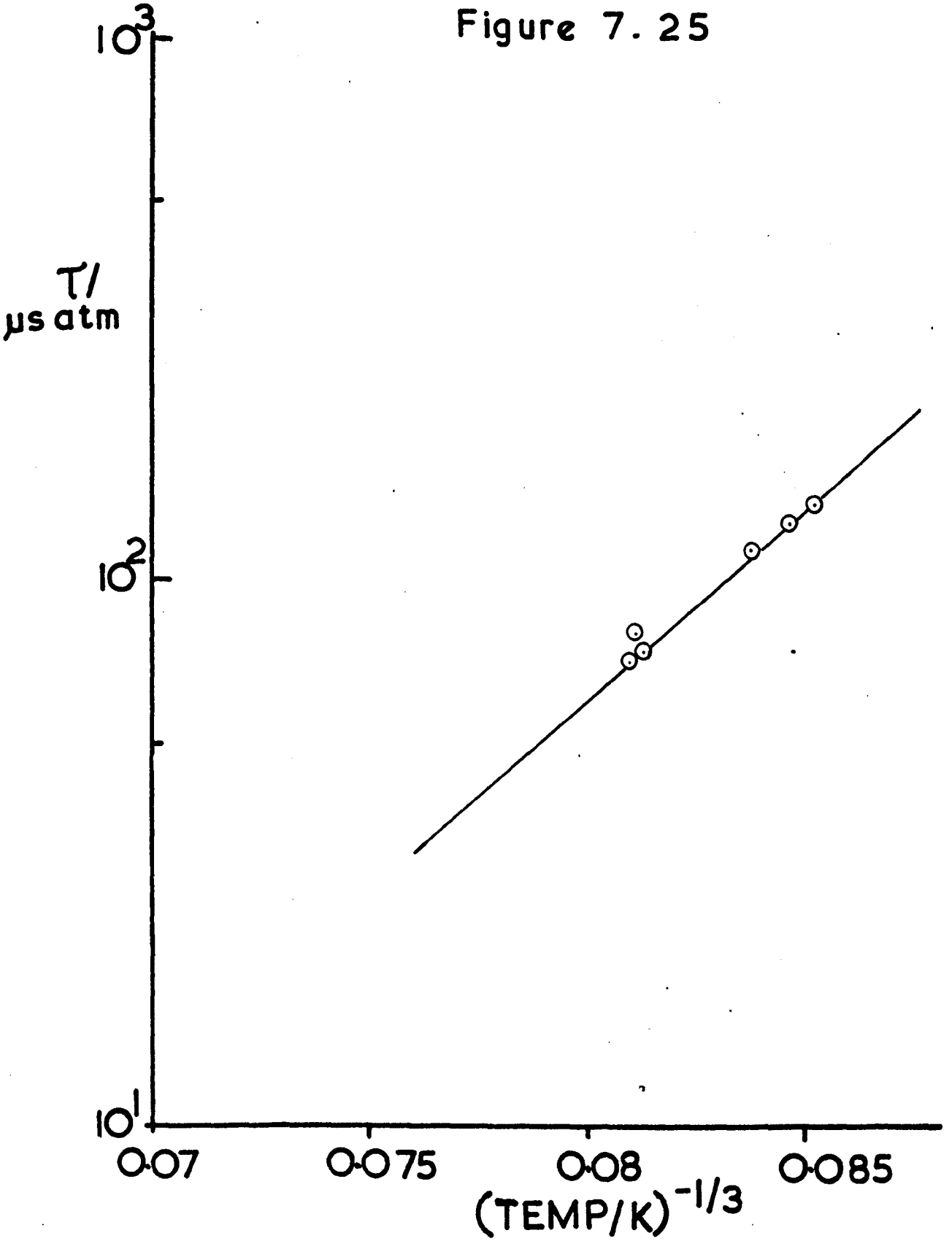

7.4.m 10% CARBON MONOXIDE - 90% NEON

Speed of Sound - 0.439; Specifc Heat Ratio - 1.625; Av. Mol. Wt. - 20.96

Photo No.	P_1 mm	Shock Speed$_1$ mm μs^{-1}	Shock Mach No.	Av.Shock Temp K	$(\text{Temp})^{-\frac{1}{3}}$	$(\rho_2/\rho_1)_{av}$	$(P_2/P_1)_{av}$	Lab Time μs	Napier Time μs atm
1281	20.0	1.7302	3.93	1734	0.08323	3.901	19.0	48.6	94.8
1282	20.8	1.7367	3.95	1734	0.08323	3.866	19.14	48.7	98.6
1283	25.0	1.6734	3.81	1628	0.08499	3.808	17.75	56.4	125.4
1285	22.3	1.7045	3.88	1681	0.08410	3.822	18.43	52.6	111.3
1286	18.7	1.7703	4.03	1807	0.08209	3.949	19.90	41.3	79.7

Figure 7.26

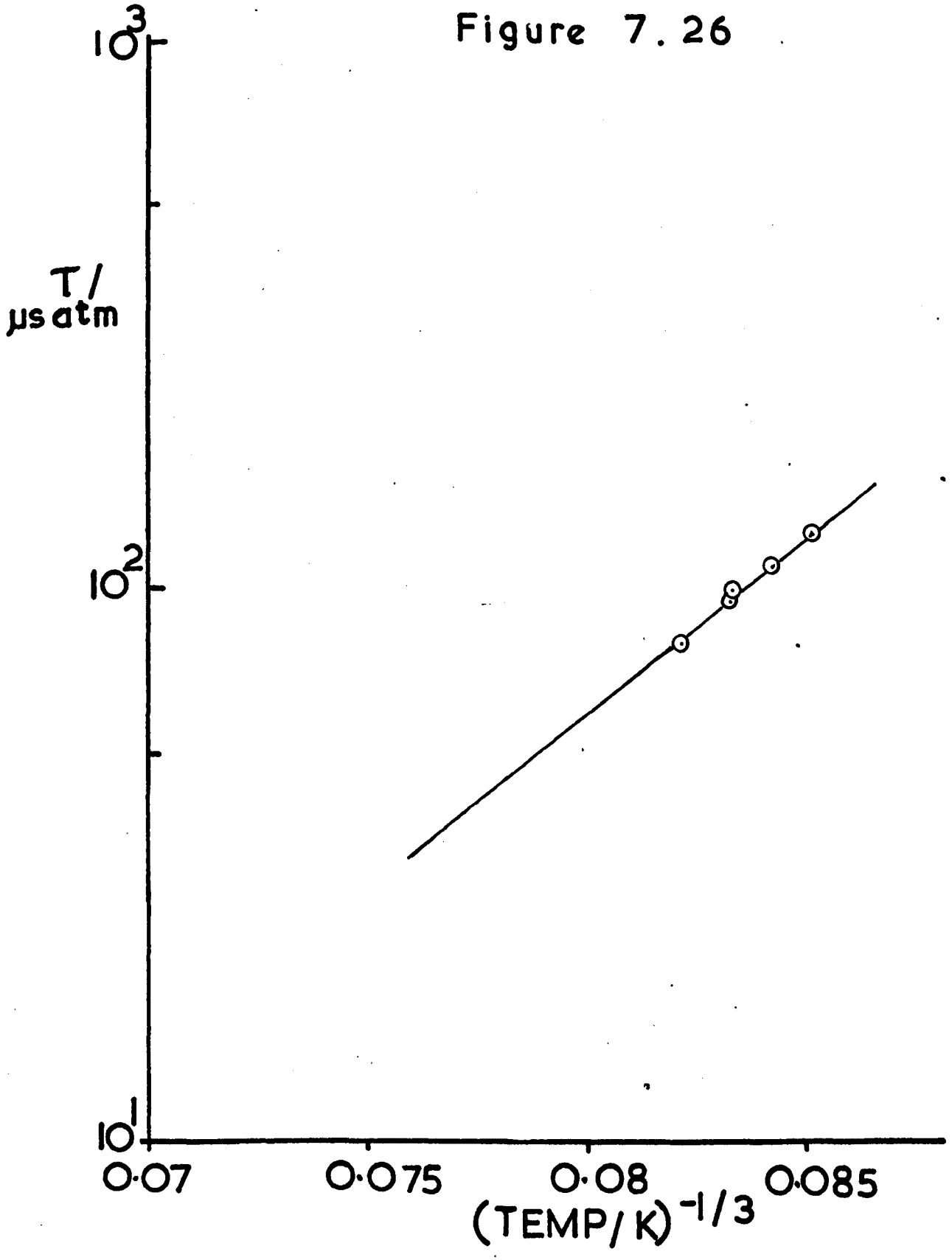

7.5 DATA OF CO/POLYATOMIC MIXTURES FOR 1ST VIBRATIONAL LEVEL

The following section contains the data obtained on the CO/CO_2, CO/N_2O, and CO/COS systems. The data for each mixture of each system is tabulated on a separate page. After the data for each system a Landau-Teller plot, of all the mixtures, is presented.

A typical experimental record of the infrared emission due to the $1 \rightarrow 0$ in CO is shown in Figure 7.27. The data corresponding to this trace is to be found in section 7.5.a.i photograph number 1404. The horizontal sweep is 20 μs cm^{-1} (i.e. with Figure 7.27 20 μs/large square) and the emission of the CO rises vertically.

Figure 7.27

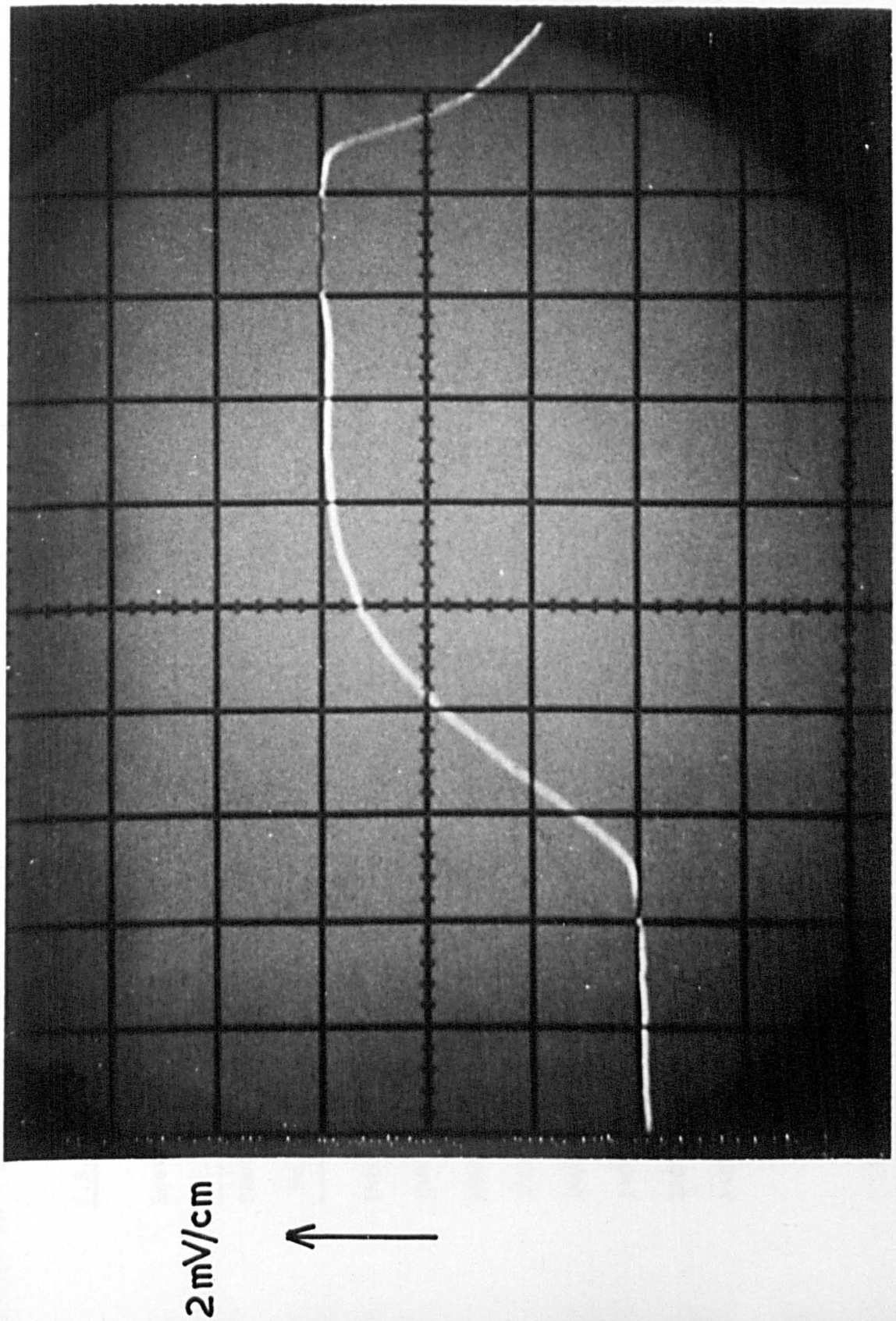

7.5.a.i 99.9% CARBON MONOXIDE - 0.1% CARBON DIOXIDE

Speed of Sound - 0.3529 km s^{-1}; Specific Heat Ratio - 1.4; Av. Mol. Wt. - 28.03

Photo No.	P_1 mm	Shock Speed$_1$ mm μs^{-1}	Shock Mach No.	Av.Shock Temp K	$(Temp)^{-\frac{1}{3}}$	$(\rho_2/\rho_1)_{av}$	$(P_2/P_1)_{av}$	Lab Time μs	Napier Time μs atm
1401	12.1	1.7591	4.98	1705	0.08370	5.636	29.19	24.0	62.9
1402	9.9	1.8412	5.22	1836	0.08166	5.768	32.00	23.0	55.3
1403	10.2	1.8347	5.20	1825	0.08182	5.749	31.76	23.4	57.3
1404	12.2	1.8228	5.18	1798	0.08223	5.705	31.35	24.0	63.2
1405	13.3	1.7531	4.97	1695	0.08386	5.628	28.98	27.0	77.4
1406	14.0	1.7264	4.89	1649	0.08463	5.562	28.08	31.0	89.2
1407	16.0	1.6791	4.76	1580	0.08586	5.508	26.56	35.0	107.7
1408	16.8	1.6592	4.70	1550	0.08640	5.47	25.93	36.0	112.9

7.5.a.ii 99.5% CARBON MONOXIDE - 0.5% CARBON DIOXIDE

Speed of Sound - 0.3524 km s^{-1}; Specific Heat Ratio - 1.4; Av. Mol. Wt. - 28.04.

Photo No.	P_1 mm	Shock Speed mm μs^{-1}	Shock Mach No.	Av.Shock Temp K	$(Temp)^{-\frac{1}{3}}$	$(\rho_2/\rho_1)_{av}$	$(P_2/P_1)_{av}$	Lab Time μs	Napier Time μs atm
1412	12.8	1.7699	5.02	1718	0.08349	5.628	29.61	18.0	50.5
1413	13.9	1.7046	4.83	1617	0.08519	5.542	27.44	20.4	56.7
1414	15.0	1.6439	4.66	1534	0.08671	5.496	25.50	24.0	66.2
1415	23.5	1.5136	4.29	1344	0.09061	5.284	21.56	30.0	105.5
1416	11.0	1.7929	5.09	1758	0.08285	5.688	30.4	17.1	42.8
2413	15.9	1.6737	4.75	1564	0.08614	5.489	26.44	22.3	67.7
2414	10.3	1.7532	4.97	1698	0.08382	5.657	29.05	21.2	47.2
2415	9.3	1.8528	5.25	1863	0.08126	5.841	32.49	16.0	37.2

7.5.a.iii 99% CARBON MONOXIDE - 1% CARBON DIOXIDE

Speed of Sound - 0.352 km s^{-1}; Specific Heat Ratio - 1.4; Av. Mol. Wt. - 28.17

Photo No.	P_1 mm	Shock Speed$_1$ mm μs^{-1}	Shock Mach No.	Av.Shock Temp K	$(Temp)^{-\frac{1}{3}}$	$(\rho_2/\rho_1)_{av}$	$(P_2/P_1)_{av}$	Lab Time μs	Napier Time μs atm
1421	12.7	1.7643	5.01	1709	0.08364	5.613	29.52	12.6	34.9
1422	13.8	1.7367	4.93	1662	0.08442	5.537	28.59	12.8	36.8
1423	15.1	1.6890	4.80	1590	0.08567	5.472	27.02	14.1	41.4
1424	16.4	1.6788	4.77	1572	0.08599	5.438	26.69	13.9	43.5
1425	18.3	1.6391	4.66	1514	0.08707	5.380	25.43	13.2	43.5
1426	19.5	1.5965	4.53	1451	0.08718	5.297	24.11	14.0	45.9
1427	23.0	1.5562	4.42	1393	0.08954	5.213	22.88	15.1	54.5
2421	24.5	1.5178	4.31	1341	0.09067	5.141	21.75	18.3	66.0
2422	26.7	1.4853	4.22	1296	0.09170	5.076	20.82	18.7	68.7
2424	9.9	1.8716	5.32	1879	0.08103	5.756	33.27	11.4	28.4
2425	8.8	1.8908	5.37	1882	0.08099	5.788	33.97	11.5	26.2
2426	12.5	1.7643	5.01	1705	0.08370	5.593	29.52	12.2	33.1

7.5.a.iv 98% CARBON MONOXIDE - 2% CARBON DIOXIDE

Speed of Sound - 0.351 km s^{-1}; Specific Heat Ratio - 1.4; Av. Mol. Wt. - 28.33

Photo No.	P_1 mm	Shock Speed mm μs^{-1}	Shock Mach No.	Av.Shock Temp K	$(Temp)^{-\frac{1}{3}}$	$(\rho_2/\rho_1)_{av}$	$(P_2/P_1)_{av}$	Lab Time μs	Napier Time μs atm
1431	14.5	1.6839	4.80	1582	0.08582	5.457	27.03	9.0	25.3
1432	21.1	1.5432	4.40	1376	0.08989	5.194	22.64	9.6	31.2
1433	24.0	1.5178	4.32	1340	0.09071	5.132	21.90	9.6	34.1
1434	28.2	1.4579	4.15	1263	0.09249	5.038	20.17	10.4	39.2
1435	30.9	1.4352	4.09	1232	0.09327	4.987	19.54	10.9	43.2
1436	18.3	1.6294	4.64	1499	0.08736	5.349	25.28	8.8	28.6
2431	20.2	1.6011	4.56	1459	0.08816	5.315	24.4	8.1	27.9
2433	25.0	1.5095	4.30	1331	0.09091	5.128	21.65	10.0	36.5
2434	27.0	1.4973	4.26	1314	0.09129	5.117	21.29	10.0	38.7

Figure 7.28

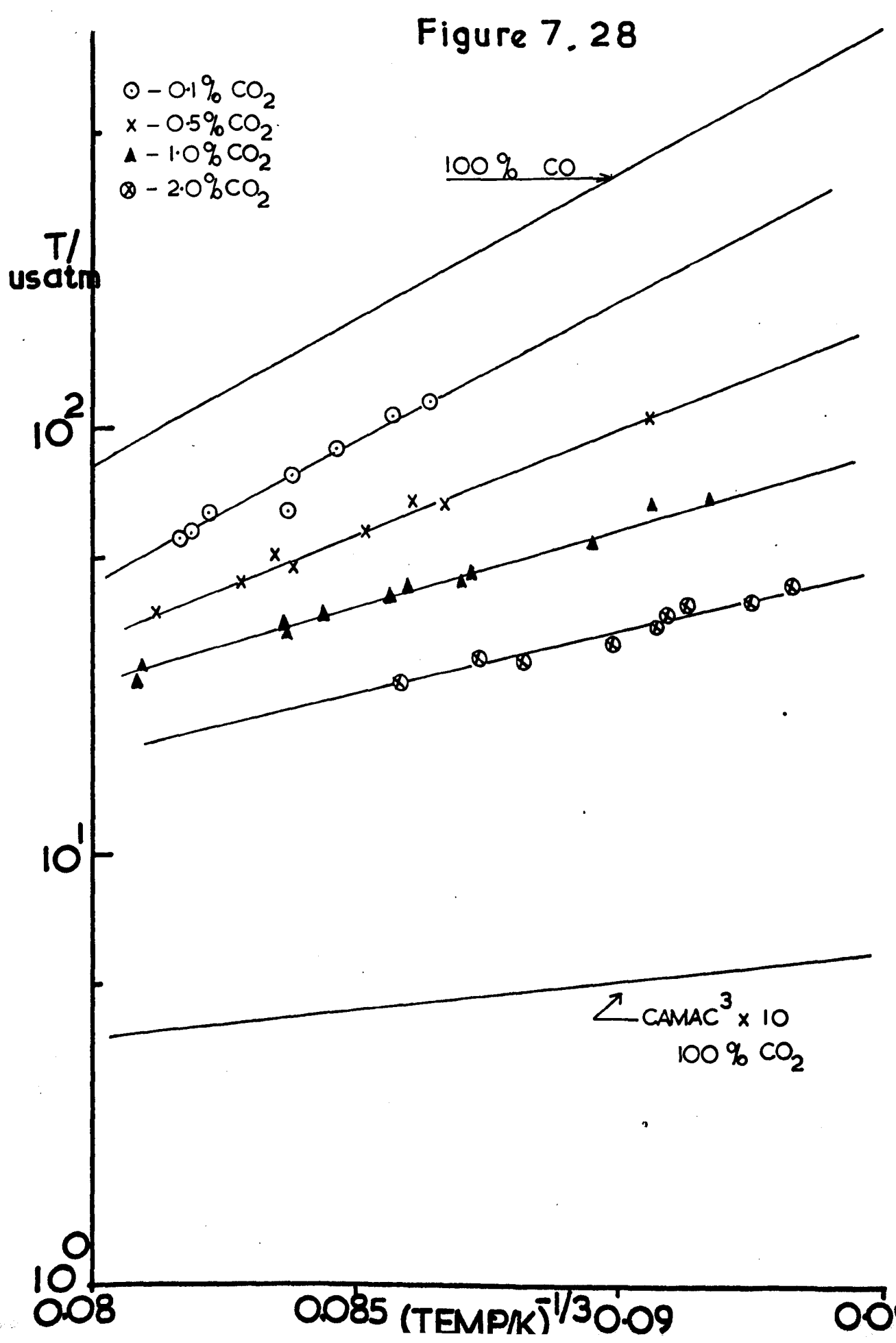
⊙ – 0·1% CO_2
x – 0·5% CO_2
▲ – 1·0% CO_2
⊗ – 2·0% CO_2
100 % CO
T/ usatm
10^2
10^1
10^0
CAMAC^3 x 10
100 % CO_2
0·08
0·085
(TEMP/K)$^{-1/3}$
0·09
0·095

7.5.b.i 99.9% CARBON MONOXIDE - 0.1% NITROUS OXIDE

Speed of Sound - 0.3529 km s^{-1}; Specific Heat Ratio - 1.4; Av. Mol. Wt. - 28.03

Photo No.	P_1 mm	Shock Speed$_1$ mm μs^{-1}	Shock Mach No.	Av.Shock Temp K	$(Temp)^{-\frac{1}{3}}$	$(\rho_2/\rho_1)_{av}$	$(P_2/P_1)_{av}$	Lab Time μs	Napier Time μs atm
1501	13.1	1.7484	4.95	1683	0.08406	5.592	28.82	22.1	61.4
1503	14.8	1.6991	4.81	1610	0.08531	5.536	27.20	25.1	73.6
1504	15.5	1.6591	4.70	1555	0.08631	5.51	25.93	26.3	76.7
1505	14.5	1.7203	4.87	1645	0.08470	5.594	27.88	22.0	65.5
1506	17.6	1.6591	4.70	1557	0.08627	5.53	25.93	24.2	80.4
1507	19.1	1.6104	4.56	1483	0.08772	5.429	24.39	28.3	94.1
1508	20.0	1.5925	4.51	1456	0.08826	5.391	23.84	31.8	107.5
1509	10.0	1.8657	5.28	1871	0.08115	5.766	32.85	19.7	49.1

7.5.b.ii 99.5% CARBON MONOXIDE - 0.5% NITROUS OXIDE

Speed of Sound - 0.3525 km s^{-1}; Specific Heat Ratio - 1.4; Av. Mol. Wt. - 28.09

Photo No.	P_1 mm	Shock Speed $mm\ \mu s^{-1}$	Shock Mach No.	Av.Shock Temp K	$(Temp)^{-\frac{1}{3}}$	$(\rho_2/\rho_1)_{av}$	$(P_2/P_1)_{av}$	Lab Time μs	Napier Time μs atm
1511	12.1	1.7699	5.08	1733	0.08325	5.728	30.47	13.9	38.6
1512	14.9	1.7046	4.90	1628	0.08500	5.608	28.24	14.4	44.7
1513	18.3	1.6246	4.61	1496	0.08741	5.388	24.89	16.4	52.9
1514	21.5	1.5606	4.45	1403	0.08937	5.261	22.95	18.3	62.2
1516	9.9	1.8344	5.27	1840	0.08160	5.853	32.77	11.9	29.7
1517	9.3	1.8716	5.38	1904	0.08068	5.92	34.14	11.0	27.1
2511	8.8	1.8908	5.46	1923	0.08041	5.866	33.85	12.8	23.4
2512	10.8	1.8344	5.20	1820	0.08190	5.719	31.84	12.0	31.0
2513	11.8	1.7587	4.99	1698	0.08382	5.595	29.24	13.7	34.8
2514	13.7	1.7205	4.88	1640	0.08479	5.554	27.96	14.5	40.6

7.5.b.iii 99% CARBON MONOXIDE - 1% NITROUS OXIDE

Speed of Sound - 0.352 km s^{-1}; Specific Heat Ratio - 1.4; Av. Mol. Wt., - 28.17

Photo No.	P_1 mm	Shock Speed$_1$ mm μs^{-1}	Shock Mach No.	Av.Shock Temp K	$(Temp)^{-\frac{1}{3}}$	$(\rho_2/\rho_1)_{av}$	$(P_2/P_1)_{av}$	Lab Time μs	Napier Time μs atm
1521	25.5	1.4943	4.25	1306	0.09157	5.073	21.09	10.0	35.9
1522	11.1	1.8233	5.18	1795	0.08228	5.658	31.55	7.9	20.6
1523	14.0	1.7264	4.90	1644	0.08473	5.514	28.25	8.1	23.3
1524	16.2	1.7248	4.74	1556	0.08630	5.405	26.39	8.5	25.8
1525	19.4	1.5886	4.51	1436	0.08865	5.265	23.86	9.1	29.0
1526	22.5	1.5439	4.38	1354	0.09038	5.174	22.52	9.8	33.5
2521	26.1	1.4891	4.23	1300	0.09185	5.041	20.94	10.8	39.1
2522	24.2	1.5145	4.30	1335	0.09093	5.136	21.66	9.8	34.7
2523	28.2	1.4701	4.18	1270	0.09242	5.041	20.40	11.0	41.9

7.5.b.iv 98% CARBON MONOXIDE - 2% NITROUS OXIDE

Speed of Sound - 0.351 km s^{-1}; Specific Heat Ratio - 1.4; Av. Mol. Wt. - 28.33

Photo No.	P_1 mm	Shock Speed$_1$ mm μs^{-1}	Shock Mach No.	Av.Shock Temp K	$(Temp)^{-\frac{1}{3}}$	$(\rho_2/\rho_1)_{av}$	$(P_2/P_1)_{av}$	Lab Time μs	Napier Time μs atm
1531	14.5	1.7102	4.89	1630	0.08490	5.513	28.07	5.1	15.0
1532	19.2	1.6203	4.62	1463	0.08810	5.336	25.00	6.5	21.9
1533	24.1	1.5314	4.36	1360	0.09027	5.165	22.29	6.0	21.9
1534	27.2	1.4709	4.19	1277	0.09216	5.052	20.53	6.4	23.8
1535	29.2	1.4356	4.09	1232	0.09329	5.052	19.55	7.3	27.7
1536	32.0	1.4207	4.05	1211	0.09379	4.943	19.13	6.5	25.9

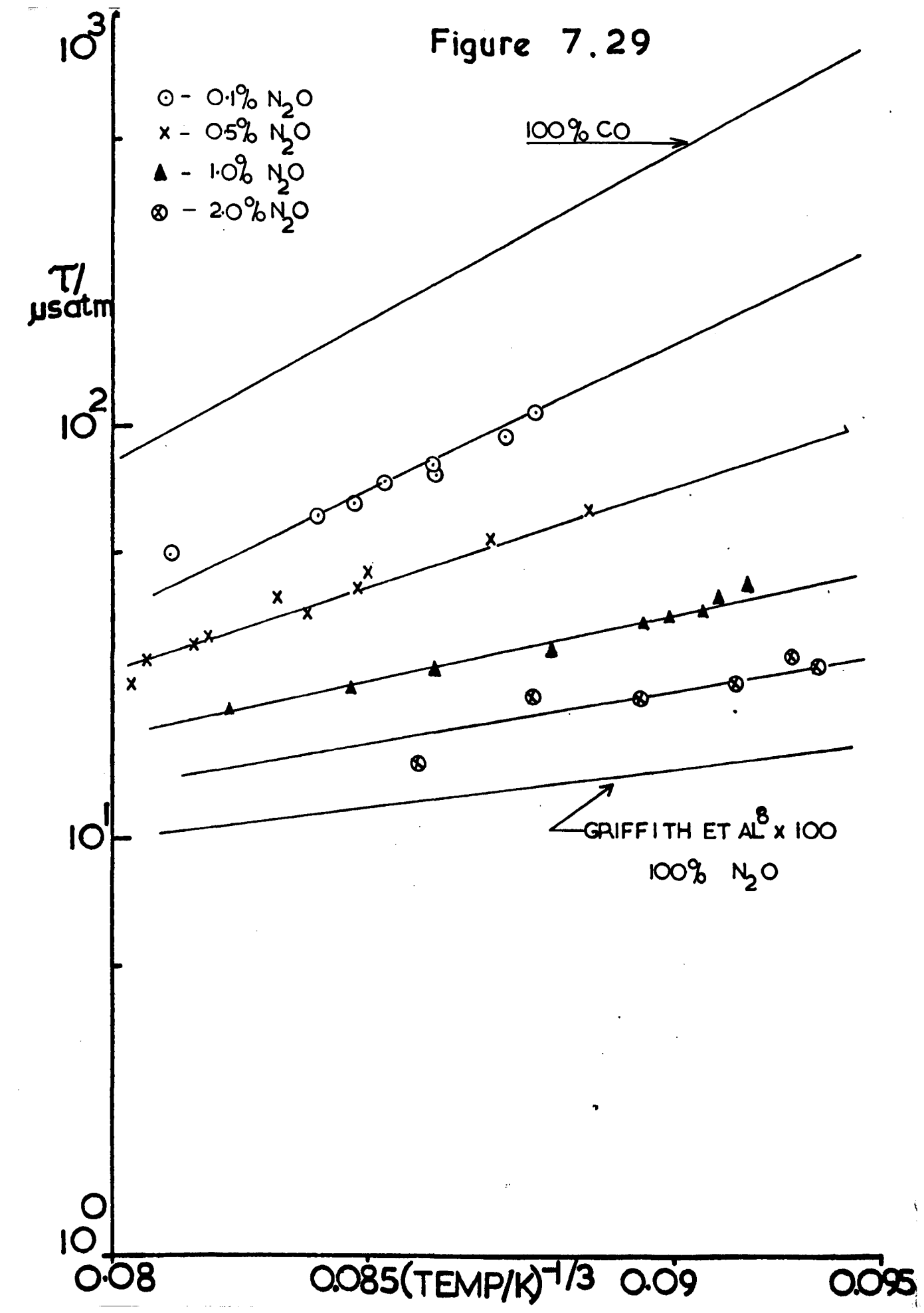
Figure 7.29
⊙ - 0·1% N_2O
× - 0·5% N_2O
▲ - 1·0% N_2O
⊗ - 2·0% N_2O
100% CO
GRIFFITH ET AL[8] x 100
100% N_2O
τ/ μsatm
10^3
10^2
10^1
10^0
0·08
0.085(TEMP/K)$^{-1/3}$
0·09
0·095

7.5.c.i 99% CARBON MONOXIDE - 1% CARBONYL SULPHIDE

Speed of Sound - 0.351 km s^{-1}; Specific Heat Ratio - 1.4; Av. Mol. Wt. - 28.33

Photo No.	P_1 mm	Shock Speed mm μs^{-1}	Shock Mach No.	Av.Shock Temp K	$(Temp)^{-\frac{1}{3}}$	$(\rho_2/\rho_1)_{av}$	$(P_2/P_1)_{av}$	Lab Time μs	Napier Time μs atm
1621	13.1	1.7061	4.86	1630	0.08497	5.515	27.74	5.8	15.3
1622	18.1	1.5975	4.55	1454	0.08827	5.248	24.28	6.1	18.5
1623	19.5	1.5749	4.49	1422	0.08892	5.203	23.58	6.3	19.9
1625	22.1	1.5462	4.40	1380	0.08982	5.127	22.72	6.8	24.0
1626	25.0	1.4986	4.27	1311	0.09137	5.049	21.33	6.6	23.4

Figure 7.30

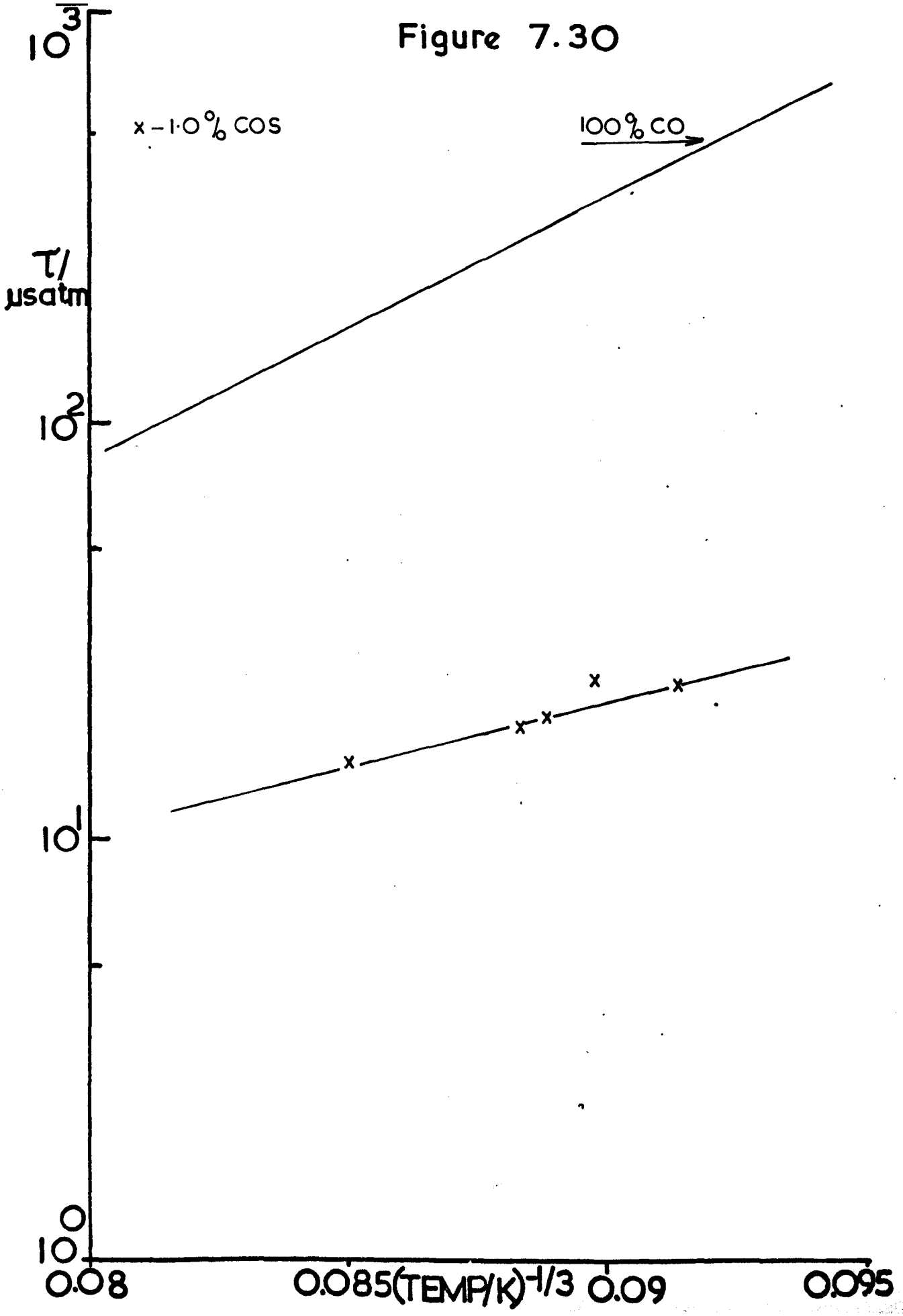
x - 1·0% COS
100% CO
τ/ μsatm
10^3
10^2
10^1
10^0
0.08
0.085(TEMP/K)^-1/3
0.09
0.095

REFERENCES

1. W.J. Hooker and R.C. Millikan, *J. Chem. Phys.*, 1963, 38, 214.

2. R.L. Belford and R.A. Strehlow, *Ann. Rev. Phys. Chem.*, 1969, 20, 247.

3. M. Camac, *Avco Report*, 1964, 195.

4. S.J. Colgan and B.P. Levitt, *Private communication*

5. C.J.S.M. Simpson, K.B. Bridgman and T.R.D. Chandler, *J. Chem. Phys.*, 1968, 49, 513.

6. C.J.S.M. Simpson, K.B. Bridgman and T.R.D. Chandler, *J. Chem. Phys.*, 1968, 49, 509.

7. J.M. Simmie, W.J. Quiring and E. Tschuikow-Roux, *J. Phys. Chem.*, 1969, 73, 3830.

8. W. Griffith, D. Brickl and, V. Blackman, *Phys. Rev.*, 1956, 102, 1209.

8. DISCUSSION

This chapter will firstly interpret and discuss the results obtained in the pure CO and CO/Ne systems, for the fundamental and overtone of CO. The results will be compared to computer studies of idealised relaxation models. A conclusion will follow the discussion. Secondly, the interpretation and discussion of the CO/polyatomic system is presented. A conclusion follows this section. Then a summary is presented which draws together relevant information from both pieces of work. Finally, suggestions for further study are made.

8.1 PURE CO AND CO/Ne MIXTURES

8.1.a 1ST VIBRATIONAL LEVEL

The results for the fundamental of CO are presented in section 7.2 and those of CO/Ne mixtures in section 7.3 of Chapter 7. The Napier time-temperature data is plotted in Figure 7.4, according to the Landau-Teller[1] equation.

$$\ln\tau = A + BT^{-\frac{1}{3}}$$

where $\tau/\mu s\ atm$ = relaxation time

$B/K^{-\frac{1}{3}}$ = constant

A = constant (only very slightly temperature dependent)

In the case of the pure gas the constants A and B are found to be:-

$$A = -22.2 \quad (-22.2)$$

$$B = 160.2 \quad (160.0)$$

These constants agree very well with the values (in brackets) obtained by Hooker and Millikan.[2] Measurements on total properties of the system,[3,4] in pure CO, also have good agreement with the above constants. This is an interesting result since measurements of total properties have $\tau^{-1} = k_{10}(1-\exp(-h\nu/kT))$ while spectroscopic measurements have $\tau^{-1} = k_{10}(1+\exp(-h\nu/kT))$.

Thus as the temperature increases, the discrepancy between the two experimental techniques should increase. The computer results, mentioned later, indicate this.

In the case of mixtures it is possible to plot τ^{-1} versus mole fraction X, according to the equation:-

$$\frac{1}{\tau_{mix}} = \frac{1-X}{\tau_{CO-CO}} + \frac{X}{\tau_{CO-Ne}}$$

where X = mole fraction of Ne

τ_{CO-Ne} = Napier time of 1 molecule of CO in Ne

Figures 8.1, 2 and 3 show plots of τ^{-1} vs X for the constant temperatures 1953K, 1813K and 1628K respectively. The data is extracted from Figures 7.6 through 7.12. Extrapolation of the straight line to the case where X=1 gives a value of τ_{CO-Ne} at the particular temperature. By applying this to another temperature,

Figure 8.1

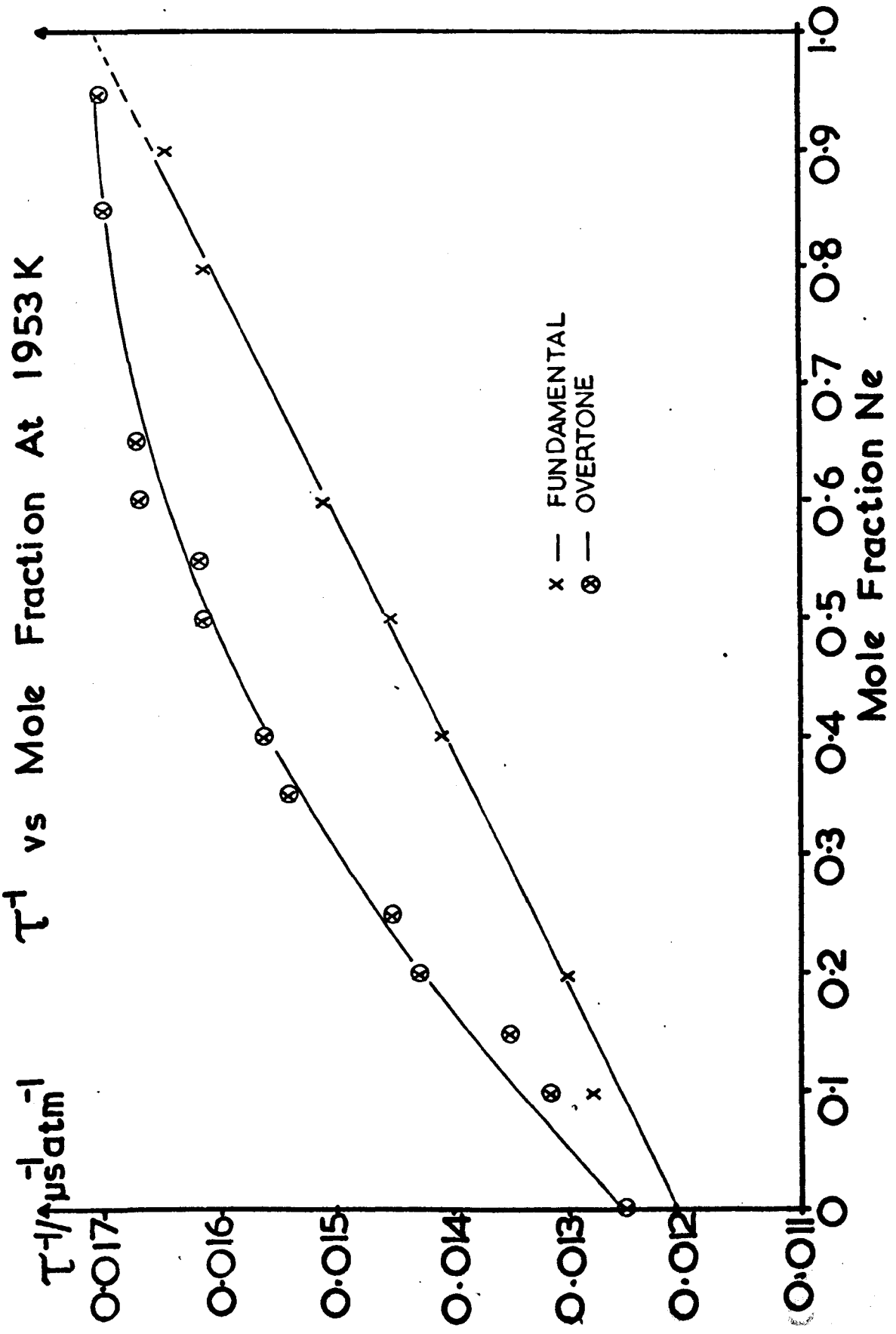
τ⁻¹ vs Mole Fraction At 1953 K
τ⁻¹/μs atm⁻¹
0·017
0·016
0·015
0·014
0·013
0·012
0·011
0
0·1
0·2
0·3
0·4
0·5
0·6
0·7
0·8
0·9
1·0
Mole Fraction Ne
x — FUNDAMENTAL
⊗ — OVERTONE

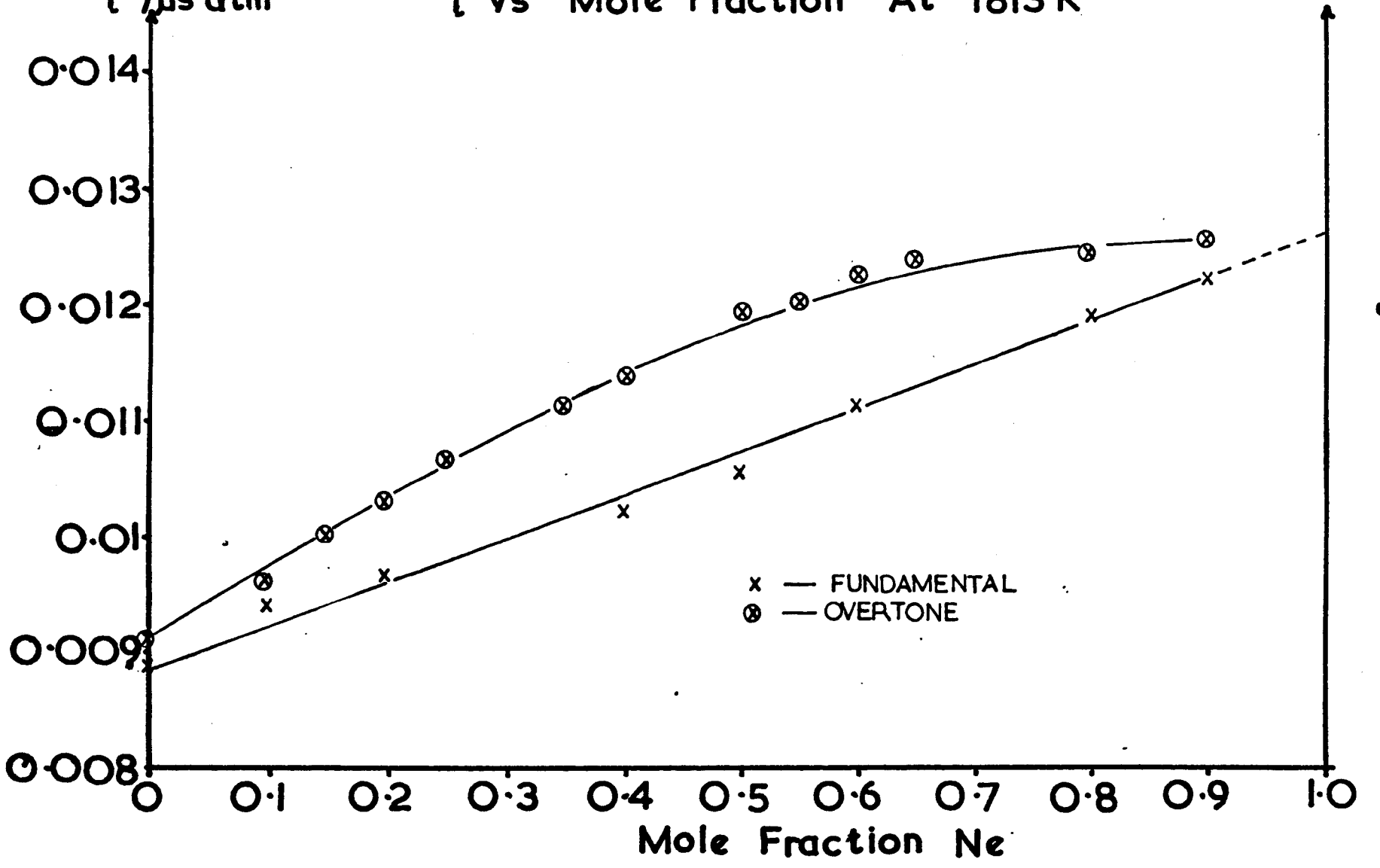
τ⁻¹/μs⁻¹atm⁻¹
τ⁻¹ vs Mole Fraction At 1813 K
0·014
0·013
0·012
0·011
0·01
0·009
0·008
0
0·1
0·2
0·3
0·4
0·5
0·6
0·7
0·8
0·9
1·0
Mole Fraction Ne
x — FUNDAMENTAL
⊗ — OVERTONE

Figure 8.2

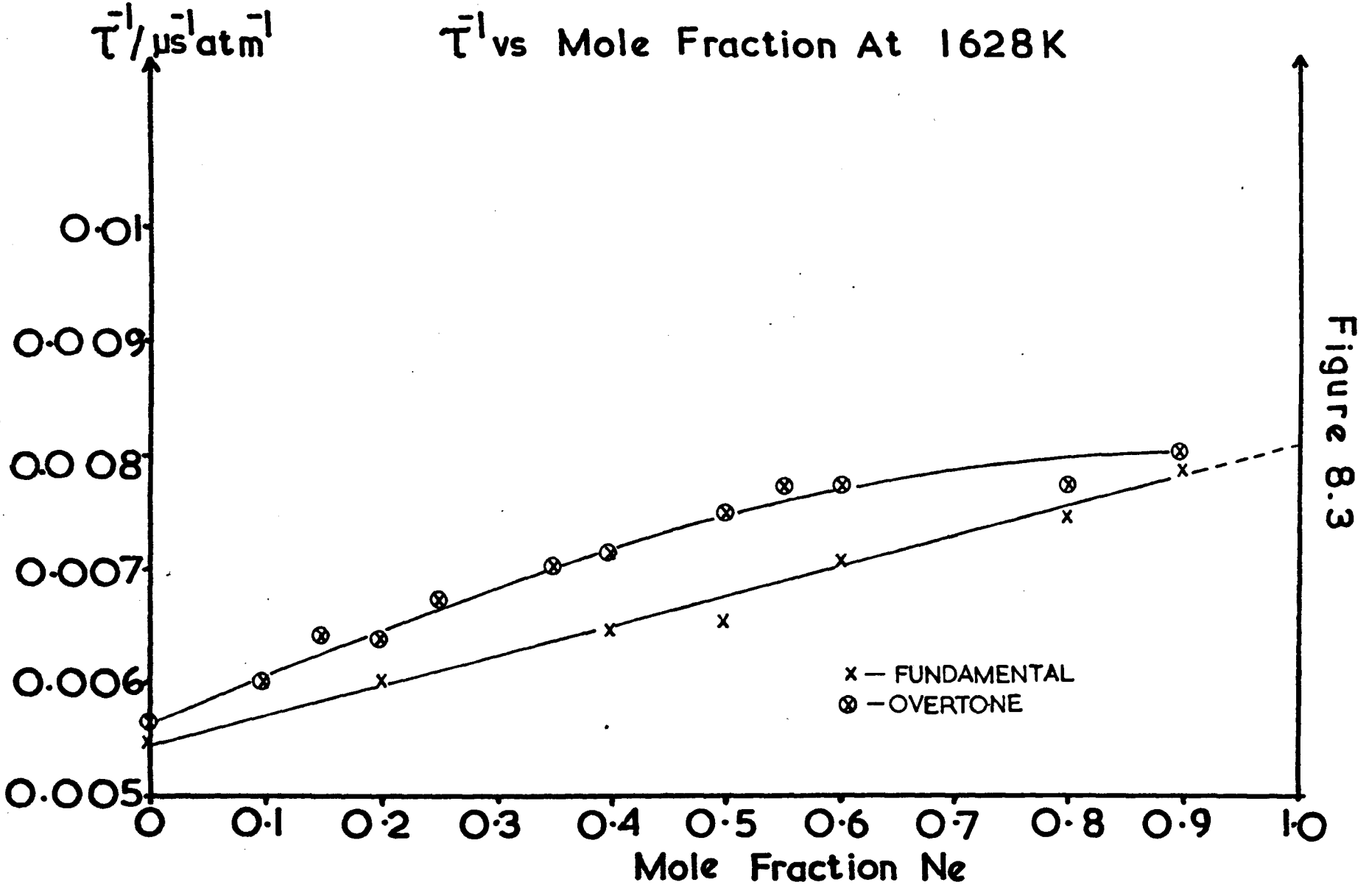
$\tau^{-1}/\mu s^{-1} atm^{-1}$
τ^{-1} vs Mole Fraction At 1628K
0·01
0·009
0·008
0·007
0·006
0·005
0
0·1
0·2
0·3
0·4
0·5
0·6
0·7
0·8
0·9
1·0
Mole Fraction Ne
x — FUNDAMENTAL
⊗ — OVERTONE

Figure 8.3

the values of A and B in the Landau-Teller equation are:-

$$A = -21.66 \quad (-21.1)$$

$$B = 148.9 \quad (142.0)$$

The values are higher by 2.7% for A and 6.3% for B than the values (in brackets) obtained by Millikan.[5] The constant B gives a steeper temperature dependence. It is most probable that the present constants are more reliable since the effect of the diluent was studied over a number of concentrations. This is in contrast to the study of Millikan,[5] who must have obtained his values by extrapolation of the line between pure CO and 3% CO in 97% Ne.

The temperature dependence of τ_{CO-CO} and τ_{CO-Ne} is shown in Figure 8.4. This figure also shows the values given by the S.S.H. theory and the M.W. correlation. The constants used in the S.S.H. calculations are shown below:-

TABLE 8.1

	ϵ/k K	r_0 nm	$\bar{\nu}_B$ cm^{-1}
CO	88.0	27.49	2143
Ne	35.6	37.06	-

The S.S.H. calculations give good agreement with the experimental value for pure CO, but the values are about 3 times shorter than the measured value for τ_{CO-Ne}. The discrepancy in the latter case

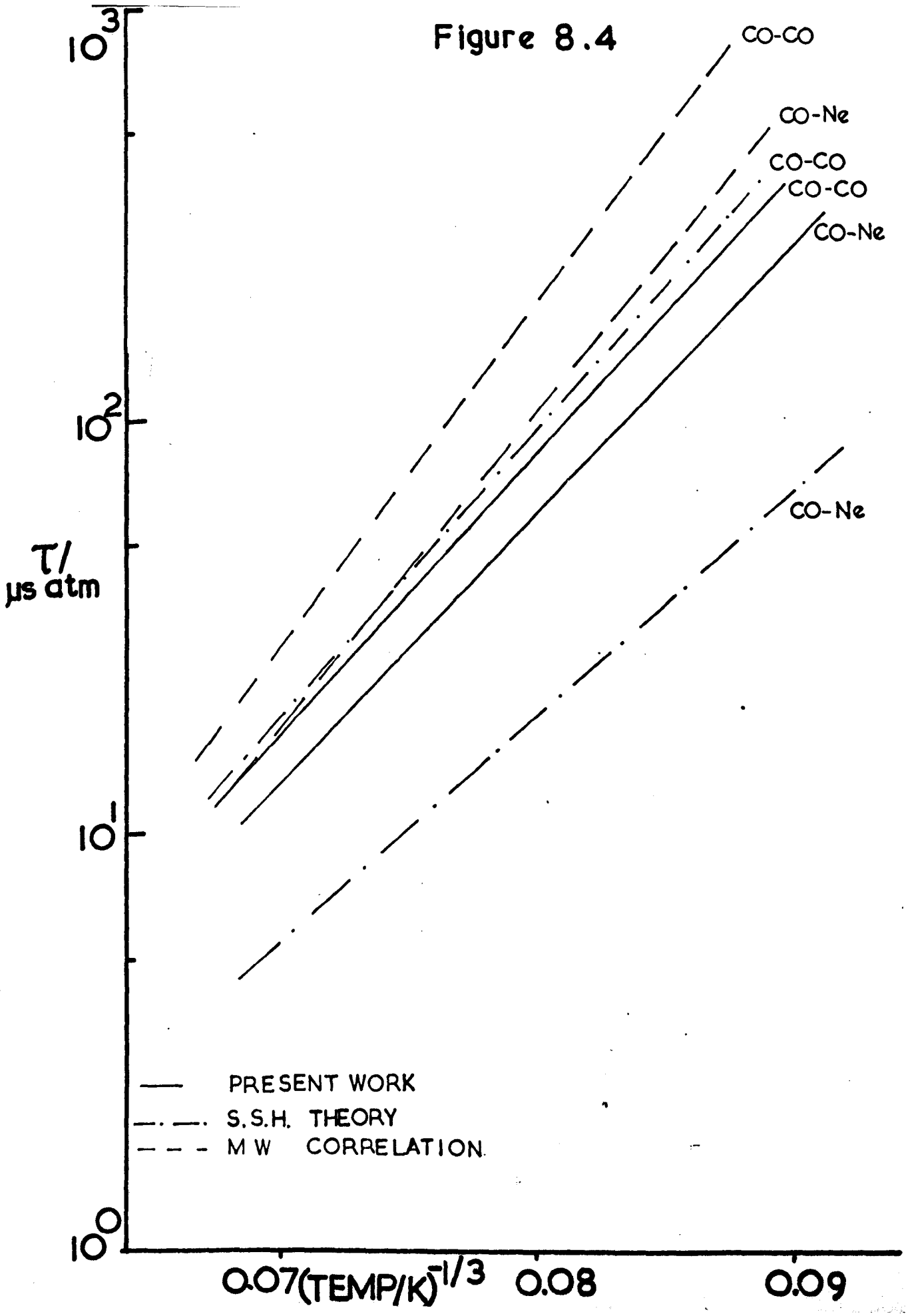
Figure 8.4
CO-CO
CO-Ne
CO-CO
CO-CO
CO-Ne
CO-Ne
10^3
10^2
10^1
10^0
τ/ μs atm
PRESENT WORK
S.S.H. THEORY
M W CORRELATION
0.07(TEMP/K)$^{-1/3}$
0.08
0.09

is difficult to explain. The value of ε/k and r_0 for Ne come from viscosity measurements on the pure gas. The error may arise because the geometric mean is taken for ε/k and the arithmetic mean for r_0, in gas mixtures. The means may not accurately represent the L-J parameters in the CO-Ne case. The M.W. correlation gives values of τ_{CO-CO} and τ_{CO-Ne} which are both a factor of 2 too long. This may be due to the assumption of a single value for the repulsion parameter, ℓ, in all cases. Further, the correlation contains no terms relating to ε/k or r_0.

8.1.b 2ND VIBRATIONAL LEVEL

The results for the overtone of pure CO are presented in section 7.4.a of Chapter 7. The Napier time-temperature data is plotted, in Figure 7.14, according to the Landau-Teller equation. In the case of the pure gas the constants are found to be:-

$$A = -21.98 \quad (-22.2)$$

$$B = 156.7 \quad (160.0)$$

The constant B is slightly less, by 2.1%, than the value obtained previously,[2] and thus it gives a less steep temperature dependence.

The population of the 2nd vibrational level may be by a direct $0 \rightarrow 2$ process or by stepwise processes obeying the selection rule $\Delta v = 1$. If the direct process predominated, then the infrared emission trace Figure 7.13 would show an exponential rise, similar

to Figure 7.5. The trace, Figure 7.13, does show a zero initial slope, which cannot be ascribed to effects of the rise time of the system. The zero initial slope arises from the fact that the first vibrational level, v = 1 must have appreciable population before the excitation to v = 2 can occur. Using an harmonic oscillator 3 state model, see sections 5.2.b.ii and iii, the second vibrational level may be analysed according to equation 5.12. Treatment of the experimental results of the first level by equation 5.3.a and of the second level by 5.12, leads to the fact that the first and second levels give approximately the same relaxation time, at the same temperature. This gives support for the stepwise process, since $\Delta v = \pm 1$ selection rule is incorporated in the analytical equations. Further evidence for the stepwise process, emerges from S.S.H. calculations. When a large amount of energy, corresponding to the $2 \rightarrow 0$ transition (4286 cm^{-1}), is transferred between vibration and translation, the probability P_{20} becomes very small, 1.44×10^{-11} at 1953K. Assuming that the rate of stepwise population of the 2nd level in twice the rate of population of the 1st level, then $P_{step} = 5.4 \times 10^{-7}$. This means that the direct process is 10^{-4} less probable than the stepwise process.

The CO/Ne mixtures were plotted according to the Landau--Teller equation, Figures 7.14 through 7.26. Plots of τ^{-1} vs X were made at the constant temperatures, stated previously. The reciprocal Napier time shows an unexpected concentration dependence, since the second level results for the mixtures should fall on the same line as

the first level mixtures. The discrepancy between the two lines apparently decreases as the concentration of diluent is increased.

The results on the first level were obtained in a glass--metal tube, with windows, while those of the second level in an all glass tube. It may be, then, that the trend shown in the figures is an experimental artifact. However, as mentioned in Chapter 2, strict precautions were taken to ensure the purity of the sample and the uniformity of the flow. It was also realised that the dimensions of the tube and the bursting characteristics of the diaphragm produced non uniformities in the flow. These were corrected for in the precribed manner, see Chapter 3. Thus it was felt that the trend observed in Figures 8.1, 2, 3 was genuine. It is possible that deficiencies in the analytical equations led to the discrepancy. Computer studies, using idealised models, were undertaken to test the validity of the equations. The tests are shown below.

8.1.c COMPUTER STUDIES

8.1.c.i THE MODELS

The computer calculations, section A.2.iii, Appendix 2, were carried out using three models in which the molecules were assumed to be simple harmonic oscillators.

a) The two level plus resonance model, see for example section 5.2.b.iii. The first excited state was populated by T-V processes, while higher vibrational levels were populated by vibration-vibration (V-V) exchange, at exact resonance, for example in CO:-

$$CO_{v=i} + CO_{v=j} \rightleftharpoons CO_{v=i+1} + CO_{v=j-1} \qquad 8.1$$

b) The Landau-Teller (L-T) model, in which the population of all vibrational levels was by vibration-translation (V-T) energy transfer. The ratios between the rate constants were as shown in section 5.2.a.ii of Chapter 5.

c) The L-T model, as in b, but with resonance exchange operating concurrently. It was possible to adjust the rate constants of the resonance reactions (e.g. 8.1) so that the V-V rates become fast with respect to the V-T rates.

It was possible to use the models with the molecules having up to 10 vibrational levels. The relaxation of any chosen level could be plotted as a function of time, a constant or changing bath temperature could be chosen, providing in the latter case the temperature dependence of k_{10} was fed in as the constants A and B of the L-T equation. Diluents, particularly inert gases, could be added to the system in any concentration. Their L-T constants, in the presence of 1 molecule of the other gas, would be required in a changing temperature condition. It was also possible to

calculate the oscillator energy.

Figure 8.5 shows relaxation curves plotted for the first (I) and second (II) vibrational levels, using a L-T model with 5 levels. The ordinate is the ratio of the population x at time t, to the final population at equilibrium. The abscissa is in units of time which have been normalised to the relaxation time (k_{10}^{-1}) of pure CO, at the particular temperature. These relaxation curves can be reduced in exactly the same way as the experimental curves, Chapter 6, to obtain a relaxation time.

8.1.c.ii GENERAL OBSERVATIONS

In the discussion below the molecule being considered is CO, reference will also be made to CO/Ne mixtures. Several interesting points arose from the computer studies:-

a) Using an L-T model with the bath temperature changing (initially at 2051K) runs were made with molecules having 2, 5 or 10 vibrational levels. The relaxation time was taken as being the time for the population to reach (1-(1/e))th or 63.2% of its equilibrium value. It was found that the relaxation time for a 5 level system was 3% higher than that for a 2 level. The longer relaxation time, in the former case, reflects the filtering off of vibrational energy into the higher levels. This lengthens the time required for the 1st level to reach equilibrium. Extending the number of vibrational levels to 10 resulted in a relaxation time exactly the same as that

Figure 8.5

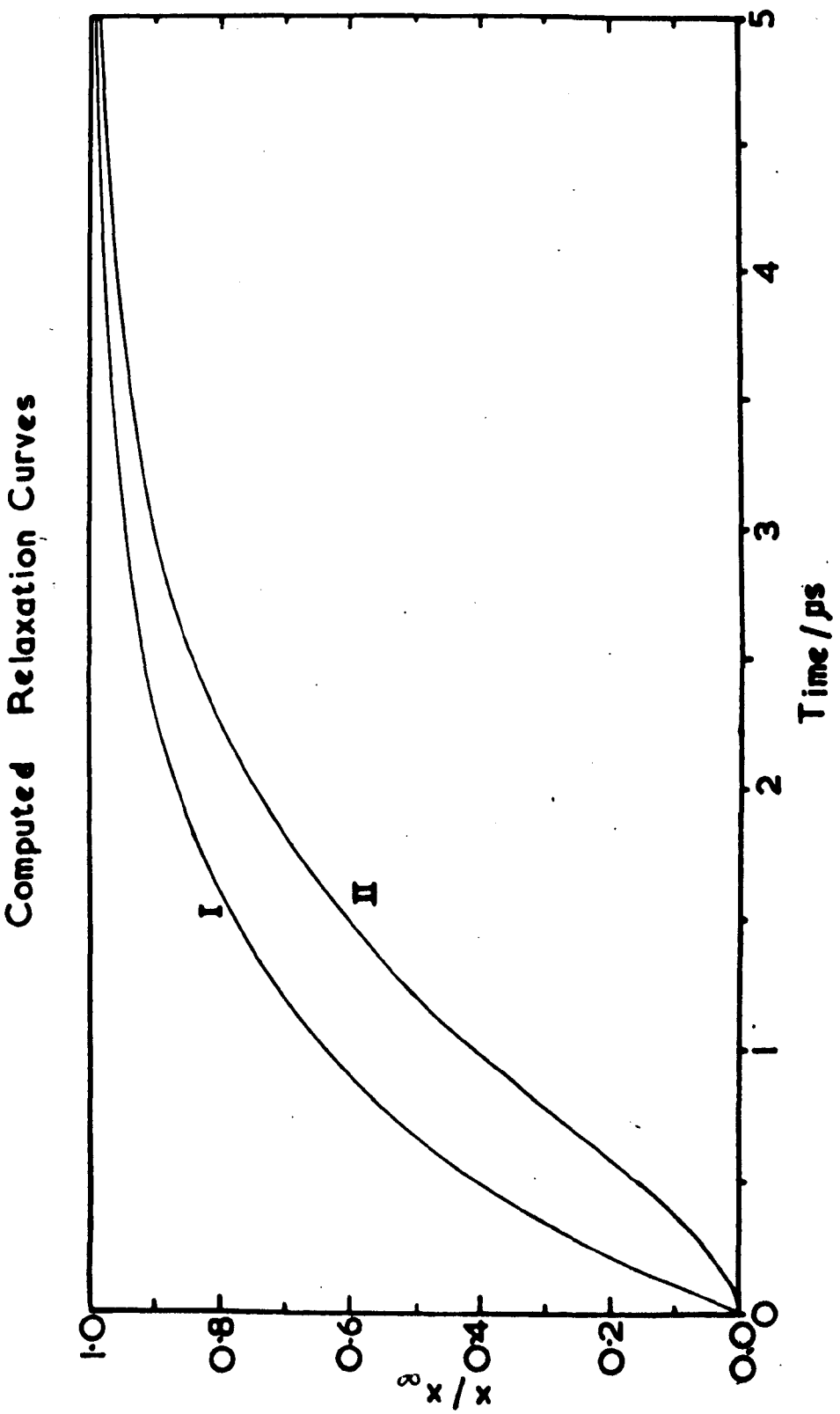
Computed Relaxation Curves
I
II
1·0
0·8
0·6
0·4
0·2
0·0
$^{\infty}x / x$
0
1
2
3
4
5
Time / μs

obtained for the 5 level system. Thus for most of the computer runs, a 5 level system was used.

b) For upper levels, the 2nd in particular, it was observed that the L-T and L-T + resonance (L-T-R) models gave exactly the same relaxation curves. This effect was independent of temperature and concentration of diluent. It was also the case no matter how fast the resonance rates were made with respect to the L-T V-T rates. (At about 2000K, for exact resonance the S.S.H. theory predicts a probability of 2.16×10^{-3}, while for the V-T process P_{10} is 4.8×10^{-6} at the same temperature. Several calculations were made where the V-V rate constants were greater than the V-T constants by factors of ten. The increase in the V-V constants did not affect the relaxation time. In order to conserve computing time, the V-V rate constants were made a factor of 10 faster than the V-T constants, for most of the calculations). The concordance of the relaxation curves demonstrates a point that theoreticians[6,7,8,9] have argued. It is that the resonance reactions serve only to redistribute the available vibrational energy, thus enabling a quasi steady state distribution to be maintained. This distribution slowly decays to equilibrium through V-T processes. It is here that the distinction between the 2 level + resonance and the L-T-R mechanisms becomes clearer. In the former system the upper vibrational levels can only obtain their energy from translation through the $0 \rightarrow 1$ transition. This means that higher

vibrational levels, in this model, would have to await significant population of the 1st vibrational level. In the L-T-R model energy is being fed from translation to every vibrational level. The computed relaxation curves showed that, for the 2nd level, the relaxation time obtained by the 2 level + resonance model was longer than that for the L-T-R model. This is one piece of evidence which strongly suggests that the 2 level + resonance model is unrealistic. The kinetic analysis of this model is shown in section 5.2.b.iii of Chapter 5.

c) The relaxation time of the oscillator energy, which is a total property of the system, is taken the time when the energy has reached 63.2% of its equilibrium value. The times obtained were compared to the relaxation times obtained, in the same way, from the populations. It was found that, for a 5 level L-T model at 1500K with temperature changing, the relaxation time for the oscillator energy was 17.9% higher than that from the populations. For a similar system at >3000K the discrepancy is >50%.

In L-T plots of the experimental data, from spectroscopic and interferometric measurements the scatter is such that these discrepancies are not noticed. Further comment will be made in section 8.1.c.iii.

d) Relaxation times obtained assuming a constant bath temperature were different from those obtained in a changing bath. The relaxation time in the case of a constant bath was always greater than that in the temperature changing case. This is due to the fact

that exp(-hν/kT) is always greater in the former system, so that it has further to go to reach equilibrium. It is also usual in shock tube studies to take the average of the shock temperature and the final equilibrium temperature. The relaxation time was quoted at the average temperature. It was found that the difference between the average temperature and the temperature corresponding to the relaxation time was about 10K in 2000K. The discrepancy was even less in the case of mixtures, where the temperature changed less as the concentration of diluent was increased. Errors from this source were negligible.

8.1.c.iii TEST OF ANALYTICAL EQUATIONS FOR 1ST AND 2ND LEVEL

This section will show the tests applied to the analysis of the relaxation curves. The tests were applied equally to both levels, in pure CO and CO/Ne mixtures.

Considering pure CO. For the first vibrational level, the best possible model and conditions, to suit the analytical equation 6.3, was an isothermal two level system. The calculations were done at 1500K, with a constant bath. Taking points off the relaxation curve and plotting $-\ln(1-x(t)/x(\infty))$ as ordinate and t as abscissa, a straight line was obtained, Figure 8.6. The reciprocal of the slope was τ, this was found to be 0.9 μs (the values of the gradations of the x axis of the Figure 8.5 were arbitrarily chosen

as 0.5 μs). The system was then revised to an L-T-R system with 5 levels, the bath temperature held constant as before. The plot of 6.3, showed an initial curvature. However, the best straight line was drawn through the points and τ was found to be 1.0 μs. This represented an 11% increase over the previous value. A further approach to reality was then made by making the bath temperature change over the relaxation period. A plot of equation 6.3 in this case is shown in Figure 8.6 (N.B. Figure 8.6 now shows the two extremes, i.e. the isothermal 2 level model and the more realistic multistate model, with changing temperature). There was a noticeable increase in curvature, over the isothermal 5 level case. The best straight line gave a relaxation time of 1.18 μs an increase of 30% over the ideal model. Experimentally the present results gave little or no curvature on plots of equation 6.3. It was thought that noise on the traces may have obscured the effect. However, Matthews[3] (interferometric study at >3000K) obtained a similar curvature by plotting $-\ln(1-(\rho/\rho_\infty))$ versus t, where ρ,ρ_∞ are the densities at time t and equilibrium respectively. He obtained the relaxation time by taking the slope of the curve at its mid point. Analysis of the computed vibrational energy by this method, for a 5 level temperature changing system, gives a value of 1.26 μs. This value is comparable to that obtained from the populations. It is realised that experimental inadequacies may account for about 15% scatter,

Figure 8.6

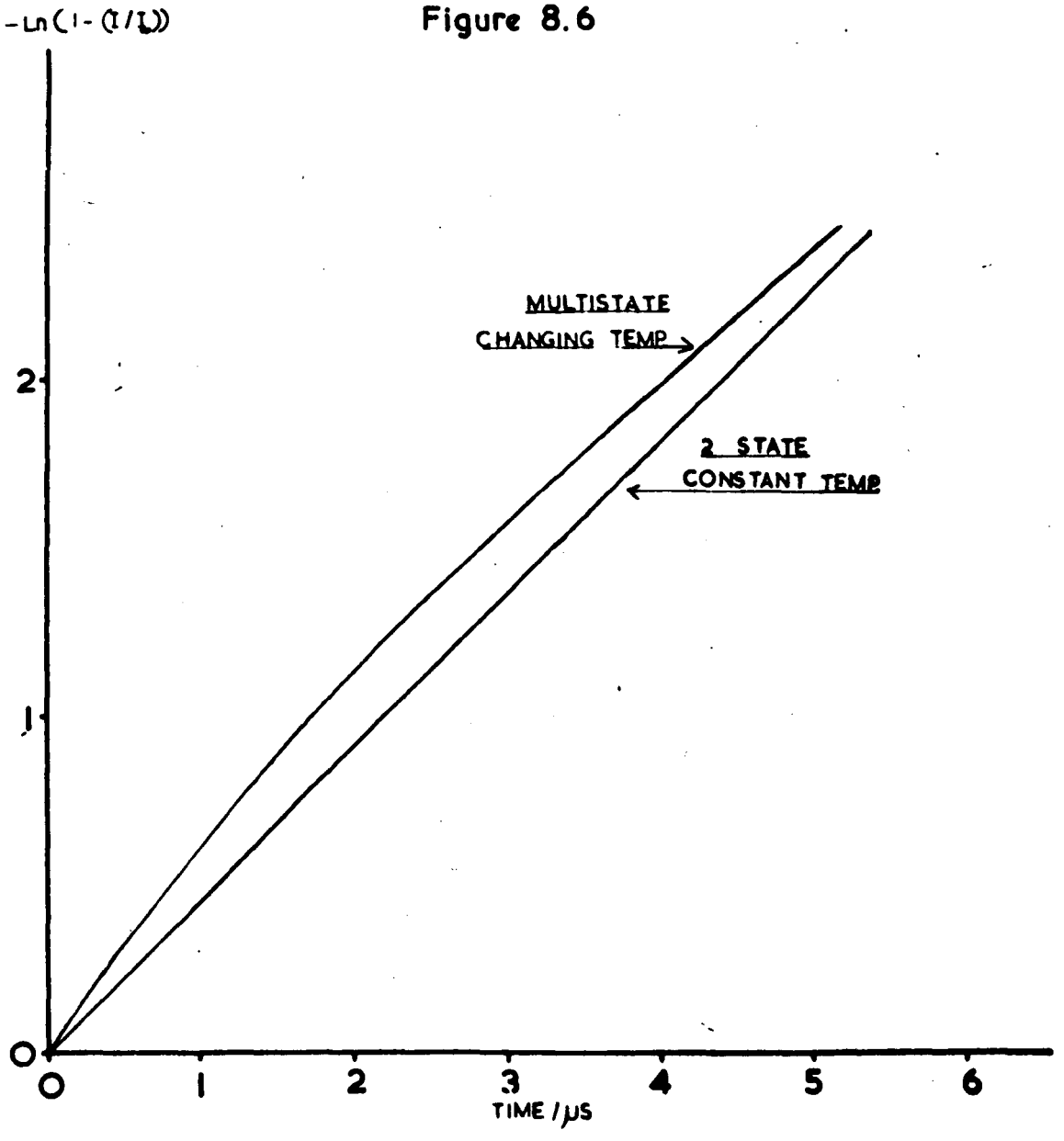
-Ln(1-(I/I))
MULTISTATE
CHANGING TEMP
2 STATE
CONSTANT TEMP
2
1
0
0
1
2
3
4
5
6
TIME /μs

about the average line on an L-T plot. However, systematic errors are introduced by taking values of the relaxation time from curves such as Figure 8.6 or from the curves given by Matthews.[3] There would also be a small random error due to say estimating the mid point of the curve. These three types of error probably account for the scatter seen on L-T plots (see, for example, ref. 25, p.236, p.257) and why the spectroscopic results and interferometric results are the same.

The same procedure was carried out with the 2nd vibrational level. The ideal model was that of an isothermal 3 level system. The relaxation curves were analysed by equation 6.4. The relaxation time obtained was exactly the same as that for the 1st level. For the other two systems which approached reality, the same treatment was applied. The resulting relaxation times, were the same as those obtained on the 1st level, with the same discrepancies between the ideal and realistic models.

The relaxation times of the 1st and 2nd levels were computed for mixtures of 50% CO - 50% Ne and 10% CO - 90% Ne. A 5 level L-T-R model, with changing temperature was used. Again the curvature was evident in plots of equations 6.3 and 6.4. However, the curvature diminished slightly in the order:-

$$\text{Pure CO} > 50\%\ \text{CO} > 10\%\ \text{CO}$$

This was due to the fact that as the concentration of diluent was

was increased, the isothermal condition was approached. In the mixtures the relaxation times obtained for both 1st and 2nd levels were the same.

Thus two facts emerge from the above discussion:-

a) that the relaxation times obtained by a realistic model are 30% above those obtained by an ideal model, for both levels, using the same method of analysis. The results of the present study, and those which have gone before,[2] may be too high. The equations 6.3 and 6.4 are not adequate for analysing the experimental curves. The inadequacy has been demonstrated by comparison with the interferometric work which gives rise to the same relaxation times.

b) that in all conditions of temperature and concentration of diluent the second level gives the same relaxation time as the first, in the case of a harmonic oscillator. The discrepancy between the results on the 1st and 2nd levels, in the present case, is not resolved. One assumption remains to be questioned. Are the Landau--Teller ratios of the rate constants correct? This is dealt with in the next section.

8.1.d THE LANDAU-TELLER RATE CONSTANTS

In the derivation of equations 6.3 and 6.4, see sections 5.2.a and 5.2.b respectively, a harmonic oscillator was assumed. The computer models used a harmonic oscillator. This model had the rate constants related in the following general way:-

$$k_{j+1,j} \quad : \quad k_{j,j-1} \quad = \quad (j+1) \quad : \quad j$$

In the case of the 1st and 2nd levels:-

$$k_{21} \quad = \quad 2k_{10}$$

and

$$k_{12} \quad = \quad 2k_{01}$$

In the case of an anharmonic oscillator it might be expected that:-

$$\frac{k_{21}}{k_{10}} \quad > \quad 2 \qquad\qquad 8.2$$

This arises because the rate constant for the 2 → 1 transition (2117 cm^{-1} in CO) is greater than that for the 1 → 0 transition (2143 cm^{-1} in CO).

Using two different theoretical approaches it is possible to put an approximate value to the coefficient in 8.2, in the anharmonic case:-

i) Using the S.S.H. theory, with the constants given in Table 8.1, a value of k_{10} can be obtained. Using the same constants, but now setting $\bar{\nu}$ = 2117 cm^{-1} it is possible to get an apparent value for k_{21}, called $k_{10}^{app.}$. The value for k_{10} is 1.07 x 10^4 s^{-1} and $k_{10}^{app.}$ is 1.23 x 10^4 s^{-1} at 1953K. Thus the ratio of rate constants in the anharmonic case may be written:-

$$\left(\frac{k_{21}}{k_{10}}\right)_{\text{anharmonic}} = 2 \times \frac{1.23}{1.07} = 2.23$$

ii) The vibrational relaxation of anharmonic oscillator molecules has been treated by Bray.[10,11] In this treatment an exponential increase in V-T probabilities was given with increase in vibrational level. The equations allow direct calculation of the transition probabilities between the various levels of an anharmonic oscillator.

The calculations are as follows:-

$$P_{v,v-1} = P(T) \frac{v}{1-\varepsilon v} F(y_{v,v-1})$$

where v = vibrational quantum number

$P(T)$ = constant, at constant temperatures, which can be chosen empirically. This factor is eliminated in the present calculations.

ε = the anharmonicity

$F(y_{v,v-1})$ = adiabaticity factor which has been evalued empirically,[12] to be

$F(y) = 0.5(3-\exp(-2y/3))\exp(-2y/3)$

$y = g(1-2\varepsilon v)$

$g = (0.5)^{\frac{3}{2}} \sqrt{\frac{\theta'}{T}}$

$$\theta' = \frac{16^{4} M \bar{\nu}^{-2} \ell^{2} c^{2}}{2N\ 10^{16} k} \qquad 8.3$$

The parameters in equation 8.3 have been described in Appendix 2, section A.2.ii.

The value of θ' was taken from the S.S.H. calculations. Thus for $\theta' = 4.33 \times 10^6$, $\varepsilon = 0.0061$ and at 1953K:-

Then for v = 1

$$y = 16.42$$

From this:- $$F = 2.63 \times 10^{-5}$$

$$\therefore \quad P_{10} = P(T)F$$

$$\therefore \quad P_{10} = 2.63 \times 10^{-5} P(T)$$

For v = 2, all the other parameters being the same as before:-

$$y = 16.21$$

From this:- $$F = 3.06 \times 10^{-5}$$

$$\therefore \quad P_{21} = P(T)F\ 2.05$$

$$\therefore \quad P_{21} = P(T)\ 6.27 \times 10^{-5}$$

From the S.S.H. calculations τ_c (time between collisions) at 1953K is 4.8×10^{-10} s. Thus the rate constants are:-

$$k_{10} = 5.4 \times 10^4\ P(T)\ s^{-1}$$

$$k_{21} = 1.3 \times 10^5\ P(T)\ s^{-1}$$

$$\therefore \quad \left(\frac{k_{21}}{k_{10}}\right)_{\text{anharmonic}} = \frac{1.3 \times 10^5}{5.4 \times 10^4} = 2.4$$

Thus the two different theoretical approaches both give approximately the same value for the Landau-Teller coefficient, in the anharmonic case. The above calculations apply to the rate constant, $(k_{10})_{CO-CO}$, in the pure gas, but presumably the same reasoning may be extended to $(k_{10})_{CO-Ne}$.

There is very little experimental evidence to indicate whether the Landau-Teller ratios between the rate constants are correct. The flash photolysis experiments of Callear and Smith[13] indicate that $k_{32} : k_{21} : k_{10}$ are in the correct ratio. Similar experiments[14] on the high vibrational levels of O_2 are consistent with a single step quantum jump. The shock tube work of Hooker and Millikan[2] also is consistent with the single quantum jump, with the ratios being correct for the lower levels. On the other hand work on high vibrational levels of I_2[15,16] has indicated that transitions where $\Delta v = 2$ play a significant part in energy transfer in I_2. Also Chow and Greene[17] have observed the 2nd, 3rd and 4th levels of HI. They found that all the levels relaxed at the same rate, with a simple exponential, not predicted by the Landau-Teller model.

The present results indicate that the stepwise model for the population of the upper states is correct, and $\Delta v > 1$ transitions play little or no part in energy transfer. However, it has been shown that ratio of $k_{21} : k_{10}$ is not 2:1. It is more likely that the Landau-Teller coefficient lies between 2.2 and 2.4, for these rate constants. Unfortunately, no method for the extraction of a value for

the coefficient, from the present results was available.

8.1.e CONCLUSIONS

The work on the 1st and 2nd vibrational levels of CO was reexamined, under carefully controlled conditions. The values of the L-T constants were in reasonable agreement with previous work.[2,5] A discrepancy between the results of work, on mixtures, of the 1st and 2nd vibrational levels was shown. The detailed conclusions are shown below:-

a) One of the objects of these experiments was to try to distinguish between the stepwise, section 5.2.b.ii, and the resonance exchange, section 5.2.b.iii, mechanisms for the population of the second vibrational level. It was shown in section 8.1.c.ii that the 3 state model assumed in 5.2.b.iii was unrealistic and this mechanism was discounted. It was concluded that the L-T-R mechanism was the most realistic model. In this process, the resonance reactions maintain a quasi Boltzmann distribution, while the general form of the relaxation is carried out through V-T processes. The experimental works of Appleton[18] and Millikan and White,[19] on N_2, seem to support this idea.

It has been demonstrated theoretically[10,11] that in the case of high vibrational temperatures and low translational temperatures V-V reactions play an important role, in the relaxation process. The result is that vibrational deactivation becomes rapid, the rates being

much faster than those predicted by the L-T model. In contrast to some recent experiments[41,42] which show an enhanced vibrational deexcitation rate, the work of Appleton et al[43] shows that when T-V collisions control the relaxation process, the characteristic vibrational relaxation time of CO dilute in Ar is the same whether measured in a compression or expansion situation. Thus it seems that the L-T model may be applicable in cases of extreme vibrational excitation.

b) The kinetic equations used to analyse the computed and experimental relaxation curves, were found to be inadequate. They cannot cater for conditions of changing temperature in multi-level harmonic oscillators. The relaxation times obtained for the real conditions are often very different from those obtained from ideal conditions. The absolute value of the present results may be too high because of this. Thus the work of Hooker and Millikan[2] may have a small systematic error. However, it is difficult to see how the equations could be changed for the better.

Johannesen and his co-workers[20,21] have derived an exact procedure which determines the relaxation time at the local conditions of T and ρ, throughout the relaxation region, behind the shock. Blythe[22] has compared this method with the approximate analysis using the average temperature. The differences between the two methods were found to be of the order of 10% - 20%. The exact method has had limited application, with interferometric[23] and laser schlieren[24]

measurements. It would be worth while extending this technique to cover spectroscopic measurements, such as thosepresented here.

c) It was thought that the difference between the 1st level and 2nd level results with the mixtures was genuine. The computer calculations showed that for all temperatures and concentrations of diluent, the lines in Figures 8.1, 2 and 3 should concur. It was assumed that the $\Delta v = \pm 1$ was still valid, and that the discrepancy was due to the fact that no account of anharmonicity was taken in the Landau-Teller model. It was shown that the Landau-Teller ratio between the rate constants k_{21} and k_{10} was >2, the actual value being some where between 2.2 and 2.4. Thus further computer calculations using anharmonic oscillators are required.

The general shape of the curves for the 2nd level in Figures 8.1, 2 and 3 is more difficult to explain. The 'tailing off' at high concentrations of Ne may be due to the weakness of the infrared emission in these mixtures. As the temperature decreases i.e. 1953K to 1628K, see Figures 8.1, 8.3, the rate constants k_{21} and k_{10} are expected to decrease. However they do so in the same relative proportions, so that the discrepancy between the 1st and 2nd levels remains constant at about 10%.

8.2 CO/POLYATOMIC MIXTURES

A detailed analysis will be presented for the CO/CO_2 system. Most of the arguments used in this analysis will be extended to the analysis of the CO/N_2O and CO/COS systems. Any minor amendments will be noted.

8.2.a CO/CO_2 SYSTEM

Assuming, initially that CO_2 is a molecule with a ground vibrational state and an excited state at 2349 cm^{-1}, then the five processes which may govern the relaxation of the CO/CO_2 systems are:

$$1)\quad CO^* + CO \underset{k_{-1}}{\overset{k_1}{\rightleftharpoons}} CO + CO \qquad V\text{-}T$$

$$2)\quad CO^* + CO_2 \underset{k_{-2}}{\overset{k_2}{\rightleftharpoons}} CO + CO_2 \qquad V\text{-}T$$

$$3)\quad CO^* + CO_2 \underset{k_{-3}}{\overset{k_3}{\rightleftharpoons}} CO + CO_2^* - 206\ cm^{-1} \qquad V\text{-}V$$

$$4)\quad CO_2^* + CO_2 \underset{k_{-4}}{\overset{k_4}{\rightleftharpoons}} CO_2 + CO_2 \qquad V\text{-}T$$

$$5)\quad CO_2^* + CO \underset{k_{-5}}{\overset{k_5}{\rightleftharpoons}} CO_2 + CO \qquad V\text{-}T$$

where * indicates a vibrational energy quantum. It is also assumed that the rate of reaction (4) >> (1), see Figure 7.28 at 1372K ($T^{-\frac{1}{3}} = 0.09$) for CO/CO_2.

Figure 7.28 shows an L-T plot of the results of the various mixtures of CO and CO_2. It is noted that small amounts of CO_2 have a dramatic effect on the relaxation time of CO. There are two explanations which arise depending on the rate of (3):-

i) if (3) is much faster than all the other processes, then it will maintain the vibrational energy of the whole system in local equilibrium. The vibrational energy will then relax via the faster of processes (4) or (5). There is a single relaxation time, with the rate controlling process being either (4) or (5). If (4) plays the dominant role, then a quadratic dependence of reciprocal relaxation time on mole fraction of CO_2 will be given (this is shown in section 5.2.c and 5.3.a of Chapter 5).

ii) if (3) is slower than (4) or (5) but faster than (1) or (2), then CO will relax by the route:- (3) followed by (4) or (5), with (3) being the rate determining step. This will give a linear dependence of the reciprocal relaxation time on mole fraction of CO_2. There will be a double relaxation process.

In general, except in the two extreme cases above, the relaxation process cannot be defined by a single relaxation time, but can be regarded as a coupled case of two relaxation processes. It has been observed, experimentally, by Taylor, Camac and Feinberg (T.C.F.)[26]

that mixtures of diatomic gases relax to some fraction of their equilibrium, then both gases relax with the same rate toward the equilibrium. The fraction to which they relax initially depends on the extent of V-V coupling, which is called, by T.C.F., the vibrational energy ratio α. They show that for weak coupling $\alpha \to 1$, and for strong coupling $\alpha \to 0$.

Plots of τ^{-1} vs mole fraction of CO_2, Figure 8.7, at constant temperature 1372K show a linear dependence. It is noted that only a small concentration range has been studied, and that the quadratic dependence may reveal itself at higher concentrations of CO_2. However the linear dependence of τ^{-1} over this concentration range allows the first qualitative conclusion. It is that CO-CO_2 are weakly coupled (according to T.C.F. $\alpha \to 1$) such that reaction (3) is much slower than the V-T processes (4) and (5), but that it is much faster than the V-T processes (1) and (2). Thus (3) dominates the relaxation of CO.

The molecule CO_2 has 4 vibrational modes, and not as suggested earlier, just one. The symbol $CO_2(XY^ZW)$ denotes a CO_2 molecule with X quanta of the symmetric stretching mode, ν_1, excited; Y quanta of the doubly degenerate bending mode, ν_2, excited with angular momentum Z; and W quanta of the asymmetric stretching mode, ν_3, excited. The symmetric stretch is at 1388 cm^{-1}; the bending mode at 667 cm^{-1}; and the asymmetric stretch at 2349 cm^{-1}. Much work has been carried out on the vibrational relaxation of the various modes of CO_2. The consensus of present opinion is that neither the symmetric stretching

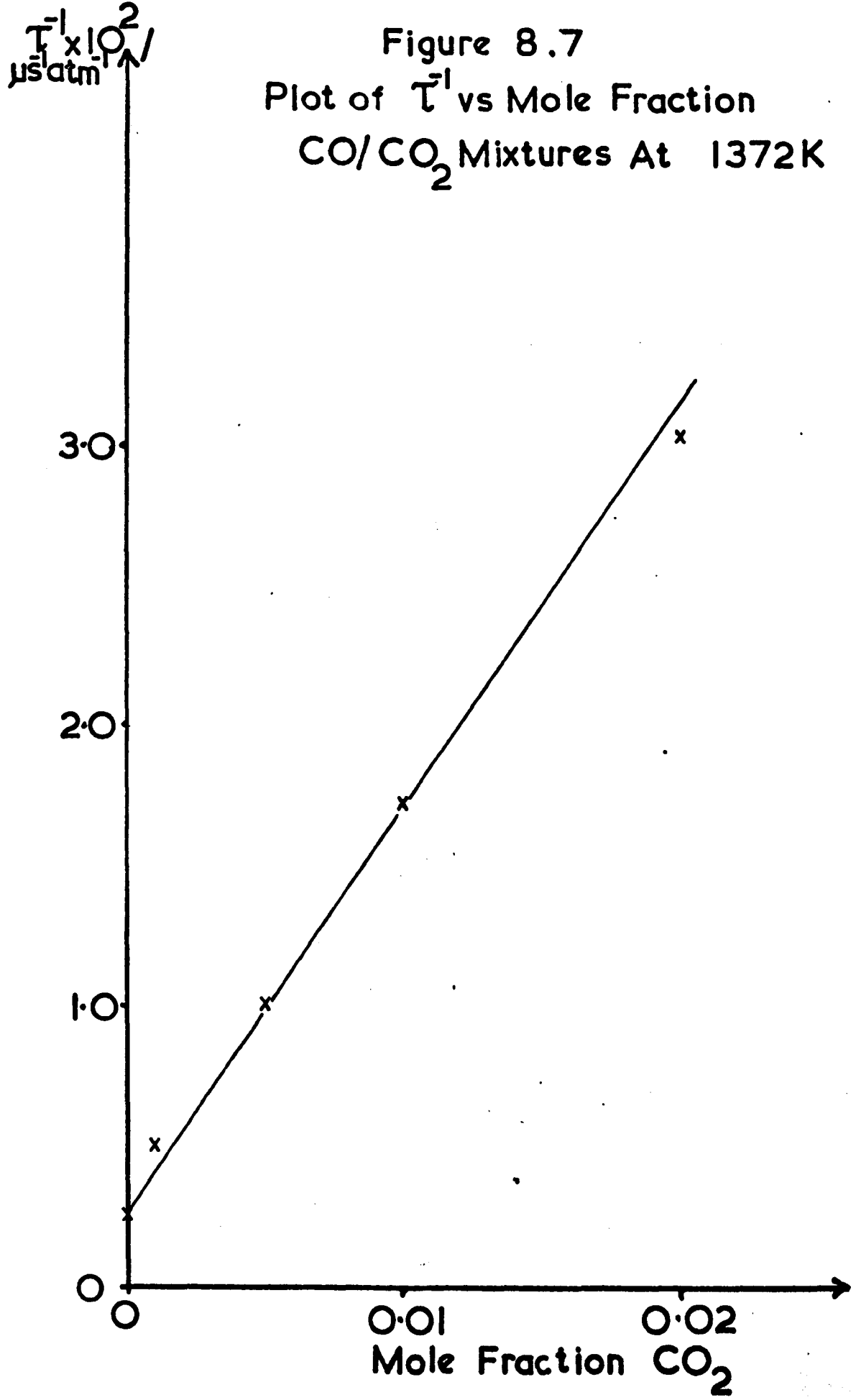

Figure 8.7
Plot of τ^{-1} vs Mole Fraction
CO/CO_2 Mixtures At 1372K

mode nor the asymmetric stretching mode have significantly longer relaxation times than the bending mode, see section 1.3, Chapter 1. These measurements are in contrast to theoretical calculations[27,28] which indicate that the asymmetric mode should have longer times than the other two. The calculations are sensitive to Lennard-Jones parameters which are used for calculating the potential energy function between colliding molecules. As indicated in Chapter 4 the parameters may not be known with sufficient accuracy, at the present time. Rapp and Sharp[29] have criticised the perturbation approximation used in the calculations, since it is invalid at high temperatures.

The energy level diagram for CO_2, Figure 8.8, shows some of the lower levels for CO_2, and some of the possible transitions for populating the upper states. T-V processes excite the lowest lying mode ν_2. There is a known Fermi Resonance between $2\nu_2$ and ν_1 so that there is very rapid energy exchange. These modes are always in equilibrium. The ν_1 and ν_2 then transfer energy to mode ν_3 via V-V processes. It is difficult to define the exact nature of these processes, since the picture regarding them is complex. A few of the possible pathways are given below:-

i) Intramolecular V-V energy transfer:-

$$CO_2(04^00) + X \rightleftharpoons CO_2(00^01) + X + 199 \text{ cm}^{-1}$$

$$CO_2(11^10) + X \rightleftharpoons CO_2(00^01) + X - 272 \text{ cm}^{-1}$$

$$CO_2(03^30) + X \rightleftharpoons CO_2(00^01) + X - 416 \text{ cm}^{-1}$$

Figure 8.8

Energy Level Diagram For

CO/CO_2 System

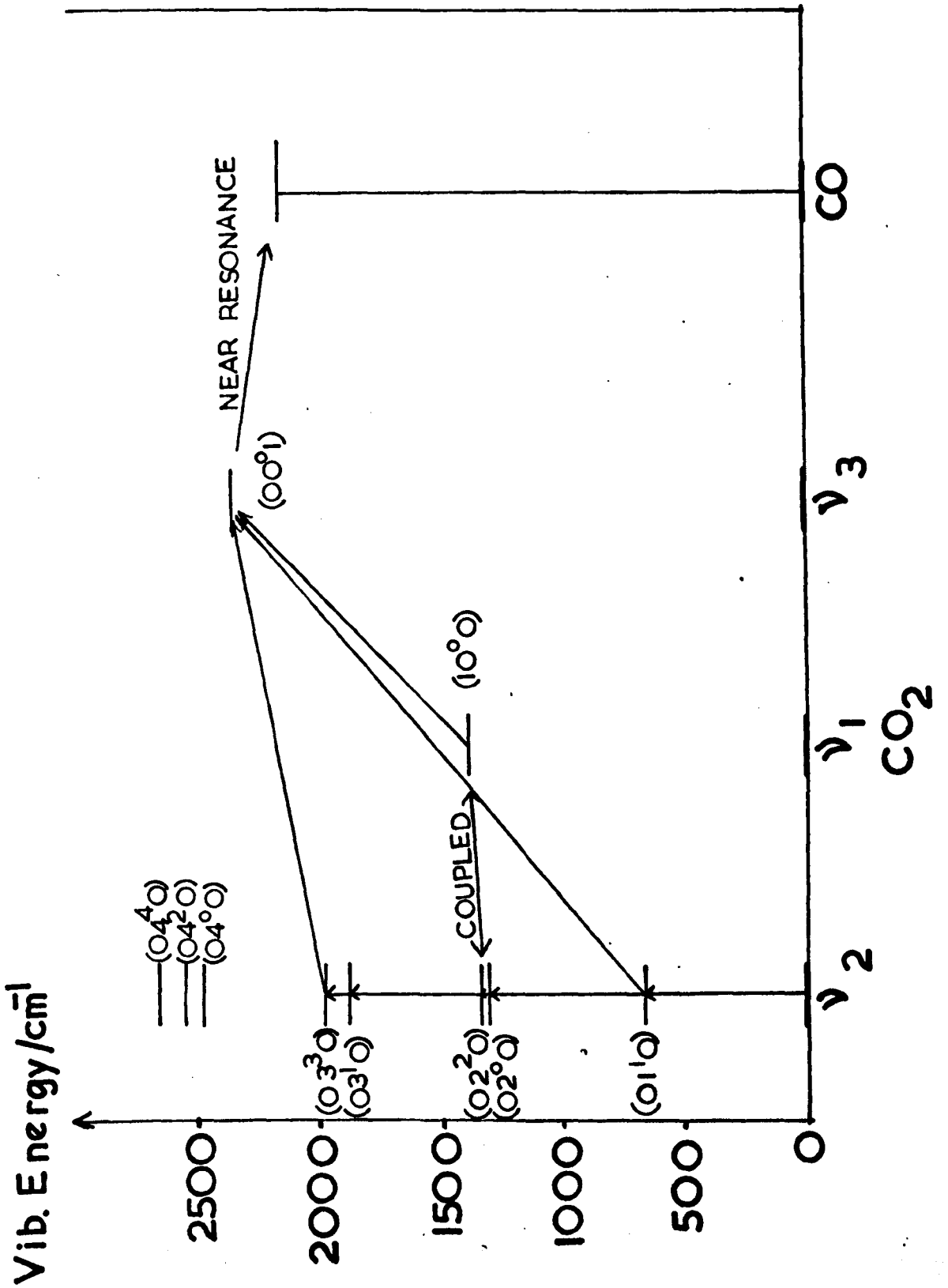

ii) Intermolecular V-V energy transfer:-

$$CO_2(01^10) + CO_2(10^00) \rightleftharpoons CO_2(00^01) + CO_2(00^00) - 294\ cm^{-1}$$

$$CO_2(00^00) + CO_2(11^10) \rightleftharpoons CO_2(00^01) + CO_2(00^00) - 272\ cm^{-1}$$

It is assumed in the present analysis that there is a rapid V-V pathway which maintains the ν_3 mode in a local equilibrium so that ν_3 and ν_1 have the same relaxation time as ν_2. It is noted, however, that by using a large excess of CO compared to CO_2, it is possible to decouple, to some extent, the relaxation of modes ν_2 and ν_3 of CO_2. At the high temperatures experienced in shock tubes, the effect of the dilution may be offset by the increase in molecular velocity, which increases the probability of the collision of 2 polyatomic molecules. The decoupling will be neglected in the present analysis. However, the decoupling may be significant at low temperatures (300K), so that the rate determining step may be some intramolecular V-V process in the polyatomic species. Studies at room temperature, with the N_2/CO_2 laser system,[44] have shown the importance of intramolecular V-V energy transfer in polyatomic molecules.

The excited ν_3 mode can now couple to the fundamental vibration frequency of CO. The possibility of direct V-V coupling between CO and modes ν_2 or ν_1 is available in the sequence:-

$$CO_2(00^01) + CO \rightleftharpoons CO_2(11^10) + CO + 272\ cm^{-1}$$

and $$CO + CO_2(11^10) \rightleftharpoons CO^{\ddagger} + CO_2(00^00) - 66\ cm^{-1}$$

Moore has concluded that the rate of the sum of reactions of the type above is at least one order of magnitude smaller than the rate of:-

$$CO_2(00^01) + CO \rightleftharpoons CO_2(00^00) + CO^* + 206\ cm^{-1}$$

This argument is consistent with the results of Rosser, Wood and Gerry,[37] on the N_2/CO_2 system.

The calculations of Herzfeld[31] indicate that for the N_2/CO_2 system, $\Delta E = 18\ cm^{-1}$, at 1500K the probability, P, for $(01^10) \rightarrow (000)$ is 1.38×10^{-2} (9.09×10^{-3} in pure CO_2), while for the V-V reaction, similar to 3, the value of P is 2.5×10^{-3}. Thus in the present case, while the values of P for (4) and (5) stay approximately the same as the N_2/CO_2 system, the value for (3) must decrease because of a ten fold increase in the energy discrepancy ΔE. The S.S.H. theory and the M.W. correlation may given an indication as to the values of k_1, k_2, k_3 and k_4. These are shown in Table 8.2:-

TABLE 8.2

At 1372K

	Reaction 1, k_1/s^{-1}	Reaction 2, k_2/s^{-1}
S.S.H.	2.09×10^3	1.61×10^2
M.W. Correlation	7.46×10^2	2.95×10^2
Expt.	2.5×10^3	

	Reaction 4, k_4/s^{-1}	Reaction 5, k_5/s^{-1}
S.S.H.	4.16×10^6	6.28×10^6
M.W. Correlation	5.29×10^6	6.8×10^6
Expt.	1.96×10^6	

In the S.S.H. calculations for CO_2, $\varepsilon/k = 213.0K$ and $r_0 = 38.97$ nm.

The conclusions to be drawn from the above discussion and table are summarised as follows:-

i) $k_1 > k_2$

ii) $k_4 \approx k_5$

iii) $k_4, k_5 >> k_1, k_2$

iv) $k_{-3} = k_3 \exp(\Delta E/kT)$

where $\Delta E = 206\ cm^{-1}$

$\therefore \quad k_{-3} = 0.8\ k_3$

$\therefore \quad k_5 > k_{-3}, k_3$

v) $X << 1$

Using these facts it is possible to make adjustments to the analytical equations:-

Taking 5.31:-

$$\frac{1}{\tau_o} = \frac{1}{\tau_{o_{AA}}} + (k_2 - k_1 + (k_3k_5/(k_{-3} + k_5)))X$$

$$+ (k_3k_{-3}(k_4 - w_1)/(k_{-3} + k_5)^2)X^2$$

Using assumption iv)

$$\frac{1}{\tau_o} = \frac{1}{\tau_{o_{AA}}} + (k_2 - k_1 + (k_3))X + (k_3k_{-3}(k_4 - w_1)/(k_5)^2)X^2$$

also $k_3 > (k_2 - k_1)$

so that:-

$$\frac{1}{\tau_o} = \frac{1}{\tau_{o_{AA}}} + k_3X + (k_3k_{-3}(k_4 - w_1)/(k_5)^2)X^2$$

The two assumptions used above may also be applied to w_1:-

$$w_1 = k_2 - k_1 + (k_3k_5/(k_{-3} + k_5))$$

which reduces to:-

$$w_1 = k_3$$

$$\therefore \quad \frac{1}{\tau_o} = \frac{1}{\tau_{o_{AA}}} + k_3X + (k_3k_{-3}(k_4 - k_3)/(k_5)^2)X^2$$

Rearranging:-

$$\frac{1}{\tau_o} = \frac{1}{\tau_{o_{AA}}} + k_3 X\left(1 + \left(\frac{k_{-3}(k_4 - k_3)}{(k_5)^2}\right)X\right)$$

Using assumptions ii), iv) and v)

$$\left(\frac{k_{-3}(k_4 - k_3)}{(k_5)^2}\right)X \to 0$$

$$\therefore \quad \frac{1}{\tau_o} = \frac{1}{\tau_{o_{AA}}} + k_3 X$$

This is the equation of a straight line, the gradient of which is the rate constant k_3. Similar approximations applied to the analysis of Tuesday and Boudart, see section 5.2.c of Chapter 5, give the same equation. The gradient was taken from Figure 8.7 and was found to be 1.45×10^6 s^{-1}, and thus the probability 5.2×10^{-4}. At 1372K, the near resonance theory of S.S.H. gives a value of P_{10-01} of 1.96×10^{-4}, while the exact resonance value is 1.097×10^{-3}. The calculations of Rapp and Golden[32] give a value P_{10-01} of 2.2×10^{-3}. The temperature dependence of P_{10-01} from the experiments was obtained by plotting figures similar to 8.7 at different temperature. The temperature dependence is shown in Figure 8.9, together with those given by the theories. The agreement between the observed probabilities and calculated ones is good considering the uncertainties in both experiment and theory. The temperature dependence seems to be more correct in the case of Rapp and Golden case than the S.S.H. As mentioned previously

Figure 8.9

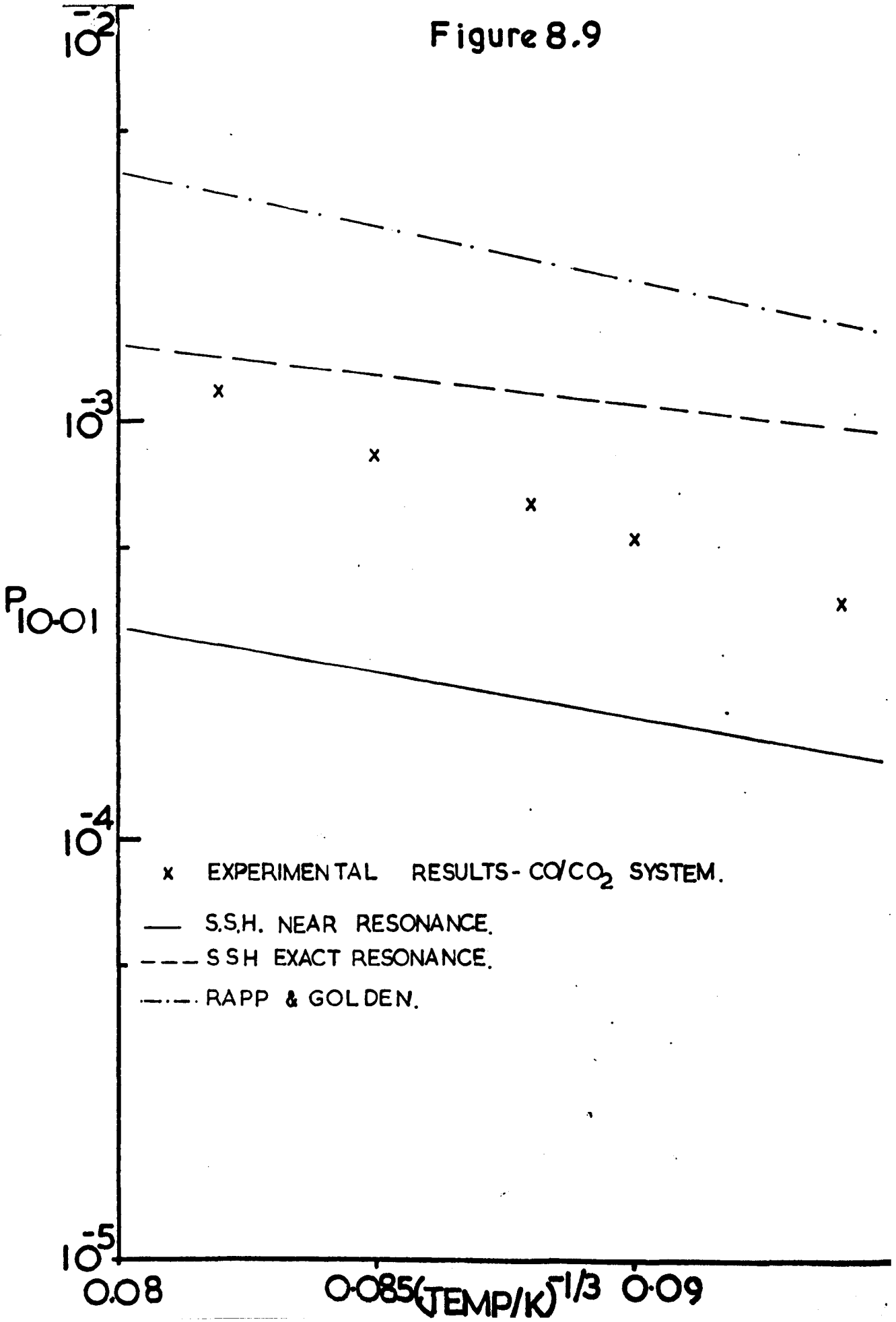
10^{-2}
10^{-3}
P_{10-01}
10^{-4}
10^{-5}
x EXPERIMENTAL RESULTS - CO/CO_2 SYSTEM.
S.S.H. NEAR RESONANCE.
S S H EXACT RESONANCE.
RAPP & GOLDEN.
0.08
0·085(TEMP/K)$^{-1/3}$
0·09

the discrepancy may be due to taking the geometric mean for ε/k and the arithmetic mean of r_0 of the corresponding two values for the pure gases. This may apply particularly in the cases of the CO/polyatomic systems, since the potential well depth of the polyatomic species is about 2 to 4 times that for CO.

Extrapolation of the present results to 300K gives a value of P_{10-01} of 2.3×10^{-6}. This value is compared to a value of 8.0×10^{-4} suggested by Moore,[30] which indicates that the process (3) may be ≈400 times more probable than the present results suggest. However, at temperatures <1000K long range forces between the dipole moment of CO_2 (ν_3) and the quadrupole moment of CO become important. The calculations of Sharma and Brau[33] indicate that the probability was inversely proportional to temperature, see section 4.7, Chapter 4. This has been demonstrated experimentally by the shock tube studies of Taylor and Bitterman[34] and Roach and Smith.[35] Thus, it is possible to conclude that there are two separate interactions for near resonant exchange processes. At low temperatures, long range forces are important and the rate is proportional to T^{-1}, while at high temperature the interaction is dominated by short range forces, the rate being proportional to T.

8.2.b CO/N_2O SYSTEM

In this case the resonance reaction (3) is written as:-

$$CO^* + N_2O \underset{k_{-3}}{\overset{k_3}{\rightleftharpoons}} CO + N_2O^* - 80\ cm^{-1}$$

The plot of τ^{-1} vs mole fraction of N_2O is shown in Figure 8.10. The dashed line indicates the possibility of a quadratic dependence, and thus that the above reaction is fast compared to k_4 for pure N_2O. However, it is pointed out that the mixture containing 2% N_2O, gave very fast experimental rise times, ≈ 5 μs, which were comparable with the rise times of the system. It was though that the point at 2% N_2O in Figure 8.10 was unreliable, and for the purposes of the present analysis it will be ignored.

N_2O has very similar properties to CO_2. However, whereas there is Fermi resonance between $2\nu_2$ and ν_1 modes of CO_2, there is a wavenumber difference of 107 cm^{-1} between the second harmonic of ν_2 and the ν_1 mode of N_2O. This results in a slower transfer of energy to the ν_1 mode from the ν_2 in N_2O than in CO_2. The excitation of the ν_2 mode is much faster in N_2O. In this case it may be expected that N_2O would exhibit separate relaxation times for the various modes. However Simpson et al,[36] in a careful shock tube study up to 1700K, have shown that neither the ν_1 mode nor the ν_3 mode have significantly longer relaxation times than the ν_2 mode.

The magnitudes of the rate constants, obtained by theory and experiment are shown in Table 8.3:-

Figure 8.10

Plot of $\bar{\tau}^{-1}$ vs Mole Fraction CO/N_2O Mixtures At 1372 K

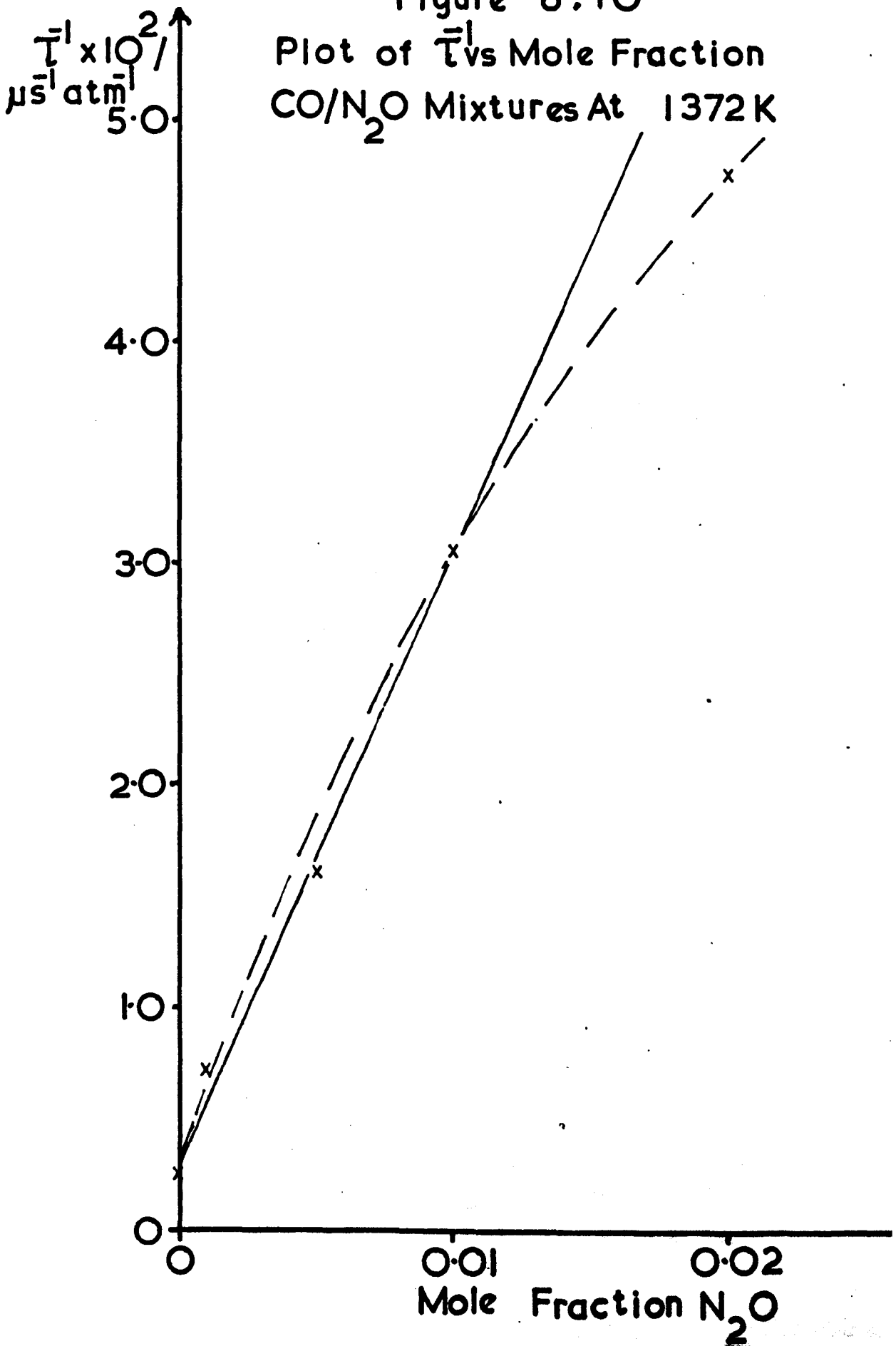

TABLE 8.3

At 1372K

	Reaction 1, k_1/s^{-1}	Reaction 2, k_2/s^{-1}
S.S.H.	2.09×10^3	1.94×10^2
M.W. Correlation	7.46×10^2	2.96×10^2
Expt.	2.5×10^3	-

	Reaction 4, k_4/s^{-1}	Reaction 5, k_5/s^{-1}
S.S.H.	1.47×10^7	2.12×10^7
M.W. Correlation	8.26×10^6	1.03×10^7
Expt.	6.99×10^6	-

In the S.S.H. calculations, for N_2O, $\epsilon/k = 237.0$ and $r_0 = 38.16$ nm. In this case the assumptions i), ii), iii) v) made in section 8.2.a still hold. However, since ΔE is reduced

$$k_{-3} = k_3$$

Although in this case k_3, k_{-3} are faster than in the CO/CO_2 case, reactions (4) and (5) in the CO/N_2O have increased by about a factor of 3 so that:-

$$k_5 > k_3, k_{-3}$$

The gradient of Figure 8.10 was found to be 2.75×10^6 s^{-1} and thus the probability is 1.05×10^{-3}. At 1372K, the near resonance theory of S.S.H. gives a value of P_{10-01} of 2.67×10^{-4} while at exact

resonance the value is 5.49×10^{-3}. The calculations of Rapp and Golden[32] give a value of P_{10-01} of 4.5×10^{-3}. The temperature dependence of P_{10-01} from the experiments was obtained by plotting figures similar to 8.7 at different temperatures. The temperature dependence is shown in Figure 8.11, together with those given by the theories. The experimental data has good agreement with the calculations, although the discrepancies may be ascribed to choice of L-J parameters in mixtures. The experimental data shows an increase of a factor of 2 in P_{10-01} for the CO/N_2O system over the CO/CO_2 system.

The present results were extrapolated to 300K, where a value of 1.9×10^{-5} was obtained for P_{10-01}. The only measurement at room temperature on this system is an old dispersion measurement of Eucken and Jaacks,[38] who found a value of 2.3×10^{-4} for P_{CO-N_2O}. The most recent comparable work is that of Roach and Smith,[35] who studied the N_2/N_2O system, $\Delta E = 107$ cm^{-1}, and found that P_{10-01} was 7.7×10^{-4} at 300K. This figure when compared to the present value, reflects again the importance of the long range forces, for the near resonance condition at low temperatures.

8.2.c CO/COS SYSTEM

In this case the resonance reaction (3) is written as:-

$$CO^* + COS \underset{k_{-3}}{\overset{k_3}{\rightleftharpoons}} CO + COS^* + 64 \text{ cm}^{-1}$$

Figure 8.11

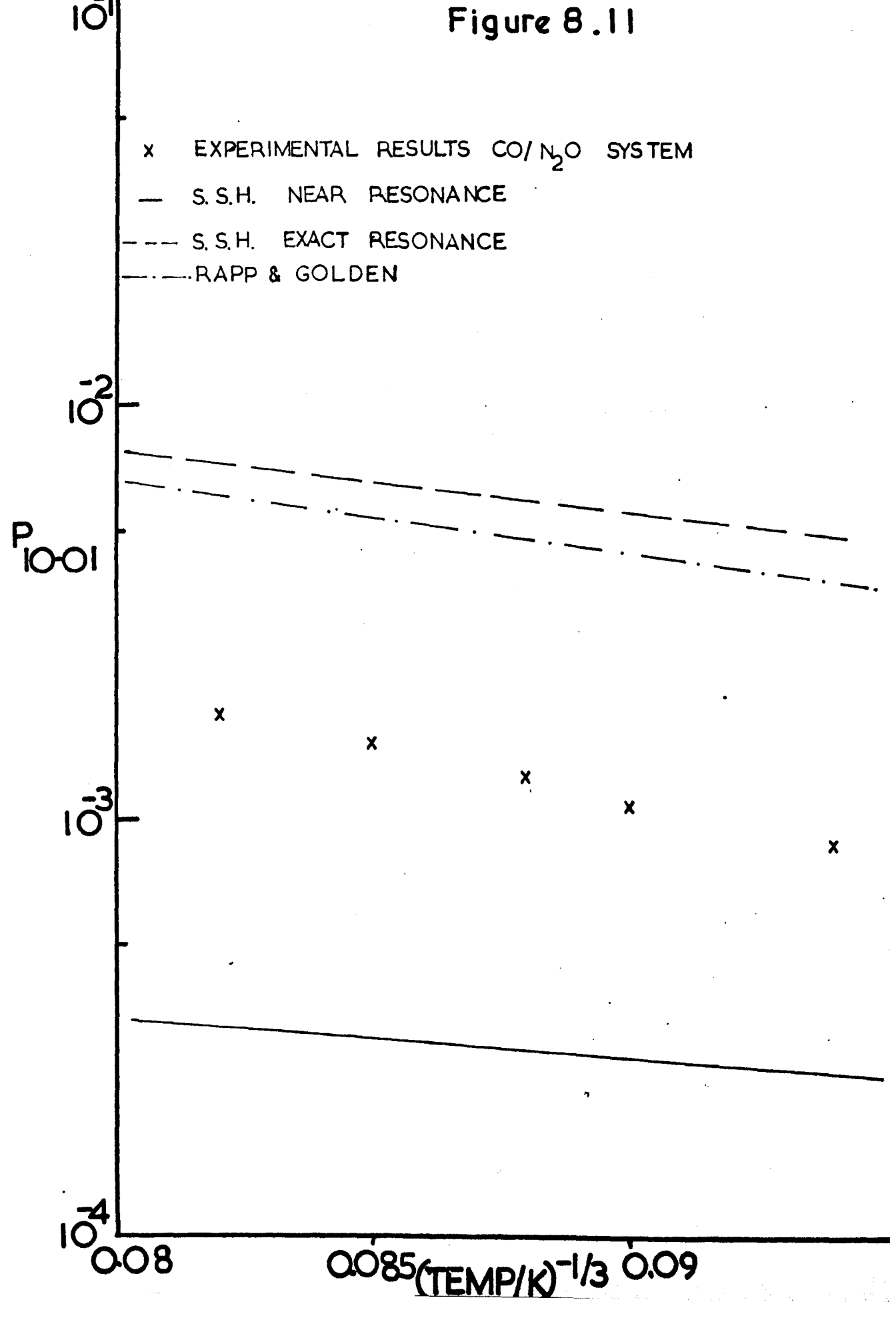
x EXPERIMENTAL RESULTS CO/ N_2O SYSTEM
— S. S. H. NEAR RESONANCE
– – – S. S. H. EXACT RESONANCE
—·—·— RAPP & GOLDEN
10^{-1}
10^{-2}
10^{-3}
10^{-4}
P_{10-01}
0.08
0.085
$(TEMP/K)^{-1/3}$
0.09

The plot of τ^{-1} vs mole fraction of COS is shown in Figure 8.12. Only one mixture of CO/COS was studied, thus no conclusions about the quadratic behaviour of the CO/COS system can be made.

COS has similar properties to CO_2 and N_2O. As with N_2O the rapid transfer of energy between the mode $2\nu_2$ and mode ν_1 is not present in COS, since the energy discrepancy is 197 cm^{-1}. The T-V excitation of the ν_2 mode is much faster than CO_2 and faster than N_2O. No high temperature data exists for the relaxation of COS, presumably because of the possibility of dissociation. However, as has been done in the previous cases, it will be assumed that all the modes relax together and there is little dissociation. The magnitudes of the rate constants obtained by theory and experiment are shown in Table 8.4:-

Figure 8.12

Plot of T^{-1} vs Mole Fraction

CO/COS Mixture At 1372K

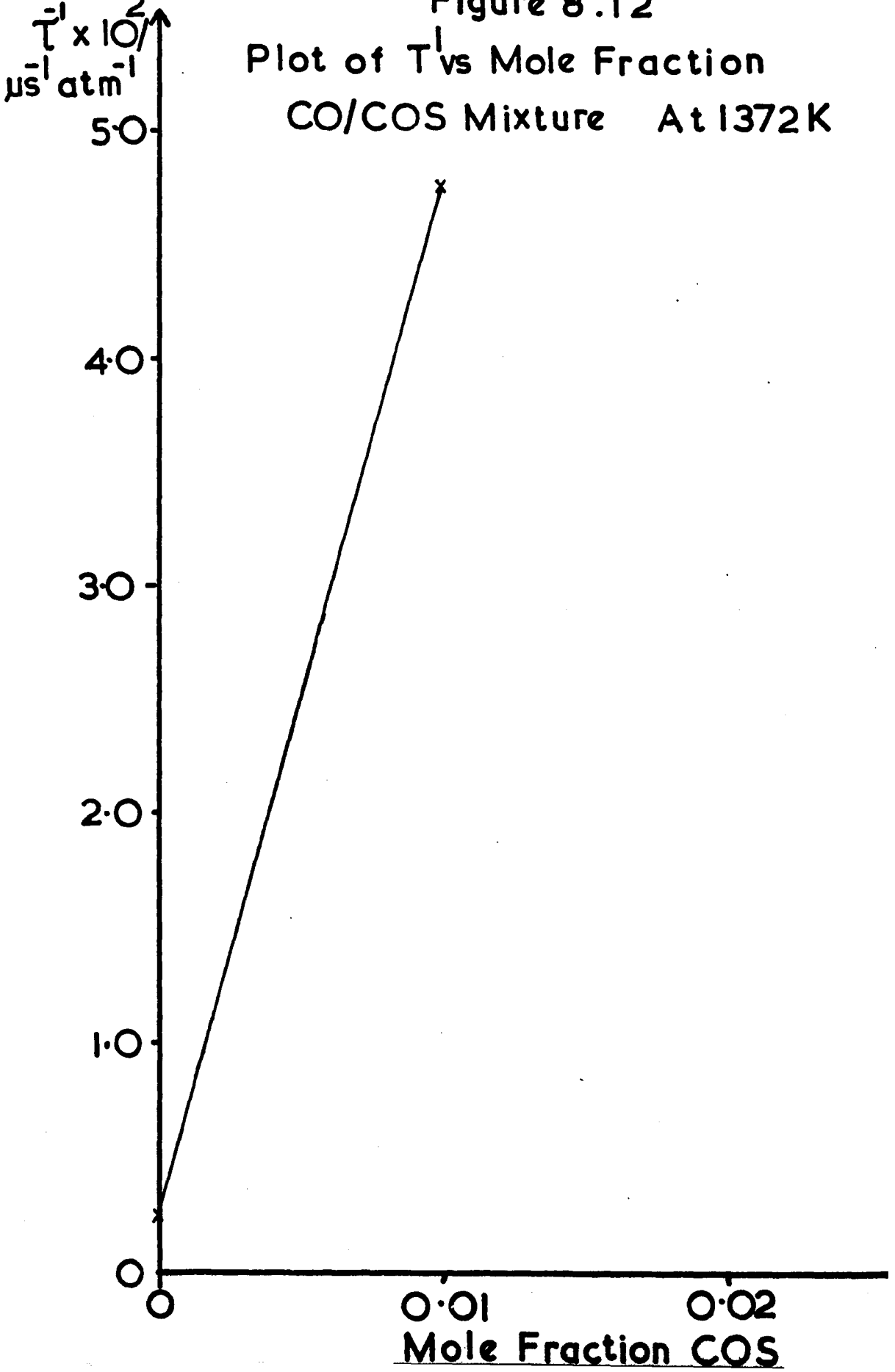

TABLE 8.4

At 1372K

	Reaction 1, k_1/s^{-1}	Reaction 2, k_2/s^{-1}
S.S.H.	2.09×10^3	1.67×10^2
M.W. Correlation	7.46×10^2	1.75×10^2
Expt.	2.5×10^3	-

	Reaction 4, k_4/s^{-1}	Reaction 5, k_5/s^{-1}
S.S.H.	5.26×10^6	1.0×10^7
M.W. Correlation	9.12×10^6	1.29×10^7
Expt.	-	-

In the S.S.H. calculations for COS, ϵ/k = 335K and r_0 = 41.3 nm. The assumptions made in 8.2.a still apply.

The comparison of the experimental data with the theoretical calculations is shown in Figure 8.13. As in the previous two cases, agreement between experiment and theory is good. The data showed an increase in the probability of a factor of 2 over the CO/N_2O data. This increase is more than expected, and more than the theory predicts. It is possible that the COS was not perfrectly pure, and may have contained traces of water.

The data was extrapolated to room temperature and a value of 1.3×10^{-4} was obtained for P_{10-01}. Again there is no recent comparable work. Eucken and Aybar,[39] in 1940, obtained a value of

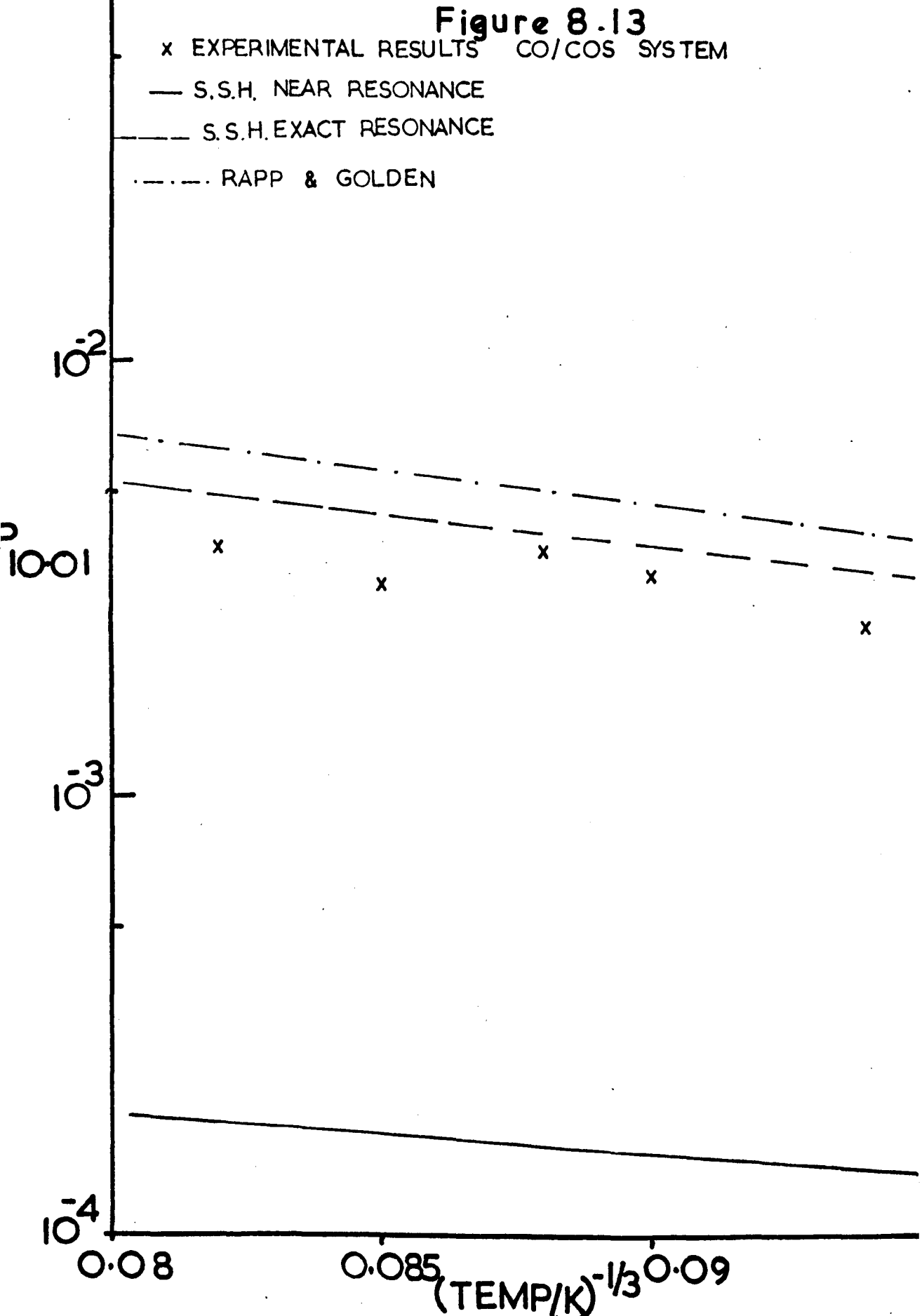
Figure 8.13
x EXPERIMENTAL RESULTS CO/COS SYSTEM
— S.S.H. NEAR RESONANCE
— — — S.S.H. EXACT RESONANCE
— · — · RAPP & GOLDEN
10^{-2}
P
10-01
10^{-3}
10^{-4}
0·08
0·085
0·09
(TEMP/K)$^{-1/3}$

6.8×10^{-4} for P_{CO-COS}.

8.2.d CONCLUSIONS

The conclusions for this section are enumerated below:-

1) It has been shown experimentally that the V-V exchange process can control the vibrational relaxation of gas mixtures. This is the case when the minor component has a rapid T-V process available for excitation. By analysis of the vibrational relaxational data on the binary systems; CO/CO_2; CO/N_2O and CO/COS, it has been shown that the smaller the energy discrepancy between the two species, the more efficient the V-V reaction. Thus the 3 systems studied were found to follow this sequence:-

$$\underset{\Delta E = 206}{P(CO, \overset{10}{\underset{\nu_3}{CO_2}})} < \underset{80}{P(CO, \overset{10}{\underset{\nu_3}{N_2O}})} < \underset{64}{P(CO, \overset{10}{\underset{\nu_3}{COS}})} \quad cm^{-1}$$

This is shown in Figure 8.14, together with the probabilities of T-V processes calculated by the S.S.H. theory. This shows that V-V processes have a steeper temperature dependence than the T-V process. Thus as the gas temperature increases the probabilities for V-V exchange and T-V exchange will approach each other. Therefore at lower temperatures (1000 - 3000K) where the T-V process of the major component is slow, V-V processes become very important.

Figure 8.14

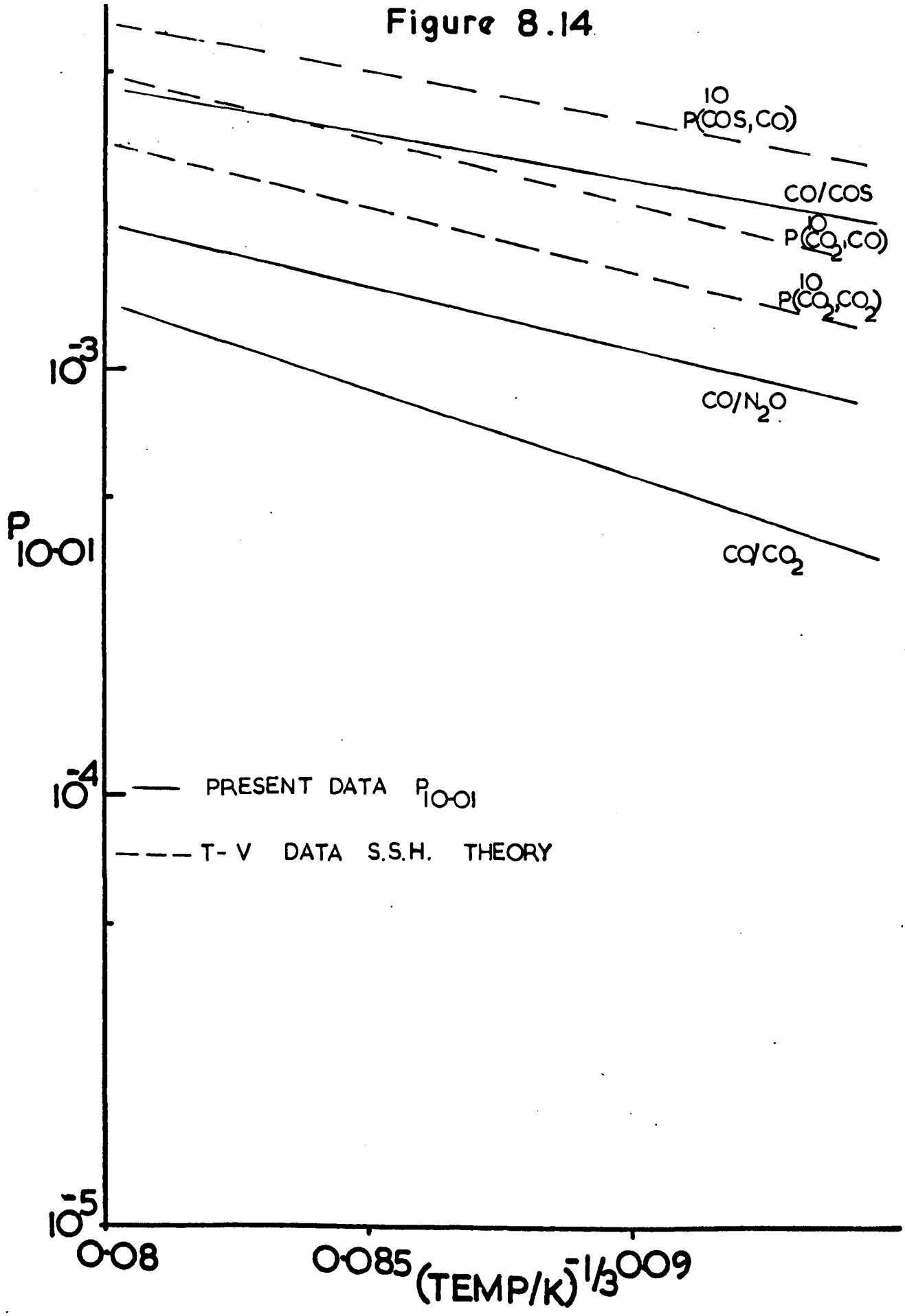
10
P(COS,CO)
CO/COS
10
P(CO2,CO)
10
P(CO2,CO2)
CO/N2O
CO/CO2
P10-01
10-3
10-4
10-5
PRESENT DATA P10-01
T-V DATA S.S.H. THEORY
0·08
0·085
(TEMP/K)-1/3
0·09

2) Comparison was made to previous or comparable work at room temperatures by extrapolation of the present data. In the cases where comparison was possible there was an apparent discrepancy between the values. It was felt that the discrepancy was due to the effect of long range forces, at temperatures below 1000K, for the near resonance condition. It has been shown by other workers that the probabilities have an inverse temperature dependence at these temperatures.

3) The present data was compared to theory, and in the three cases studied agreement was good. The major source of error in the S.S.H. calculations was thought to be the evaluation of ε/k and r_0 for gas mixtures. The geometric mean was taken for ε/k and the arithmetic mean for r_0. The error in ε/k may have been particularly large, due to the differences in potential well depth between CO and the polyatomic species.

8.3 SUMMARY

This work has studied two aspects of vibrational energy exchange. In the first part it was shown that V-V reactions played an important role in maintaining the vibrational energy distribution, while the V-T processes relaxed the gas to equilibrium. It was found that even when the V-V processes were made very fast with respect to the V-T processes, they had no effect on the rate of relaxation of the system. In the study of binary mixtures, with active modes, it was found that the V-V processes played an active part in the relaxation process. In this case one of the gases was assumed to relax very slowly with respect to the other. Thus the T-V processes would play no part in populating the excited state of the slower relaxing gas. The vibrational energy required by this gas was provided by V-V exchange from a near resonant mode of the faster relaxing gas. The rate at which the energy was exchanged depended on the matching of the two modes of the gases. The smaller the energy discrepancy between the modes, the more efficient the V-V exchange. It was also found that at high temperatures the probabilities of the V-V exchange would approach those of T-V exchange, because the temperature dependence of the two processes are different.

8.4 SUGGESTIONS FOR FUTURE WORK

1) With regard to the work on CO/Ne, the computer programme should be extended to account for anharmonicity. It is possible then that a rate constant for k_{21} may be extracted from the present work.

2) This work has indicated the importance of the T^{-1} temperature dependence of P_{10-01} at temperatures <1000K. It would be interesting to conduct a similar study to that of Taylor and Bitterman[34] which indicates that for N_2/CO_2 the cross over point, between the long range and short range interaction, is between 1000 - 1200K. Thus extending the present data to well below 1200K would probably indicate the cross over point in the three systems studied.

3) The S.S.H. theory has been used extensively throughout this work, although its limitations are fully realised. It has two main faults, one is in the evaluation of ϵ/k and r_0 for gas mixtures and the other is in the evaluation of, Z_o, the geometric factor. Shin[40] has proposed an alternative method of calculating Z_o, which may be more realistic. It is difficult to suggest alternative methods for calculating ϵ/k and r_0.

4) In view of the fact that most diatomic and simple polyatomic molecules have been studied in the pure case and in gas mixtures, it would be worth while focussing attention on the new technique of a glow discharge shock tube, as mentioned in Chapter 1.

This will provide basic information on the exchange of energy between excited atoms and diatomic molecules, at high temperatures. Comparison can be made with work done at room temperatures.

REFERENCES

1. L.D. Landau and E. Teller, *Z. Phys. Sowjetunion*, 1936, 10, 34.
2. W.J. Hooker and R.C. Millikan, *J. Chem. Phys.*, 1963, 38, 214.
3. D.L. Matthews, *J. Chem. Phys.*, 1961, 34, 639.
4. A.G. Gaydon and I.R. Hurle, *Symp. Combust. 8th*, (Williams and Wilkins, Baltimore) 1962, 309.
5. R.C. Millikan, *J. Chem. Phys.*, 1964, 40, 2594.
6. E.W. Montroll and K.E. Shuler, *J. Chem. Phys.*, 1957, 26, 454.
7. N.W. Bazley, E.W. Montroll, R.J. Rubin and K.E. Shuler, *J. Chem. Phys.*, 1958, 28, 700.
8. J.W. Rich and R.G. Rehm, *Symp. Combust. 11th*, (Combustion Institute, Pittsburg, Pa.) 1967, 37.
9. E.R. Fisher and R.H. Kummler, *J. Chem. Phys.*, 1968, 49, 1075.
10. K.N.C. Bray, *Fluid Mechanic Laboratory Publication, Massachusetts Institute of Technology*, 1967, 67-3.
11. K.N.C. Bray, *J. Phys. B (Proc. Phys. Soc.)* 1968, Ser 2, Vol 1, 705.
12. J. Keck and G. Carrier, *J. Chem. Phys.*, 1965, 43, 2284.
13. A.B. Callear and W.M. Smith, *Trans. Faraday Soc.*, 1963, 59, 1735.
14. R.V. Fitzsimmons and E.J. Blair, *J. Chem. Phys.*, 1964, 40, 451.
15. J.I. Steinfield and W. Klemperer, *J. Chem. Phys.*, 1965, 42, 3475.
16. R.L. Brown and W. Klemperer, *J. Chem. Phys.*, 1964, 41, 3072.

17. C.C. Chow and E.F. Greene, *J. Chem. Phys.*, 1965, 43, 324.

18. J.P. Appleton and M. Steinberg, *J. Chem. Phys.*, 1967, 46, 1521.

19. R.C. Millikan and D.R. White, *J. Chem. Phys.*, 1963, 39, 98.

20. N.H. Johannesen, *J. Fluid Mech.*, 1961, 10, 25.

21. H.K. Zienkiewicz and N.H. Johannesen, *J. Fluid Mech.*, 1963, 17, 499.

22. P.A. Blythe, *J. Fluid Mech.*, 1961, 10, 33.

23. N.H. Johannesen, H.K. Zienkiewicz, P.A. Blythe and J.H. Gerrard, *J. Fluid Mech.*, 1962, 13, 213.

24. R.W. Lutz and J.H. Kiefer, *Phys. Fluids*, 1966, 9, 1638.

25. P. Borrell, *Transfer and Storage of Energy by Molecules*, (Wiley - Interscience, London) 1969, 2.

26. R.L. Taylor, M. Camac and R.M. Feinberg, *11th Symp. Combustion* (Combustion Institute, Pittsburg, Pa.) 1967, 49.

27. W.J. Witteman, *Philips Res. Repts.*, 1963, 2.

28. K.F. Herzfeld, *Discussion Faraday Soc.*, 1962, 33, 22.

29. D. Rapp and T.E. Sharp, *J. Chem. Phys.*, 1963, 38, 2641.

30. C.B. Moore, *Fluorescence*, (Marcel Dekker, New York) 1967, 3, 133.

31. K.F. Herzfeld, *J. Chem.Phys.*, 1967, 47, 743.

32. D. Rapp and P.E. Golden, *J. Chem. Phys.*, 1964, 40, 573, *Ibid*, 1964, 40, 5123.

33. R.D. Sharma and C.A. Brau, *Phys. Rev. Letters*, 1967, 19, 1273.

34. R.L. Taylor and S. Bitterman, *J. Chem. Phys.*, 1969, 50, 1720.

35. J.F. Roach and W.R. Smith, *J. Chem. Phys.*, 1969, 50, 4114.

36. C.J.S.M. Simpson, K.B. Bridgman and T.R.D. Chandler, *J. Chem. Phys.*, 1968, 49, 509.

37. W.A. Rosser, Jr., A.D. Wood and E.T. Gerry, *J. Chem. Phys.*, 1969, 50, 4996.

38. A. Eucken and H. Jaacks, *Z. Phys. Chem.*, 1935, 30B, 85.

39. A. Eucken and S. Aybar, *Z. Phys. Chem.*, 1940, 46B, 195.

40. H.K. Shin, *J. Chem. Phys.*, 1967, 47, 3302.

41. J.G. Hall and A.L. Russo, *AGARD CP*, 1967, 12, Vol 2.

42. A.L. Russo, *J. Chem. Phys.*, 1967, 47, 5201.

43. T.I. McLaren and J.P. Appleton, *J. Chem. Phys.*, 1970, 53, 2850.

APPENDIX 1

FORMULAE

A.1.i TUBE DIMENSIONS AND HOT FLOW TIME

The tube dimensions mentioned in Chapter 2, section 2.2.a, were calculated using the equations set out below. The length of the tube from diaphragm to observation station is χ_c. χ_c is, in fact, the distance along the tube at which the reflected rare faction wave overtakes the contact surface. For a given hot flow time, $\Delta\tau$, and Mach number, M_s, the value of χ_c can be calculated from:-

$$\chi_c = \tau_c \left[\frac{2a_1 (M_s^2 - 1)}{(\gamma_1 + 1)M_s} \right] \qquad \text{A.1.1}$$

where

$$\tau_c = \Delta\tau \left[1 - \frac{2(M_s^2 - 1)}{(\gamma_1 + 1)M_s^2} \right]^{-1} \qquad \text{A.1.2}$$

Where τ_c = flow duration of contact surface μs

$\Delta\tau$ = $\tau_c - \tau_s$ = hot flow time μs

τ_s = flow duration of shock wave μs

a_1 = speed of sound in test gas mm μs^{-1}

γ_1 = specific heat of test gas

The minimum length of driver section, x_D, required for the given $\Delta\tau$ is calculated from:-

$$x_D = \frac{\tau_c a_4}{2}\left[1 - \frac{\gamma_4 - 1}{\gamma_1 + 1}\frac{a_1}{a_4}\left(\frac{M_s^2 - 1}{M_s^2}\right)\right]^{\frac{\gamma_4 + 1}{2(\gamma_4 - 1)}}$$

where a_4 = speed of sound in driver gas mm μs^{-1}

γ_4 = specific heat ratio of driver gas

In order that the maximum hot flow time, $\Delta\tau$, may be obtained, the observation station must be placed at a distance from the end wall to ensure no interaction of the reflected shock with the hot flow region. The minimum tolerable length of the low pressure section, x_{min}, is given by:-

$$x_{min} = \left[\frac{\tau_c + x_c/W_R}{W_s^{-1} + W_R^{-1}}\right] \qquad \text{A.1.3}$$

where

$$W_s = M_s a_1$$

$$W_R = W_s\left[\frac{2 + \left(\frac{2}{\gamma_1 - 1}\frac{P_1}{P_2}\right)}{\frac{\gamma_1 + 1}{\gamma_1 - 1} - \frac{P_1}{P_2}}\right] \qquad \text{A.1.4}$$

$$\frac{P_2}{P_1} = \frac{2\gamma_1 M_s^2 - (\gamma_1 - 1)}{\gamma_1 + 1}$$

W_s = speed of shock wave mm μs^{-1}

W_R = speed of reflected wave mm μs^{-1}

In the present calculations a value of 500 μs was used for $\Delta\tau$. For a shock of Mach 5 in pure carbon monoxide $\gamma_1 = 1.4$ and $a_1 = 0.353$ mm μs^{-1}. Equation A.1.2 gives τ_c to be 2.5×10^{-3} s and equation A.1.1 gives χ_c to be 3.53 m. At Mach 5, in pure CO, $P_2/P_1 = 29$ and $W_s = 1.77$ mm μs^{-1}, thus A.1.4 gives $W_R = 0.644$ mm μs^{-1}. From A.1.3 χ_{min} is 3.76 m. Thus the observation station needs to be at least 0.23 m from the end plate. The length of the driver section, χ_D, was calculated using $a_4 = 1.334$ mm μs^{-1}, $\gamma_4 = 1.4$ and τ_c as given above. The value of χ_D was found to be 1.5 m.

The flow correction computer programme, Appendix 2, included calculations for $\Delta\tau$, for various Mach numbers and for the length of tube used. The ideal diaphragm pressure ratios were calculated from:-

$$\frac{P_4}{P_1} = \left[\frac{2\gamma_1 M_s^2 - (\gamma_1 - 1)}{(\gamma_1 + 1)}\right]\left[1 - \frac{\gamma_4 - 1}{\gamma_1 + 1}\frac{a_1}{a_4}\left(M_s - \frac{1}{M_s}\right)\right]^{-\frac{2\gamma_4}{\gamma_4 - 1}} \qquad \text{A.1.5}$$

A.1.ii DERIVATION d ln M_s/dt

In Chapter 3, section 3.1.a, the quantity d ln M_s/dt was determined in terms of measured parameters. The shock wave is decelerating as it moves down the tube, and the change of Mach number with distance is given by:-

$$\frac{d M_s}{dx} = - Y M_s$$

where Y = velocity decrement (about 1% m^{-1})

Integrating:-

$$\ln M_s = - Yx + c$$

$$M_s = e^{-Yx} e^{c}$$

when $x = 0$, $M_s = M_{s(g)}$

where $M_{s(g)}$ = the given shock Mach number

$$M_s = M_{s(g)} e^{-Yx} \qquad \text{A.1.6}$$

Also:-

$$M_s = \frac{1}{a_1} \frac{dx}{dt} \qquad \text{A.1.7}$$

Substituting A.1.7 in A.1.6

$$\therefore \quad \frac{1}{a_1} \quad \frac{dx}{dt} \quad = \quad M_{s(g)} \, e^{-Yx} \qquad \text{A.1.8}$$

Integrating:-

$$\int e^{Yx} \, dx \quad = \quad \int M_{s(g)} \, a_1 dt$$

$$\frac{e^{Yx}}{Y} \quad = \quad M_{s(g)} \, a_1 t \; + \; d$$

when $t = 0, \; x = 0$

$$\therefore \quad d \quad = \quad Y^{-1}$$

$$\therefore \quad e^{-Yx} \quad = \quad \frac{1}{YM_{s(g)} \, a_1 t \; + \; 1}$$

$$\therefore \quad M_s \quad = \quad \frac{M_{s(g)}}{YM_{s(g)} \, a_1 t \; + \; 1}$$

Taking logs:-

$$\ln M_s \quad = \quad \ln M_{s(g)} \; - \; \ln \left(YM_{s(g)} \, at \; + \; 1\right)$$

differentiating w.r.t. t:-

$$\frac{d \ln M_s}{dt} \quad = \quad \frac{Ya_1 \, M_{s(g)}}{YM_{s(g)} a_1 t + 1} \qquad \text{A.1.9}$$

The values of Y, a_1, $M_{s(g)}$ are known and the value of t is set equal to t_m, the maximum hot flow time at the observation station. The value of t_m can be calculated from equation 3.1.

APPENDIX 2

COMPUTER STUDIES

A.2.i FLOW CORRECTION PROGRAMME

The calculational procedure for the correction of shock parameters has been set out in Chapter 3, section 3.1.a. The equations for the hot flow time and diaphragm pressure ratio were set out in Appendix 1. The calculations apply to gas mixtures, and the specific heat ratio, $\bar{\gamma}$, for a mixture is calculated from:-

$$\bar{\gamma} = \frac{\sum_{j=1}^{s} C_{pj} F_j}{\sum_{j=1}^{s} C_{vj} F_j}$$

F_j = mole fraction of species j

C_{pj} = specific heat at constant pressure of species j

C_{vj} = specific heat at constant volume of species j

Using this calculated value of $\bar{\gamma}$, the average speed of sound in the gas mixture is calculated from:-

$$a = \frac{1}{10} (0.8313\ \bar{\gamma}\ T_1/\overline{M.W.})^{\frac{1}{2}}$$

where T_1 = room temperature K

$\overline{M.W.}$ = average molecular weight

$$= \sum_{j=1}^{s} (M.W.)_j \, F_j$$

$(M.W.)_j$ = molecular weight of species j

The computer programme used to calculate the corrected parameters is set out overleaf. The more important calculational symbols and their meanings are given in Table A.2.1 where a symbol is part of the output, the output format will be included. The input symbols, their formats and meanings are detailed on the comment cards, Table A.2.2 lists the input information.

TABLE A.2.1

COMPUTATION SYMBOLS

FORTRAN	CALCULATIONS	MEANING
XM	M_s	Mach number (F6.3)
AT1MIX	a_1	Speed of sound in test gas (F8.5)
U	W_s	Speed of shock (F11.5)
GAMIX	$\bar{\gamma}$	Average specific heat ratio (F6.3)
XMWAV	$\overline{M.W.}$	Average molecular weight (F8.3)
TC	τ_c	Flow duration of contact surface
TO	$\Delta\tau$	Hot flow duration (F15.6)
PRES	P_4/P_1	Diaphragm pressure ratio (F11.4)
DER	r	Radius of tube
TM	t_m	Maximum hot flow duration (E10.4)
TP	t_p	Particle time for hot flow (E10.4)
TL	t_l	Laboratory time

FORTRAN	CALCULATIONS	MEANING
XMS2	M_{2s}	The Mach number of the hot flow behind the shock
DELTB	$(\Delta T/T_2)_b$	Temperature correction due to boundary layer
DLNMS	d ln M_s/dt	-
DELTD	$(\Delta T/T_2)_d$	Temperature correction due to deceleration
DTOTAL	$(\Delta T/T_2)_{TOTAL}$	Total temperature correction (F7.5)
DELRO	$(\Delta\rho/\rho_2/\rho_1)$	Total density correction (F8.4)
TACT	ΔT	Actual correction to temperature in K (F10.2)
ROACT	$\Delta\rho$	Actual density correction (F10.2)

TABLE A.2.2

INPUT INFORMATION

CARD No.	COL NOS.	SYMBOL & UNITS		FORMAT
1. Number of jobs for one mixture	1 - 5	NJOBS		I5
2. Experimental parameters	1 - 10	XD	mm	F10.4
	11 - 16	GAMA4		F6.3
	17 - 24	A4	$mm\ s^{-1}$	F8.5
	25 - 30	DER	cm	F6.3
	31 - 37	YID	$\%\ mm^{-1}$	F7.4
	38 - 40	IS		I3
3. Species parameters	1 - 15	ZJK		5A3
	16 - 20	XNJ		F5.2
	21 - 27	XMWJ		F7.3
	28 - 34	GJ		F7.3
4. Mole fraction. Up to five species per mixture are allowed, and read across the card	1 - 10	FJ		F10.5
5. Input Mach numbers for one job	1 - 6	XMS		F6.3
	7 - 12	XME		F6.3
	13 - 19	XMI		F7.3
	20 - 27	T1	K	F8.3

CARD No.	COL NOS.	SYMBOL & UNITS		FORMAT
6. Experimental	1 - 7	P1	torr.	F7.3
input parameters	8 - 17	TL	μs	E10.4
for one job	18 - 25	RHOS		F8.4
	26 - 33	T2	K	F8.2
7. Recycle card	1 - 2	ISSW		I2

For any set of experimental parameters (card 2) and species parameters (cards 3, 4) there are a certain number of jobs (card 1). For any one job there will be a pair of experimental input cards (cards 5, 6). If the programme is recycled (card 7), then a new number of jobs (card 1) is read, and the species parameters (cards 2, 3, 4) are read. Then the experimental parameters cards are read in pairs until the number of jobs is completed.

```
C
C      G MILLWARD(KEELE) CORRECTIONS FOR NON-UNIFORM FLOW IN SHOCK TUBES.
C      THEORY OF H.MIRELS DEVELOPED FOR EXPLICIT USE BY R.A.STREHLOW.
C
       DIMENSION ZJK(5,5),XNJ(5),XMWJ(5),CPJ(5),CVJ(5),CPAJ(5),CVAJ(5),FJ
      1(5),GAJ(5),GJ(5)
       COMMON IS,T1,AY,RY,AT1MIX,AAMIX,GMIX,GAMIX,XMWAV,FJ,ZJK,XMWJ,GJ,PR
      1ES,TO,XM,U,JJ,XNJ
     4 CONTINUE
     1 FORMAT(30X,65H**********FLOW NONUNIFORMITY-EFFECT ON SHOCK PARAMET
      1ERS**********)
     2 FORMAT(30X,53H                ADAPTED BY G.E.MILLWARD 25 AUGUST 196
      18)
       WRITE(2,1)
       WRITE(2,2)
       JJ=0
C
C      READ IN DATA
C
C
C      CARD 1 START COL 1. NJOBS=NUMBER OF JOBS(I5)FOR ONE MIXTURE
C
       READ(7,21)NJOBS
    21 FORMAT(I5)
C
C      CARD 2 START COL 1. XD=TUBE LENGTH FROM DIAPHRAGM TO OBSERVATION
C      STATION(F10.4),GAMA4=SPECIFIC HEAT RATIO OF DRIVER GAS(F6.3),
C      A4=SPEED OF SOUND IN DRIVER GAS(F8.5),DER=RADIUS OF TUBE(F6.3),
C      YID=VELOCITY DECREMENT(F7.4),IS=NUMBER OF SPECIES IN MIXTURE(I3)
C
       READ(7,20)XD,GAMA4,A4,DER,YID,IS
    20 FORMAT(F10.4,F6.3,F8.5,F6.3,F7.4,I3)
```

```
C
C       CARD 3 START COL 1. ZJK=SPECIES NAME(5A3),XNJ=NUMBER OF ATOMS IN
C       SPECIES(F5.2),XMWJ=MOLECULAR WEIGHT OF SPECIES(F7.3),GJ=SPECIFIC
C       RATIO OFSPECIES(F7.3)
C       NUMBER OF SPECIES CARDS SIMILAR TO CARD 3 DEPENDS ON THE VALUE
C       OF IS
C
        DO 51 J=1,IS
   90   FORMAT(5A3,1X,F5.2,F7.3,F7.3)
        READ(7,90)(ZJK(J,K),K=1,5),XNJ(J),XMWJ(J),GJ(J)
   51   CONTINUE
C
C       CARD 4 START COL 1. FJ=MOLE FRACTIONS OF SPECIES A TOTAL OF FIVE
C       SPECIES IS POSSIBLE,READ ACROSS THE CARD(5F10.5)
C
        READ(7,100)(FJ(J),J=1,IS)
  100   FORMAT(5F10.5)
C
C       CARD 5 START COL 1. XMS=STARTING MACH NUMBER(F6.3),XME=ENDING MACH
C       NUMBER(F6.3),XMI=MACH NUMBER INCREASE(F7.4),T1=ROOM TEMPERATURE(F
C       8.3)
C
        DO 2000 M=1,NJOBS
        READ(7,7)XMS,XME,XMI,T1
    7   FORMAT(F6.3,F6.3,F7.4,F8.3)
C
C       CARD 6 START COL 1. P1=DOWNSTREAM PRESSURE(F7.3),TL=OBSERVATION
C       TIME(E10.4),RHOS=DENSITY RATIO AVERAGE(F8.4),T2=AVERAGE SHOCK

C       TEMPERATURE(F8.2)
C
        READ(7,18)P1,TL,RHOS,T2
   18   FORMAT(F7.3,E10.4,F8.4,F8.2)
        JJ=JJ+1
        WRITE(2,22)JJ
   22   FORMAT(1H0,41X,11HJOB NUMBER=,I5)
   23   FORMAT(42X,16H----------------)
        WRITE(2,23)
```

```
C
C      CALCULATIONS ON DIAPHRAGM PRESSURE RATIO,AND THEORETICAL
C      OBSERVATION TIME
C
       CALL BLOOD
       CALL COFFIN
       XM=XMS
     9 U=XM*AT1MIX
       AM=U/AAMIX
       CY=AM**2
       B=((2*GAMIX*CY)-RY)/(AY)
       C=((GAMA4-1.)*AT1MIX)/(AY*A4)
       D=(AM-(1./AM))
       E=(-2*GAMA4)/(GAMA4-1.)
       PRES=((1.-(C*D))**E)*B
       TC=XD/((2.*AT1MIX*(CY-1.))/(AM*AY))
       TO=TC*(1-((2.*(CY-1.))/(CY*AY)))
       WRITE(2,11)U,XM,PRES,TO
    11 FORMAT(27X,F11.5,5X,F6.3,6X,F11.4,4X,F15.6)
       XM=XM+XMI
       IF(XM-XME)9,9,12
    12 CONTINUE
C
C      CALCULATIONS OF EFFECT OF NON UNIFORM FLOW ON THE EXPERIMENTAL
C      INPUT PARAMETERS PRINT OUT OF TEMPERATURE AND DENSITY INCREASE
C
       CALL DEATH(DER,P1,TL,RHOS,YID,T2)
       XM=XMS
    53 CONTINUE
       U=XM*AT1MIX
       AM=U/AAMIX
       CY=AM**2
       AZ=3.142*(DER**2)
       AP=2*3.142*DER
       TM=5.85*((4*AZ)**2)*P1/((XM**1.7)*(AP**2)*AT1MIX*10.0**5)
       TP=TL*RHOS*(1+(0.7*((TL/TM)**0.5)))
       XMS2=(((BY*CY)+2)/((2*GAMIX*CY)-BY))**0.5
```

```
      DELTR=((TL/TM )**0.5)*(((XMS2**2)*RY)/((XMS2**2)-1))*(-1.00)
      DLNMS=(YID*AT1MIX*XM)/((YID*AT1MIX*TM)+1)
      DELTD=TP*((2*((CY-1)**2))/((1+((RY*CY)/2))*(((2*GAMIX*CY)/RY)-1)))
      DTOTAL=DELTR+DELTD*DLNMS
      DELRO=DTOTAL/RY
      TACT=DTOTAL*T2
      ROACT=DELRO*RHOS
      WRITE(2,91)XM,TM,TP,DTOTAL,TACT,DELRO,ROACT
   91 FORMAT(7X,F6.3,9X,E10.4,4X,E10.4,7X,F7.5,3X,F10.2,10X,F8.4,6X,F10.
     12)
      XM=XM+XMI
      IF (XM-XME)53,53,52
   52 CONTINUE
 2000 CONTINUE
C
C     CARD 7 START COL 1 RECYCLE CARD IF ISSW(I2) 01 WILL RECYCLE,IF 00
C     THEN PROGRAMME CONCLUDES. ON RECYCLING THE FOLLOWING CARDS ARE
C     REQUIRED FOR A NEW MIXTURE 1,2,3,4,5,6, ETC.
C
      READ(7,3)ISSW
    3 FORMAT(I2)
      IF (ISSW.EQ.1) GO TO 4
      STOP
      END
C
C     THIS SUBROUTINE CALCULATES THE SPECIFIC HEAT RATIO,THE AVERAGE
C     MOLECULAR WEIGHT AND THE SPEED OF SOUND IN THE MIXTURE.
C
      SUBROUTINE BLOOD
      DIMENSION ZJK(5,5),XNJ(5),XMWJ(5),CPJ(5),CVJ(5),CPAJ(5),CVAJ(5),FJ
     1(5),GAJ(5),GJ(5)
      COMMON IS,T1,AY,RY,AT1MIX,AAMIX,GMIX,GAMIX,XMWAV,FJ,ZJK,XMWJ,GJ,PR
     1ES,T0,XM,U,JJ,XNJ
      XMWAV=0.0
      GMIX=0.0
      CP=0.0
      GAMIX=0.0
```

```
      PCM=0.0
      VCM=0.0
      PCAM=0.0
      VCAM=0.0
      DO 50 J=1,IS
      XMWAV=XMWAV+FJ(J)*XMWJ(J)
      IF(XNJ(J)-1.0)42,42,43
   42 GAJ(J)=1.6667
      GO TO 47
   43 IF(XNJ(J)-2.0)44,44,45
   44 GAJ(J)=1.4
      GO TO 47
   45 GAJ(J)=1.33333
   47 CONTINUE
      CPJ(J)=1.9872*GJ(J)/(GJ(J)-1.)
      CVJ(J)=CPJ(J)-1.9872
      CPAJ(J)=1.9872*GAJ(J)/(GAJ(J)-1.)
      CVAJ(J)=CPAJ(J)-1.9872
      PCM=PCM+FJ(J)*CPJ(J)
      VCM=VCM+FJ(J)*CVJ(J)
      PCAM=PCAM+FJ(J)*CPAJ(J)
      VCAM=VCAM+FJ(J)*CVAJ(J)
   50 CONTINUE
      GMIX=PCM/VCM
      GAMIX=PCAM/VCAM
      AAMIX=1./10.*SQRT(GAMIX*0.8313*T1/XMWAV)
      AT1MIX=1./10.*SQRT(GMIX*0.8313*T1/XMWAV)
      AY=GAMIX+1.
      BY=GAMIX-1.
      RETURN
      END
```

```
C
C      THIS SUBROUTINE PRINTS OUT THE SPECIES CHARACTERISTICS AND
C      THE HEADINGS FOR P4/P1 AND HOT FLOW TIME
C
       SUBROUTINE COFFIN
       DIMENSION ZJK(5,5),XNJ(5),XMWJ(5),CPJ(5),CVJ(5),CPAJ(5),CVAJ(5),FJ
      1(5),GAJ(5),GJ(5)
       COMMON IS,T1,AY,BY,AT1MIX,AAMIX,GMIX,GAMIX,XMWAV,FJ,ZJK,XMWJ,GJ,PR
      1FS,TO,XM,U,JJ,XNJ
  510  FORMAT(1H0,21X,27H                          SPECIES,10X,10HMOLE FRACT,5X
      1,2HMW,5X,6HGAMMA1)
       WRITE(2,510)
       DO 530 J=1,IS
       WRITE(2,540)(ZJK(J,K),K=1,5),FJ(J),XMWJ(J),GJ(J)
  530  CONTINUE
  540  FORMAT(42X,5A3,F10.5,F12.3,F9.3)
       WRITE(2,550)T1,XMWAV,AT1MIX,GMIX
  550  FORMAT(31H0                        T1 (DEGK)=,F6.1,5X,7HAV MW =,F8.3,
      15X,17HMIX SOUND SPEED =,F8.5,5X,12HGAMMA(MIX) =,F6.3)
       WRITE(2,10)
   10  FORMAT(//34X,3HVEL,7X,5HMACHN,10X,5HP4/P1,10X,18HTEST TIME(MU-SECS
      1))
       RETURN
       END
```

```
C
C      THIS SUBROUTINE PRINTS OUT HEADINGS FOR THE NON UNIFORM
C      CORRECTION CALCULATIONS
C
       SUBROUTINE DEATH(DER,P1,TL,RHOS,YID,T2)
       DIMENSION ZJK(5,5),XNJ(5),XMWJ(5),CPJ(5),CVJ(5),CPAJ(5),CVAJ(5),FJ
      1(5),GAJ(5),GJ(5)
       COMMON IS,T1,AY,BY,AT1MIX,AAMIX,GMIX,GAMIX,XMWAV,FJ,ZJK,XMWJ,GJ,PR
      1ES,TO,XM,U,JJ,XNJ
       WRITE(2,700)
  700 FORMAT(1H0,20X,75H**********CORRECTION TO NON UNIFORM FLOW USING M
      1IRELS   EQUATIONS**********)
  750 FORMAT(1H0,10X,10HT2 (DEGK)=,F6.1,5X,14HINITIAL PRES =,F8.3,5X,8HR
      102/R01=,F8.4)
       WRITE(2,750)T2,P1,RHOS
       WRITE(2,752)TL,YID,DER
  752 FORMAT(10X,17HOBSERVATION TIME=,E10.4,5X,19HVELOCITY DECREMENT=,F7
      1.4,5X,7HRADIUS=,F9.5)
       WRITE(2,751)
  751 FORMAT(1H0,6X,8HMACH NO.,7X,8HMAX TIME,6X,10HIDEAL TIME,6X,7HDELT/
      1T2,6X,13HTEMP INCREASE,5X,7HDELR/R0,6X,16HDENSITY INCREASE)
       RETURN
       END
```

A.2.ii S.S.H. PROGRAMME

A résumé of the calculational procedure used in this programme is set out below. The most important parameter in the calculations is ℓ, the range of repulsive forces, which is evaluated by an iterative procedure. It is assumed for most pure gases and gas mixtures, that ℓ has a value between 1.5 and 2.5 nm. If the value of ℓ is outside these limits then the programme indicates this and stops. Usually ℓ is calculated as follows:-

$$\ell' = 2\pi\ell \qquad \text{A.2.5}$$

The value of ℓ inserted initially in A.2.5 is 1.5 then the calculated value of ℓ' is substituted in:-

$$\frac{\varepsilon'}{k} = \frac{\mu(2\pi c\, \bar{\nu}\ell')^2}{10^{16}\, k} \qquad \text{A.2.6}$$

where $$\mu = \frac{M_A\, M_{BC}}{(M_A+M_{BC})N}$$

N = Avagadro's number

M's = molecular weights of A and BC

k = Boltzmann Constant

c = speed of light cm s^{-1}

$\bar{\nu}$ = fundamental vibration frequency of BC cm^{-1}

The value of ε'/k is then used in:-

$$\frac{Em}{k} = \frac{T}{2} \left(\frac{\varepsilon'}{kT}\right) \qquad A.2.7$$

where T = a specified temperature K (input)

Values of ε/k are obtained from the tables of Hirschfelder et al,[1] and for 2 colliding particles A and B, the geometric mean of the pair of values is taken:-

$$\varepsilon/k = \sqrt{\frac{\varepsilon_A}{k} \quad \frac{\varepsilon_{BC}}{k}} \qquad A.2.8$$

where ε = geometric mean of L-J potential well depth

Em = effective collision energy

Thus from A.2.7 and A.2.8 a value for Em/ε may be found. Then using Method B a value of ℓ can be obtained:-

$$\ell = r_\theta \left[\ln\left(\frac{Em}{\varepsilon} + 1\right)\right]^{-1} \left[1 - \left(\tfrac{1}{2}\left[1 + \sqrt{Em/\varepsilon + 1}\right]\right)^{\frac{1}{6}}\right] \text{A.2.8}$$

Where r_0 is the arithmetic mean of the L-J constant. The values of r_{OA} and r_{OBC} being obtained from Hirschfelder et al.[1]

$$r_0 = \frac{r_{OA} + r_{OBC}}{2}$$

Thus the programme returns to a value of ℓ, which is compared with the input value. If the two match exactly, then the programme continues. However, if the values are not equal, then the value of ℓ may be incremented by as little as 0.0001 nm and the procedure is

recycled, until the values of ℓ do coincide.

Now putting

$$\theta' = \frac{\varepsilon'}{k} \quad \text{and} \quad \theta = \frac{\bar{\nu}_{BC} hc}{k}$$

Then Z_{10}, the collision number for deactivation is:-

$$Z_{10} = 1.017(r_0/r_c)^2 \; Z_o \; Z_{osc} \; Z_{trans} \; Y(2,2) \; e^{-\varepsilon/kT} \; (1 - e^{-\theta/T})^{-1}$$

where $Z_o = 2.5 \; (\ell/L)^2 + L/\ell$

L = internuclear distance of BC

$$Z_{osc} = \frac{M_B M_C (M_A + M_B + M_C)}{(M_B^2 + M_C^2) M_A} \; \frac{1}{\pi} \left(\frac{\theta'}{\theta}\right)$$

$$Z_{tran} = \pi^2 \left(\frac{\theta}{\theta'}\right)^2 \sqrt{\frac{3}{2\pi}} \left(\frac{T}{\theta'}\right)^{\frac{1}{6}} \exp\left[\frac{3}{2} \left(\frac{\theta'}{T}\right)^{\frac{1}{3}} - \frac{\theta}{2T}\right]$$

$$Y(2,2) = 0.76 \; (1 + 1.1 \; \varepsilon/kT)$$

The relaxation time of one molecule of BC in all A is calculated from

$$\tau = Z_{10} \; \tau_c$$

where τ = relaxation time s

τ_c = average time between collisions s

For an ideal gas with rigid sphere molecules:-

$$\eta = 1.271\, p\tau_c$$

where η = viscosity in μP

p = 1 atms = 1.013×10^6 dyne cm^{-2}

The viscosity of the gas mixture, η, is calculated from:-

$$\eta \times 10^7 = \frac{266.93 \sqrt{2M_A M_{BC} T/(M_A + M_{BC})}}{r_0^2 \ (\Omega^{(2,2)} \text{ at } T^*)}$$

The viscosity is calculated assuming the molecules interact according to a potential curve specified by interaction parameters r_0 and ε (since T^* is kT/ε). The quantity ($\Omega^{(2,2)}$ at T^*) is obtained in a special way. The transport coefficients of a diatomic gas, of which the viscosity is one, may be expressed in terms of a set of linearly combined integrals, given the name $\Omega^{(2,2)}$. For a given interaction potential $\Omega^{(2,2)}$ can be evaluated, and the values of $\Omega^{(2,2)}$ and the reduced temperature T^* to which they correspond have been tabulated by Hirschfelder et al.[2] A value of T^* is calculated, and the tabulated data is searched for the values of T^* between which the calculated T^* lies. The value of the calculated $\Omega^{(2,2)}$ to which the calculated T^* corresponds is then obtained by interpolation.

Calculations of vibration-vibration exchange collision numbers may also be made. In the case of near resonance, the collision

number for deactivation of BC is given by:-

$$Z_{10(n.r.)} = Z_o \, Z_{osc} \, Z_{trans}$$

where Z_o = 9 steric factor

$$Z_{osc} = \frac{1}{4\pi^4} \left(\frac{4M_BM_C}{M_B^2+M_C^2}\right)_A \left(\frac{4M_BM_C}{M_B^2+M_C^2}\right)_{BC} \left(\frac{\theta'_A}{\theta_A}\right) \left(\frac{\theta'_{BC}}{\theta}\right)$$

$$Z_{trans} = \pi^2 \sqrt{\frac{3}{2\pi}} \left(\frac{T}{\theta'_{ABC}}\right)^{\frac{1}{6}} \left(\frac{\theta - \theta_A}{\theta'_{ABC}}\right)^2$$

$$\exp \frac{3}{2} \left[\left(\frac{\theta'_{ABC}}{T}\right)^{\frac{1}{3}} \pm \left(\frac{\theta - \theta_A}{2T}\right) - \frac{\epsilon}{T}\right]$$

where $\theta'_A = \dfrac{16\pi^4 M_A \bar{\nu}_A^2 c^2 \ell^2}{2 N 10^{16} k}$

$$\theta'_{BC} = \frac{16\pi^4 M_{BC} \bar{\nu}_{BC}^2 c^2 \ell^2}{2 N 10^{16} k}$$

$$\theta'_{ABC} = \frac{16\pi^4 \mu \ell^2 c^2 (\bar{\nu}_A - \bar{\nu}_{BC})}{10^6 k}$$

c = speed of light cm s^{-1}

$\bar{\nu}_A$ = vibration frequency of A cm^{-1}

$\bar{\nu}_{BC}$ = vibration frequency of BC cm^{-1}

k = Boltzmann constant

N = Avagadro's number

In the case of exact resonance:-

$$Z_{10(e.r.)} = Z_o \, Z_{osc} \, Z_{trans}$$

The values of Z_o, Z_{osc} are the same as for near resonance, but

$$Z_{trans} = \frac{h^2 \; 10^{16}}{64\pi^2 \; \mu \; kT \; \ell^2}$$

The computer programme used to calculate the collision numbers by the S.S.H. method is set out overleaf. The programme was written in collaboration with Mr. R. Gutteridge and Mrs P.M. Borrell. The more important calculational symbols and their meanings are given in Table A.2.3 where a symbol is part of the output, the output format will be included. The input symbols, their formats and meanings are detailed on the comment cards included in the programme, Table A.2.4 lists the input information.

```
C
C      G.MILLWARD(KEELE) QUANTUM THEORY OF VIBRATION ENERGY EXCHANGE.
C      THIS USES A 3-DIMENSIONAL S.S.H. METHOD.
C
       DIMENSION TEMP(100),ZED(100),EXPEK(100),ETHETA(100),ZTRAN(100),X(1
      100),Y(100),GAMA(100),TAUC(100),TAU(100),BL(100),ZEK(100),Z(100),
      2CTAU(100),ZEKBC(100),ZEKA(100),ZEKABC(100),TS(100),Z10NR(100),ZEX(
      3100),ZEKBCA(100),ZOS(100),ZTRA(100),ZTR(100)
       COMMON M,X,Y
C
C      READ IN DATA
C
C
C      THE FIRST TWO DATA CARDS CONTAIN CONSTANTS.
C      CARD 1 START COL 16.F=PI(F7.4),BK=BOLTZMAN CONSTANT(1PE12.4)
C      DL=INITIAL VALUE OF L(0PF10.5),BLI=INCREMENTAL VALUE OF L(0PF10.5)

C      CARD 2 START COL 1.AN=AVAGADRO NUMBER(1PE10.3),CE=SPEED OF LIGHT(1PE10.3),
C      H=PLANCKS CONSTANT(1PE10.3)
C

       READ(7,5)F,BK,DL,BLI,AN,CE,H
     5 FORMAT(15X,F7.4,1PE12.4,0P2F10.5/1P3E10.3)
C
C      CARD 3 START COL 1. N=NUMBER OF TEMPERATURE CARDS(I2)
C
   108 READ(7,101)N
   101 FORMAT(I2)
C
C      CARD 4 START COL 1.TEMP=TEMPERATURE(F7.1).
C
   112 DO 110 I=1,N
   111 READ(7,109)TEMP(I)
   109 FORMAT(F7.1)
   110 CONTINUE
```

```
C
C       CARD 5 START COL 1. M=NUMBER OF INTEGRALS IN HIRSCHFELDERS DATA(I3).
C       SEE THE TEXT
C
        READ(7,170)M
  170 FORMAT(I3)
C
C       CARD 6 START COL 1.HIRSCHFELDERS DATA T* & O(2,2) (12F0.0)
C       EACH CARD IS ALLOWED 6 PAIRS OF DATA.
C
        READ(7,171)(X(J),Y(J),J=1,M)
  171 FORMAT(12F0.0)
  501 CONTINUE
C
C       CARD 7 START COL 1.DI=INTERNUCLEAR DISTANCE OF BC(F10.6).
C
        READ(7,9)DI
    9 FORMAT(F10.6)
C
C       CARD 8 START COL 1.SPECIES CARD MOLECULE A.20 SPACES ALLOCATED FOR
C       SPECIES NAME(20H).THEN,COL 21 COA=L-J POTENTIAL WELL DEPTH(F10.4),
C       DRA=CONSTANT IN L-J POTENTIAL(F10.4),XMA=MOLECULAR WEIGHT OF A(F10.4),
C       XMA1,2,=ATOMIC WEIGHTS OF ATOMS 1,2(BOTH F10.4),XNUA=FUNDAMENTAL VIBRATION
C       FREQUENCY (F10.4).
C
        READ(7,7)COA,DRA,XMA,XMA1,XMA2,XNUA
    7 FORMAT(20H                    ,6F10.4)
C
C       CARD 9 .SPECIES CARD FOR MOLECULE BC;EXACTLY SIMILAR TO CARD 8.
C
        READ(7,8)COBC,DRBC,XMBC,XMB,XMC,XNU
    8 FORMAT(20H                    ,6F10.4)
```

```
C
C      CARD 10 START COL 1.RECYCLE CARD.IF 01(I2) WILL RECYCLE IF 00 THEN THE
C      PROGRAMME CONCLUDES.ON RECYCLING 3 CARDS ARE REQUIRED IE CARDS 7,8,9,
C      WHICH WILL CONTAIN THE PARAMETERS OF THE NEXT PAIR OF MOLECULES.
C
       READ(7,500)IPW
  500  FORMAT(I2)
C
C      PRINTING OF THE HEADINGS.
C
    1  FORMAT(100H1CALCULATIONS OF VIBRATIONAL RELAXATION IN PURE GASES A
     1ND GAS MIXTURES USING THE 3-D S.S.H. THEORY  )
    2  FORMAT(52H ADAPTED BY R.GUTTERIDGE & G.F.MILLWARD 23 JULY 1968 )
    3  FORMAT(33HOGAS A  DEACTIVATING  GAS BC                )
    4  FORMAT(86HOCONSTANTS USED  F=PI    BK=BOLTZ.   INIT.LO   LO INC. A
     1N=AVAGAD C(CM/SEC)  PLANCKS       )
       WRITE(2,1)
       WRITE(2,2)
       WRITE(2,3)
       WRITE(2,4)
       WRITE(2,41)F,BK,DL,BLI,AN,CE,H
   41  FORMAT(15X,F7.4,1PE12.4,0P2F10.5,1P3E10.3)

    6  FORMAT(29HOMOLECULAR CONSTANTS    EPS/K,7X,2HRO,5X,39HMOL.WT.   AT
     1.WT.B   AT.WT.C   NUBAR                  )
       WRITE(2,6)
       WRITE(2,7)CQA,DRA,XMA,XMA1,XMA2,XNUA
       WRITE(2,8)CQBC,DRBC,XMBC,XMB,XMC,XNU
C
C      COMPUTE MOLECULAR PARAMETERS;MATCHING OF THE EXPONENTIAL
C      POTENTIAL WITH LENNARD JONES POTENTIAL VIA METHOD B.
C
       DR=(DRA+DRBC)/2.
       CQ=SQRT(CQA*CQBC)
   20  FORMAT(20H AVERAGE FOR A & BC ,2F10.4)
       WRITE(2,20)CQ,DR
   91  FORMAT(1H0,47X,45H****** CALCULATED MOLECULAR PARAMETERS ******)
```

```
      WRITE(2,91)
   16 FORMAT(1H0,19X,7HT(DEGK),5X,5HEM/EP,7X,4HRO/L,6X,5HRO/RC,8X,3HL,A,
     1 8X,6HTHETAD,7X,6HY(2,2),2X,22HEXP(-EP/KT)       1-EXP)
      WRITE(2,16)
      XMW=XMA*XMBC/((XMA+XMBC)*AN)
      THETA=XNU*H*CE/BK
      THETAA=XNUA*H*CE/BK
  113 DO30I=1,N
      BL(I)=0.1500
   15 AL=2.0*F*BL(I)
      ZEK(I)=XMW*(2.0*CE*F/10.0**8*XNU*AL)**2/BK
      ZEMK=TEMP(I)/2.0*(ZEK(I)/TEMP(I))**0.33333
      ZEMKA=ZEMK/CQ
      BLC=DR*(1.-(0.5*(1.+SQRT(ZEMKA+1.)))**(-.16667))/(ALOG(ZEMKA+1.))
      IF(BLC-BL(I))104,104,22
   22 BL(I)=BL(I)+BLI
      IF(0.2500-BL(I))27,27,15
   27 WRITE(2,24)
   24 FORMAT(47H0BL LESS THAN 0.150000R GREATER THAN 0.25000          )
      GO TO 26
   31 GO TO 15
  104 DROC=(0.5*(1.+SQRT(ZEMKA+1.)))**0.16667
      ROL=DR/BL(I)
      ZEDO=(2.5*((BL(I)/DI)**2))+(DI/BL(I))
      BLN=BL(I)
      Y22=0.76*(1.+(1.1*CQ/TEMP(I)))
      IF(0.7-TEMP(I)/ZEK(I))28,29,29
   28 WRITE(2,10)
   10 FORMAT(22H KT/EPSILON TOO SMALL    )
      GO TO 26
   29 CONTINUE
      IF(10.0-TEMP(I)/ZEK(I))11,13,13
   11 WRITE(2,12)
   12 FORMAT(22H KT/EPSILON TOO LARGE    )
      GO TO 26
   13 EXPEK(I)=EXP(-CQ/TEMP(I))
```

```
C
C      COMPUTE COLLISION NUMBERS VIBRATION TRANSLATION ENERGY TRANSFER.
C
       ZOSC=(XMB*XMC*(XMA+XMBC)*ZEK(I))/((XMB**2+XMC**2)*XMA*F**2*THETA)
       ETHETA(I)=1./(1.-EXP(-THETA/TEMP(I)))
       ZTRAN(I)=((F*THETA/ZEK(I))**2)*(SQRT(1.5/F))*((TEMP(I)/ZEK(I))**0.
      116667)*(EXP((1.5*(ZEK(I)/TEMP(I))**0.33333)-(THETA/(2*TEMP(I)))))
       ZED(I)=1.017*DROC**2*Y22*ETHETA(I)*ZEDO*ZOSC*ZTRAN(I)*EXPEK(I)
       WRITE(2,17)TEMP(I),ZEMKA,ROL,DROC,RLN,ZEK(I),Y22,EXPEK(I),ETHETA(I
      1)
   17 FORMAT(1H0,19X,F7.1,4X,F6.2,5X,F6.2,5X,F6.3,5X,F8.5,3X,1PE10.3,5X,
      10PF6.3,4X,F7.4,8X,F7.4)
       RL(I)=RLN
   30 CONTINUE
   94 FORMAT(1H0,23X,92H****** VIBRATIONAL-TRANSLATIONAL ENERGY TRANSFER
      1--COLLISION NUMBERS--RELAXATION TIMES ******)
       WRITE(2,94)
   93 FORMAT(1H0,19X,7HT(DEGK),4X,7HT(-1/3),5X,2HZ0,6X,4HZOSC,6X,5HZTRAN
      1,12X,3HZ10,10X,4HTAUC,10X,3HTAU)
       WRITE(2,93)
C
C      COMPUTE RELAXATION TIMES VIA TABULATED VISCOSITY DATA.
C
       DO 50 I=1,N
       T3(I)=1.0/TEMP(I)**0.33333
       Z(I)=1.013249E-10*DRA**2*SQRT(16*AN*F/XMA/BK/TEMP(I))
       CTAU(I)=ZED(I)/Z(I)
       XX=TEMP(I)/CQ
       CALL LOOKUP(XX,YY)
       GAMA(I)=(266.93*SQRT(2*XMA*XMBC*TEMP(I)/(XMA+XMBC)))/((DR**2.)*YY*
      1(10.0**7.0))
       TAUC(I)=GAMA(I)/1.271/1.013249E6
       TAU(I)=ZED(I)*TAUC(I)
       WRITE(2,51)TEMP(I),T3(I),ZEDO,ZOSC,ZTRAN(I),ZED(I),TAUC(I),TAU(I)
   51 FORMAT(1H0,19X,F7.1,3X,F8.5,3X,F6.3,2X,F6.1,6X,1PE10.3,5X,E11.4,4X
      1,1PE11.5,4X,1PE11.5)
   50 CONTINUE
       IF(XNUA.EQ.0.0)GO TO 26
```

```
C
C      COMPUTE COLLISION NUMBERS FOR NEAR RESONANCE ENERGY TRANSFER.
C
       DO 61 I=1,N
       ZEKA(I)=16.0*F**4*XMA/AN/2.0*(BL(I)/10.0**8*XNUA*CE)**2/BK
       ZEKABC(I)=16.0*F**4* XMW*(BL(I)**2/10.0**16)*CE**2*(XNU-XNUA)**2
      1/BK
       ZEKBCA(I)=16.0*F**4*XMW*(BL(I)**2/10.0**16)*CE**2*((XMB+XMC)**2)/4
      1.0
       ZEKBC(I)=16.0*F**4*XMBC/AN/2.0*(BL(I)/10.0**8*XNU*CE)**2/BK
       ZOS(I)=((4.0*XMA1* XMA2)/(XMA1**2+XMA2**2))/4.0/F**4*((4.0*XMB*XMC
      1)/(XMB**2+XMC**2))*ZEKA(I)/THETAA*ZEKBC(I)/THETA
   61  CONTINUE
       ZONR=9.0
       IF (ZEKABC(1).EQ.0.0) GO TO 98
   95  FORMAT(1H0,24X,88H****** VIBRATIONAL-VIBRATIONAL ENERGY TRANSFER--
      1NEAR RESONANCE--COLLISION NUMBERS ******)
       WRITE(2,95)
       WRITE(2,96)
   96  FORMAT(1H0,32X,7HT(DEGK),4X,7HT(-1/3),5X,2HZ0,10X,4HZOSC,10X,5HZTR
      1AN,9X,9HZ10(N.R.))
       DO 73 I=1,N
       ZTRA(I)=(F**2)*(SQRT(3.0/2.0/F))*((TEMP(I)/ZEKABC(I))**0.16667)
      1*(((THETA-THETAA)/ZEKABC(I))**2)*EXP(1.5*((ZEKABC(I)/TEMP(I))**
      20.33333)-(ABS(THETA-THETAA)/2.0/TEMP(I))-(CQ/TEMP(I)*BK))
       Z10NR(I)=ZONR*ZOS(I)*ZTRA(I)
       WRITE(2,97)TEMP(I),T3(I),ZONR,ZOS(I),ZTRA(I),Z10NR(I)
   97  FORMAT(1H0,32X,F7.1,3X,F8.5,3X,F4.1,4X,E12.5,4X,E12.5,4X,E12.5)
   73  CONTINUE
C
C      COMPUTE COLLISION NUMBERS FOR EXACT RESONANCE ENERGY TRANSFER.
C
   98  FORMAT(1H0,24X,89H****** VIBRATIONAL-VIBRATIONAL ENERGY TRANSFER--
      1EXACT RESONANCE--COLLISION NUMBERS ******)
       WRITE(2,98)
   99  FORMAT(1H0,32X,7HT(DEGK),4X,7HT(-1/3),5X,2HZ0,10X,4HZOSC,10X,5HZTR
      1AN,9X,9HZ10(E.R.))
```

```
C
C       THIS SUBROUTINE TAKES AVALUE OF XX FROM THE MAIN PROGRAMME AND
C       FINDS A VALUE OF YY .THIS IS DONE BY SIFTING THROUGH THE TABULATED
C       VISCOSITY DATA OF HIRSCHFELDER,CURTISS AND BIRD.THE VALUE OF YY
C       IS THEN USED IN FURTHER CALCULATIONS IN THE MAIN PROGRAMME.
C
      SUBROUTINE LOOKUP(XX,YY)
      COMMON M,X,Y
      DIMENSION X(100),Y(100)
      DO 178 J=1,M
      IF(XX.GT.X(J))GO TO 178
      IF(XX.EQ.X(J))GO TO 177
      IF(.NOT.(J.EQ.1))GO TO 181
      WRITE(2,179)
      YY=(XX-X(J))*((Y(J+1)-Y(J))/(X(J+1)-X(J)))+Y(J)
      RETURN
  177 YY=Y(J)
      RETURN
  178 CONTINUE
      WRITE(2,180)
  180 FORMAT(/39H POINT ABOVE TABLE LIMITS-EXTRAPOLATION)
  179 FORMAT(/39H POINT BELOW TABLE LIMITS-EXTRAPOLATION)
  181 YY=(XX-X(J))*((Y(J)-Y(J-1))/(X(J)-X(J-1)))+Y(J)
      RETURN
      END
```

TABLE A.2.3

COMPUTATION SYMBOLS

FORTRAN	CALCULATIONS	MEANING
DR	r_0	Average L-J constant
CQ	ε	Geometric mean of L-J potential well
XMW	μ	Reduced mass of collision partners
THETA	θ	Characteristic temperature of vibration of BC
THETAA	θ_A	Characteristic temperature of vibration of A
AL	ℓ'	
ZEK	θ'	(1PE10.3)
ZEMK	Em/k	Em effective energy of collision
ZEMKA	Em/ε	(F6.2)
BLC	ℓ	Range of repulsive forces from Method B. (F8.5)
ROL	r_0/ℓ	(F6.2)

FORTRAN	CALCULATIONS	MEANING
Y22	$Y(2,2)$	(0PF6.3)
EXPEK	$\exp(-\varepsilon/kT)$	(F7.4)
ETHETA	$(1-e^{-\theta/T})^{-1}$	(F7.4)
ZOSC	Z_{osc}	Vibrational collision number (F6.1)
ZTRAN	Z_{trans}	Translational collision number (1PE10.3)
ZED	Z_{10}	Collision number of deactivation (E11.4)
T3	$T^{-\frac{1}{3}}$	(F8.5)
XX	T^*	Reduced temperature
YY	$\Omega^{(2,2)}$	
GAMA	η	viscosity
TAUC	τ_c	Time between collisions (1PE11.5)
TAU	τ	Relaxation time (1PE11.5)
ZEKBC	θ'_{BC}	
ZEKA	θ'_{A}	

FORTRAN	CALCULATIONS	MEANING
ZEKABC	θ'_{ABC}	
ZOS	$Z_{osc(n.r.)}$	Vibrational collision number for near resonance (E12.5)
ZTRA	$Z_{trans(n.r.)}$	Translational collision number for near resonance (E12.5)
Z1ONR	$Z_{1O(n.r.)}$	Collision number for deactivation at near resonance (E12.5)
ZTR	$Z_{trans(e.r.)}$	Translational collision number for exact resonance (E12.5)
ZEX	$Z_{1O(e.r.)}$	Collision number of deactivation in the exact resonance condition (E12.5)

TABLE A.2.4

INPUT INFORMATION

CARD No.	COL NOS.	SYMBOL & UNITS	FORMAT
1. Constant Card	15 - 21	F	F7.4
	22 - 33	BK	1PE12.4
	34 - 43	DL	0PF10.5
2. Constant Card	1 - 10	AN	1PE10.3
	11 - 20	CE cm s^{-1}	1PE10.3
	21 - 30	H	1PE10.3
3. Number of Temperatures	1 - 2	N	I2
4. Temperatures (N cards)	1 - 7	TEMP K	F7.1
5. Number of values from Hirschfelders data	1 - 3	M	I3
6. Hirschfelders data, usually 14 cards, each card has 6 pairs of data	1 - 66	X, Y	12F0.0
7. Internuclear distance of BC	1 - 10	DI Å	F10.6

CARD No.	COL NOS.	SYMBOL & UNITS	FORMAT
8. Species card for molecule A	1 - 20	Species name	20H
	21 - 30	CQA	F10.4
	31 - 40	DRA	F10.4
	41 - 50	XMA	F10.4
	51 - 60	XMA1	F10.4
	61 - 70	XMA2	F10.4
	71 - 80	XNUA cm^{-1}	F10.4
9. Species card for molecule BC	Similar to card 8		
10. Recycle card	1 - 2	ISSW	I2

A.2.iii MISCELLANEOUS PROGRAMMES

Several programmes were used in the analysis of results, Chapter 6. These were the polynomial curve fitting, the calculation of shock parameters and the Demac plotter programme. The programmes were constructed and developed by workers in this laboratory (Mrs P.M. Borrell and Mr. R. Gutteridge). The programmes are documented elsewhere.[3]

The programme to calculate the populations of the vibrational levels of a harmonic oscillator by various mechanisms, was written and developed by Dr. P. Borrell.

REFERENCES

1. J.O. Hirschfelder, C.F. Curtiss and R.B. Bird, *Molecular Theory of Gases and Liquids*, (Wiley, New York) 1954, 1110.

2. J.O. Hirschfelder, C.F. Curtiss and R.B. Bird, *Molecular Theory of Gases and Liquids*, (Wiley, New York) 1954, 1126.

3. R. Gutteridge, *Ph.D. Thesis* to be published.